Oncogene-induced senescence in melanocytes

Onkogen-induzierte Seneszenz in Melanozyten

-

Doctoral thesis for a doctoral degree at the Graduate School of Life Sciences,
Juluis-Maximilians-Universität Würzburg,
Biomedicine

submitted by

Claudia Leikam

from

Roth, Germany

Würzburg, 2012

Submitted on:	24th September 2012

Members of the thesis committee

Chairperson:	Prof. Dr. Manfred Gessler
Primary Supervisor:	Prof. Dr. Dr. Manfred Schartl
Secondary Supervisor:	Dr. Svenja Meierjohann
Third Supervisor:	Prof. Dr. Martin Eilers

Date of Public Defence:	1st August 2013
Date of receipt of Certificates:	

"Something has changed within me,
something is not the same.
I'm through with playing by
the rules of someone else's game!
Too late for second-guessing,
too late to go back to sleep.
It's time to trust my instincts,
close my eyes
and leap...

It's time to try defying gravity,
I think I'll try defying gravity...
and you can't pull me down!"

- Elphaba, "Defying Gravity", Wicked -

To my mum in this world
and
my dad in the other.

I love you!

Affidavit

I hereby confirm that my thesis entitled "Oncogene-induced senescence in melanocytes" is the result of my own work. I did not receive any help or support from commercial consultants. All sources and / or materials applied are listed and specified in the thesis.

Furthermore, I confirm that this thesis has not yet been submitted as part of another examination process neither in identical nor in similar form.

Abenberg, 21.09.2012

Place, Date Signature

Eidesstattliche Erklärung

Hiermit erkläre ich an Eides statt, die Dissertation "Onkogen-induzierte Seneszenz in Melanozyten" eigenständig, d.h. insbesondere selbständig und ohne Hilfe eines kommerziellen Promotionsberaters, angefertigt und keine anderen als die von mir angegebenen Quellen und Hilfsmittel verwendet zu haben.

Ich erkläre außerdem, dass die Dissertation weder in gleicher noch in ähnlicher Form bereits in einem anderen Prüfungsverfahren vorgelegen hat.

Abenberg, 21.09.2012

Ort, Datum Unterschrift

Contents

1. Summary

Melanoma is the most aggressive skin cancer with very limited treatment options. Upon appearance of metastases chemotherapeutics are used to either kill or slow down the growth of cancer cells by inducing apoptosis or senescence, respectively. With melanomas originating from melanocytes, it is vital to elucidate the mechanisms that distinguish senescence induction from proliferation and tumourigenicity.

Xmrk (*Xiphophorus* melanoma receptor kinase), the fish orthologue of the human epidermal growth factor receptor (EGFR), causes highly aggressive melanoma in fish. Using an inducible variant, HERmrk, I showed that high receptor levels result in melanocyte senescence, whereas low and medium expression allows for cell proliferation and tumourigenicity. Mechanistically, HERmrk leads to increased reactive oxygen species (ROS) levels, which trigger a DNA damage response. Consequently, multinucleated, senescent cells develop by both endomitosis and fusion. Furthermore, oncogenic N-RAS (N-RAS^{61K}) induces a similar multinucleated phenotype in melanocytes.

In addition, I found that both overexpression of C-MYC and the knockdown of *miz-1* (Myc-interacting zinc finger protein 1) diminished HERmrk-induced senescence entry. C-MYC prevent ROS induction, DNA damage and senescence, while acting synergistically with HERmrk in conveying tumourigenic features to melanocytes. Further analyses identified cystathionase (*CTH*) as a novel target gene of Myc and Miz-1 crucial for senescence prevention. *CTH* encodes an enzyme involved in the synthesis of cysteine from methionine, thereby allowing for increased ROS detoxification.

Even though senescence was thought to be irreversible and hence tumour protective, I demonstrated that prolonged expression of the melanoma oncogene N-RAS^{61K} in pigment cells overcomes initial OIS by triggering the emergence of tumour-initiating, mononucleated stem-like cells from multinucleated senescent cells. This progeny is dedifferentiated, highly proliferative, anoikis-resistant and induces fast-growing, metastatic tumours upon transplantation into nude mice. Our data demonstrate that induction of OIS is not only a cellular failsafe mechanism, but also carries the potential to provide a source for highly aggressive, tumour-initiating cells.

2. Zusammenfassung

Das Melanom ist der aggressivste Hautkrebstyp mit äußerst begrenzten Therapiemöglichkeiten. Sobald Metastasen diagnostiziert werden, kommen Chemotherapeutika zum Einsatz, deren Aufgabe darin besteht, die Krebszellen durch Apotoseinduktion zu töten oder ihre Verbreitung mittels Seneszenz zu verlangsamen. Da Melanome aus Melanozyten hervorgehen, ist es essentiell, die Mechanismen zu analysieren, die entscheiden, ob Zellen seneszent oder tumorigen werden.

Xmrk, die *Xiphophorus*-Melanom-Rezeptor-Kinase und Fischortholog des humanen epidermalen Wachstumsfaktors (EGFR), verursacht aggressive Melanome in Fischen. Durch den Einsatz von HERmrk, einer induzierbaren Variante des Rezeptors, konnte ich zeigen, dass hohe Expressionslevel Seneszenz in Melanozyten zur Folge haben, wohingegen niedrige oder mittlere Rezeptorlevel mit erhöhter Zellproliferation und Tumorigenität der Zellen einhergehen. Mechanistisch gesehen, führt die Aktivierung von HERmrk zu gesteigerten Level an reaktiven Sauerstoffspezies (ROS), die wiederum DNA-Schäden verursachen und dadurch bestimmte Signalwege auslösen. Durch Endomitose und Fusion entstehen letztendlich multinukleäre, seneszente Zellen. Interessanterweise, führte die Expression von onkogenem N-RAS (N-RAS^{61K}) in Melanozyten zu einem sehr ähnlichen Phänotyp.

Des Weiteren konnte ich zeigen, dass sowohl die Überexpression von C-MYC als auch der Knockdown von *miz-1* (Myc-interagierendes Zinkfingerprotein 1) der HER-mrk-induzierten Seneszenz entgegenwirkten. C-MYC verhindert einerseits die Entstehung von ROS, die dadurch verursachten DNA-Schäden und damit die Seneszenz und wirkt andererseits synergistisch mit HERmrk, indem es den Melanozyten tumorigene Eigenschaften verleiht. In weiteren Analysen wurde Cystathionase (*CTH*) als neues Zielgen von Myc und Miz-1 identifiziert, dem eine zentrale Rolle in der Seneszenzverhinderung zukommt. *CTH* kodiert für ein Enzym, das die Synthese von Cystein aus Methionin und damit die Entsorgung von ROS ermöglicht.

Obwohl man davon ausgeht, dass Seneszenz einen irreversiblen Mechanismus darstellt, der die Tumorentstehung verhindert, konnte ich zeigen, dass die langfristige Expression des Melanomonkogens N-RAS^{61K} die initiale Seneszenzinduktion durchbricht. Dabei gehen mononukleäre, tumorigene, stammzellähnliche Zellen aus seneszenten Zellen hervor. Diese Tochterzellen sind dedifferenziert, hochproliferativ, Anoikis-resistent und induzieren schnellwachsende, metastasierende Tumoren in Nacktmäusen. Damit machen meine Daten deutlich, dass Seneszenz nicht nur als zellulärer Schadensbegrenzungsmechanismus fungiert, sondern auch das Potential hat, äußerst aggressive Tumorzellen zu generieren.

3. Introduction

3.1 Melanoma

Malignant melanoma is the most aggressive form of skin cancer with the number of melanoma cases worldwide increasing faster than that of any other type of cancer [1]. Estimates even suggest a doubling of melanoma incidence every 10–20 years [2]. Although melanoma only accounts for about 4% of skin cancer cases, it does so for as many as 74% of all related deaths. In 2002, the World Health Organization (WHO) estimated 160.000 new cases of malignant melanoma worldwide and reported 41.000 deaths caused by this dreadful disease [3]. Even though there is a good chance for the recovery of patients suffering from melanoma if the primary lesion is detected and excised very early (more than 90% survival in stage I melanomas), prognosis for 5-year survival for more advanced melanomas drops to approximately 60% of cases (stage II) and to as low as 10% (stage III) before reaching almost complete fatality (stage IV) usually within less than 6-8 months [4–6]. Notably, melanomas of as little as 4 millimeters in diameter are usually associated with distant metastases. Hence, metastasis occurs very early in the progression of the disease. Once melanomas have metastasized to distant organs, they are classified as stage IV melanoma (*Figure 1*) [7]. These data underline the current lack of therapeutic approaches to treat advanced melanoma. Beyond an early surgical removal of the primary tumour after diagnosis, there is currently no promising standard therapy available for treatment of advanced melanomas.

Hence, it is not surprising that malignant melanoma is one of the most aggressive types of human cancers [8]. Most frequently arising in the skin, melanomas can evolve from benign or pre-malignant aggregations of melanocytes, termed nevi [9]. It is noteworthy that nevi are considered permanently growth-arrested (or "senescent") and are thought to rarely progress into melanoma. Indeed, studies showed that human nevi, most of which bear a $BRAF^{V600E}$ mutation, are invariably positive for senescence-associated-β-galactosidase (SA-β-Gal), one of the classical senescence markers [10–12]. Nevertheless, traditionally, five distinct steps of melanoma development and progression are distinguished: A dysplastic nevus (2) showing a high level of structural and architectural changes arises from a common nevus (1). The subsequent radial growth phase (RGP) primary melanoma (3; stage I melanoma) is the first recognizable malignant stage in which cells do not yet possess metastatic potential but are already locally invasive. This means that the epidermis that covers a portion of the primary tumour might no longer be intact. The RGP can be followed by a VGP (vertical growth phase) leading to primary melanoma lesions (4) in which melanoma cells infiltrate and invade the dermis and finally the subcutis (late stage I melanoma). Besides, the tumour cells bear metastatic potential even though they have not metastasized to local or distant lymph nodes (stage II melanoma). Once the melanoma has metastasized to local but not

distant lymph nodes, it is classified as stage III melanoma. This process finally results in metastasis to distant lymph nodes and organs (5; stage IV melanoma; *Figure 1 and 2*) [13].

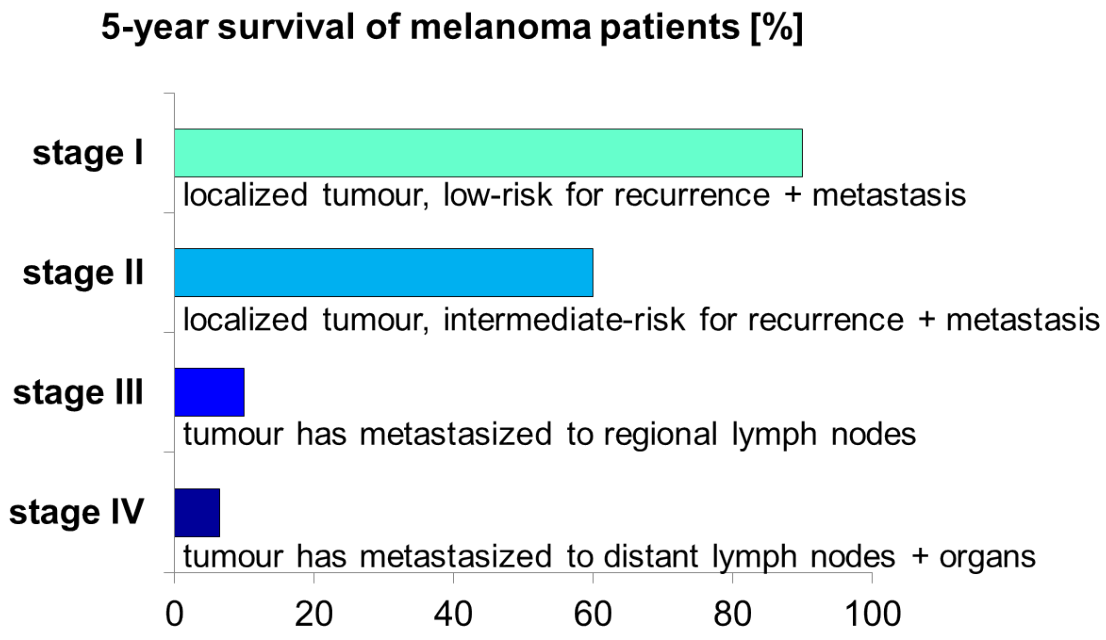

Figure 1: Characteristics of melanoma stages and the corresponding 5-year survival rates
Melanomas are staged (I-IV) according to tumour size, localization, recurrence and metastasis risk level as well as the presence and location of metastases. The corresponding 5-year survival rates for melanoma patients dramatically drop with stage progression.

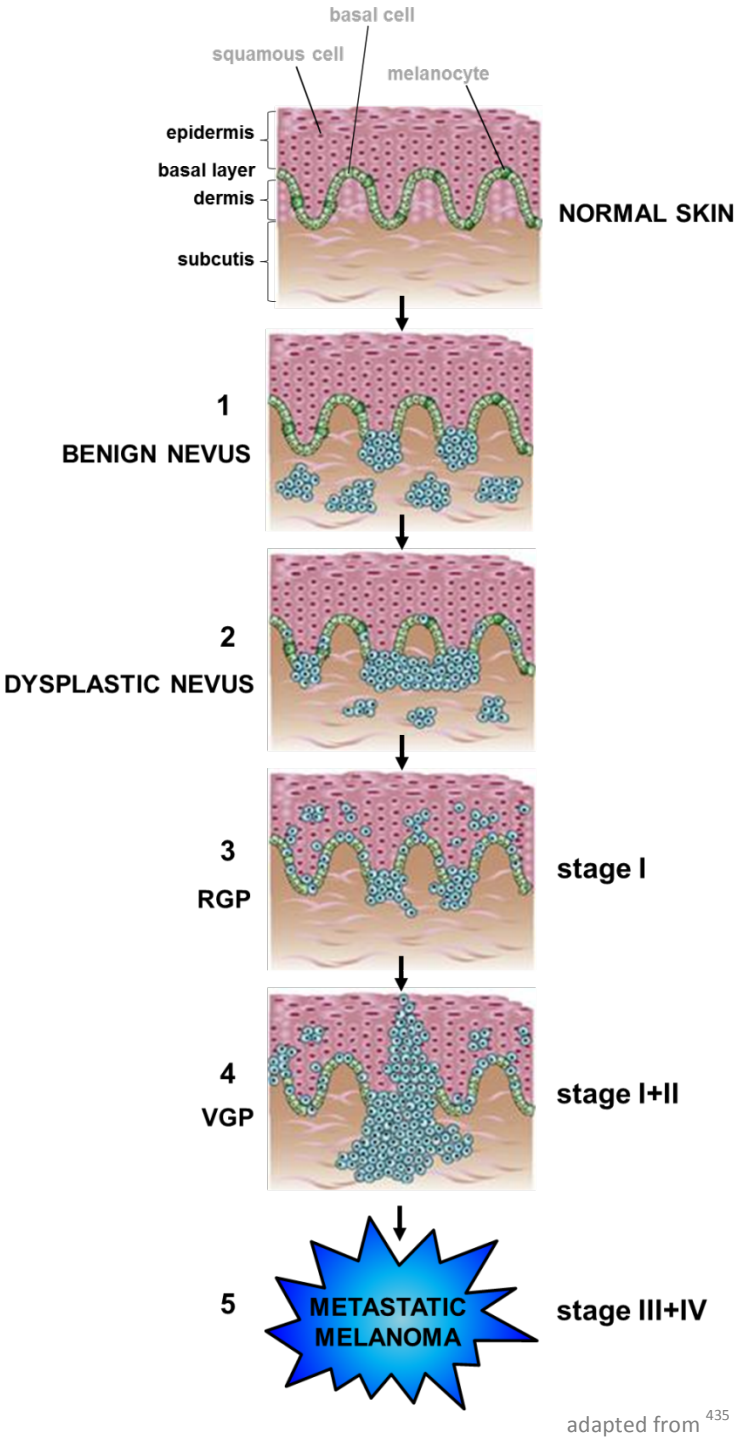

Figure 2: Five steps of melanoma development

Traditionally, five steps of melanoma development are distinguished: the dysplastic nevus (2) arises from a benign nevus (1), followed by a subsequent radial growth phase melanoma (RGP). Then the tumour cells become locally invasive forming a vertical growth phase melanoma (VGP) before metastasizing to regional and distant sites of the body.

The neoplastic transformation of melanocytes often involves onco-proteins that up-regulate the mitogen-activated kinase pathway [9]. In particular, activating mutations of BRAF (e.g. V600E) or NRAS (e.g. Q61K or Q61R) are found in approximately 60% and 20% of melanomas from non-chronically sun-damaged skin, respectively [14–16]. However, $BRAF^{V600E}$ mutations in

melanomas from chronically sun-damaged skin or from skin relatively unexposed to sun are less common [14]. Intriguingly, $BRAF^{V600E}$ mutations are detected at even higher frequencies in benign acquired nevi (82%) [17], whereas 81% of benign congenital nevi harbour mutations in the *NRAS* gene [18]. Besides, inducing *NRAS* point mutations are detected in 33% of primary melanomas and 26% of metastatic melanoma samples [19]. Moreover, activating *HRas* mutations (*H-ras*^{G12V}) in mouse melanocytes in cooperation with inactivating mutations in tumour suppressors like *CDKN2A* (cyclin dependent kinase inhibitor 2A) or *TP53* (tumour protein 53) can lead to cell transformation [20,21]. Apart from oncogenic mutations in RAS or B-RAF, the hyperactivation of upstream-acting receptor tyrosine kinases (RTKs) is frequently observed in melanoma [22–26]. In murine $H\text{-}RAS^{V12}$-driven melanoma, transcriptional induction of epidermal growth factor receptor (EGFR) ligands is observed, resulting in an autocrine EGFR-stimulating loop important for melanomagenesis [27]. Moreover, the RTK Xmrk induces highly malignant melanoma in several backcross hybrids of the fish *Xiphophorus* [28,29]. Besides, a forward genetic screen in benign and malignant human melanocytic neoplasms lacking a BRAF or NRAS mutation identified the oncogenic mutation $GNAQ^{Q209L}$ in 83% of blue naevi (n=529), 50% of 'malignant blue naevi' (n=52) and 46% of uveal melanomas (n=548) [30]. Even though $GNAQ^{Q209L}$ was long ago demonstrated to transform 3T3cells [31], it has only recently been shown that Q209L or R183C mutations in GNA11, a paralogue of GNAQ, are capable of transforming melan-a cells and induce tumours in non-obese diabetic mice with severe combined immunodeficiency and depletion of the interleukin-2 receptor γ chain [32]. Furthermore, in about 45% of melanomas, the lipid phosphatase PTEN is deleted and the downstream Akt3 gene is amplified [33,34], with both mutations resulting in aberrant Akt activity [34].

The most significant risk factor for melanoma is a strong family history of this cancer. A meta-analysis of family history found that the presence of at least one first-degree relative with melanoma increases the risk by 2.24-fold [35,36]. Genetic studies of this heritable trait in large melanoma-prone families finally led to the initial identification of CDKN2A as the familial melanoma gene. Located on chromosome 9p21, LOH (loss of heterozygosity) or mutation at this locus goes along with increased melanoma susceptibility [37,38]. Interestingly, 9p21 homozygous deletions on CDKN2A were frequently observed in various cancer cell lines [39,40] and somatic mutations in this gene are also found in most sporadic melanomas [41,42]. Furthermore, several physical characteristics have been shown to increase the risk for melanoma development, e.g. fair skin, an inability to tan, red hair, and blue eyes [43]. Likewise, the presence of multiple pigmented lesions, including freckles and banal or clinically atypical moles, is associated with increased melanoma risk [44].

To date, the failure of current approaches to provide successful melanoma treatment reflects an underlying problem, which is only poorly understood at the molecular level: cancer cell population heterogeneity. Increasing evidence suggests that tumours comprise multiple subpopulations of cancer cells, some of which may be resistant to therapy. Two models that aim at explaining tumour heterogeneity and treatment failure are being

discussed: the melanoma stem cell and the melanoma switch model. The melanoma stem cell model claims that cancers develop from a small, therapy-resistant subset of cells with self-renewal properties analogous to organ stem cells [45]. Several melanoma stem cell markers have been suggested, e.g. the rhodamine efflux transporter ABCB5 [46], the neural crest nerve growth factor receptor CD271 (Ngfr / p75) [47], the H3K4 demethylase JARID1B [48] or the stem cell marker combination $CD34^{+}CD271^{-}$ [49]. However, contradictory results concerning the tumour-initiating potential of the marker-bearing versus the marker-negative subpopulations [50], the expression of differentiation markers on subsets of apparent melanoma stem cells, the impact of technical issues (e.g. the prior embedding in matrigel) and the fact that 25% of single melanoma cells isolated from patients initiated tumourigenesis [51] have caused some debate concerning these findings. That is probably the reason why the melanoma switch theory is gaining recognition. This model suggests that metastasis and phenotypic heterogeneity is driven by specific gene expression programs that might be imposed by the cellular microenvironment rather than by the accumulation of genetic events. Thereby, the changing microenvironmental conditions, to which melanoma cells themselves also contribute, are suggested to allow virtually every melanoma cell to switch back-and-forth between proliferative or migratory phenotypes. The phenotype-switch model theory is e.g. supported by the reversible E-cadherin expression during melanoma development [52], an intrinsic migratory capacity switch [53] and the fact that matrix-modifying components secreted by metastatic melanoma cells can reprogram normal melanocytes to a reversible invasive phenotype [54]. On top, gene expression profiling of 86 melanoma cell lines in culture identified two major expression signatures, namely the proliferative and the invasive one [55], all of which generated heterogenous tumours containing cells with both kinds of expression profiles when transplanted into mice [56]. Furthermore, the expression of the transcription factor Brn-2 revealed a striking heterogeneity in melanoma [57]. Brn-2 expression is positively associated with melanoma proliferation, up-regulated by BRAF and β-catenin and associated with invasiveness. Besides, Brn-2 actively represses the microphthalmia-associated transcription factor Mitf, which controls survival, differentiation, proliferation and migration in melanocytes [58]. Hence, it is not surprising that motile cells in the primary tumour tend to express higher levels of Brn-2 while showing low Mitf levels and pigmentation, whereas low Brn-2 cells predominate in the resulting lung metastases [57].

Regardless of which model one favours, animal models are considered a helpful and often necessary tool to more deeply and relevantly investigate the mechanisms underlying melanoma formation. One of the oldest ones for human cancer are *Xiphophorus* fish, in which the oncogene *Xmrk* drives spontaneous melanoma formation specifically in certain hybrid genotypes.

3.2 The *Xiphophorus* melanoma model

Xmrk is the acronym for *Xiphophorus* melanoma receptor kinase (Xmrk) that acts as a very strong oncogene when overexpressed in *Xiphophorus* melanoma. It is a transmembrane glycoprotein belonging to the receptor tyrosine kinases (RTKs) that is permanently dimerized due to disulfide bridges in the extracellular domain. Xmrk shows full transformation potential as it is not only involved in proliferation and resistance to apoptosis but also interferes with differentiation and induces migration [59].

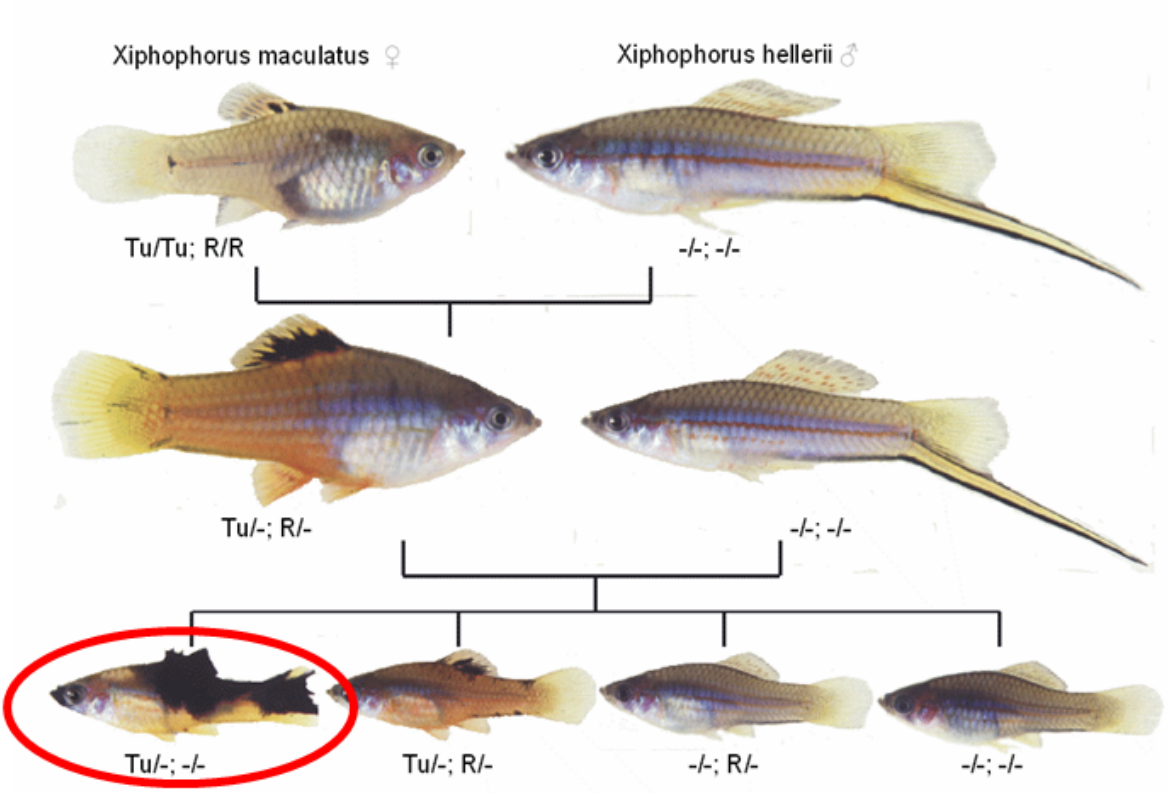

Figure 3: Gordon/Kosswig/Anders melanoma model
Fish of the species *Xiphophorus maculatus* and *Xiphophorus hellerii* very rarely develop neoplastic lesions. Nevertheless, certain backcross hybrids (highlighted by a red ellipse) develop highly malignant melanoma at high frequency due to the presence of the dominant oncogene locus Tu. This Tu locus encodes *Xmrk* and its expression is presumably repressed by the presence of the regulator R in the platyfish *Xiphophorus maculatus*. The closely related swordtail *Xiphophorus hellerii* contains neither of these genes. Crossing conditioned elimination of R leads to the development of highly malignant melanoma.

As Xmrk is one fish orthologue of the well-studied mammalian epidermal growth factor receptor (EGFR), its dimerization results in autophosphorylation and activation of various pathways that are largely identical to those mapped for EGFR signalling (*Figure 4*) [60]. Phosphatidyl-inositol 3-kinase (PI3K) is one of the downstream proteins activated by Xmrk. Alone, or in combination with the src-kinase fyn, it results in activation of the PI3K/protein

kinase B (PKB/Akt) signalling pathway and consequently in protection from apoptosis [28,59,61]. Furthermore, Xmrk activation leads to an increase in cell motility via interactions with focal adhesion kinase (FAK) and fyn [62] . Changes in FAK activity are then followed by modulation of focal adhesions and appearance of stress fibres [63]. Moreover, Xmrk expressing cells show continuous binding and phosphorylation of the signal transducer and activator of transcription 5 (STAT5) [60]. Phosphorylated STAT5 translocates to the nucleus and activates specific target genes resulting in proliferation signals and the expression of the anti-apoptotic protein bcl-x [64]. Importantly, the Xmrk receptor was found to bind to growth factor receptor binding protein 2 (GRB2), which initiates the activation of the mitogen-activated-protein-kinase (MAPK) through Ras and Raf, resulting in a strong activation of the MAP kinases' extracellular signal-regulated kinases 1 and 2 (ERK1 and ERK2) [65]. This pathway is not only essential for proliferation, but also for cell survival in 3D-matrices as it up-regulates the RNA and protein levels of the secreted protein osteopontin (Opn) [29]. Opn binds to $\alpha_V\beta_3$ integrins on the cell surface, which is in turn associated with neoplastic progression and tumourigenicity in melanoma [66,67]. Besides, the MAPK-dependent induction of the matrix metalloprotease MMP13 enhances proliferation while decreasing the pigmentation of melanocytes [68]. As Xmrk is known to be a potent inducer of all three proteins, understanding the effects of Xmrk on transformation serves as an important step in melanomagenesis comprehension.

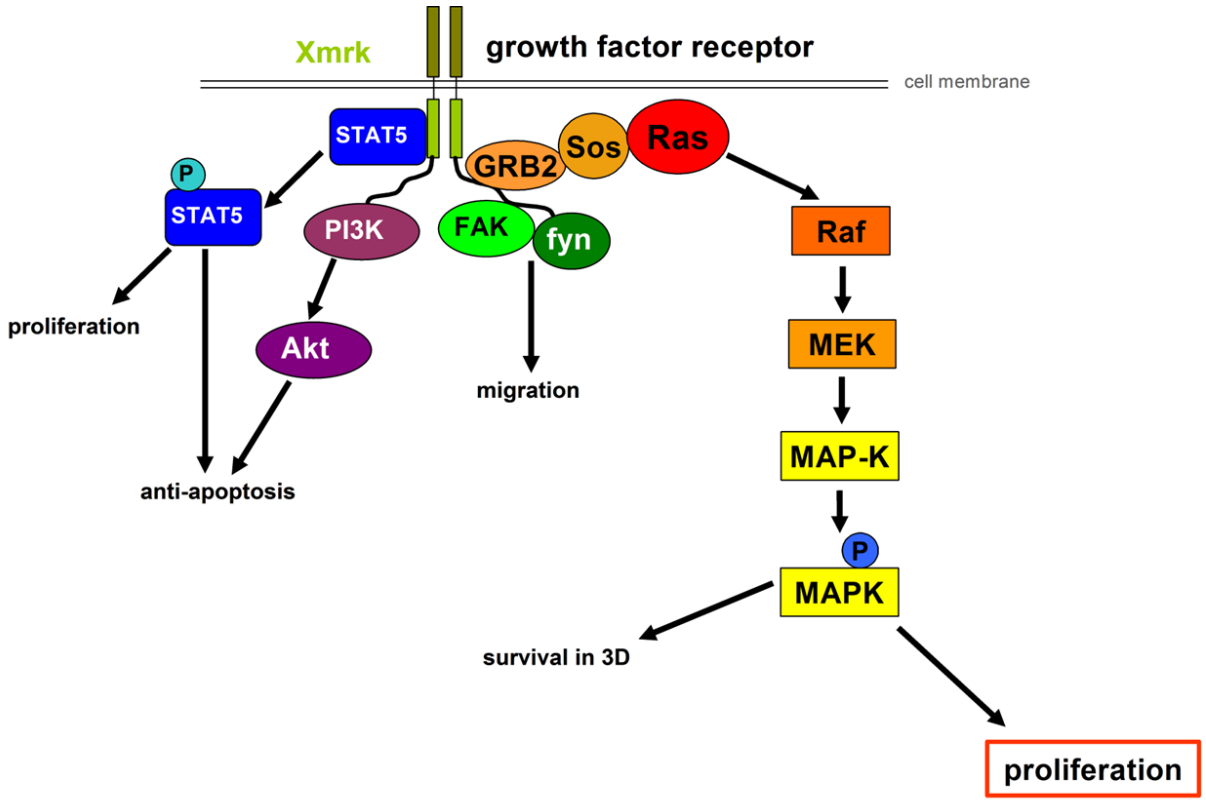

Figure 4: Pathways induced by Xmrk

Dimerization of the receptor tyrosine kinase Xmrk results in the induction of various pathways. STAT5 is phosphorylated upon binding to Xmrk, translocates to the nucleus and activates target genes that promote proliferation as well as anti-apoptotic signals. Anti-apoptotic signals are also transmitted via the PI3K/Akt pathway. The interaction of FAK and fyn with Xmrk leads to an increase in cell motility. In addition, binding of GRB2 initiates the activation of MAPK through Ras and Raf resulting in cell survival and proliferation. Besides, MAPK-dependent MMP13 expression enhances proliferation and diminishes melanocyte pigmentation.

3.3 HERmrk

The receptor tyrosine kinase and EGFR orthologue Xmrk is constitutively active due to at least two dimerizing mutations in the extracellular domain of the receptor. The first one is the substitution of a conserved cysteine for a serine (C578S) involved in intramolecular disulfide bonding. The second one is a glycine to arginine exchange (G359R) in subdomain III. Either mutation leads to constitutive dimer formation, thereby activating the oncogenic version of the Xmrk receptor [67,69]. Interestingly, these mutations not only result in constitutive activity of the oncogene, but also slow down its processing in the endoplasmic reticulum [70].

The problem of continuous Xmrk acitivity can be circumvented by the use of an EGF-inducible chimeric receptor ('HERmrk' or shortly 'Hm'). Hm consists of the extracellular part of the human EGFR (HER) and the cytoplasmic part of Xmrk (mrk). To analyze Xmrk signalling specifically in the pigment cell lineage, the mouse melanocyte cell line melan a [71] was stably

transfected with the chimeric HERmrk receptor [72]. This allows HERmrk signalling induction by providing the cells with human EGF (*Figure 5*), which is readily available as a recombinant protein, while keeping the cytoplasmic kinase domain and docking sites of the fish receptor intact.

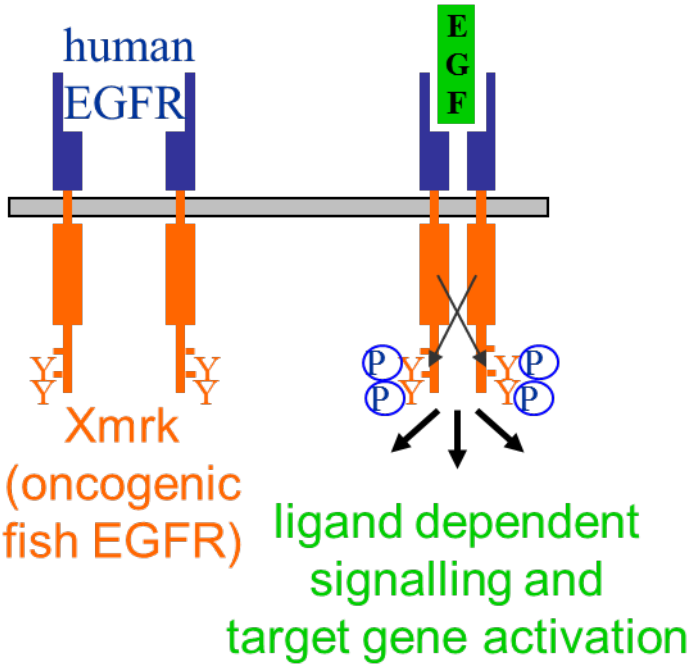

Figure 5: HERmrk receptor
The chimeric receptor HERmrk (shortly Hm) consists of the extracellular part (HER) of the human epidermal growth factor receptor (EGFR) and the intracellular part (mrk) of Xmrk. Supplementing the culture medium of stably transfected melan a-Hm cells with human epidermal growth factor (EGF) results in ligand-dependent signalling and target gene activation.

3.4 Senescence

Apoptosis and senescence are cellular failsafe programs. The term "senescence" derives from the Latin word "senescere" which translates to "ageing". Cellular senescence was first described by Hayflick and Moorhead in 1961 [73] as a process that prevents human fibroblasts from growing indefinitely in culture, as for all differentiated cell types proliferation ceases after a cell type specific number of divisions [74].

The phenotype of senescent cells is generally characterized by an irreversible growth arrest, an increased cell size, a distinct flat, enlarged morphology, the accumulation of lipofuscin granules and senescence associated-β-galactosidase activity. In addition, an increased expression of genes, e.g. those involved in cell cycle regulation, as well as gain and loss of various biological functions has been observed for senescent cells while they remain in a metabolically active state [75]. Besides, senescent cells have been shown to secrete factors associated with senescence induction, inflammation (e.g. the chemokines IL-6 and IL-8) and

tumour development. This so-called senescence-associated phenotype (SASP) not only occurs in cultured cells, but also in vivo upon DNA-damage, e.g. chemotherapy [4].

Two major types of senescence have been described. Replicative senescence (RS) is a complex and heterogeneous process and is thought to occur once the telomeres have reached a critically short length [76]. Every other kind of senescence is referred to as premature senescence (PS), occurring due to stress after fewer cell divisions compared to RS. As one example, stress-induced senescence is caused by extrinsic factors, like lack of nutrients or oxidative stress. One particular source of stress derives from the aberrant proliferative signals of oncogenes, such as the activated form of the small G-protein Ras which can eventually trigger senescence. This process is referred to as oncogene-induced senescence (OIS). OIS counteracts the excessive mitogenic signalling from activated oncogenes by restricting their cell division rate, so that the tumour remains in a non-aggressive, premalignant state. Therefore, OIS is observed in the vast majority of premalignant neoplastic lesions, both in mouse models and humans, but is scarce in malignant tumours [77].

3.5 Mediators of OIS

Mutant-Ras-induced OIS has been linked to two major cell-signalling pathways that are often disrupted in cancer cells: the $p19^{ARF}$-p53 and the $p16^{INK4A}$-Rb pathway [78]. Interestingly, human melanocytes have been implied to senesce primarily via the pRb pathway upon $N\text{-}Ras^{Q61K}$ oncogene expression *in vitro* [79]. However, p53 not only induced a cell-cycle arrest in primary human melanocytes, but also effectively prevented the progression of small benign lesions to malignant and metastatic melanoma in a $TP\text{-}ras^{0/+}$: $Mdm4^{+/-}$ mouse model. These mice expressed activated $HRAS^{V12G}$ under a mouse tyrosinase promoter and lack one allele of Mdm4, a negative regulator of p53. The $TP\text{-}ras^{0/+}$ mouse is a highly appreciated model of melanoma progression because a topical treatment of DMBA induces all the stages of melanomagenesis [80]. Thus, mutations in both, the $p19^{ARF}$ and the $p16^{INK4A}$-Rb pathway allow the oncogene-driven progression into malignant tumours.

Both potent tumour suppressors, $p16^{INK4a}$ (inhibitor of cyclin dependent kinase 4) and $p19^{ARF}$ (alternative reading frame), are found on the same mammalian gene locus *CDKN2A* (*cyclin-dependent kinase inhibitor 2A*), also known as *MTS1* (*multiple tumour suppressor 1*). It is deleted, mutated or silenced in a wide variety of human malignancies [81]. A unique gene structure generates two distinct open reading frames that initiate in different first exons and continue in alternative reading frames in a common second exon. This unusual utilization of overlapping exonic sequences in mammalian cells enables a single gene to encode two structurally and biochemically completely unrelated protein products [82]. The $p16^{INK4a}$ protein inhibits the association of D-type cyclins and CDK4/6, thereby blocking phosphorylation of Rb and exit from G1 phase [83] (*Figure 6*). The $p19^{ARF}$ protein blocks the MDM2 (Murine

Double Minute Clone 2) inhibition of p53 and induces G1 and G2 checkpoint arrests [84]. The fact that the two structurally and biochemically dissimilar products of the *CDKN2A* locus can modulate different tumour suppressor pathways, makes it uniquely effective, yet, at the same time, exquisitely vulnerable as a tumour suppressor [85].

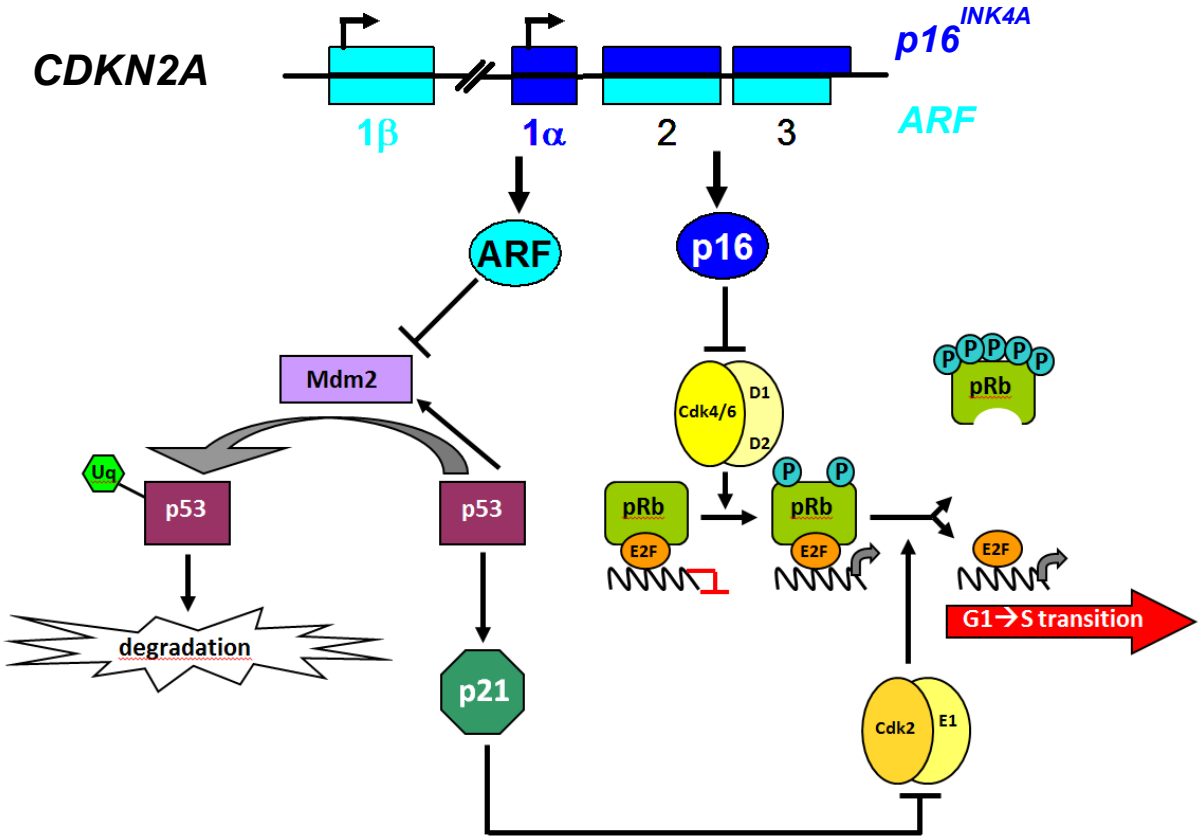

Figure 6: Role of *CDKN2A* in cell cycle regulation
The mammalian gene locus *CDKN2A* encodes two potent tumour suppressors that differentially regulate cell cycle progression. $P19^{ARF}$ protein blocks MDM2-mediated inhibition of p53, leading to a G1 and G2 check-point arrest via upregulation of p21. $P16^{INK4a}$ inhibits the association of D-type cyclins and CDK4/6, thereby inducing a pRb-depending G1 arrest.

Since senescent cells are abundant in premalignant lesions like nevi, but scarce in malignant tumours, it is vital to investigate the mechanisms underlying OIS. Besides, a detailed understanding of senescence might identify crucial aspects for the switch from the benign to the malignant state of melanoma.

3.6 INK4 proteins

$P16^{INK4a}$ is one of four INK4 isoforms sharing a structural motif, the ankyrin repeats, that are involved in cyclin dependent kinase 4/6 (CDK4/6) binding [86]. INK4 proteins are differentially expressed during development [87,88].

Interestingly, p16^{INK4a} expression increases with age [89]. The expression of *p16^{INK4a}* is tightly regulated on the transcriptional level by a number of proteins. Inhibitor of differentiation 1 (Id1) usually represses the *p16^{INK4a}* promoter and keeps p16^{INK4a} expression in check. This effect is potentiated by mitogen-activated/extracellular signal-regulated kinase kinase (Mek) expression. The polycomb protein and transcriptional repressor B lymphoma Mo-MLV insertion region 1 (Bmi-1) is another negative regulator of p16^{INK4a}. Id1 as well as Bmi-1-deficient mice undergo premature senescence [75]. Members of the erythroblast transformation specific domain (Ets) transcription factors have been described as activators of *p16^{INK4a}*, whereas the Twist and E2F3 proteins act as repressors of *p19^{ARF}* transcription. Proteins like T-box 2 transcription factor (Tbx2), T-box-3 transcription factor (Tbx3), Jun-like transcription factor B (JunB) and others have also been implicated in the regulation of *CDKN2A.* The T-box factors repress *p19^{ARF}* transcription, whereas JunB activates p16^{INK4a} expression [90,91]. Interestingly, *p16$^{INK4a-/-}$ p19$^{ARF-/-}$* mice develop normally with spontaneous tumours occurring with rather short latency and these mice are highly sensitive to carcinogenic insults. Mice exclusively lacking *p19^{ARF}* show the same phenotype [92], yet *p16$^{INK4a-/-}$* mice suffer from a variety of tumours with rather long latency and from thymocyte hypercellularity [93]. Surprisingly, mice solely lacking exon 1α of *p16^{INK4a}* develop tumours at a higher rate. This suggests an indirect effect of the exclusive lack of exon 1α on p19^{ARF} expression in this mutant mouse strain [93]. The ablation of each of the other INK4 loci does not result in significant developmental abnormalities [94–96].

The cyclin dependent kinase inhibitor p15^{INK4b} shows significant similarities to p16^{INK4a} [85] and is one of the best-established OIS markers. CDKN2B encodes for p15^{INK4b}, which inhibits Cdk4 and Cdk6, thereby arresting the cells in G1 [88] and acting as a tumour suppressor [97]. P15^{INK4b} shows increased expression levels specifically in premalignant neoplastic lesions of the skin, lung and pancreas but not in corresponding malignant tumours [77]. The frequent alteration of *p15^{INK4b}* in human and murine hematopoietic malignancies suggests that its absence might predispose hematopoietic cells to malignant transformation [89]. In addition, p15^{INK4b} has been described to be involved in growth arrest that is imposed during mutant-Ras-induced senescence and was shown to oppose transformation by Ras in cultured cells [77].

In contrast to *CDKN2A,* mutations in the neighbouring *CDKN2B* gene encoding p15^{INK4b} occur less frequently in human malignancies. Even though p15$^{INK4b-/-}$ mice have been described as less cancer-prone than p16$^{INK4a-/-}$ animals [85], some mice do develop tumours with hemangiosarcoma being the most frequent type [98].

Genetic alterations of p18^{INK4c} gene are rare events in human tumours. However, several studies reported that p18^{INK4c} is a haploinsufficient tumour suppressor in mice, suggesting the possibility that a quantitative decrease of this INK4 may be involved in human tumourigenesis [99]. Besides, p18^{INK4c} is down-regulated in human pituitary adenoma [100]. Additionally, p18^{INK4c} gene silencing by promoter methylation has been observed in Hodgkin

lymphoma [101] and medulloblastoma [102]. Furthermore, deletions of *CDKN2C*, which encodes for $p18^{INK4c}$, are frequently found in multiple myeloma [103]. Taken together, these data suggest a possible role for p18INK4c as a tumour suppressor.

In contrast, $p19^{INK4d}$ null mice do not develop tumours or other types of proliferative disorders. Furthermore, they are not more susceptible to tumour formation than wild-type mice in response to carcinogenic treatment [98]. The only phenotype observed for $p19^{INK4d}$-deficient mice is testicular atrophy even though the mice remain fertile [96]. These results render it unlikely that p19INK4d alone acts as a tumour suppressor.

Even though neither $p18^{INK4c}$ nor $p19^{INK4d}$ have been reported to play a role in senescence, both $p15^{INK4b}$ and $p16^{INK4a}$ are important for this tumour-protecting mechanism. Hence, it is important to further investigate the detailed mechanisms underlying senescence induction in melanocytes to better understand melanoma formation. Since *CDKN2A* is most frequently lost in tumours and seems to be the vital player in senescence induction, I will focus on $p16^{INK4a}$.

3.7 The $p16^{INK4a}$-Rb pathway

The $p16^{INK4a}$/Rb pathway plays a key role in controlling cell growth by integrating multiple mitogenic and antimitogenic stimuli. In addition, this pathway is deregulated in more than 80% of human tumours either by genetic or epigenetic alterations that target at least some of its key members like Cyclin D1, cyclin dependent kinase 4 (CDK4), INK4a or retinoblastoma protein (pRb) [98]. $P16^{INK4a}$ expression is low in young and high in senescent cells, whereby demethylation or overexpression often goes along with a senescent phenotype. In addition, $p16^{INK4a}$ is highly expressed in human nevi, the benign precursors of malignant melanoma, and frequently deleted in melanoma cells [78]. Linkage-analysis studies have shown a high incidence of *CDKN2A* and *CDK4* mutations in familial melanomas, which represent approximately 10% of all melanoma cases [90].

$P16^{INK4a}$ protein sequesters Cdk4 and 6 and prevents them from phosphorylating and inactivating Rb. The Rb family of proteins, pRb, p107 and p130 ultimately regulate the critical transition from mitogen dependence to mitogen independence, the so-called restriction point (R) or point of no return. Having passed through R that divides early and late G1, cells become committed to a new round of replication. Early in G1 the synthesis of D-type cyclins which heterodimerize with CDK4 and 6 to phosphorylate pRb, leads to the release of the E2F transcription factor and progression of the cell cycle [104–106] (*Figure 6 and 7*).

The histone-lysine N-methyltransferase suppressor of variegation 3-9 homolog 1 (Suv39h) functions in concert with Rb by methylating histone proteins [78]. This global heterochromatin formation initiated by Rb results in the permanent and stable repression of genes with

crucial roles in proliferation, such as those regulated by the E2F family of transcription factors[107].

Most cells carrying a null mutation in the Rb gene senesce normally, yet inactivation of additional Rb family members, p107 and p130, is sufficient to prevent senescence [108].

3.8 p53, the p19^{ARF}-p53 pathway and the p53-Mdm2 loop

The gene locus *TP53* encodes p53 which is also known as the "guardian of the genome" [109,110] as it is involved in checkpoint control, cell-cycle arrest, chromosomal stability, apoptosis and senescence [111] by acting as a transcription factor for more than 60 known target genes. P53 is regulated by at least ten feedback loops, seven of which are negative and three are positive. As all of them are autoregulatory, they are either induced or repressed by p53 transcriptional activity or p53-induced proteins [112]. Hence, it is not surprising that a malfunction or mutation of p53 is observed in far more than half of all human cancers. P53 mutations are mainly missense mutations (80% of tumours) resulting in aberrant proteins with an increased half-life, which in turn leads to the appearance of dominant negative and/or gain of function phenotypes associated with tumour progression and metastasis [113]. However, as p53 is generally functional in melanoma, other events must contribute to p53 inactivation.

P53 is highly conserved among mammalian species (74-90%) and even though sequence identity is divergent among lower vertebrates (38-53%), DNA binding domains as well as crucial residues involved in oligomerization and MDM2 binding are highly conserved [110]. Intrinsic or extrinsic stress results in posttranslational modification of the p53 protein [112]. One of the major players in the p53-mediated G1 arrest induced by p19^{ARF} overexpression is the p21 gene product that inhibits the cyclin E-dependent cyclin dependent kinase 2 (CDK2) (*Figure 7*).

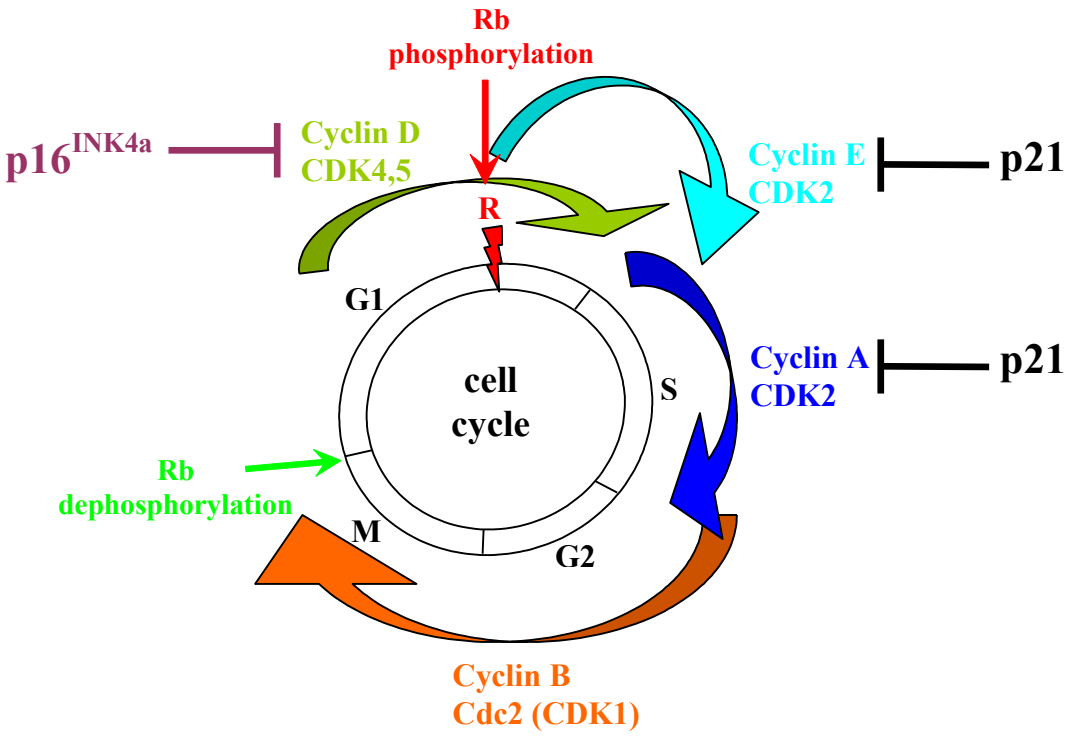

Figure 7: Cell cycle control

Combinatorial interactions of CDKs and cyclins promote the transition through the cell cycle. Cyclin D/CDK4,5 and Cyclin E/CDK2 complexes promote pRb phosphorylation and transition from G1 (cell prepares for DNA synthesis) to S (DNA synthesis occurs) phase. Cyclin A/CDK2 interaction supports DNA synthesis and the onset of G2 (cells prepare to complete the cell cycle by undergoing mitosis). Cyclin B/CDK1 complexes then promote transition through G2 and M (mitosis) before pRb is finally dephosphorylated again. Two families of CDK inhibitors, INK4 and CIP1/KIP1 proteins ($p21^{CIP1/WAF1}$, $p27^{KIP1}$, $p57^{KIP2}$), provide the major negative regulation of CDKs.

As CDK2 usually promotes the progress from G1 to S phase of the cell cycle the expression of p21 induces G1 arrest of the cells [112]. It does not seem surprising that $p21^{-/-}$ cells bypass senescence [75], supporting the proposed linear model linking p53 and Rb via p21 [114]. In contrast to that, MEFs carrying a null mutation in p21 undergo senescence normally [115], indicating that other proteins compensate for the function of p21. Supporting this suggestion, Li-Fraumeni patients, who suffer from a rare autosomal dominant syndrome characterized by multiple cases of early-onset primary tumours, are defective for p53 and therefore do not express any p21. Yet, their cells can still undergo senescence, indicating that p53 and p21 must be dispensable for RS [75].

Similar to the situation in Li-Fraumeni patients, the absence of p53 leads to induction of cancer at low age [112] in other mammals and in *Xenopus* [75]. In mouse embryonic fibroblasts (MEFs), inactivation of p53 is sufficient to prevent senescence, allowing these cells to divide indefinitely [116]. Surprisingly, $p53^{+/-}$ patients show a decrease in tumour incidence, but also a highly reduced lifespan [75]. In zebrafish, the deletion of p53 leads to nerve sheath tumour

development after eight months in approximately 30% of all fish [117]. Nevertheless, no effect of UV irradiation and chemicals on p53 expression in medaka and other fish cells could be observed, even though a three to ten-fold increase in p53 expression is detected in human cell lines [110,118] upon such treatment. This difference might be due to the different p53 gene regulation because of different intron sizes as the medaka gene of 8.7 kb is smaller than that of mouse (12 kb) and human (20 kb). These structural differences might point to species-dependent, functional differences in transcriptional control [118].

The tumour suppressor $p19^{ARF}$ (Alternative Reading Frame) is a positive regulator upstream of p53 that is induced in situations of stress and senescence and activated by ectopic expression of oncoproteins such as Myc, Ras, E2F1 and E1A [90]. The disruption of the $p19^{ARF}$-p53 pathway, the primary failsafe cascade engaged by Myc, is shown to facilitate Ras-initiated transformation [111]. $P19^{ARF}$ protein binds to Mdm2 protein, one of the key players in p53 regulation [119] mediating the downmodulation of its p53-ubiquitin ligase activity, which in turn leads to a higher p53 protein level within the cell.

The transcription of the tumour suppressor $p19^{ARF}$ is positively regulated by E2F-1 and beta-catenin and negatively regulated by p53. High levels of E2F-1 not bound to pRb switches the p53 response from G1 arrest to apoptosis [112]. Besides, p53 binds specifically to the *mdm2* gene and stimulates its transcription [120,121]. Hence, p53 itself induces one of its negative feedback regulators in order to diminish p53 levels. Mdm2/p53 binding is mediated by phosphorylation of p53 at the Mdm2-N-terminal binding site.

Overexpression of Mdm2 leads to tumour formation in mammals and *Xenopus* but not in zebrafish, indicating a MDM2-independent p53 regulation [110] which fits to the fact that fish lack $p19^{ARF}$.

In mice, inactivation of the *mdm2* gene results in early embryonic lethality, which is completely prevented by simultaneous inactivation of p53 [122,123]. This shows that a tight regulation of p53 is important for development and growth control.

Since p53 is a potent tumour suppressor with a vital role in senescence induction, it is important to elucidate the possible role of p53 in melanocyte senescence and melanoma development.

3.9 Myc and its role in cancer

3.9.1 Growth-promoting functions of Myc

Almost 30 years ago, MYC, the human homologue of the retrovirus *v-gag-myc,* was discovered. To date, more than 22.000 scientific articles on MYC have been published indicating its pivotal role in development and disease. MYC transcription factors are commonly deregulated in tumourigenesis. All three known MYC protein family members (c-Myc, N-Myc and L-Myc) promote proliferation, growth and apoptosis; inhibit terminal differentiation; and are involved in the genesis of an extremely wide range of cancers [124]. Moreover, MYC can also drive vasculogenesis [125], reduce cell adhesion [126,127] and promote metastasis [128] as well as genomic instability [129]. The basic-helix-loop-helix-zipper (bHLHZ) domain of MYC heterodimerizes with the bHLHZ Max to form a sequence-specific DNA binding complex, which recognizes the E-box sequence CACGTG (as well as related non-canonical sites) and activates transcription (*Figure 8*) [130–132]. Intriguingly, MYC can also function as a negative regulator of transcription [133,134]. Most, but not all, functions of MYC depend on interaction with MAX, but there are exceptions. For example, in *Drosophila* MYC forms a complex with TfIIIb to stimulate transcription of RNA polymerase III genes independently of MAX [135].

The c-MYC proto-oncogene is one of the most frequently activated oncogenes, regulating as many as 15 - 20% of all genes [136,137]. Hence it is not surprising that both, targeted c-Myc and N-Myc deletions, lead to early embryonic lethality in mice [138,139]. However, to date, little is known about which target genes are actually crucial for MYC function. Nevertheless, $p21^{CIP1}$ suppression by MYC expression is postulated to be responsible for the G1 arrest failure of MYC-transformed cells upon DNA damage [140,141]. Furthermore, observations indicate that cyclin-D–CDK4 functions downstream of MYC in transformation. Accordingly, fibroblasts lacking all three D-type cyclins fail to be transformed by MYC and Ras oncogenes, while the defects in cell proliferation are moderate [142]. Similarly, the loss of CDK4 inhibits C-MYC's tumourigenic activities in epithelial tissues [143]. Even though further, crucial MYC targets remain to be elucidated, c-MYC is estimated to be involved in 20% of all human cancers [144], especially in hematopoietic lesions by causing inappropriate gene expression, which in turn results in autonomous cellular proliferation and blocks cellular differentiation [145]. In all cases, the relative amounts of MYC protein are increased in the tumour tissue relative to the surrounding normal tissues, which indicates that the elevated expression of MYC contributes to tumourigenesis. Several studies using transgenic animals, which express MYC proteins in a deregulated manner, support this view [146]. High *C-MYC* expression was also reported to enhance melanoma growth in SCID mice [147] while being associated with IFN-α resistance in human melanoma treatment [148]. Besides, *C-MYC* amplifications are observed in about one third of uveal melanoma [149]. In accordance, *C-MYC* downregulation sensitizes melanoma cells for chemo- and radiotherapy [150,151]. Interestingly, both N-RAS and BRAF but not K-RAS

can induce *C-MYC* expression [152,153]. Conversely, lymphomas undergo proliferative arrest, differentiation and apoptosis associated with sustained regression upon C-MYC inactivation in transgenic mice. Similarly, C-MYC inactivation in osteosarcoma results in the differentiation into mature osteocytes and the formation of bone, whereas in hepatocellular carcinoma, C-MYC inactivation differentiates tumour cells into normal hepatocytes and biliary cells, while a subpopulation of the cells retains its neoplastic properties. Taken together, C-MYC inactivation can reverse the process of transformation - even in tumours with genomic complexity [154,155]. In accordance, C-MYC downregulation by expression of constitutively active STAT5 in human fibroblasts induced p53 and pRb-dependent senescence, which could be circumvented when C-MYC was overexpressed [156]. Furthermore, *C-MYC* inactivation by RNA interference has been shown to trigger cellular senescence in diverse cancer cell lines including melanoma cells [157–159]. However, C-MYC overexpression alone is not sufficient to transform cells. Only in cooperation with other oncogenes, e.g. Ras, is C-MYC capable of inducing cellular transformation and tumourigenesis [160,161]. Whether deregulated C-MYC actually drives transformation or forces cells to enter apoptosis might rely on its expression level [162].

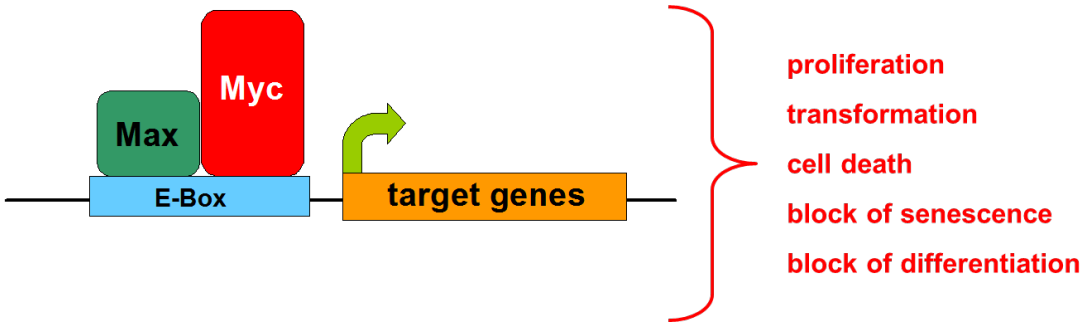

Figure 8: The Myc-Max complex activates transcription
Once MYC has associated with MAX, the MYC-MAX complex recognizes and binds to the E-box sequence CACGTG before activating transcription. MYC target gene expression results in proliferation, transformation and apoptosis, while blocking senescence and differentiation.

3.9.2 Growth-suppressive functions of Myc and the role of Miz-1

Interestingly, oncogenically activated c-Myc (from now referred to as Myc) is not only a potent inducer of cell proliferation but also engages growth-suppressive programs that restrict Myc's oncogenic potential. In a Myc transgenic mouse, where latent Myc is expressed under the control of the ubiquitously active Rosa26 promoter, apoptosis can be detected exclusively in the tissue with the highest Myc levels, namely in colonial epithelium. Since Myc also dimerizes with MAX when inducing programmed cell death, a threshold model might explain the different Myc functions [162]. Like apoptosis, induction of $p19^{ARF}$ by oncogenic Myc via inhibition of Mdm2 and the subsequent activation of p53 can either drive

apoptosis [163–165] or suppress proliferation [166]. Besides, repression of Miz-1 (Myc-interacting zinc finger protein 1) activity by Myc is important in Myc-induced apoptosis as Miz-1 activates the cell cycle inhibitor p21, leading to growth arrest instead of apoptosis [140].

The transcription factor MYC-interacting protein 1 (MIZ-1) was identified by virtue of its ability to bind MYC. MIZ-1 targets include the genes encoding the low-density lipoprotein receptor gene LDLR, $p21^{CIP1}$, $p15^{INK4B}$, and MAD4 [140,167–169]. MIZ-1 directly binds to the core promoters of these genes and activates their transcription.

Miz-1 upregulates the expression of $p15^{INK4B}$ leading to its accumulation, which is strongly linked to cellular senescence [168]. Accordingly, Miz-1 overexpression induces replicative senescence by arresting the cells in G1 via upregulation of $p15^{INK4B}$ [168,170]. A number of studies provided evidence to support a model in which C-MYC serves to repress the transcriptional activation function of MIZ-1 [171], e.g. for the regulation of $p15^{INK4B}$ expression [168,170]. C-MYC does not directly bind to Miz-1 target genes, but is recruited to them via Miz-1. Transcriptional activation by Miz-1 is abolished upon c-Myc recruitment and the Miz-1/C-MYC/MAX complex functions to repress transcription (*Figure 9*). However, MYC-mediated suppression of MIZ-1 transcriptional activation can be counteracted by transforming growth factor β signalling, which results in decreasing levels of the inhibitory MYC protein [170]. Furthermore, MIZ-1 transcriptional activity can also be modulated by UV exposure, which induces a decrease in topoisomerase II-binding protein (TopBP1). TopBP1, like MYC, associates with MIZ-1 and inhibits its ability to activate transcription of certain target genes such as the cyclin-dependent kinase inhibitors, $p21^{CIP1}$ [141]. Moreover, the transcriptional repressor Gfi-1 was reported to interact with Miz-1 to repress *CDKN1A* transcription by forming a ternary complex in cooperation with C-MYC [172].

Thus, MIZ-1 is a tightly regulated transcription factor whose activity can be modulated by association with various regulatory partners.

Apart from its interaction with binding partners, the subcellular localization of MIZ-1 is vital for its regulation. Cytoplasmic localisation of MIZ-1 has been reported together with its coactivator p300 and MYC [168,171]. However, physiological signals that regulate the subcellular localization of endogenous MIZ-1 have been difficult to pinpoint. Since MYC is mainly localized to the nucleus at low cell densities, but accumulates in the cytoplasm upon growth at high density or serum withdrawal [173], this might also be relevant to the control of MIZ-1 localization and activity. In addition to these diverse mechanisms of MIZ-1 regulation, MIZ-1 activity can also be regulated by its association with microtubules. According to this regulatory pathway, MIZ-1 is sequestered in the cytoplasm by association with microtubules. Upon drug-induced microtubule depolymerization, MIZ-1 is free to enter the nucleus, where it binds to target sequences and activates transcription [174]. An essential co-activator of Miz-1, nucleophosmin, is required for Miz-1-induced cell cycle arrest. By retaining nucleophosmin in the nucleolus, the ribosomal protein L23, which is encoded by a direct

target gene of Myc, acts as a negative regulator of Miz-1-dependent transactivation. This regulatory circuit may provide a feedback mechanism that links translation of Myc target genes and cell growth to Miz-1-dependent cell-cycle arrest [175].

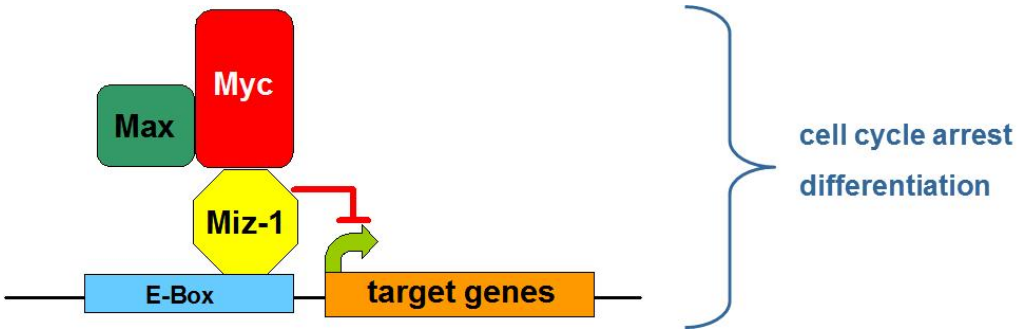

Figure 9: The MIZ-1-MYC-MAX complex represses transcription
Association of the MYC-MAX complex to MIZ-1 results in a repressive MIZ-1-MYC-MAX complex. The repression of MIZ-1 target genes in turn leads to cell cycle arrest and differentiation.

Taken together, several intrinsic tumour suppressor mechanisms limit Myc's oncogenic potential. However, the factors that determine whether proliferation or cell death is the predominant outcome of Myc activation remain unclear. With Myc´s potential role in up to 20% of human cancers and the fact that the down-regulation of Myc protein activates apoptosis in melanoma cells and increases the susceptibility of cells to various antitumoural treatments [151,176,177] suggests a possible role for Myc in melanoma.

3.10 Polyploidy and aneuploidy in cancer development

Polyploidy, a state in which cells possess more than the usual two sets of homologous chromosomes, occurs frequently in nature. Cellular stress, ageing, and various diseases trigger polyploidy, which are normally diploid [178,179]. Besides, polyploidy is also a frequent event during evolution as genome sequencing reveals many contemporary genomes, including those of higher vertebrates, to have evolved from ancient genome duplications [180]. However, mounting evidence suggests that polyploid cells are genetically unstable and can act as intermediates on the road to aneuploidy and, ultimately, cancer [178,181].

Aneuploidy, the numeric aberrations of chromosomes, is frequently observed in human cancer. It has long been known that malignant cells accumulate a large number of genetic mutations that affect differentiation, proliferation and cell death. In addition, it is also recognized that most cancers are clonal, although they display extensive heterogeneity with respect to karyotypes and phenotypes of individual clonal populations. It has been proposed that an underlying acquired genetic instability is responsible for the multiple mutations detected in cancer cells that lead to tumour heterogeneity and progression [182,183].

Aneuploidy is suggested to have a causative role in tumourigenesis since chromosomal instabilities and aberrations correlate with tumour grade and prognosis [184,185]. Further supporting this argument, genes involved in maintaining chromosome stability are frequently deregulated in human tumours [186].

However, even though aneuploidy is one of the most obvious differences between normal and cancer cells, there remains debate over how aneuploid cells arise and whether or not they are a cause or consequence of tumourigenesis. Accumulating evidence suggests unstable tetraploid intermediates to be the prerequisite for aneuploidy and cancer. Several mechanisms promote the genesis of tetraploid cells, e.g. DNA replication without subsequent cell division, a process termed endoreplication [187]; cytokinesis failure [188]; defective chromosome segregation [189,190]; chromosome non-disjunction [191]; defective kinetochore-microtubule attachment [192]; cell fusion [193] or mitotic slippage [194,195]. This theory is in accordance with the observation of tetraploid cells in early-stage cervix cancer [196] or the premalignant condition Barrett´s oesophagus [197], whereas more mature tumours have near-tetraploid karyotypes [198]. On top, inoculation of tetraploid, actin inhibitor DCB (dihydrocytochalasin B)-treated, *p53*$^{-/-}$ mouse mammary epithelial cells resulted in malignant mammary epithelial tumours in nude mice. By contrast, diploid cells carried through the same isolation procedure, did not. Interestingly, the tetraploid-derived tumours displayed massive chromosomal instability, including both numerical and structural chromosome aberrations, the hallmarks of aneuploidy [199].

Several cell cycle regulation-relevant genes, which are involved in G2/M or cytokinesis phases of the cell cycle have been described. One of these genes is *B-myb*, which is induced during G1/S transition of proliferating cells [200,201]. B-myb not only activates anti-apoptotic genes such as *Bcl-2* thereby promoting cell survival [202], but also bears essential functions in stem cell formation [203,204]. Accordingly, murine *B-myb* knockouts are early embryonic lethal [204], while shRNA knockdown of B-myb in mouse embryonic stem cells results in delayed G2/M transit and polyploidy [205]. Aurora kinase B is also vital for chromosome segregation and cytokinesis [206]. Inhibition of Aurora B function results in multinucleation and polyploidy[207]. Interestingly, Aurora B is overexpressed in several tumour types and in some melanoma cell lines [208]. Progression through the cell cycle mainly relies on two classes of molecules, namely cyclin-dependent kinases (Cdks) and cyclins [209]. In late G1 Cdk2 is activated by binding Cyclin E, which completes the phosphorylation of Rb family members, followed by further transcription of E2F-responsive genes ultimately allowing cells to pass the G1/S boundary [210,211]. Finally, Cdk1/cyclin B complexes actively participate in mitosis and allow its completion [212]. Besides, degradation of cyclin B was shown to be the prerequisite to drive human cells out of mitosis [194] and overexpression of cyclin E1 is frequently observed in tumours [213]. DNA damage induces p53-dependent transcription of Krüppel-like factor 4 (KLF4) [214] in turn causing a G1/S or G2/M arrest of the damaged cells [215,216]. Moreover, KLF4

was shown to exhibit anti-apoptotic activity by arresting γ-irradiated cancer cells and fibroblasts in a p21-dependent manner [217]. Last but not least, KLF4 directly interacts with Oct4 and Sox2 when ectopically expressed to reprogram somatic cells into induced pluripotent stem cells [218]. Another factor implicated to be important for cell division and apoptosis suppression is a 16.5 kDa protein, the smallest inhibitor of apoptosis (IAP) gene family member survivin [219,220]. Therefore, it is not surprising that survivin is not only overexpressed in 67% of malignant melanoma but also associated with poor prognosis in a variety of human cancers [221]. Besides, survivin expression peaks during G2/M as survivin functions as a chromosome passenger protein to enable correct cytokinesis [222,223]. Furthermore, survivin ablation was shown to activate a p53-dependent mitotic checkpoint, followed by upregulation of p21 and polyploidy [224]. For megakaryocytes, even though both survivin and Aurora B were thought to be vital for the chromosome passenger complex and the course of endomitosis [225], a megakaryocyte-specific knockout of *Survivin*, did not influence cell survival but instead enhanced polyploidy [226].

4. Aim of project

Cancers are prevented by the activation of intrinsic tumour suppressor programmes that either fix the damage in cells or ensure that the damaged cells cannot propagate. Cancers can only arise once these tumour suppressor pathways are abrogated. Importantly, activation of such tumour suppressor pathways must be restricted only to oncogenic, not normal, growth signals. Using the HERmrk system, my PhD project was to analyze whether and if so how the highly potent oncogene Xmrk was capable of inducing senescence in mouse melanocytes.

5. Materials and Methods

5.1 Software

- Microsoft Word 2007, 2010
- Microsoft Excel 2007, 2010
- Microsoft Powerpoint 2007, 2010
- CorelDraw X5
- Image J
- SigmaPlot 10.0
- Leica DMI6000 software
- Mendeley Desktop

5.2 Kits

kit	manufacturer	order #
PureYield Plasmid Miniprep System	Promega	A1223
PureYield Plasmid Midiprep System	Promega	A2495
Wizard SV Gel & PCR Clean-Up System	Promega	A9282
Total RNA Isolation Reagent (TRIR)	Thermo Scientific	AB-0304
RevertAid First Strand cDNA Kit	Fermentas/Thermos Scientific	K1622
DNase I, RNase-free	Fermentas/Thermos Scientific	EN0521
miRNeasy Mini Kit (50)	Quiagen	217004
SuperSignal West Pico Chemiluminescent Substrate	Pierce/Thermo Scientific	34080

5.3 Special Technical Devices

- Inverted, fluorescence microscope: DMI6000 (Leica) and Zeiss Axiovert 100 (Zeiss)
- Microscope cameras: DFC350 FX (black and white; Leica), DFC 320R2 (color; Leica), Nikon Coolpix 990 (Nikon) and Zeiss Axiocam HRc (Zeiss)
- Quantitative Realtime PCR: iCycler (Bio-Rad)
- PCR cycler: T3000 Thermocycler (Biometra)
- DNA/RNA quantification: NanoDrop 1000 (Thermo Scientific)
- DNA gel documentation: Decon Science Tec GmbH Imaging Systems
- Incubators: Heraeus Typ B 5061 EK-CO2 (Heraeus), Galaxy S (RS Biotech/nunc) and HERAcell 150i (Thermo Scientific)
- Western blotting: Image Station 4000MM (Kodak)

5.4 Vectors

- pSUPER (kindly provided by Prof. Martin Eilers, Univerity of Wuerzburg, Wuerzburg, Germany)
- pSUPER-sh*Miz-1* (kindly provided by Prof. Martin Eilers, University of Wuerzburg, Germany)
- pRetroSUPER (pRS)
- pRS-survivin-shRNA#1
- pRS-survivin-shRNA#2
- pRS-survivin-shRNA#3
- pBabe-puro-MYC-wt (kindly provided by Prof. Martin Eilers, University of Wuerzburg, Wuerzburg, Germany)
- pBabe-puro-MYC^{V394D} (kindly provided by Prof. Martin Eilers, University of Wuerzburg, Wuerzburg, Germany)
- pBabe-puro-MYC^{T58A} (kindly provided by Prof. Martin Eilers, University of Wuerzburg, Wuerzburg, Germany)
- pBabe-puro
- pBabe-puro-CTH-flag
- pBabe-MN[EF1a-red membrane and green nucleus]-2A-puro (kindly provided by Dr. Toni Wagner, University of Wuerzburg, Wuerzburg, Germany)
- pTetON
- pTRE2hyg
- pTRE2hyg-N-RAS^{61K}
- PL-SIN-EOS-S(4+)-eGFP (a gift from James Ellis, University of Toronto, Canada, kindly provided by Dr. Toni Wagner, University of Wuerzburg, Wuerzburg, Germany)
- pH2B-eGFP (kindly provided by Dr. Toni Wagner, University of Wuerzburg, Wuerzburg, Germany)
- pH2B-eBFP2 (kindly provided by Dr. Toni Wagner, University of Wuerzburg, Wuerzburg, Germany)
- pCDH-CMV-N-RAS^{61K}-EF1-copGFP (kindly provided by R. Houben, University of Wuerzburg, Wuerzburg, Germany)
- p-mOrangeN1 (kindly provided by Dr. Toni Wagner, University of Wuerzburg, Wuerzburg, Germany)
- p-mCherry-LYN (kindly provided by Dr. Toni Wagner, University of Wuerzburg, Wuerzburg, Germany)

5.5 Antibodies

5.5.1 Primary Antibodies

antibody	supplier	order #	weight [kDa]	origin	dilution [WB]
β-actin (C-4)	Santa Cruz	sc-47778	43	mouse	1:10000
c-Myc	Cell Signaling	9402	67	rabbit	1:4000
Erk2 (C-14)	Santa Cruz	sc-154	42	rabbit	1:5000
γ-H2AX	Cell Signaling	2577	15	rabbit	1:1500
GKLF4 (KLF4)	Santa Cruz	sc-20691	55	rabbit	1:100
MIZ-1 (hybridoma supernatant, clone 10E2)	kindly provided by Prof. Martin Eilers		89	mouse	1:100
Nanog	Novus Biologicals	NB 100-587	40	rabbit	1:2000
N-Ras (F155)	Santa Cruz	sc-31	21	mouse	1:1000
Oct-4A (C30A3; Oct4)	Cell Signaling	2840	45	rabbit	1:1000
P-Chk1 (Ser345)	Cell Signaling	2348	56	rabbit	1:1000
P-Chk2 (Thr68)	Cell Signaling	2661	62	rabbit	1:1000
P-MAPK (Thr202/Tyr204)	Cell Signaling	9101	42/44	rabbit	1:5000
P-p53	Cell Signaling	9284	53	rabbit	1:1000
p15INK4B (M-20)	Santa Cruz	sc-1429	15	goat	1:200
p16INK4A (M-156)	Santa Cruz	sc-1207	16	rabbit	1:500
p19ARF	abcam	ab80	19	rabbit	1:1000
p21 (N-20)	Santa Cruz	sc-469	21	rabbit	1:200
p27 (F8)	Santa Cruz	sc-1641	27	mouse	1:2000
p53 (hybridoma supernatant, clone PAB-122)	kindly provided by Dr. Thorsten Stiewe		53	mouse	1:100
Rb (C-50)	Santa Cruz	sc-50	105	rabbit	1:500
survivin	Novus Biologicals	NB 500-201	16.5	rabbit	1:1000
Xmrk (S388) sequence DDVVDADEYLLPYKR	BioGenes		160	rabbit	1:1000

Antibody dilutions used for Western blotting (WB) are indicated.

5.5.2 Secondary antibodies

antibody	supplier	dilution [WB]
rabbit-anti-goat	Abcam	1:3000
goat-anti-mouse-POD	Thermo Scientific	1:10000
goat-anit-rabbit-POD	Bio-Rad	1:3000
CY3-conjugated goat-anti-rabbit	Jackson ImmunoResearch Laboratories	

Antibody dilutions used for Western blotting (WB) are indicated.

5.6 Oligonucleotides

gene	forward 5`-> 3`	reverse 5`-> 3`	product [bp]
AurkB	TCGCTGTTGTTTCCCTCTCT	GGCTCCTTCCGTAGGACTCT	150
B-myb	GGGACTGCAAGCCTGTCTAC	CACCCTGGTGCTGTTCCT	60
Cth	GCACAAATTGTCCACAAAC	CGAAGCCGACTATTGAGGTC	194
Cth-overex	GCGCGGATCCATGCAGAAGGACGCCTCT	GCGCGTCGACTTACTTATCGTCGTCATCC TTGTAATCAGGGTGCGCTGCCTTCAAAG	
Cyclin B1	TCTTGACAACGGTGAATGGA	TCTTAGCCAGGTGCTGCATA	94
Cyclin E1	CACCACTGAGTGCTCCAGAA	CTGTTGGCTGACAGTGGAGA	230
HPRT	TGTTGTTGGATATGCCCTTG	ACTGGCAACATCAACAGGACT	150
KLF4	CTGAACAGCAGGGACTGTCA	GTGTGGGTGGCTGTTCTTTT	218
Miz-1	GGCAGAAAGTGCATCCAGTG	GGCCCTGCACCCTCTTCCTCTT	204
pBabe_seq	CTCTCCCCCTTGAACCTCCTCTTT	GGACTTTCCACACCTGGTTGCT	depends on insert
pRS_seq	CCCTTGAACCTCCTCGTTCGACC	GAGACGTGCTACTTCCATTTGTC	depends on insert
p15^{INK4B}	TTACCAGACCTGTGCACGAC	GCAGATACCTCGCAATGTCA	159
p16^{INK4A}	CCGCTGCAGACAGACTGG	GGGGTACGACCGAAAGAGTT	112
p19^{ARF}	GTCGCAGGTTCTTGGTCACT	CGAATCTGCACCGTAGTTGA	246
p21$^{CIP/WAF1}$	ACGGTGGAACTTTGACTTCG	CAGGGCAGAGGAAGTACTGG	160
p27^{KIP1}	TTGGGTCTCAGGCAAACTCT	TCTGTTCTGTTGGCCCTTTT	157
survivin	ATCGCCACCTTCAAGAACTG	CAGGGGAGTGCTTTCTATGC	193

All oligonucleotides were purchased from Sigma-Aldrich, Mannheim, Germany.

5.7 shRNA Oligonucleotides

oligo	sequence 5`-> 3`
Miz-1 shRNA_fwd	GATCCCCGCTGAGCCTTAGCCCTGAGTTCAAGAGACTCAGGGCTAAGGCTCAGCTTTTTGGAAA
Miz-1 shRNA_rev	AGCTTTTCCAAAAAGCTGAGCCTTAGCCCTGAGTCTCTTGAACTCAGGGCTAAGGCTCAGCGGG
survivin shRNA #1_fwd	GATCCCCCGATAGAGGAGCATAGAAATTCAAGAGATTTCTATGCTCCTCTATCGTTTTTGGAAA
survivin shRNA #1_rev	AGCTTTTCCAAAAACGATAGAGGAGCATAGAAATCTCTTGAATTTCTATGCTCCTCTATCGGGG
survivin shRNA #2_fwd	GATCCCCTCAAGAAGCAGATGGAAGATTCAAGAGATCTTCCATCTGCTTCTTGATTTTTGGAAA
survivin shRNA #2_rev	AGCTTTTCCAAAAATCAAGAAGCAGATGGAAGATCTCTTGAATCTTCCATCTGCTTCTTGAGGG
survivin shRNA #3_fwd	GATCCCCGAACTAACCGTCAGTGAATTTCAAGAGAATTCACTGACGGTTAGTTCTTTTTGGAAA
survivin shRNA #3_rev	AGCTTTTCCAAAAAGAACTAACCGTCAGTGAATTCTCTTGAAATTCACTGACGGTTAGTTCGGG

All shRNA oligonucleotides were purchased from Sigma-Aldrich, Mannheim, Germany.

6. Methods

6.1 PCR

Polymerase chain reaction was used to screen bacterial clones and to amplify CTH DNA prior to sequencing and subsequent cloning into the pBabe-puro expression vector.

PCR reaction:

- 19µl H2O
- 2µl reaction buffer (10x)
- 1µl forward primer (10pM)
- 1µl reverse primer (10pM)
- 0.7µl dNTP mix (10mM each)
- 0.3µl Taq polymerase (5U/µl)
- 1µl template

PCR programme:

step	temperature [°C]	duration	repetition
1	95	pre-heating	
2	95	5 min	
3	57	30 sec	30 times
4	72	2 min	
5	72	10 min	
6	10	until removed from the cycler	

6.2 Sequencing

Sequencing was performed by GATC Biotech, Konstanz, Germany. DNA samples were prepared as follows: First, DNA was diluted using ddH_2O to a final concentration of 60ng/µl. 30µl were pipetted into a 1.5ml reaction tube, which was then labeled with a green bar code, which had previously been purchased. Then 35µl of each sequencing primer (10pmol/µl) were put in two 1.5ml reaction tubes labeled with according yellow oligonucleotide bar codes. Upon online registration on the GATC homepage the barcodes were registered and the primer sequences were deposited. Finally, a small box containing the prepared reaction tubes were taken to the university´s pick up point. After e-mail notification, the obtained sequences can be downloaded.

6.3 Realtime PCR

Cells were starved and EGF-treated as described and RNA isolation was performed with TRIR solution (ABGene, Hamburg, Germany). Whole RNA (4 µg) was reversely transcribed using the RevertAidTM First Strand cDNA Synthesis Kit (Fermentas, Leon-Rot, Germany). Fluorescence- based quantitative real-time polymerase chain reaction (qRT-PCR) was performed using the iCycler (Bio-Rad, Munich, Germany). See materials section for oligonucleotides used. Gene expression was normalized to hypoxanthineguanine phosphoribosyltransferase. Relative expression levels were calculated applying REST software [227].

25µl qRT-PCR reactions consisted of 14.25µl sterile ddH_2O, 2.5µl 10x PCR buffer, 0.7µl dNTPs (10 mM), 0.25µl FITC (0.5 nM in DMSO), 0.75µl SYBRGreen (2.5x10^{-3}units/µl in DMSO), 0.75µl of each primer (10pmol/µl), 4µl template and 0.3µl (1.5 units) Taq polymerase.

A 95°C denaturation step for 3min was followed by an amplification parameter of 40 cycles of denaturation at 95°C for 25sec, annealing at 60°C- 63°C for 25sec and primer extension at 72°C for 45sec. In order to record the melting curves, a 95°C incubation for 1 min was performed before the starting temperature of 55°C for 1min was steadily increased by a final incubation of 80 times 10sec followed by a 15°C hold. Products were electrophoresed on 2% agarose/ 1xTAE, stained with ethidium bromide (to 0.5µg / ml) and visualized with a Herolab E.A.S.Y. 429K gel documentation system.

6.4 Microarray Analysis

$NRAS^{61K}$ cells were treated for 6, 14 or 28 days with 1µg/ml doxycycline (Sigma) and $NRAS^{61K}$-AR cells underwent the same treatment for 10 days before being harvested. RNA was isolated using the miRNeasy Kit (Qiagen). The following analysis was performed by Dr. Susanne Kneitz [Microarray Core Unit, IZKF (Interdisciplinary Center for Clinical Research), University of Wuerzburg, Wuerzburg, Germany], using the Affymetrix Gene Chip Mouse Genome 430 2.0. All data were analyzed using different R packages from the Bioconductor project (www.bioconductor.org).

6.5 Cloning

6.5.1 Survivin shRNA vectors

150pg (1.5µl of 10pM dilution in H_2O) of each shRNA oligonucleotide pair were mixed with 50µl annealing buffer (100mM NaCl, 50mM Hepes pH 7.4) in a 1.5ml Epperdorf reaction tube before being boiled for 5 minutes at 95°C. Upon switching off the water bath the tube was left floating in the slowly but steadily cooling water over night. The following day 1µl of a 1:20 dilution of the annealing reaction and 50ng of purified (Wizard SV Gel & PCR Clean-Up System; Promega, Mannheim, Germany), previously digested (BglI and HindIII in Buffer R

(red) (Fermentas/Thermo Scientific, St. Leon-Rot, Germany) for 1.5 hours at 37°C) pRetroSUPER vector were used for ligation with T4 Ligase (Fermentas/Thermo Scientific, St. Leon-Rot, Germany) in the corresponding buffer for 1 hour at room temperature.

6.5.2 Transformation

The ligation reaction was then mixed with 50µl of competent DH5α bacteria (freshly thawed on ice upon removal from storage at -80°C) and put at 42°C for 90 seconds, followed by a 45 minute incubation period on ice at 4°C. Transformed bacteria were supplemented with 800µl LB and incubated on a shaker at 37°C for about 1 hour followed by centrifugation at 3000rpm for 5 minutes. Supernatant was discarded and pellets were re-suspended in 100µl LB before plated onto LB-Amp-agar dishes before being incubated upside-down at 37°C.

6.5.3 Colony Screen

Colonies were screened for successful insertion of annealed shRNA oligos performing colony PCR with pRS_seq forward and reverse primers. The DNA of two positive clones was amplified via Midipreps (Pure Yield Midiprep System; Promega, Mannheim, Germany) according to manufacturer´s instructions. Prior to transfection into Hm^{hi} cells, the insert was sequenced.

6.5.4 CTH overexpression vector

Mouse CTH DNA was amplified via PCR using Cth-overex oligonucleotides (CTH-5-BamHI and CTH-3flag Sal1) and 25ng of Hm^{hi}-MYC-TA-14 days EGF-cDNA as template. Upon gel electrophoresis to visualize PCR products followed by gel purification (Wizard SV Gel & PCR Clean-Up System, Promega) both CTH DNA and pBabe-puro DNA was sequentially digested using Sal1 (Buffer O, orange; Fermentas/Thermo Scientific, St. Leon-Rot, Germany) and BamHI (BamHI Buffer; Fermentas/Thermo Scientific, St. Leon-Rot, Germany) for 1 hour each at 37°C followed by a purification step upon each digestion step (Wizard SV Gel & PCR Clean-Up System; Promega, Mannheim, Germany). Ligation, transformation and screening for positive clones followed by DNA amplification was performed as described above. Prior to transfection into Hm^{hi} cells, the insert was sequenced.

6.6 Cell Culture

The EGF-inducible version of the oncogenic EGFR orthologue Xmrk (“HERmrk” or shortly “Hm”), consisting of the extracellular domain of the human EGF receptor (“HER”) and the intracellular part of Xmrk (”mrk”’), was used to establish stable cell lines of the mouse melanocyte cell line melan a [71,228]. Three cell clones with different expression levels were chosen for further analyses.

In accordance with RTK expression levels, cell lines were termed Hm^{lo}, Hm^{me} and Hm^{hi}. Cells were then transfected with pWHE459 vector, that allows the expression of the doxycyclin-

inducible reverse transactivator [229], using Gene Juice transfection reagent (Novagen/Merck, Schwalbach, Germany). Cells were selected applying 2mg/ml puromycin for 14 days. pTRE2hyg2-NRAS^{61K} was transfected into melan a–pWHE459 cells using Gene Juice reagent according to manufacturer´s instructions. After hygromycin selection (350mg/ml) for 3 weeks, cells were used for further analyses.

To overexpress MYC-TA in melan-a-N-RAS* cells, melan a cells were first transfected with the TetON (see TetON/OFF section for detailed description) plasmid. Upon neomycin selection (800µg/mlfor 14 days), melan a-pTetON cells underwent a subsequent round of transfection with pTRE2hyg or pTRE2hyg-N-RAS61K followed by hygromycin selection (350mg/ml for 3 weeks) and the final transfection with pBabe-puro or pBabe-puro-MYC^{T58A} (kindly provided by Prof. Martin Eilers, University of Wuerzburg, Wuerzburg, Germany). Melan a-pTRE2hyg-N-RAS*-pBabe-MYC-TA and the respective control line were selected applying 2 mg/ml puromycin for 14 days and used for further analyses.

All melan a-derived cell lines were grown at 37°C and 5% CO_2 in DMEM medium containing 10% fetal calf serum (FCS; PAN Biotech, Aidenbach, Germany) supplemented with antibiotics [penicillin (100 U/ml; Gibco/Invitrogen, Karlsruhe, Germany), and streptomycin (100 µg/ml, Gibco/Invitrogen, Karlsruhe, Germany)], 12nM cholera toxin (Sigma-Aldrich, Munich, Germany) to support melanin synthesis and tetradecanoyl-phorbol-acetate (TPA; PMA) (200nM; Sigma-Aldrich, Munich, Germany) (complete medium). TPA supports the cells` proliferation and acts as an inducer of protein kinase C (PKC) followed by activation of the mitogen-activated-protein-kinase (MAPK) pathway.

For senescence and proliferation assays, cells were cultured in starving medium [DMEM with 10% dialyzed FCS (Invitrogen, Karlsruhe, Germany)] for three days before the assay was started. Where indicated, 100ng/ml human epidermal growth factor (EGF) (Tebu-bio, Offenbach, Germany), 1mg/ml doxycycline (Dox; Sigma-Aldrich, Munich, Germany) or 2mM N-acetylcysteine (NAC; Sigma-Aldrich, Munich, Germany) was added. Medium was supplemented with EGF, Dox and NAC every second day and renewed every four days.

Normal human embryonic melanocytes (NHEM) cells were purchased from PromoCell (Heidelberg, Germany) and transfected with pCDH-CMV-NRAS^{61K}-EF1-copGFP (kindly provided by R. Houben, University of Wuerzburg, Germany) before being cultivated in melanocyte growth medium (Promocell, Heidelberg, Germany) throughout the assay period.

B16-F1 murine melanoma cells were purchased from LGC Standards/ATCC (Wesel, Germany) and cultured in DMEM (Invitrogen, Karlsruhe, Germany) supplemented with 10% FCS (PAN Biotech, Aidenbach, Germany) and antibiotics [penicillin (100 U/ml; Gibco/Invitrogen, Karlsruhe, Germany), and streptomycin (100 µg/ml, Gibco/Invitrogen, Karlsruhe, Germany)].

6.7 SA-β-Galactosidase Assay

For the first part of my thesis (as published in [230]), cells were plated in 12-well dishes at a density of $4x10^4$ cells / well. The cells were incubated in serum-free DMEM supplemented with 10% dialysed FCS (Gibco/Invitrogen, Karlsruhe, Germany; starving medium) and antibiotics for 3 days before EGF stimulation (100ng/ml; Tebu-bio, Offenbach, Germany), NAC (2mM) or doxycycline (1mg/ml) treatment (Sigma-Aldrich, Munich, Germany) TPA treatment (200 nM) or culturing in complete medium. These media were also used for all other senescence-associated assays. Cells were washed with PBS (pH 7.2) and fixed with ice cold 0.5% glutardialdehyde in PBS (pH 7.2) for 10 min at room temperature. After washing the cells with PBS (pH 7.2, 1mM $MgCl_2$) they were stained (PBS pH 6.0, 1 mg/ml X-Gal, 0.12mM $K_3Fe(CN)_6$, 0.12mM $K_4Fe(CN)_6$, 1mM $MgCl_2$) protected from light for 3.5 hours at 37°C and 5% CO_2. Cells were washed with PBS (pH 7.2) and examined by light microscopy.

In the following, an enhanced SA-β-Gal staining protocol was used. Cells were cultured in starving medium (Dulbecco's Modified Eagle's Medium with 10% dialysed fetal calf serum (Gibco/Invitrogen, Karlsruhe, Germany) for 3 days before the assay was started. Cells were plated in six-well dishes at a density of $1x10^5$ cells / well. Where indicated, 100ng/ml human EGF (Tebu-bio, Offenbach, Germany), 2mM NAC or 1 mg/ml doxycycline (Sigma-Aldrich, Munich, Germany) was added. Medium was renewed every 4 days, and EGF or NAC were freshly supplied every second day. After 3, 7 and 14 days, cells were analysed as described below.

At indicated staining time points cells were washed with PBS (pH 7.2) and fixed with 3.7% formaldehyde in PBS (pH 7.2) for 5 min at room temperature. After rinsing the cells twice with PBS (pH 7.2), they were stained in the dark for 12 h at 37°C (using 1 mg/mL of X-Gal, 40mM citric acid/sodium phosphate buffer (pH 6.0), 5mM potassium ferricyanide, 5mM potassium ferrocyanide, 150mM NaCl, and 2mM $MgCl_2$). Cells were then washed with PBS (pH 7.2) and examined by light microscopy.

6.8 Crystal violet staining

Cells were cultured and prepared as described for the SA-β-Gal assay and fixed at day 14 using methanol (-20°C) before cells and colonies were stained with 0.1% crystal violet in distilled water. To ensure equal staining distribution, six-well cell culture dishes were incubated on a shaker. Upon staining, cells were washed 10 times for 5 minutes each using distilled water. Intensive washing ensures removal of stain excess. Afterwards cells were examined by light microscopy.

6.9 Cell Quantification

Multinuclear as well as SA-β-Gal stained multinuclear cells were enumerated manually. Per assay, four phase contrast images (altogether approximately 12.6mm^2 per well) and their brightfield counterparts, both taken at 100-fold magnification, were used to determine the propotion of senescent and multinucleated cells on the total cell number manually.

6.10 Cell Proliferation Assay

5x10^4 cells per well were seeded onto a six-well plate and either left untreated or stimulated with 100ng/ml EGF or 1µg/ml Dox. Cells were harvested by trypsinization at indicated time points, pelleted, resolved in PBS and enumerated manually using a standard Neubauer counting chamber.

6.11 Soft Agar Growth Assay

One millilitre of 1.2% agar in H_2O, which had been boiled until completely dissolved, autoclaved and then cooled down and kept at 50°C for further usage, was mixed with 1ml 2x-Dulbecco's Modified Eagle's Medium (DMEM) prepared from DMEM powder purchased from Gibco (#52100-039 containing 4.5g/l glucose, lacking pyruvate and $NaHCO_3$) and plated onto six-well plates (BD Falcon). Upon polymerization, the solid agar was overlain with an equal amount of soft agar mix (0.6% agar) containing 4x10^{4}cells per well. The polymerized soft agar was supplied with 100µl of starving media for the controls and the same amount of starving media including EGF (final concentration per well: 100ng/ml), doxycycline (final concentration per well: 1µg/ml), medium supplemented with FCS alone (D10, final concentration per well: 10%) or supplemented with TPA and cholera-toxin (complete, final concentration per well: 200nM and 12nM, respectively). This solution was added every second day and six-wells were left open until liquid had been completely absorbed by the agar. After 14 days of growth under standard culture conditions (37°C, 5% CO_2), the number of cell colonies was counted, with "colony" being defined as more than eight cells per spot. If counting was impossible due to high colony numbers, phase contrast images were taken at 25-fold magnification using the DMI-6000 inverted microscope.

6.12 Reactive Oxygen Species Detection Assay

Cells were starved and treated as described for the SA-β-Gal assay. At times indicated, 20mM 2´,7´-dichlorofluorescein diacetate was added to the medium, thoroughly mixed by pipetting up and down twice and cells were stained for 5min before being washed with PBS and overlain with fresh starving medium. Cells were analysed microscopically at 200-fold magnification for the presence of ROS-induced dichlorofluorescein (excitation 488 nm) using the DMI-6000 Leica inverted microscope.

6.13 Comet Assay

Cells were cultured in starving medium for three days before $5x10^4$ cells per well were seeded onto six-well dishes. Cells were either left untreated or stimulated with 100ng/ml EGF for 14 days. Cells were then trypsinized and used for the assay as described in http://www.cometassayindia.org/Dusinska-protocol.PDF. Shortly, $2x10^4$ cells were mixed with 140µl low melting agarose (LMP) in PBS at 37°C. The mixture was then transferred as two equal drops to coated slides (1% standard agarose in H_2O, homemade: dip, clean one side, leave the other at room temperature until solidified, store at room temperature until needed). Upon polymerization, the slides were put into lysis solution (2.5M NaCl, 0.1M EDTA, 10mM Tris, 1% Triton X-100) for 1 hour at 4°C. After washing the slides three times in enzyme reaction buffer (40mM HEPES, 0.1M KCl, 0.5mM EDTA, 0.2mg/ml BSA, pH 8.0) they were treated with enzyme solution (0.5mg/ml proteinase K in enzyme reaction buffer) and left in a moist box for 1 hour at 37°C followed by alkaline treatment in electrophoresis solution (0.3M NaOH, 1mM EDTA) for 40 minutes at 4°C. Subsequent electrophoresis was performed at room temperature and 25V for 30 minutes. Slides were then washed in neutralising solution (0.4M Tris, pH 7.5) before DNA was stained with 5µg/ml Hoechst 33258 in ddH_2O.

6.14 Time Lapse Analysis

Melan a-N-RAS^{61K} cells were transiently transfected with pBabe-MN [EF1a-red membrane and blue nucleus]-2APuro (kindly provided by Dr. Toni Wagner, University of Wuerzburg, Wuerzburg, Germany) before being plated onto glass cover-slips or Ibidi chambers. Upon 16 to 28 days of doxycycline treatment, cells were monitored for up to 30 hours at a 100-fold magnification with pictures being taken every 15 to 20 minutes.

6.15 Confocal Imaging

Confocal scans were taken by Dr. Toni Wagner with a Nikon C1 confocal laser scanning microscope using a 60x oil immersion objective. Dr. Wagner stained the cells' membranes with cell mask deep red and DNA with Hoechst 33342. Imaging areas were randomly chosen. Z-stacks covered the full depths of all imaged cells and overlapped 3-fold to allow for maximum accuracy during reconstruction. 3-dimensional reconstruction and rendering were performed using Volocity 4.0 Software from PerkinElmer. The same software was used to calculate cytoplasmic and nuclear volumes. Cellmask staining allowed to deterimine total 3D cell volume modelling, while nuclear volumes were reconstructed using the saturated Hoechst signal. By 3-dimensional subtraction of the resulting virtual objects the cytoplasmic volume was calculated before the ratio between nuclear and cytoplasmic volumes could be determined. No cells in metaphase were used; otherwise selection was purely random.

6.16 *In Vivo* Growth

Before injection into nude mice, melan-a control cells (stably transfected with pTRE2hyg as empty vector control) and N-RAS^{61R} cells were cultured in DMEM containing 10% foetal calf serum supplemented with antibiotics, 12nM cholera toxin to support melanin synthesis and 200nM tetradecanoyl-12,13-phorbolacetate (TPA) to allow proliferation. In contrast, N-RAS^{61R}-AR cells were cultured in the absence of both cholera toxin and TPA. The following experiments were done by Dr. Christoph Otto and coworkers [Experimental Surgery, Experimental Transplantation Immunology, Clinic of General, Visceral, Vascular and Pediatric Surgery (Surgical Clinic I), University of Wuerzburg Hospital, Wuerzburg, Germany]: Nude mice (NMRI, Harlan strain) were subcutaneously injected with 2.5x10^6 melan-a, N-RAS^{61R} or N-RAS^{61R}-AR cells per flank. Where indicated, 2mg/ml doxycycline (Sigma) dissolved in 10% saccharose solution was supplied *ad libitum* by administration to the drinking water. After four weeks, N-RAS^{61R}-AR mice were sacrificed due to considerable tumour load. In all other mice, growth of injected cells was monitored for 10 weeks after injection before sacrificing the mice.

6.17 Statistical Analysis

Generally, all graphs depict the mean values of at least three independent experiments unless stated otherwise, standard deviations are indicated. Student`s t test (two-tailed, paired) revealed statistical significance highlighted by asterisks (*: $p<0.05$; **: $p<0.01$, ***: $p<0.001$).

6.18 Protein Methods

6.18.1 Cell Lysis and Immunoblot Analysis

All stimulation experiments were performed in serum-free DMEM containing antibiotics and 2.5% (characterization of HERmrk clones) or 10% dialysed FCS (senescence assays). Stimulating reagents were added every second day and culturing medium was changed after four days. Cells were harvested, transferred into a 1.5ml tube, pelleted at 10.000 rpm for 2 min and washed twice in PBS before being lysed in lysis buffer (20mM 4-(2-hydroxyethyl)-1-piperazineethanesulphonic acid (pH 7.8), 500mM NaCl, 5mM MgCl2, 5mM KCl, 0.1% deoxycholate, 0.5% Nonidet-P40, 10mg/ml aprotinin, 10mg/ml leupeptin, 200mM Na_3VO_4, 1mM phenylmethanesulphonylfluoride and 100mM NaF) for 1-3 hours at 4°C and pelleted at 13.000rpm for 15min. Cell extracts were standardized for protein content using the Bradford protein assay. 25 to 100µg were used for Western blot analysis. Proteins were resolved by SDS/PAGE using SDS running buffer (50mM Tris, 150mM glycine, 0.1% SDS) and transferred to nitrocellulose according to standard Western blotting protocols. Membranes were blocked for 1h with TBS/0.1 % Tween/1.5 or 5 % BSA and incubated with the first antibody

over night at 4°C. Blots were then washed with TBS/0.1 % Tween 3-5 times for 5-10min before being incubated with the secondary antibody diluted in TBS/0.1 % Tween/1.5% or 5% BSA for 1h at room temperature. After a final round of washing in TBS/0.1 % Tween, protein levels were detected. Chemiluminescent detection relied on horseradish peroxidase–conjugated secondary antibodies (SuperSignal West Pico Chemiluminescent Substrate, Pierce/Thermo Scientific). To reprobe Western blots, membranes were stripped with 62.5mM Tris/HCl pH 6.7, 2% SDS, 100 mM 2-mercapto-ethanol for 20 min at 50°C and then washed in PBS and TBS/0.1% Tween.

6.18.2 Immunolocalization

Melan a-HERmrk cells were plated onto glass coverslips at a density of $1x10^5$ cells / well in 6-well-dishes. The cells were incubated in serum-free DMEM supplemented with 10% dialysed FCS and antibiotics for 3 days before EGF stimulation (100ng/ml), TPA (200nM) and/or NAC treatment (2mM). Cells were washed with PBS, fixed with methanol (-20°C for 5 min) and permeabilized with aceton (-20°C for 2min). Coverslips were blocked with PBS/ 1% BSA for 40min before incubation with the primary antibody [anti-ɣH2AX (1:100; Cell Signalling, Danvers, USA) or survivin (1:100; Novus Biologicals, Littleton, USA)] and CY3-conjugated goat-anti-rabbit secondary antibody (1:100; Jackson ImmunoResearch Laboratories, Newmarket, Suffolk, UK) for 1h each. DNA was DAPI stained by mounting the coverslips in Vectashield containing DAPI. Cells were examined under epifluorescent illumination.

7. Results

7.1 HERmrk expression levels determine cellular fate in melanocytes

Three different mouse melan a-HERmrk (termed `HERmrk`, abbreviation `Hm`) cell clones expressing different levels of the EGF-inducible variant of the oncogenic EGFR orthologue Xmrk were used to exemplarily study the transformation capacity of receptor tyrosine kinases. According to their relative HERmrk expression, these clones were termed Hm^{lo}, Hm^{me} and Hm^{hi}, indicating low, medium and high receptor levels. Western blot analysis of serum-deprived and EGF-stimulated cells revealed, that apart from Hm levels, the downstream signalling molecules were likewise affected (*Figure 10*). Interestingly, the basal protein level of phosphorylated mitogen-activated protein kinase ERK1/2 (Thr202/Tyr204) was higher in unstimulated Hm^{me} and Hm^{lo} cells compared to Hm^{hi} cells. This increased basal expression level is likely to account for the stronger P-MAPK signal of Hm^{me} and Hm^{lo} upon EGF stimulation compared to the Hm^{hi} response.

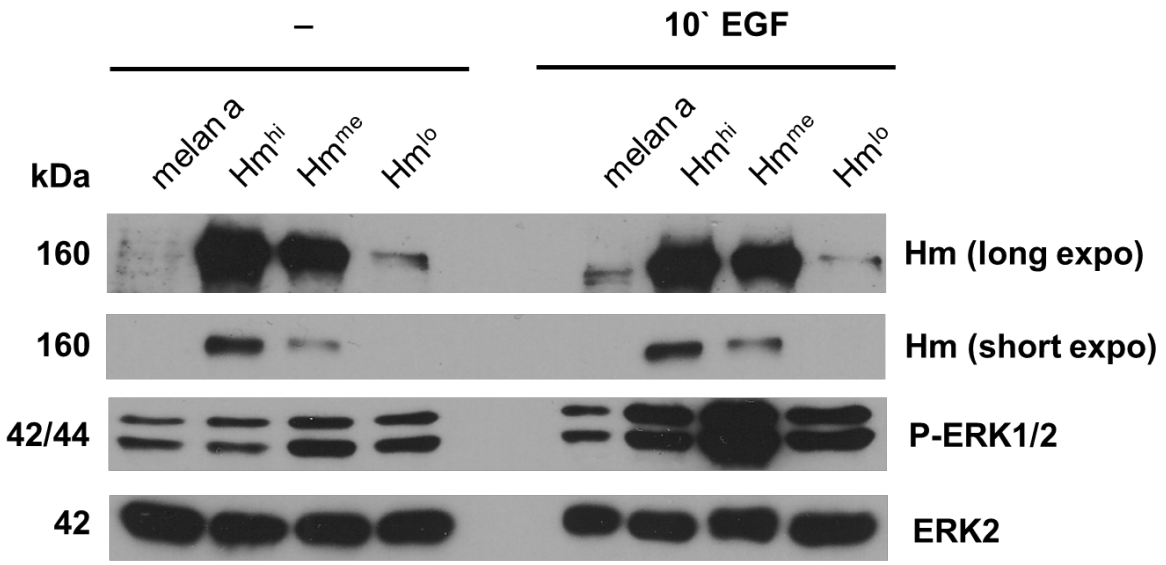

Figure 10: Western blot analysis determining Hm receptor levels and downstream ERK1/2 signalling
Western blot analysis of whole-cell lysates of melan a and the melan a Hm cell clones Hm^{hi}, Hm^{me} and Hm^{lo} probed against the C-terminal part of Xmrk, P-ERK1/2 [(the antibody detects endogenous levels of p44 and p42 mitogen-activated protein kinase (ERK1 and ERK2) when dually phosphorylated at Thr202 and Tyr204 of ERK1 or Thr185 and Tyr187 of ERK2, and singly phosphorylated at Thr202 thus generating a double band] and ERK2 (loading control). Protein weights are indicated in kDa.

To see whether the difference in receptor abundance and downstream signalling has an impact on proliferation and transformation capacity, I performed proliferation and soft agar assays. Long-term EGF stimulation did not affect the proliferation of the parental cell line

melan a, but it stimulated proliferation of all three Hm clones. Hm^{hi} cells showed a modest proliferation increase upon EGF treatment, whereas both Hm^{me} and Hm^{hi} showed a more than threefold higher proliferation capacity (*Figure 11*).

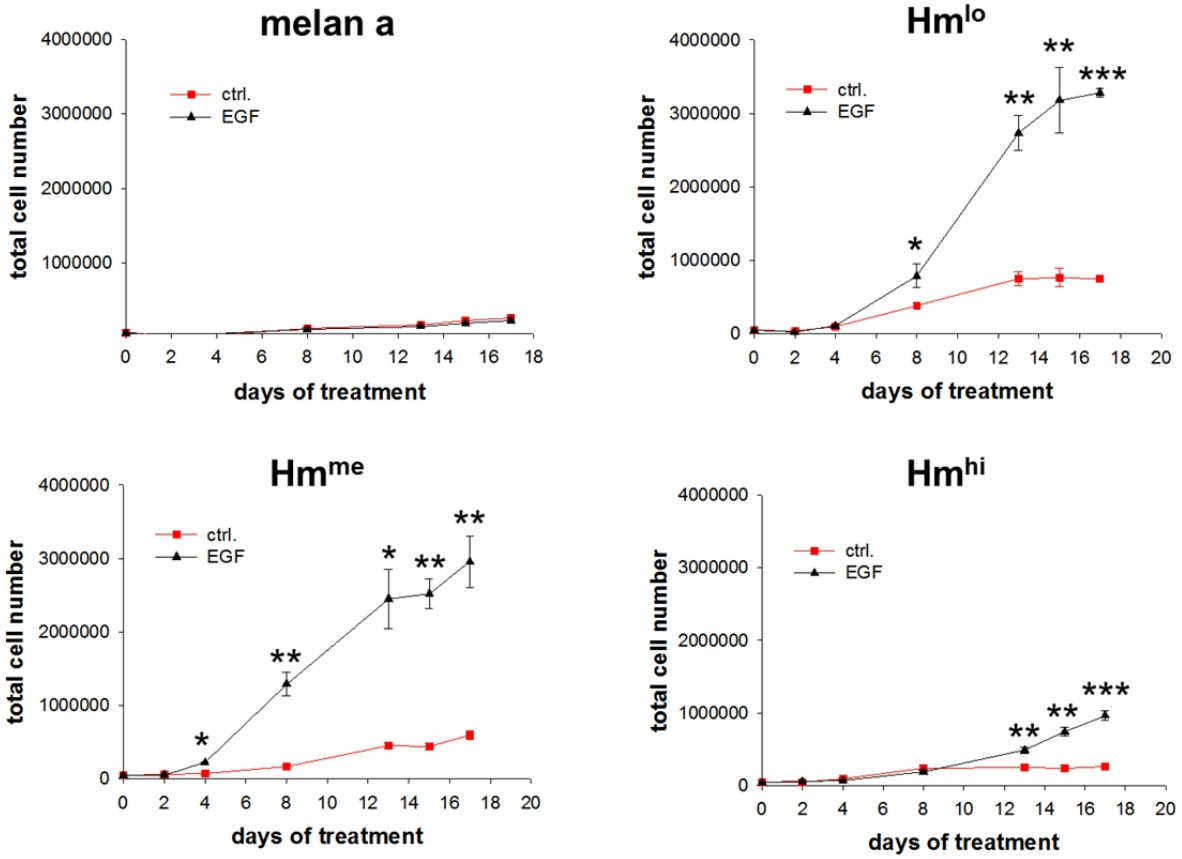

Figure 11: Hm receptor level determines proliferation extent of melanocytes
Graphs depict the total cell number (mean values of three independent experiments) of melan a and the melan a-Hm cell clones Hm^{hi}, Hm^{me} and Hm^{lo} over time in the absence (ctrl.) or presence of EGF (EGF). Student´s t-test revealed statistical significances indicated by asterisks (*p<0.05, **p<0.01, ***p<0.001).

These findings were in accordance with the soft agar colony numbers observed upon 14 days of treatment. Neither melan a, nor any of the Hm clones formed colonies in starving media-supplemented agar. However, EGF treatment led to colony formation in the Hm clones with the number of colonies observed being inversely related to the receptor levels. Notably, melan a cells did not form colonies upon EGF stimulation (*Figure 12*). Taken together, I found the Hm receptor level to negatively correlate with both proliferation and transformation.

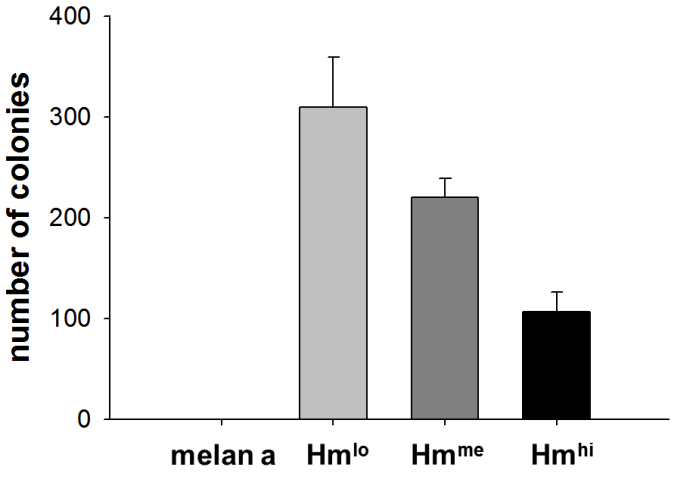

Figure 12: Hm receptor level determines transformation capacity of melanocytes
The graph depicts the total number of soft agar colonies (mean values of three independent experiments) per 6-well upon 14 days of EGF treatment of indicated cell clones.

To check whether the limited proliferation capacity of Hm^{hi} might be the consequence of senescence induction, I performed senescence-associated β-galactosidase (SA-β-Gal) stainings (*Figure 13*). Even though long-term cultivation of melan a as well as all three Hm clones in starving medium increased the number of SA-β-Gal positive cells over time, their proportion never exceeded 1.1%. Besides, melan a cells were indifferent to EGF stimulation, but Hm^{lo} and Hm^{me} melanocytes responded with a modest increase in the number and proportion of SA-β-Gal positive cells over time. However, Hm^{hi} cells showed a strong shift towards senescence, resulting in about one third being multinucleated and 15% being SA-β-Gal positive upon 14 days of EGF stimulation (*Figure 14*). Hence, high expression levels of oncogenic Hm apparently protect the melanocytes from becoming tumourigenic by inducing senescence.

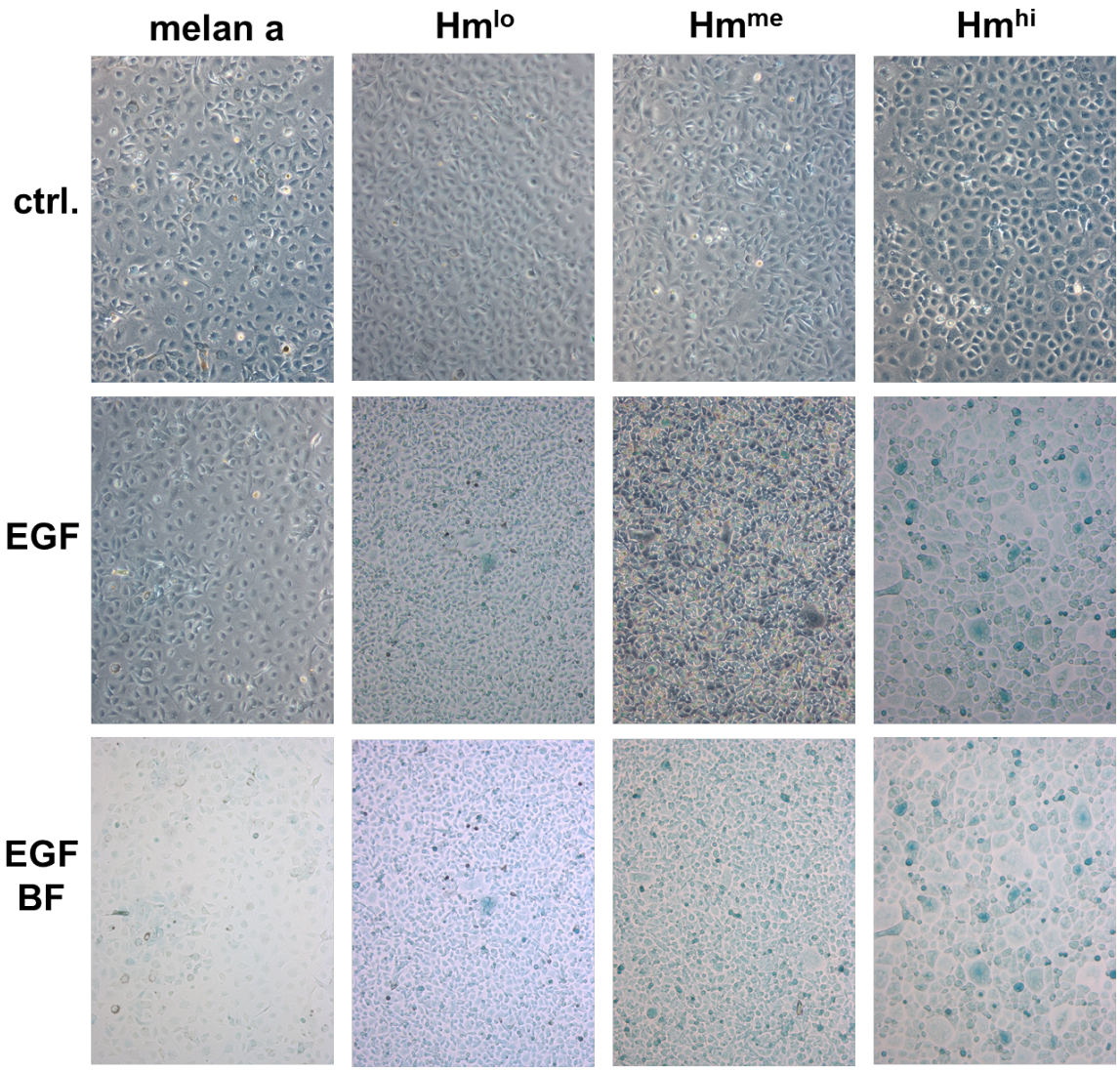

Figure 13: Hm receptor level determines senescence extent of EGF-treated melanocytes
SA-β-Gal pictures (100-fold magnification) illustrating the parental cell line melan a and the three Hm clones upon 14 days of cultivation in starving medium alone (ctrl.) or supplemented with EGF (EGF). The upper two panels show phase contrast and the lower one brightfield (BF) images.

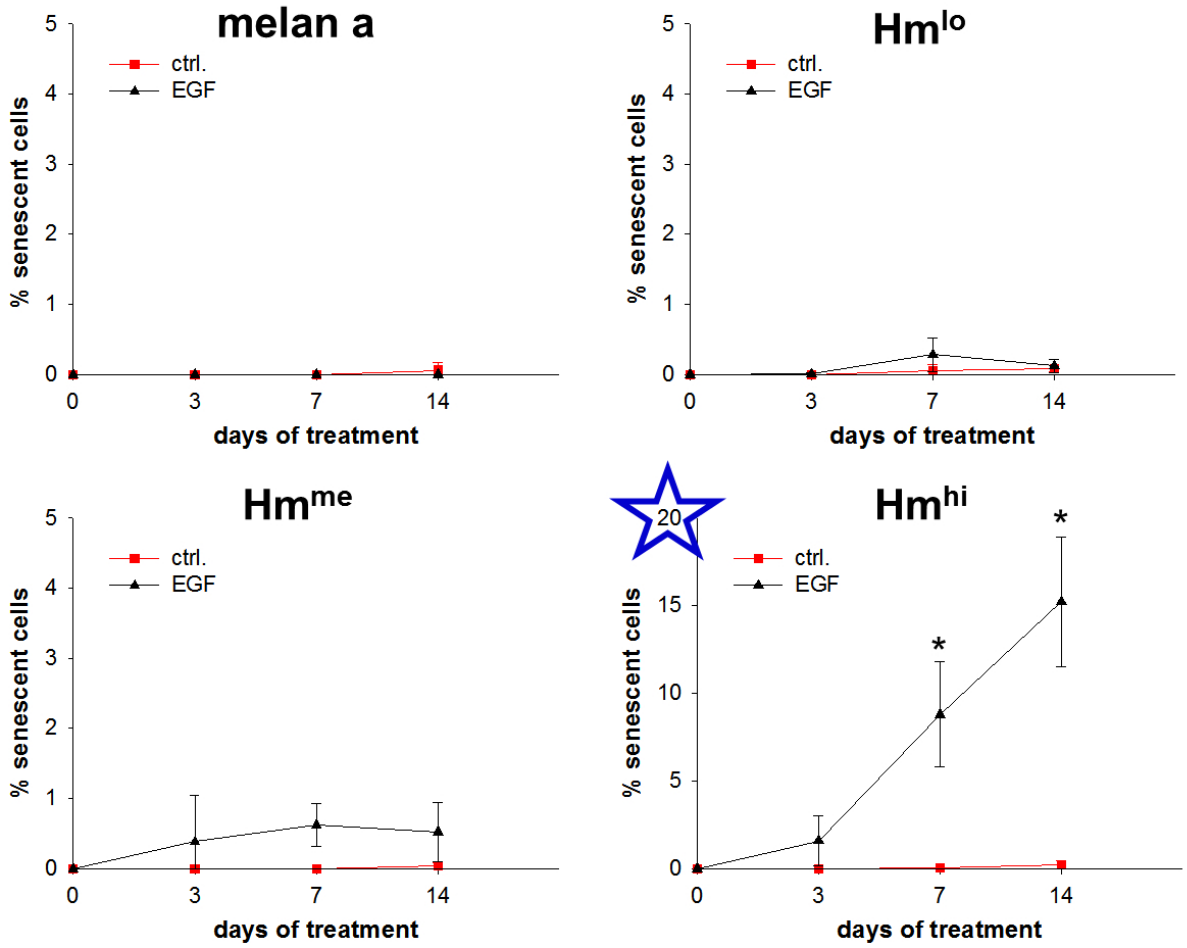

Figure 14: Hm receptor level determines senescence extent of EGF-treated melanocytes
The graphs depict the proportion of SA-β-Gal positive cells on the total cell number observed over time for the parental cell line melan a and the three Hm clones when cultivated in starving medium alone (ctrl.) or supplemented with EGF (EGF). At indicated time points SA-β-Gal stainings were performed. Graphs display the mean values of three independent experiments, standard deviations are shown. Statistical significance was assessed by student´s t-test (2-sided, paired) comparing ctrl. to EGF samples at each time point and highlighted by an asterisk (*p<0.05). Please note the different scales of the y-axes.

7.2 Multinuclear melanocytes are senescent and generated by endomitosis and fusion

One of the most notable features of the Hm^{hi} line was the occurrence of enlarged, highly multinucleated cells upon long-term EGF stimulation, which preceded the positive SA-β-Gal response. Moreover, the vast majority of blue cells had multiple nuclei, suggesting that the multinucleated phenotype is the prerequisite for senescence induction in our melanocyte system. To gain insight into the mechanistic processes, which allow the cells to become multinucleated, I stimulated a mixture of 50% Hm^{hi} cells stably transfected with mOrange (cytosolic), 25% Hm^{hi} cells transiently transfected with H2BeGFP (nuclear), and 25% untransfected Hm^{hi} cells with EGF. Upon 14 days of EGF treatment I analysed 16 pictures

taken at randomly chosen positions and found the vast majority of multinucleated cells had been generated by endomitosis and only few had undergone fusion events.

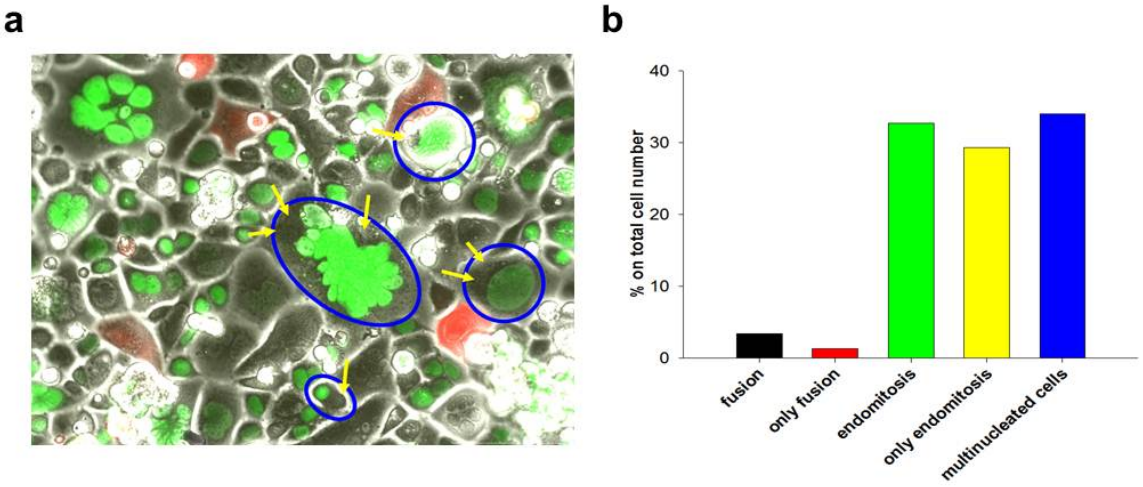

Figure 15: Multinucleated cells are mainly generated by endomitosis
(a) Image of Hm^{hi} mix (50% stably transfected with mOrange, 25% transiently transfected with H2BeGFP, 25% untransfected) upon 14 days of EGF treatment at 100-fold magnification. Encircled cells are those with green and unstained nuclei (highlighted by yellow arrows), which have undergone one or several fusion events upon 14 days of EGF stimulation. (b) The graph depicts the proportion of cells which have undergone either fusion (differently coloured nuclei or red cytoplasm and stained nucleus/nuclei) or endomitosis (two or more nuclei of the same colour in a single cell) or both on the total cell number. Bars represent mean values of the cellular events observed in 16 pictures taken at randomly chosen positions within the 6-wells. Cells were enumerated manually.

To ensure that multinucleated cells, which contain many equally coloured nuclei, were indeed the result of nuclear divisions without successive cytokinesis rather than the effect of numerous fusion events, we performed time lapse analyses of EGF-stimulated Hm^{hi} cells (*Figure 16*). With the help of Professor J. Hoppe´s heatable incubation chamber attached to a microscope (see acknowledgement section in[230]), I could observe endomitoses as well as rare fusion events. Interestingly, even in cases of fusion, endomitosis frequently occurred in one or even both of the cells.

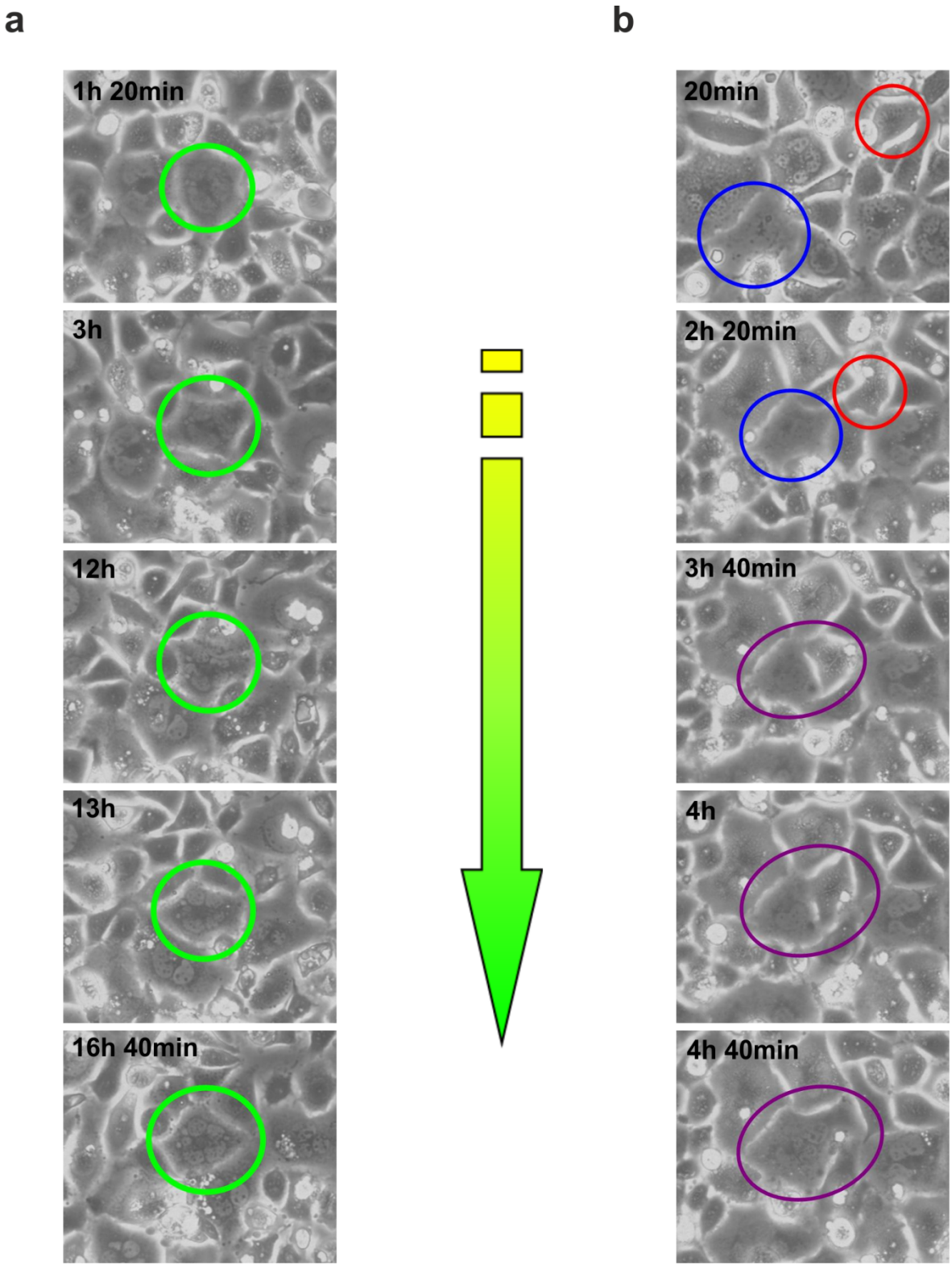

Figure 16: Endomitosis and fusion generate multinucleated melanocytes

Hm^{hi} cells were monitored for 17 hours upon 7 days of EGF treatment. Pictures were taken every 20 minutes at 100-fold magnification. Equally cropped images are shown. Time points are indicated. (a) Endomitosis. (b) Fusion.

7.3 pRB and p53 are induced by HERmrk

The two major senescence-inducing pathways are p53 and pRb [231]. To identify crucial players in our melanocyte senescence model, I examined the transcript as well as the protein levels of these senescence inducers and their upstream activators $p19^{ARF}$ (*Arf*), the cyclin-dependent kinase inhibitors $p16^{INK4A}$ (*Ink4a*), $p15^{INK4B}$ (*Ink4b*), $p21^{WAF}$ (*p21*) and $p27^{KIP1}$ (*p27*) (*Figure 17*). *Arf* transcription and protein levels were elevated upon long-term EGF stimulation in Hm^{lo} and Hm^{hi} cells, whereas the induction in Hm^{me} melanocytes was only modest. Interestingly, ARF´s downstream target p53 was found to increase concurrently with the p53 protein level being highest in the senescent Hm^{hi} cells. However, data obtained for the cyclin-dependent kinase inhibitor genes were inconclusive. While *Ink4a* transcript was slightly induced in the non-senescing Hm^{lo} and Hm^{me} as well as the senescing Hm^{hi} clone, increased protein levels could only be detected in Hm^{hi} cells. Besides, *Ink4b* mRNA levels were exclusively elevated in Hm^{lo} cells, whereas INK4B protein was detected in Hm^{hi} cells at day 14. Moreover, even though *p21* transcripts were found to be highly up-regulated in the senescent cell line Hm^{hi}, only a faint increase of p21 protein was observed, while p27 protein remained undetectable. Finally, investigaton of the protein levels of the downstream effector pRB revealed the hyperphosphorylated, inactive form was no longer detectable in Hm^{hi} cells at late time points, while hypophosphorylated, active pRB accumulated similarly in Hm^{lo}, Hm^{me} and Hm^{hi} cells.

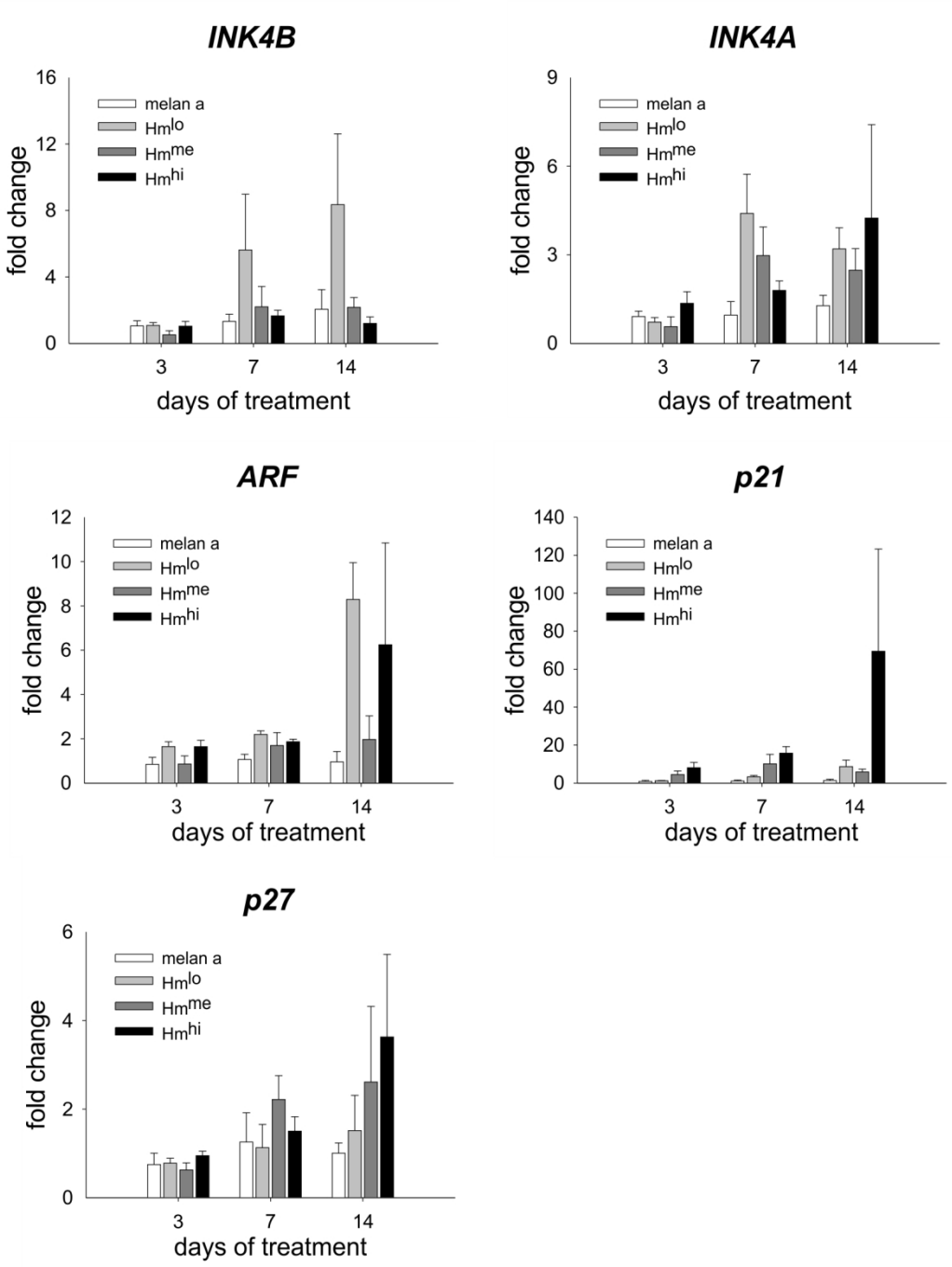

Figure 17: Inconclusive mRNA expression levels of known senescence-associated genes

qRT-PCR analyses of known senescence-associated p53 and pRb pathway components for the parental cell line melan a and the Hm clones Hm^{lo}, Hm^{me} and Hm^{hi}. The graphs depict the mean values of 3-5 independent experiments; each bar represents the mRNA fold induction upon EGF treatment in reference to starved cells. Expression levels were normalized to *HPRT*.

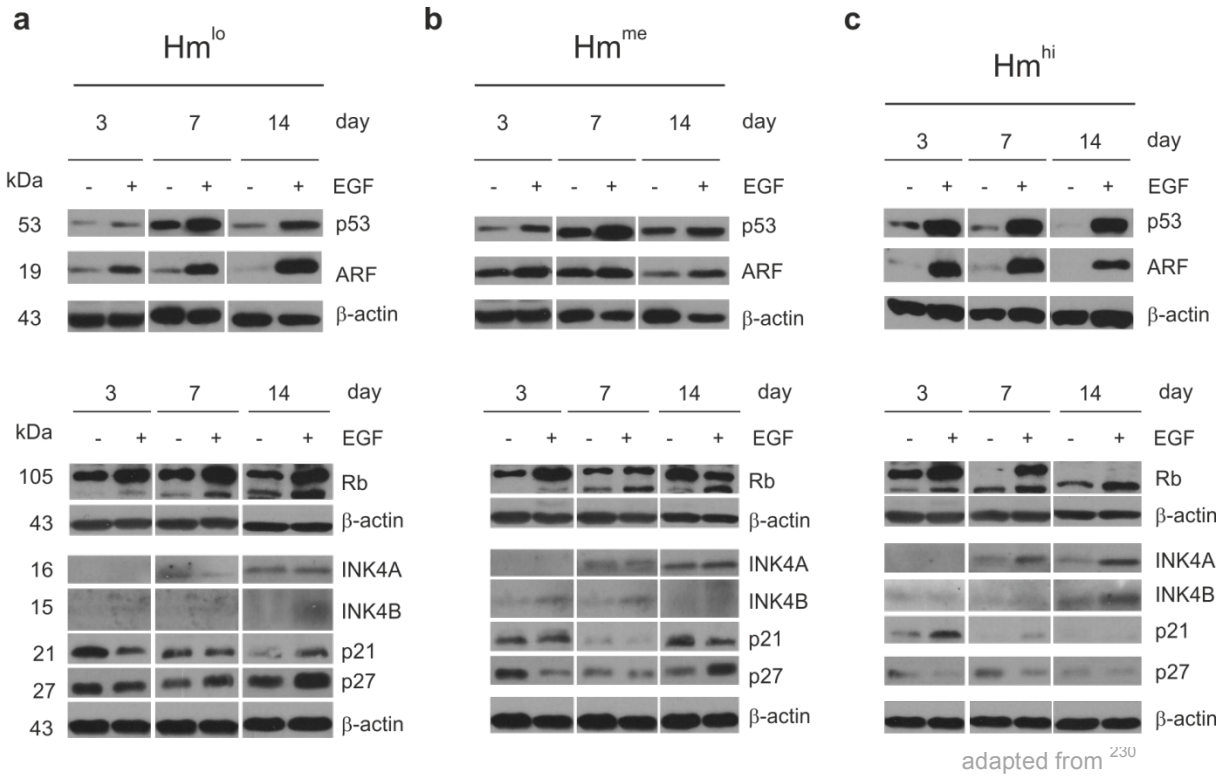

Figure 18: Analysis of protein levels of senescence markers

Western blot analyses of known senescence-associated p53 and pRb pathway components for melan a Hm clones Hm^{lo} (a), Hm^{me} (b) and Hm^{hi} (c). β-actin served as loading control. The respective protein weight is indicated in kDa.

Taken together, the molecular events accompanying HERmrk-induced senescence did not point to a single senescence mediator. Besides, the changes we observed in cyclin-dependent kinase inhibitor expression were only humble compared to those observed in other premature senescence systems [10,88,232,233]. However, the combination of high ARF and p53 protein together with the slightly enriched INK4A and INK4B levels accompanied by the lack of hyperphosphorylated pRb exclusively observed for Hm^{hi} cells might account for senescence induction.

7.4 DNA damage response is activated in cells bearing high levels of active HERmrk

Since the p53 pathway was found to be strongly activated in Hm^{hi} cells, I was interested in p53 regulation in this melanocyte clone. Besides, DNA damage response pathways are known to play a crucial role for p53 function and senescence induction [234–236]. The DNA damage response is activated when DNA-damaging events, e.g. oxidative stress, threaten the cell. Then, ataxia telangiectasia mutated (ATM) is one of the first components to be activated and recruited to the DNA damage site. In turn, the ATM target checkpoint kinase 2 (CHK2) is activated and blocks cell cycle progression. Interestingly, CHK2 activation has been described to be both necessary and sufficient for senescence induction in various non-melanocyte cell culture systems [237–239]. The DNA damage response components ATM and ataxia telangiectasia and Rad3 related (ATR) share a common target, namely p53, and phosphorylate the protein at Ser15 (human) or Ser18 (mouse). This activating modification allows p53 to interact with vital transcriptional co-activators [240,241]. To scrutinize a possible role for DNA damage response in our melanocyte senescence model, I monitored the protein levels of P-CHK2 Thr77 (= human Thr68) and P-p53 Ser18 (*Figure 19*). Western blot analyses revealed EGF treatment of Hm^{hi} cells to augment both P-CHK2 and P-p53 protein levels (*Figure 19c*). This strong increase was neither observed for EGF-stimulated, non-senescing Hm^{lo} nor for Hm^{me} cells (*Figure 19a and b*). Hence, the DNA damage response seems to contribute to senescence in our melanocyte model.

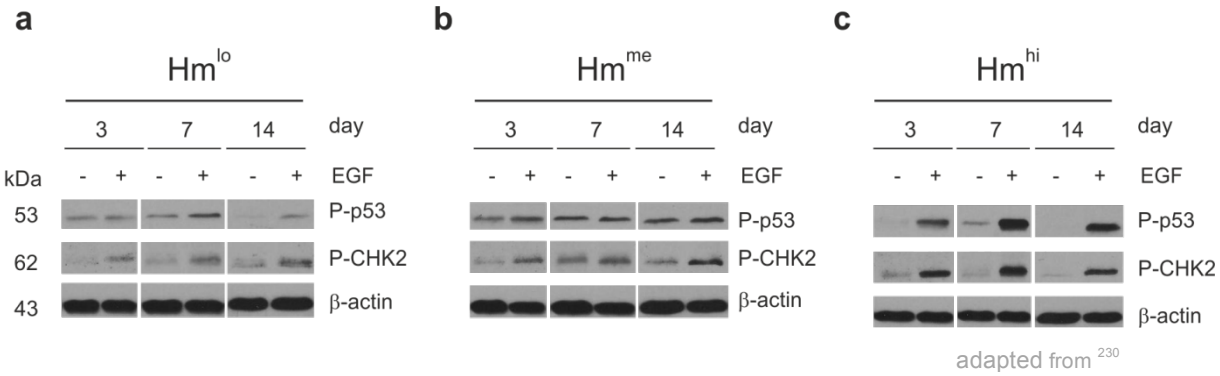

Figure 19: DNA damage response is activated in senescent Hm^{hi} cells

Western blot analyses of the DNA damage markers P-p53 (Ser18) and P-CHK2 (Thr 77) for melan a Hm clones Hm^{lo} (a), Hm^{me} (b) and Hm^{hi} (c). β-actin served as loading control. The respective protein weight is indicated in kDa.

To investigate the DNA damage level more closely, we performed an immunofluorescence staining using an antibody recognizing phospho-histone 2A.X (Ser139) (ɣ-H2AX). At sites of double-strand breaks, ɣ-H2AX accumulates in a distinctive, spotty pattern. Even though a basal level of DNA damage was detectable for all Hm clones upon long-term starvation, EGF

treatment exclusively augmented ɣ-H2AX in senescent Hm^{hi} cells (*Figure 20*). Fittingly, highest ɣ-H2AX levels could be detected in multinucleated Hm^{hi} cells.

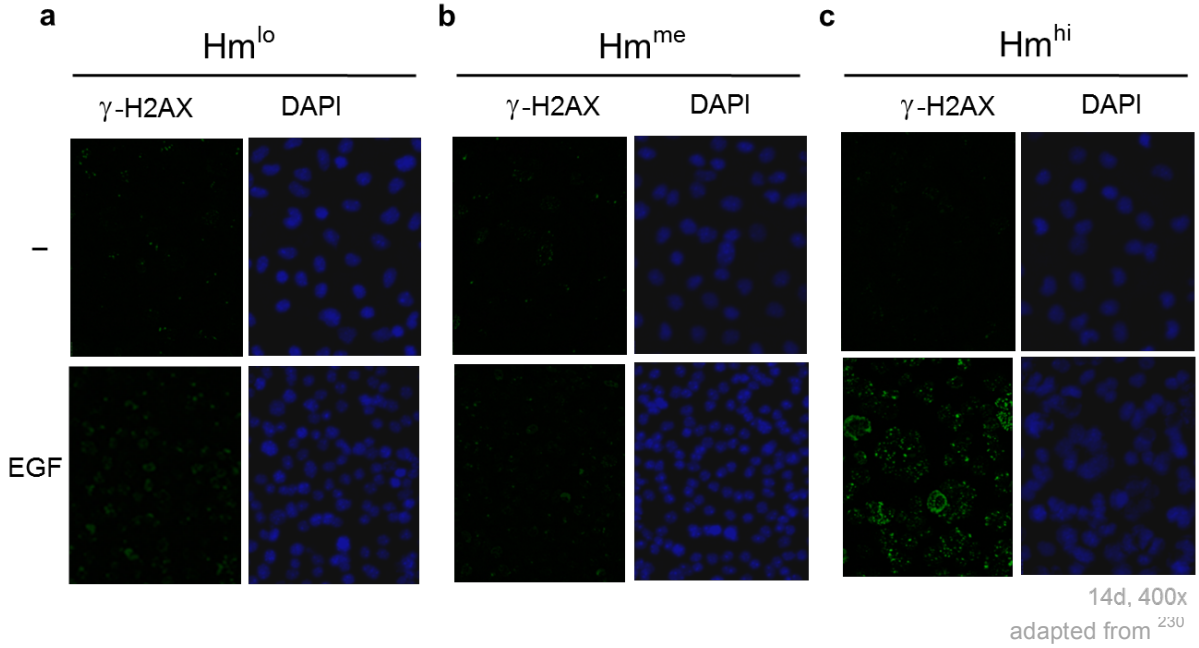

Figure 20: DNA double strand breaks in senescent Hm^{hi} cells
ɣ-H2AX immunofluorescence images (400x magnification) illustrating the level of DNA double strand breaks for melan a Hm clones Hm^{lo} (a), Hm^{me} (b) and Hm^{hi} (c) after 14 days in starving medium alone (-) or supplemented with EGF (EGF). DAPI was used to counterstain DNA.

7.5 Reactive oxygen species mediate the senescence response

DNA damage can be caused by reactive oxygen species (ROS). Aberrant RAS signalling often goes along with ROS [242,243], which cause senescence in fibroblasts [74,244]. Therefore, we performed senescence assays to analyse ROS production in Hm^{hi} cells applying 2`,7`-dichlorodihydrofluorescein diacetate (DCF-DA). This non-fluorescent dye is converted to fluorescent DCF only in presence of ROS. In accordance with the data obtained in the DNA damage assays, ROS were exclusively present in EGF-stimulated Hm^{hi} cells at stages when cells had become senescent. Then, I co-treated EGF-stimulated Hm^{hi} cells with the ROS scavenger N-acetylcysteine (NAC). NAC treatment both lowered the senescence degree (to ~33%) and induced proliferation of Hm^{hi} cells upon EGF stimulation (*Figure 21*) further supporting the role of ROS for senescence induction in our melanocyte model.

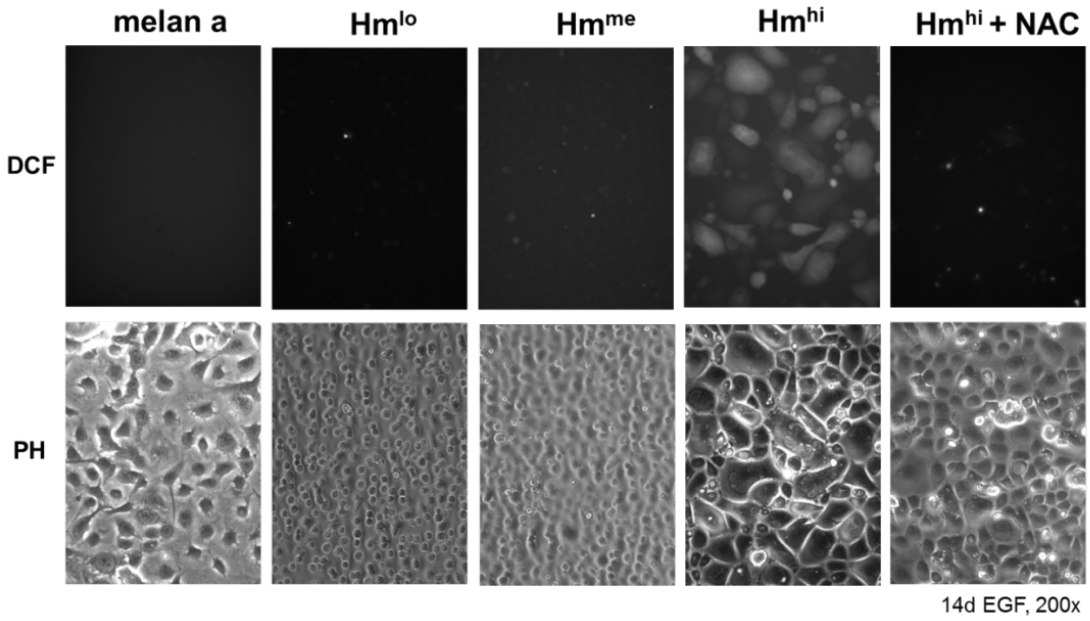

Figure 21: NAC treatment counteracts HERmrk-induced senescence
DCF staining images (200-fold magnification; DCF) of melan a cell clones melan a, Hm^{lo}, Hm^{me} and Hm^{hi} in absence or presence of the reactive oxygen species scavenger NAC upon 14 days of EGF treatment. Corresponding phase contrast images (PH) are shown.

These data allow for the conclusion that ROS mediate the HERmrk-induced appearance of multinucleated and senescent cells.

7.6 Oncogenic N-RAS expression also drives melanocytes into a multinucleated, senescent state

To check if oncogenes other than Xmrk were also capable of inducing senescence in mouse melanocytes, I performed senescence assays with melan a cells bearing a doxycycline-inducible version of the human melanoma oncogene N-RAS^{61K} ('N-RAS*'). SA-β-Gal stainings, DCF-DA assays as well as DNA damage assays of empty vector control cells (ctrl.) were compared to N-RAS*-expressing melanocytes (N-RAS*, *Figure 22*). Interestingly, N-RAS* expression mimicked the phenotype observed upon Hm^{hi} stimulation in our melanocyte model. Not only did N-RAS* force melanocytes into a SA-β-Gal-positive, multinucleated state (*Figure 22a*) but also induced the DNA damage marker P-p53 and allowed for γ-H2AX presence (*Figure 22c*), as well as ROS detection (*Figure 22d*). However, ROS levels in N-RAS* cells were lower than those observed upon EGF treatment of Hm^{hi} cells. Hence, oncogenic N-RAS alone also lead to increased ROS levels, DNA damage and a multinucleated and senescent phenotype that resembled the situation observed upon activation of HERmrk, an upstream activator of the RAS/RAF/MAPK pathway.

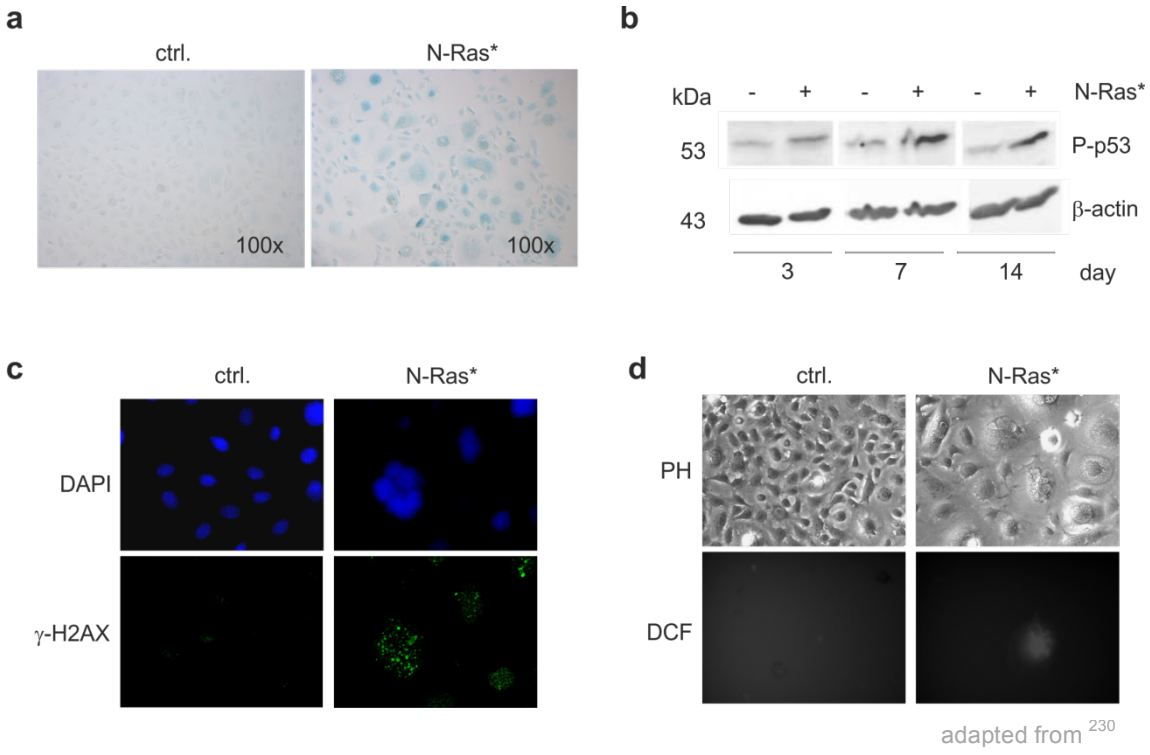

Figure 22: Oncogenic N-RAS results in ROS generation, DNA damage and senescence
(a) Brightfield images (100-fold magnification) of melan a cells bearing the empty vector control (ctrl.) or the doxycycline-inducible oncogenic N-RAS (N-RAS*) upon 14 days of doxycycline treatment. (b) P-p53 (Ser18) Western blot analyses of melan a-control (ctrl.) and N-RAS* cells upon long-term doxycycline treatment. β-actin served as loading control and protein weights are stated in kDa. (c) γ-H2AX (Ser139) immunofluorescence images (400-fold magnification) of melan a-control (ctrl.) and N-RAS* cells upon 14 days of doxycycline treatment. DNA was counterstained with DAPI. (d) Phase contrast (PH) and corresponding DCF fluorescence images upon 14 days of doxycyclin treatment (400-fold magnification).

Taken together, the data obtained from Hm^{hi}- and N-RAS*-expressing melanocytes, provide evidence for a ROS-dependent activation of the DNA damage response, which ultimately drives melanocytes into multinucleation and senescence. This in vitro phenomenon is oncogene level dependent and likely resembles the multinucleated phenotype observed in human nevi. These data are summarized in a published manuscript [230].

7.7 Expression analyses of cytokinesis-associated genes

Since multinucleation seemed to be the prerequisite for senescence induction in our melanocyte model, I analysed the expression of cell cycle regulation-relevant genes which are involved in G2/M or cytokinesis phases of the cell cycle (*Figure 23)*.

I therefore chose to look at the mRNA regulation of a number of cell-cycle relevant genes: *B-myb*, a cell-cylce regulator usually induced during G1/S transition [200,201], *Aurora Kinase B*, which is vital for chromosome segregation and cytokinesis [206], *KLF4* (*Krüppel-like factor 4*) , which is DNA damage-induced [214], *Cyclin E1* that influences Rb phosphorylation [210,211], while *Cyclin B1* is involved in the regulation of mitosis exit [212] and *Survivin* which plays a critical role in ploidy-control [224].

Quantitative realtime PCR experiments were performed to compare the mRNA expression levels of cell cycle-related genes in the three Hm lines. Fold induction of *B-myb*, *Aurora kinase B* (*Aurk B*), *Cyclin B1* and *E1*, as well as *KLF4* and the inhibitor of apoptosis *Survivin* proved to be high in EGF-treated, senescing Hm^{hi} cells, whereas the mRNA expression levels in the parental cell line melan a as well as the non-senescing clones Hm^{lo} and Hm^{me} remained low throughout the experiment (*Figure 23*).

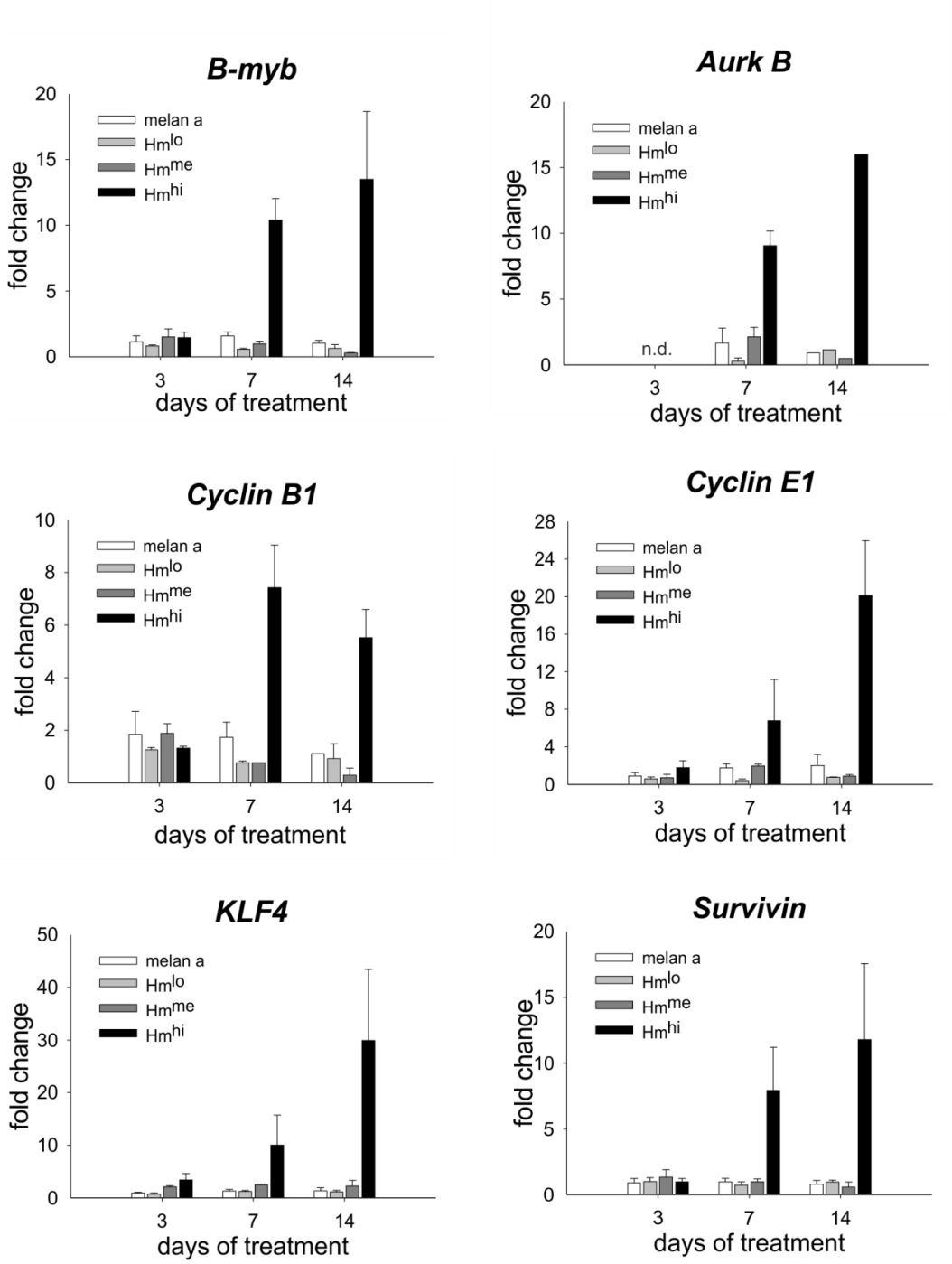

Figure 23: Cell cycle-associated genes whose expression pattern parallels Hm levels

qRT-PCR analyses of cell cycle-associated genes for the parental cell line melan a and the Hm clones Hm^{lo}, Hm^{me} and Hm^{hi}. The graphs depict the mean values of 3-5 independent experiments (exception: *Aurk B* 14 days, where only 1 experiment was performed); each bar represents the mRNA fold induction upon EGF treatment in reference to starved cells. Expression levels were normalized to *HPRT*.

7.8 Survivin expression in HERmrk-mediated senescence

Interestingly, *Survivin* is suggested to be a promising tumour marker as it usually lacks expression in terminally differentiated tissue, but is up-regulated in most cancers [220,245,246]. Additionally, *Survivin* is a vital player in chromosome segregation and associated with cytokinesis defects [224]. As described earlier, Hm^{hi} cells do become multinucleated – probably due to endomitosis based on a failure of cytokinesis. Matching these facts, I found *Survivin* mRNA levels to be exclusively increased in senescing Hm^{hi} cells. Concluding that *Survivin* was a logically linked target between DNA-damage and multinucleation in our system, I investigated *Survivin* mRNA levels upon addition of the ROS scavenger NAC. As expected, NAC treatment not only reduced the number of EGF-induced, multinucleated, senescent Hm^{hi} cells, but also lowered *Survivin* expression (*Figure 24*), pointing to a link between the observed phenomena and *Survivin* expression. In case of starved Hm^{hi} cells (ctrl.), NAC treatment slightly enhanced *Survivin* mRNA levels (*Figure 24*).

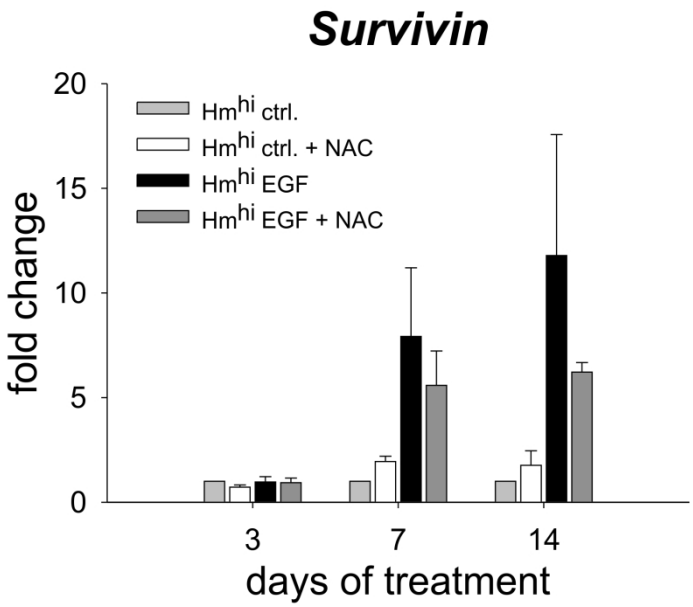

Figure 24: ROS scavenger NAC limits Survivin induction upon EGF treatment of Hm^{hi} cells
Survivin qRT-PCR analyses for senescing Hm^{hi} melanocytes. Where indicated, Hm^{hi} cells were starved (ctrl.), stimulated with EGF and/or treated with the ROS scavenger N-acetylcysteine (NAC). The graph depicts the mean values of 3-5 independent experiments; each bar represents the mRNA fold induction normalized to *HPRT*.

To check if *Survivin* mRNA induction goes along with an increase in protein abundance, I performed immunofluorescence assays comparing starved (-) or EGF-treated (EGF) Hm^{hi} cells (*Figure 25*). Even though low levels of survivin protein could be detected in nuclei of starved Hm^{hi} cells at any time point, survivin protein levels were much higher upon EGF treatment (*Figure 25*). Interestingly, survivin protein could not only be detected in nuclei but also in the cytoplasm of multinucleated, senescent Hm^{hi} cells.

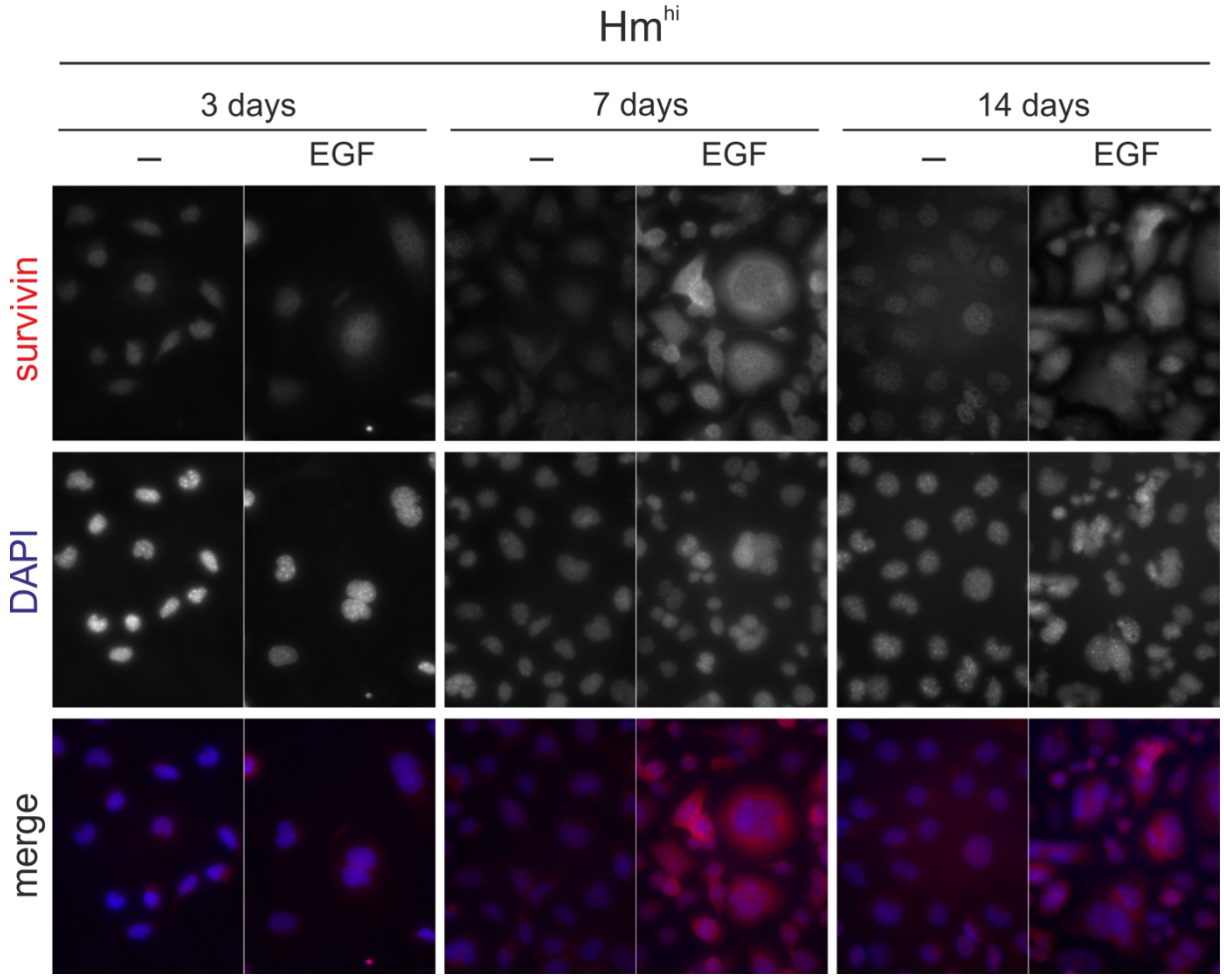

Figure 25: Survivin protein levels increase upon EGF treatment of Hm^{hi} cells
Representative survivin immunofluorescence images (400-fold magnification) of starved (-) and EGF-treated (EGF) Hm^{hi} cells upon 3, 7 and 14 days of treatment. DNA was counterstained with DAPI.

To investigate the effect of lowered *Survivin* mRNA levels on the senescing Hm^{hi} melanocytes, I transduced them with either an empty pRetroSUPER vector (ctrl.) or one expressing one of three different short hairpin RNAs directed against *Survivin* before selecting with antibiotics for cells, which had stably integrated the vector. Quantitative realtime PCR and Western blot analyses of cells cultured in complete medium revealed only a slight knockdown on mRNA level (*Figure 26a*) and apparently an increase in survivin protein (*Figure 26b*). However, phase contrast images proved the presence of

multinucleated cells under standard culture conditions in complete medium with the effect being strongest for shRNA #3 (*Figure 26c*). Notably, the survivin protein level in any of the three knockdown clones was much lower than than that in both melan a and Hm^{hi} cells. While the knockdown assay should be repeated due to the low survivin protein level in the ctrl. clone, my observations strongly point towards a functional link between survivin and Hm^{hi} multinucleation. Unfortunately, I was not allowed to perform long-term senescence assays with these cells, so I can neither comment on the cellular features under starving conditions, nor upon EGF stimulation.

Taken together, we could demonstrate that melan a cells undergo oncogene-induced, ROS-mediated senescence upon HERmrk activation or N-RAS* expression. This effect is oncogene level-dependent. However, even though some well-known senescence inducers as well as the mRNA expression levels of several cell cycle-related genes were found to parallel Hm expression, I could not identify the one crucial senescence mediator for our melanocyte system.

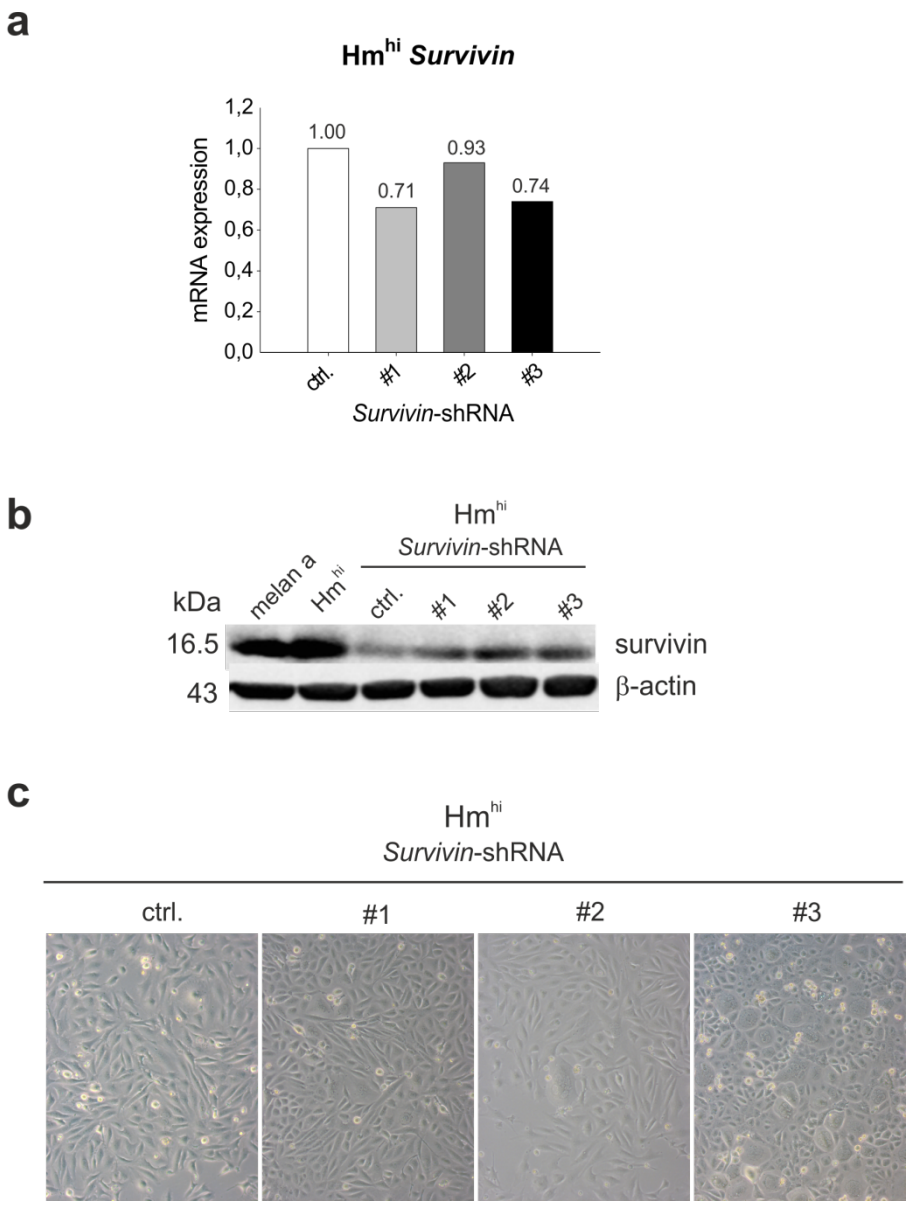

Figure 26: Effects of *Survivin* shRNA knockdown in Hm^{hi} cells

(a) *Survivin* qRT-PCR analysis of Hm^{hi} melanocytes bearing an empty vector control (ctrl.) or stably expressing one of three different shRNAs directed against *Survivin*. The graph depicts the *Survivin* mRNA expression level normalized to the empty vector control (ctrl.); prior to that, *Survivin* mRNA fold induction had been normalized to *HPRT*. (b) Survivin Western blot analysis of melan a and Hm^{hi} cells as well as Hm^{hi} cells bearing an empty vector (ctrl.) or one with one of three shRNAs directed against *Survivin*. Cells had been cultured in complete medium prior to harvesting. β-actin served as loading control. (c) Phase contrast images of Hm^{hi} cells stably expressing the empty pRS vector (ctrl.) or one bearing a shRNA directed against *Survivin* (shRNA #1, #2 and #3) upon puromycin selection (100-fold magnification).

7.9 HERmrk receptor expression status in long-term stimulation assay

Since we experienced some difficulties concerning our long-term experiments after using different kinds of serum as well as dialyzed serum, I was wondering what happened to the Hm receptor status within the two weeks of the experiment. Prior to these Western blots, Hm receptor status had only been determined upon short-term receptor stimulation (10 minutes up to 2 hours of EGF treatment).

HERmrk Western blot analyses (*Figure 27*) confirmed the difference in receptor protein level for the Hm clones in starving medium: Hm^{lo} showed the lowest HERmrk level, followed by Hm^{me} and Hm^{hi}, which proved to express receptors at a very high level. Interestingly, these levels changed upon EGF stimulation as protein levels diminished after EGF treatment. The only exception seemed to be Hm^{me} upon 3 days of treatment: The detected HERmrk levels were found to be rather constant even though the detected band in case of EGF stimulation appears to have a lower protein weight compared to its untreated counterpart. Additionally, treatment with the ROS scavenger N-acetylcysteine (NAC) apparently stabilized or enhanced the HERmrk receptor level in Hm^{hi} cells at day 3, despite a lower HERmrk status upon EGF stimulation. Nevertheless, after 7 and 14 days in culture, NAC-treated Hm^{hi} cells showed lower HERmrk levels compared to Hm^{hi} cells cultured in absence of the ROS scavenger. Interestingly, even within each cell line and treatment, receptor levels varied over time. However, one should keep in mind that we are looking at three independent blots, although the same amount of whole cell lysate, antibodies and comparable SDS gels were used.

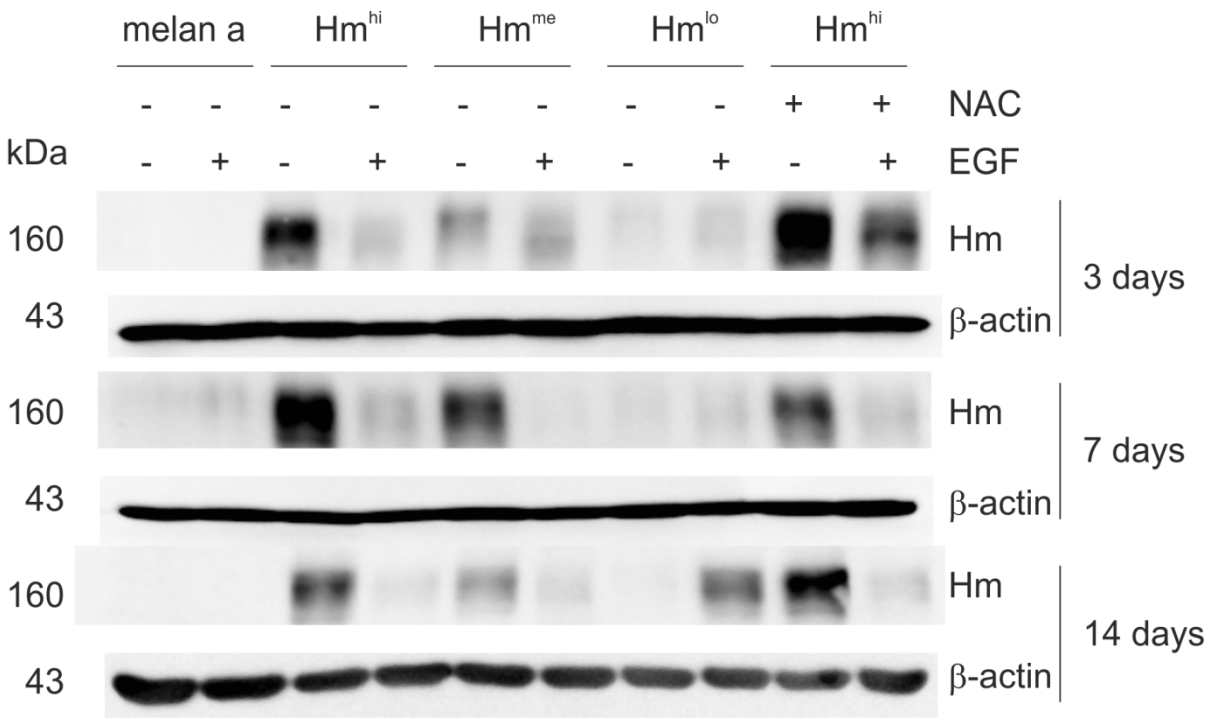

Figure 27: Hm receptor status of Hm clones during long-term assay
HERmrk Western blot analyses of Hm^{lo}, Hm^{me} and Hm^{hi} cells after 3, 7 and 14 days in starving medium (-) or EGF treatment (EGF) in absence or presence of the ROS scavenger N-acetylcysteine (NAC). 35µg of whole cell lysates were separated using 10% SDS gels. β-actin served as loading control. Protein weights are indicated in kDa.

Taken together, these Western blots suggest the Xmrk receptor to be internalized upon EGF stimulation. However, these analyses only give us a first hint at what is likely to be taking place. Hence, fluorescent labelling followed by realtime imaging of the receptor might be a useful tool to further investigate the intracellular scenarios.

While this result can only be considered to be a primer for further investigation, it demonstrates that there is an important additional level of complexity. Furthermore, it shows that one would be ill-advised to base conclusions on the assumption that HERmrk receptor, and consequently signalling levels are constant and can always be categorized by the average level assigned to the Hm^{lo}, Hm^{me} and Hm^{hi} lines. This statement is further supported by the varying P-ERK1/2 (Thr202/Tyr204) protein levels in the different Hm lines upon EGF stimulation (*Figure 10*).

Hence, this observation leads to a series of fascinating questions, such as: do HERmrk receptors continue to signal after internalization [247–249]? Are they recycled to the membrane or destroyed in lysosomes [247,250]? Is the HERmrk receptor surface-density regulated by ER-retention [251]? Is EGF degraded after internalization, or maybe transported and re-released from the cell [252]? Is the multimerisation mode changed due to changes in ER- or surface density of the receptor [253]?

7.10 The impact of MYC overexpression on HERmrk-induced melanocyte senescence

Since *C-MYC* is a well-known hEGFR target gene [254,255], which has been reported to be involved in senescence prevention in melanoma [159], we investigated the effect of C-MYC overexpression on Hm^{hi}-driven senescence. Hm^{hi} cells were transfected with expression plasmids containing either wildtype human MYC (MYC-wt), MYC^{V394D} (MYC-VD) or the mutant MYC^{T58A} (MYC-TA) (*Figure 28a*). Notably, MYC-VD is deficient in binding Miz-1 [256], while the MYC-TA mutant cannot be phosphorylated by the ubiquitin ligase Fbw7 at Thr58, leaving us with a much more stable C-MYC protein compared to its wildtype equivalent [257,258]. First, I performed proliferation assays (*Figure 28b*). Hm^{hi} cells transfected with the empty control vector did not grow when cultured in starving medium alone and became multinucleated upon EGF stimulation. Hm^{hi}-MYC-TA, Hm^{hi}-MYC-VD and Hm^{hi}–MYC-wt cells, however, only showed a limited proliferation potential in starving medium alone, but strongly proliferated upon EGF treatment.

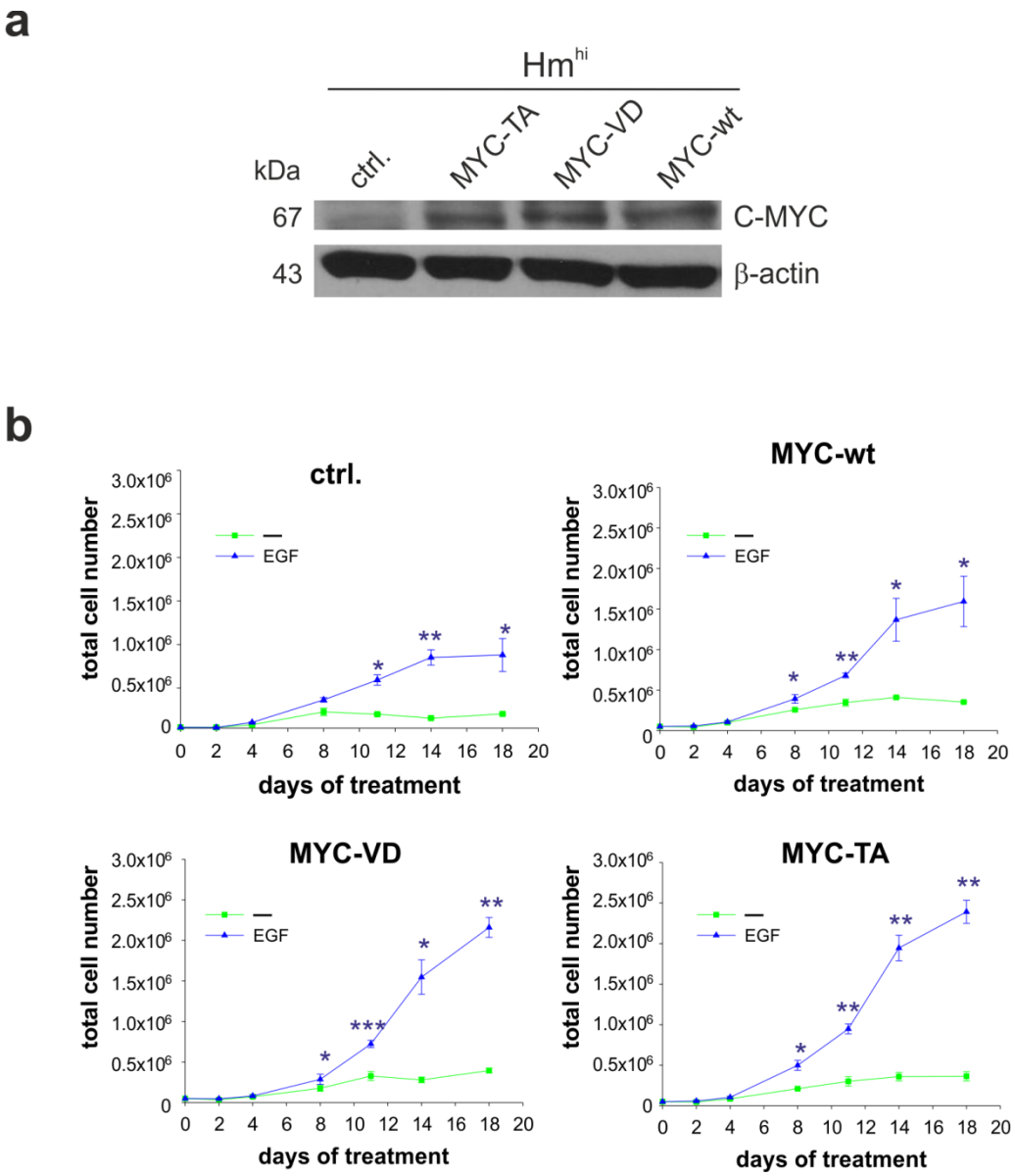

Figure 28: MYC overexpression enhances proliferation potential in Hm^{hi} cells

(a) C-MYC Western blot analysis of Hm^{hi} cells stably transfected with an empty control vector (ctrl.) or overexpressing one of three human C-MYC versions, namely MYC-wt, MYC-VD and MYC-TA. 100µg of whole cell lysates were separated using a 10% SDS gel. Cells had been cultured in complete medium prior to harvesting. β-actin served as loading control. Protein weights are indicated in kDa. (b) Graphs depict the total cell number (mean values of three independent experiments) of Hm^{hi}-ctrl. (ctrl.), Hm^{hi}-MYC-wt (MYC-wt), Hm^{hi}-MYC-VD (MYC-VD) and Hm^{hi}-MYC-TA (MYC-TA) cells over time in the absence (-) or presence of EGF (EGF). Student´s t-test (paired, 2-tailed) revealed statistical significance comparing starved (-) and EGF-stimulated cells at each time point indicated by asterisks (*p<0.05, **p<0.01, ***p<0.001).

To investigate the effect of MYC overexpression on the senescence extent of Hm^{hi} cells, I performed senescence assays. In accordance with the positive impact of MYC on melanocyte proliferation upon EGF treatment, I found MYC overexpression to diminish Xmrk-induced senescence in our cell culture model (*Figure 29*) with the effect being most prominent for MYC-TA cells (*Figure 29a*). Enumeration revealed the proportion of multinucleated, SA-β-

Gal-positive cells on the total cell number not to exceed 0.5% under starving conditions (-) regardless of MYC expression status (*Figure 29b*). EGF stimulation induced multinucleation and senescence in Hm^{hi} cells expressing the empty vector control (ctrl.) mounting to about 15% after 14 days in culture. Concomitant overexpression of MYC, however, diminished HERmrk-induced senescence to an average of 2.7% for MYC-wt, 0.75% for MYC-VD, and dropping to as low as 0.43% for MYC-TA cells upon EGF treatment (*Figure 29b*).

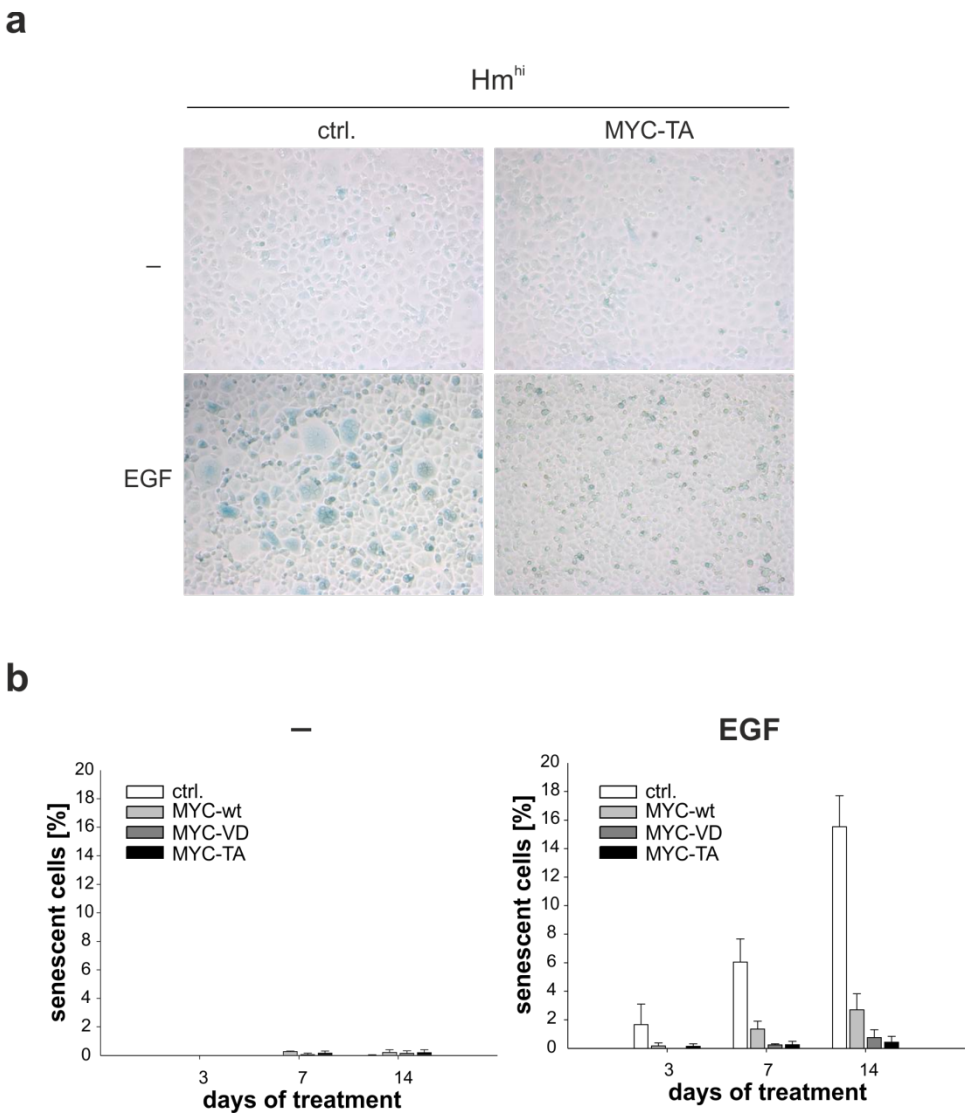

Figure 29: MYC overexpression diminishes HERmrk-induced senescence in Hm^{hi} cells
(a) Brightfield images (100-fold magnification) of SA-β-Gal-stained Hm^{hi} cells stably transfected with an empty control vector (ctrl.) oroverexpressing MYC-TA upon 14 days of treatment. Where indicated, cells were cultured in starving medium alone (-) or stimulated with EGF (EGF). (b) Graphs depict the proportion of senescent cells on the total cell number over time. Cells were either cultured in starving medium alone (-) or stimulated with EGF. Bars represent the mean values of three independent assays and standard deviations are indicated.

To test whether the enhanced proliferation potential of the Hm^{hi}-MYC clones correlated with an increase in tumourigenic capacity, soft-agar growth assays were performed (*Figure 30*).

While Hm^{hi} cells did not form colonies under starving conditions when HERmrk was inactive regardless of MYC expression status, MYC proved to dramatically enhance HERmrk-mediated colony forming capacity of melanocytes upon EGF stimulation. Notably, EGF-treated Hm^{hi}-MYC-TA cells formed extremely large colonies which were visible to the naked eye.

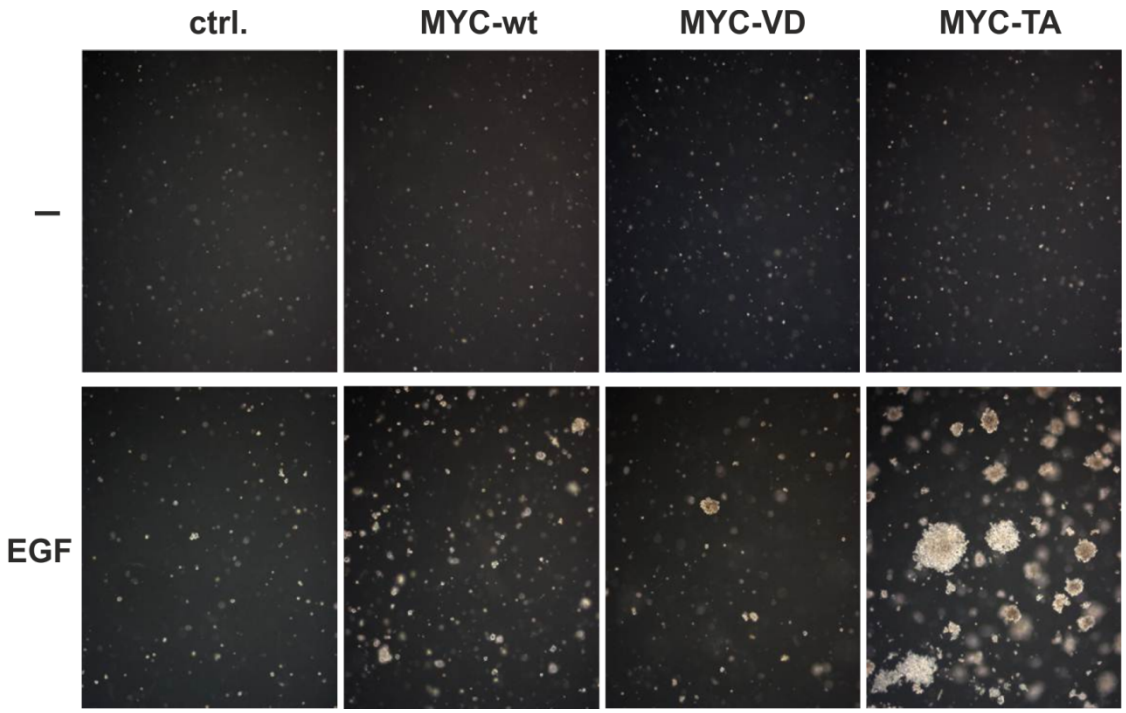

Figure 30: MYC overexpression enhances HERmrk-mediated tumourigenic potential
Phase contrast images (25-fold magnification) of Hm^{hi} cells stably transfected with an empty control vector (ctrl.), or overexpressing MYC-wt, MYC-VD or MYC-TA upon 14 days in soft agar. Where indicated, agar was overlain with starving medium alone (-) or supplemented with EGF (EGF).

To analyse the ROS extent in MYC-overexpressing Hm^{hi} cells, DCF-DA assays were performed (*Figure 31*). As expected, no fluorescent DCF and hence no ROS could be detected in starved Hm^{hi} cells upon 11 days in culture, regardless of MYC expression status. However, I found DCF-DA to convert to fluorescent DCF in multinucleated melanocytes upon EGF stimulation. The ROS level in EGF-treated Hm^{hi} cells expressing the empty control vector (ctrl., *Figure 31*) was equivalent to the one observed for Hm^{hi} cells (*Figure 21*). Since DCF was restricted to multinucleated cells, the fluorescence signal decreased from MYC-wt over MYC-VD and was lowest in MYC-TA-expressing Hm^{hi} cells (*Figure 31*). Notably, due to the high cell density observed for MYC-TA cells upon 11 days of EGF treatment, some cells had detached and died. Thus, the very bright, compact and round signals are very likely dead cells still attached to the dense cell-layer occupying to the dish. In clear contrast are the multinucleated large and flat cells emitting the DCF signal over larger areas.

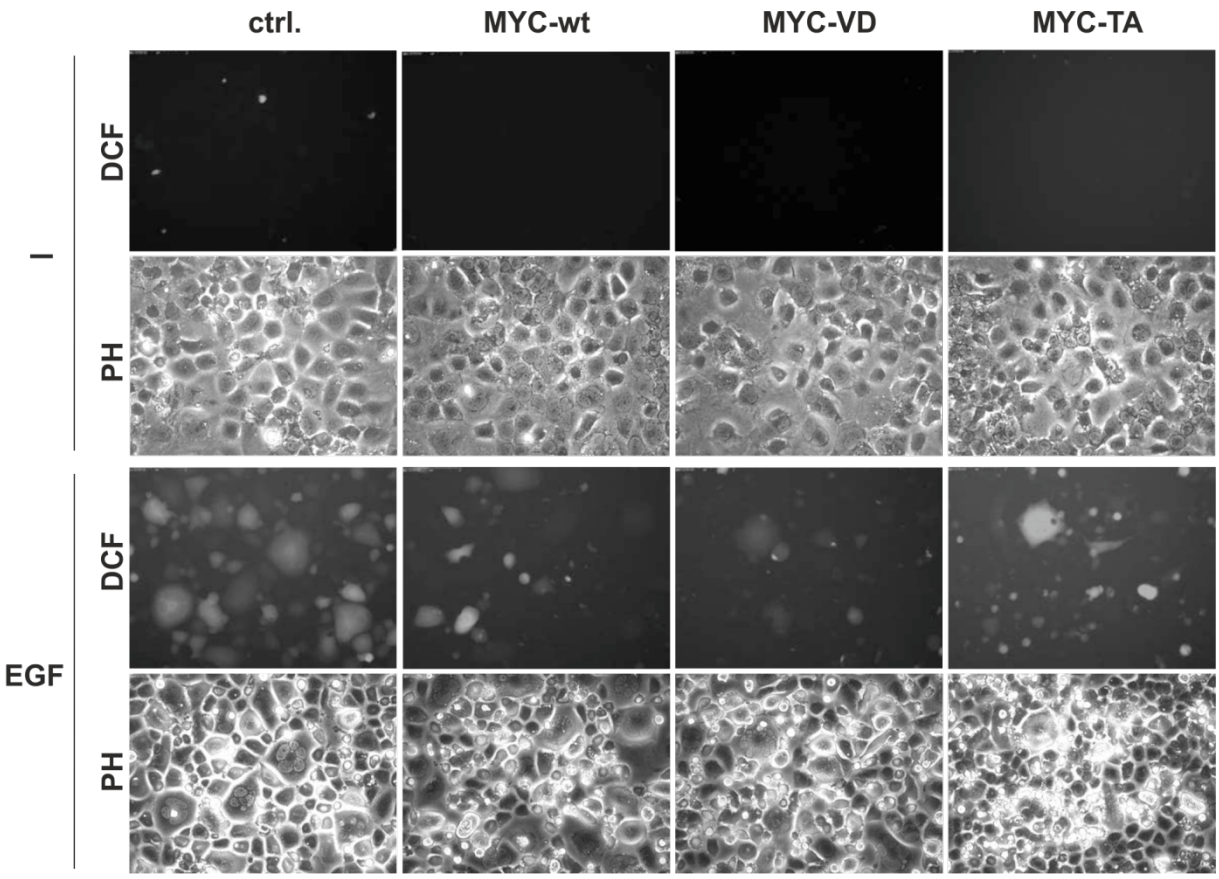

Figure 31: MYC overexpression counteracts Xmrk-induced ROS

DCF staining images (200-fold magnification; DCF) of Hm^{hi} cells stably transfected with an empty control vector (ctrl.), overexpressing MYC-wt, MYC-VD or MYC-TA upon 11 days in culture. Where indicated, cells were cultured in starving medium alone (-) or stimulated with EGF (EGF). Corresponding phase contrast images (PH) are shown.

To test whether the ROS levels correlated with the DNA damage extent, I performed comet assays under alkaline conditions (*Figure 32*). Even though a background level of DNA damage was observed regardless of MYC expression status upon 14 days in starving medium (-), it became obvious that MYC expression limits the DNA damage effect upon EGF stimulation and subsequent HERmrk activation. The number and extent of the detected comets already decreased when MYC-wt was co-expressed, but DNA damage was even lower in the MYC-VD clone and only rarely evident in MYC-TA cells.

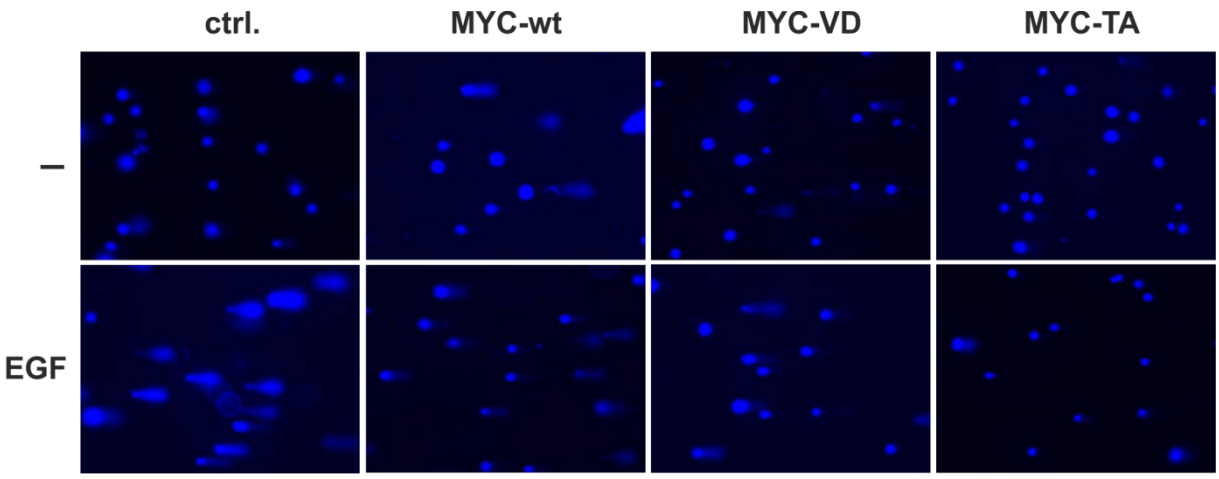

Figure 32: MYC overexpression counteracts HERmrk-induced DNA damage
Comet assay images (100-fold magnification) of Hm^{hi} cells stably transfected with an empty control vector (ctrl.) or overexpressing MYC-TA upon 14 days in culture. Where indicated, cells were cultured in starving medium alone (-) or stimulated with EGF. DNA was visualized using Hoechst 33342.

Taken together, MYC overexpression was not only found to diminish HERmrk-induced senescence, but also significantly enhanced the proliferation potential as well as the *in vitro* tumourigenic capacity of Hm^{hi} melanocytes. In accordance with these findings, MYC overexpression also limited the ROS and DNA damage extent upon HERmrk activation. Intriguingly, all these phenomena were most prominent for the stable MYC-TA mutant.

7.11 The impact of *Miz-1* knockdown on melanocyte senescence

Since MYC negatively regulates Miz-1 [259], we were wondering about the role of MIZ-1 in our senescence model. I first checked whether *Miz-1* was expressed in our Hm clones. Quantitative realtime PCR analyses of HERmrk cells revealed *Miz-1* mRNA to be induced after 14 days of treatment (*Figure 33a*). Interestingly, I found the ROS scavenger NAC to suppress *Miz-1* induction in EGF-stimulated Hm^{hi} cells to some extent (*Figure 33b*). Moreover, Western blot analysis of Hm^{hi} whole cell lysates proved MIZ-1 protein to accumulate over time upon EGF treatment, while in serum-starved Hm^{hi} cells only a weak MIZ-1 band was evident at day 7 (*Figure 33c*). Hence, HERmrk activation induced MIZ-1.

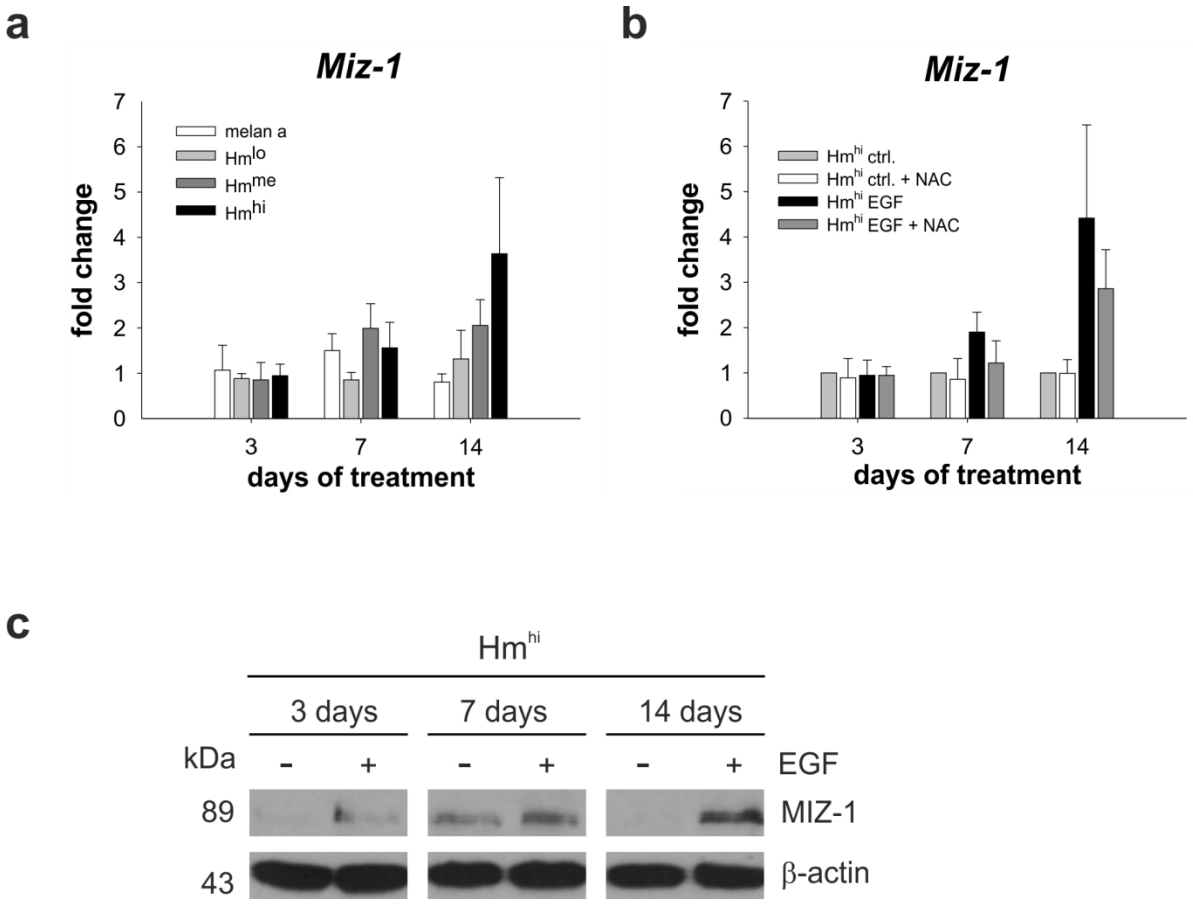

Figure 33: Activated HERmrk induces *Miz-1* on mRNA and protein level

(a) *Miz-1* qRT-PCR analyses for the parental cell line melan a, the non-senescing Hm-clones Hm^{lo} and Hm^{me} as well as the senescing Hm^{hi} melanocytes upon long-term EGF stimulation. Expression levels were normalized to *HPRT* and shown in reference to the serum-starved equivalent of each cell line. Bars depict the mean values of four independent experiments. Standard deviations are shown. (b) *Miz-1* qRT-PCR analyses for the the senescing Hm^{hi} clone upon long-term serum starvation (ctrl.) or EGF stimulation (EGF) in absence or presence of the ROS scavenger N-acetylcysteine (NAC). Expression levels were normalized to *HPRT*. Bars depict the mean values of four independent experiments. Standard deviations are shown. (c) MIZ-1 Western blot analysis of Hm^{hi} whole cell lysates upon 3, 7 and 14 days in culture in absence (-) or presence of EGF (EGF). β-actin served as loading control. Protein weights are indicated in kDa.

To elucidate the role of MIZ-1 in HERmrk-induced melanocyte senescence, I used Hm^{hi} clones stably expressing either an empty control vector (Hm^{hi}-pS, simply termed pS later on) or a shRNA directed against *Miz-1* (Hm^{hi}-pS-*Miz-1*, simply termed pS-*Miz-1* later on). Notably, both clones had been generated prior to my studies. Quantitative realtime PCR analyses proved *Miz-1* mRNA levels to be significantly down-regulated in pS-*Miz-1* cells compared to pS cells (*Figure 34*).

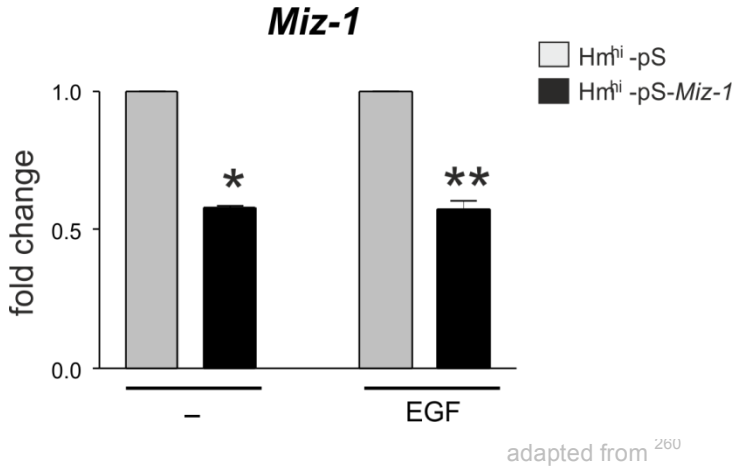

Figure 34: pS-Miz-1 significantly down-regulates *Miz-1* mRNA levels in Hm^{hi} cells
Miz-1 qRT-PCR analyses for Hm^{hi} cells stably expressing pS-Miz-1or the empty control vector (pS) after 3 days in culture. Where indicated, cells were cultured in starving medium alone (-) or supplemented with EGF (EGF). Expression levels were normalized to *HPRT* and shown in reference to pS. Bars depict the mean values of three independent experiments. Standard deviations are shown. Student´s t-test (paired, 2-tailed) revealed statistical significance indicated by asterisks (*p<0.05, **p<0.01, ***p<0.001).

Long-term stimulation assays revealed a senescence-protective effect of *Miz-1* knockdown on Hm^{hi} cells. Unlike Hm^{hi}-pS cells, which started to become enlarged and multinucleated after 3 days of EGF treatment, Hm^{hi}-pS-Miz-1 melanocytes did not become multinucleated regardless of EGF treatment duration (*Figure 35*).

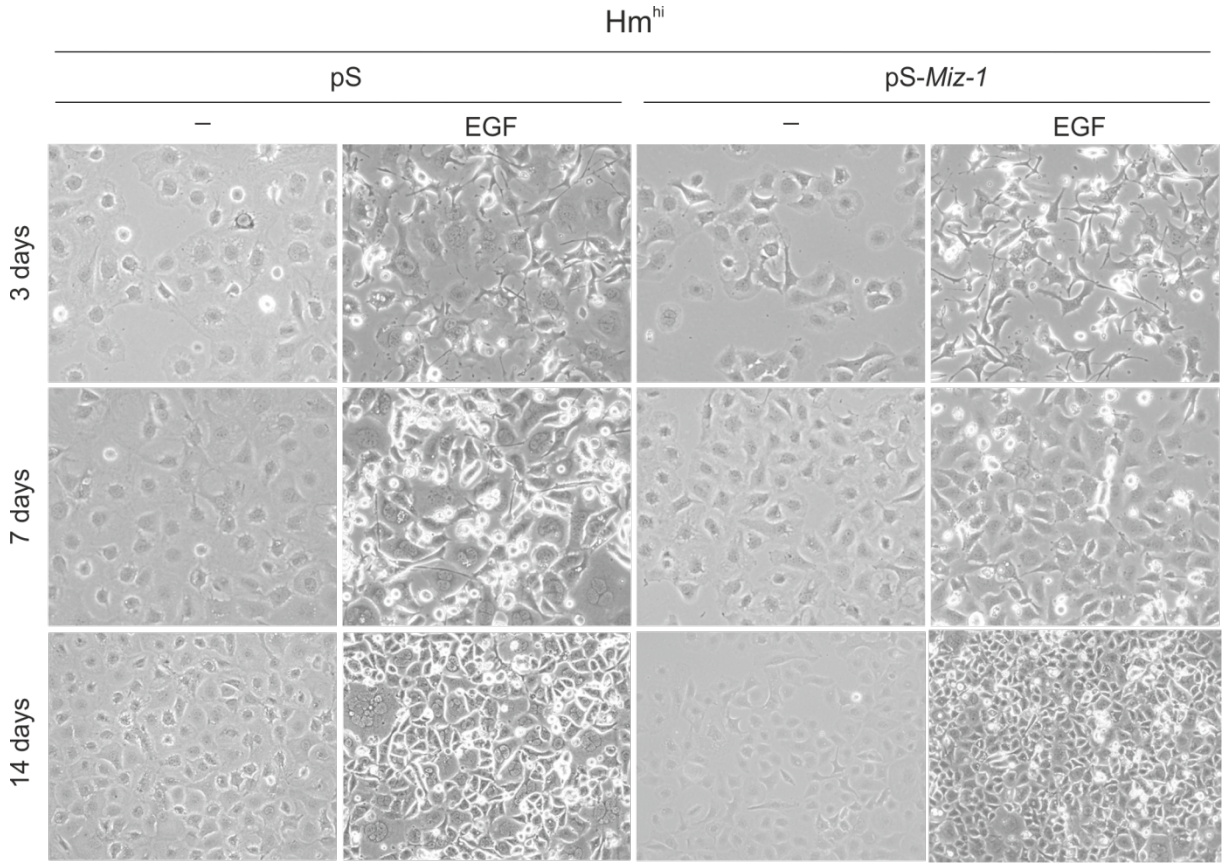

Figure 35: Long-term senescence assay comparing Hm^{hi}-pS and Hm^{hi}-pS-Miz-1 cells
Phase contrast images (100-fold magnification) comparing the cellular features of Hm^{hi} cells stably expressing pS or pS-Miz-1 in a long-term senescence assay. Where indicated, cells were cultured in starving medium alone (-) or supplemented with EGF (EGF).

To check and quantify the senescence extent in Hm^{hi}-pS and Hm^{hi}-pS-Miz-1 cells, SA-β-Gal stainings were performed. I found *Miz-1* knockdown to diminish HERmrk-induced senescence (*Figure 36*).

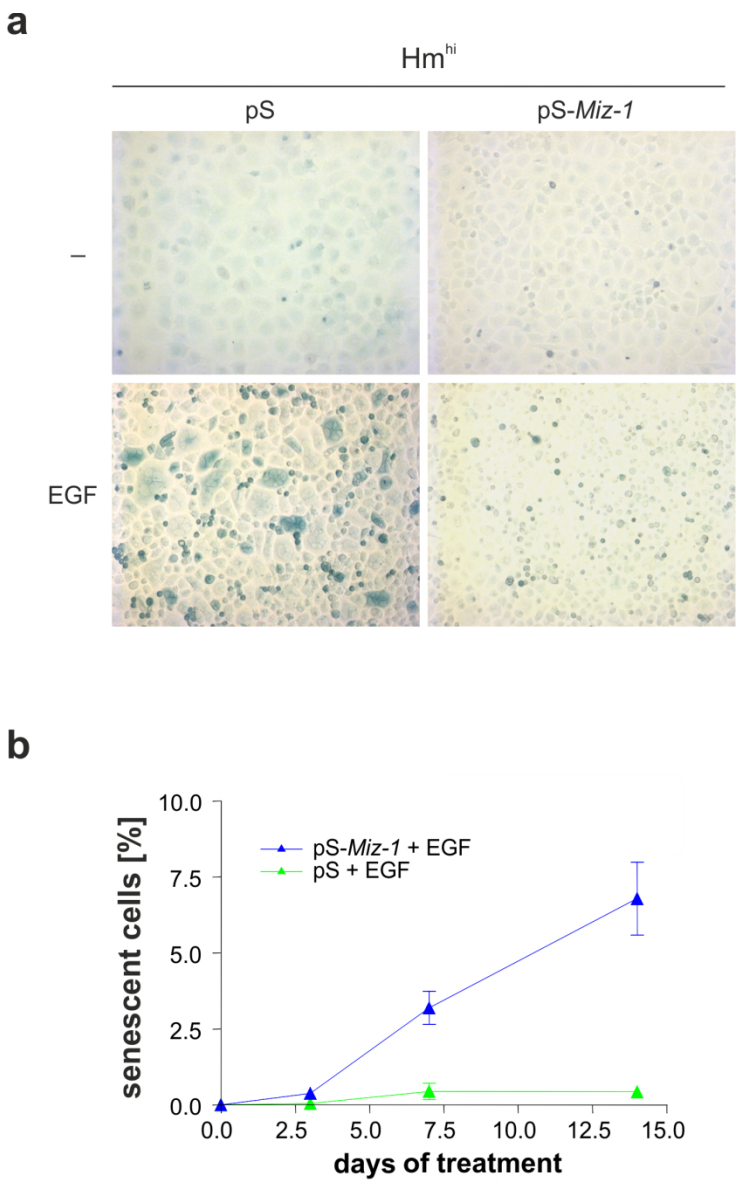

Figure 36: *Miz-1* knockdown diminishes HERmrk-induced senescence in Hm^{hi} cells
(a) Brightfield images (100-fold magnification) of SA-β-Gal-stained Hm^{hi}-pS and Hm^{hi}-pS-Miz-1 cells upon 14 days of treatment. Where indicated, cells were cultured in starving medium alone (-) or supplemented with EGF (EGF). (b) The graph depicts the proportion of multinucleated, SA-β-Gal-positive cells over time (mean values of three independent experiments; standard deviations are shown). *Miz-1* knockdown proved to diminish HERmrk-induced senescence in EGF-treated Hm^{hi} cells.

Not only did the stable *Miz-1* knockdown prevent HERmrk-induced senescence, it also significantly enhanced the proliferation potential of Hm^{hi} cells (*Figure 37*). Even though pS cells proliferated better in presence of EGF than when cultured in starving medium alone, the EGF-mediated proliferation boost observed for pS-Miz-1 cells was much stronger (*Figure 37a*).

Using a different visualisation of the same data an additional, interesting effect becomes clear: both pS and pS-Miz-1 cells reach a growth plateau when cultured in starving medium

alone (-) for about 8 days, whereas unlike pS cells, pS-Miz-1 do not stop to proliferate in presence of the growth stimulus EGF (*Figure 37b*).

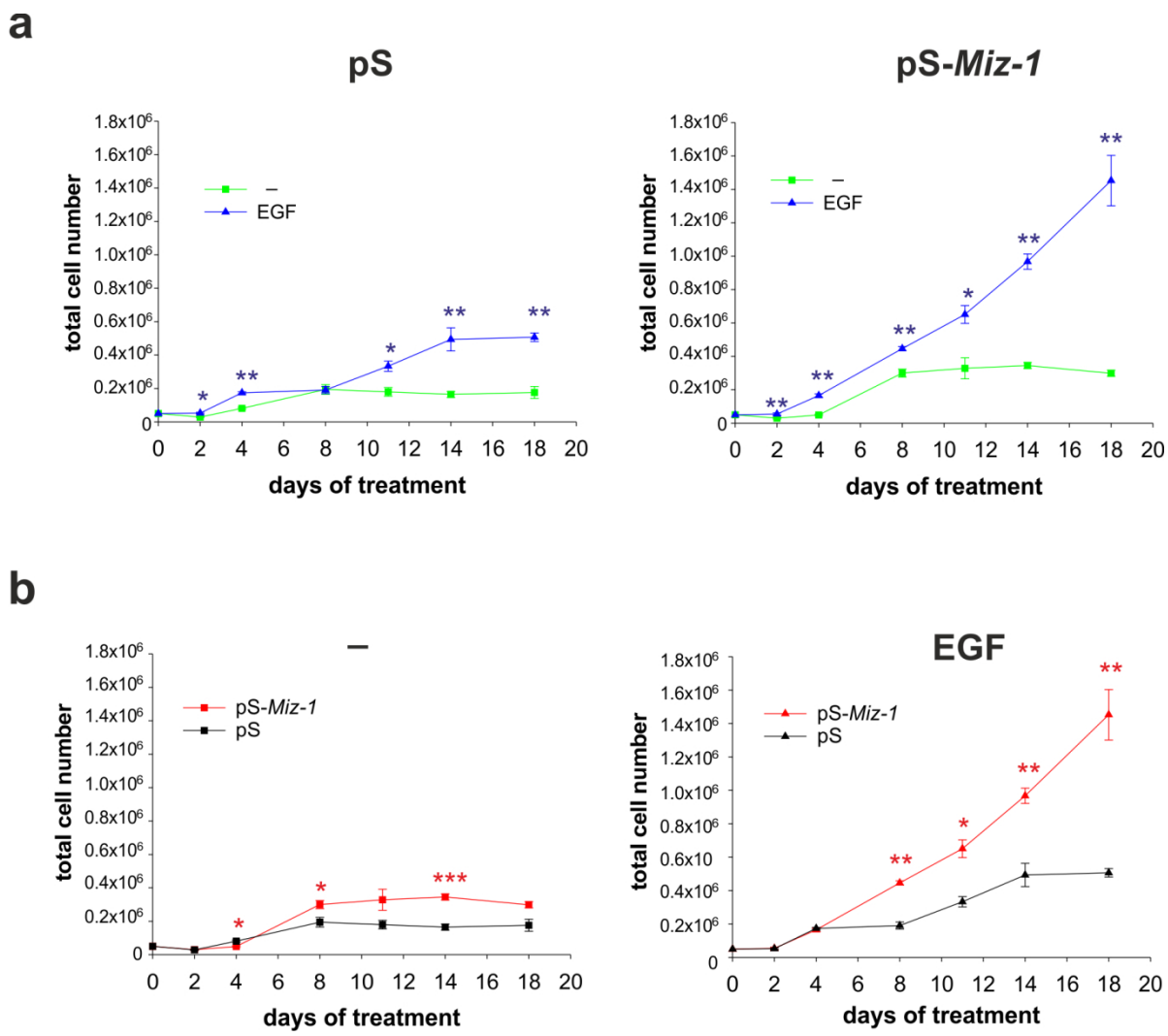

Figure 37: *Miz-1* knockdown enhances proliferation potential of Hm^{hi} cells

(a) Graphs depict the total cell number (mean values of three independent experiments) of Hm^{hi}-pS (pS) and Hm^{hi}-pS-Miz-1 (pS-Miz-1) cells over time in the absence (-) or presence of EGF (EGF). Student´s t-test (paired, 2-tailed) revealed statistical significance comparing starved (-) and EGF-stimulated (EGF) cells at each time point indicated by asterisks (*p<0.05, **p<0.01, ***p<0.001). (b) As in (a), but statistics compare starved (-) and EGF-stimulated (EGF) Hm^{hi}-pS cells with their Hm^{hi}-pS-Miz-1 counterparts at each time point.

To test whether the enhanced proliferation potential of Hm^{hi}-pS-Miz-1 cells correlated with an increase in tumourigenic capacity, soft-agar growth assays were performed (*Figure 38*). *Miz-1* knockdown enhanced the *in vivo* transformation potential by about 3-fold compared to Hm^{hi}-pS control cells upon EGF treatment. Notably, the colonies observed were much smaller than those formed in MYC-overexpressing Hm^{hi} cells.

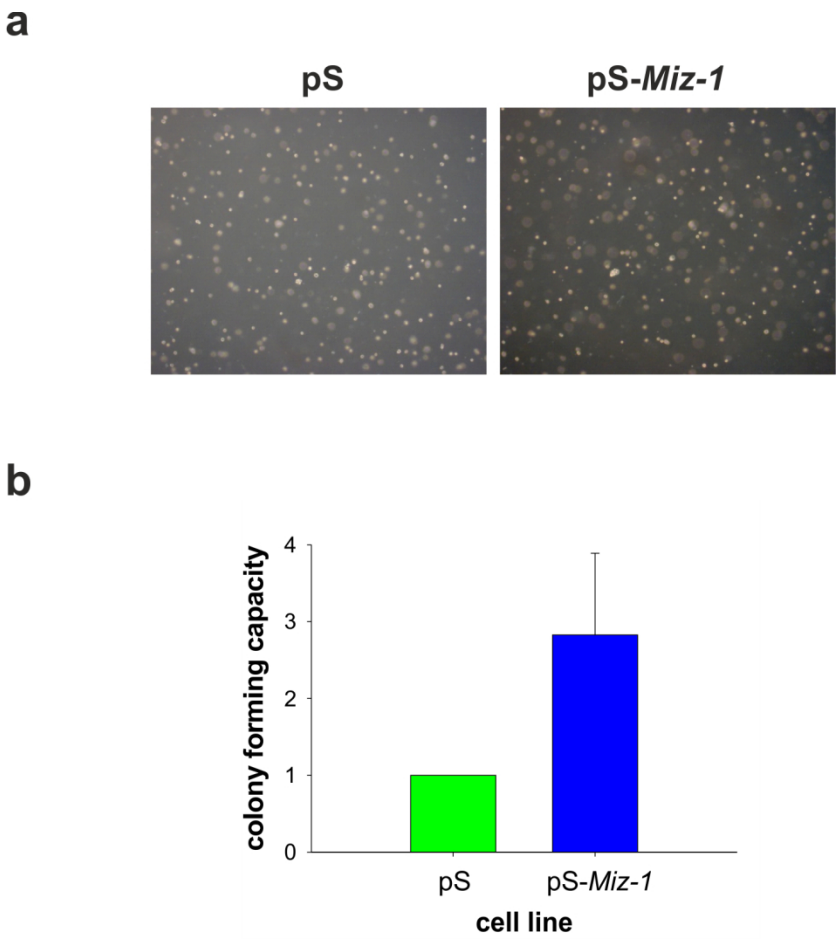

Figure 38: *Miz-1* knockdown enhances HERmrk-mediated tumourigenic potential
(a) Phase contrast images (25-fold magnification) of Hm^{hi} cells stably transfected with an empty control vector (pS) or a *Miz-1* knockdown plasmid (pS-Miz-1) upon 14 days in soft agar supplemented with EGF. (b) Graph depicts the transformation capacity of EGF-stimulated Hm^{hi}-pS-Miz-1 cells in reference to Hm^{hi}-pS cells. Bars represent the mean values of three independent experiments. Standard deviation is shown.

To investigate the influence of MIZ-1 on intracellular ROS levels, DCF-DA stainings were performed (*Figure 39*). While a strong DCF signal could be detected for Hm^{hi}-pS cells upon 10 days of EGF stimulation, only a minor fluorescence signal became evident in case of Hm^{hi}-pS-*Miz-1*. Besides, neither was a DCF signal detectable in serum-starved Hm^{hi}-pS cells nor in *Miz-1* knockdown melanocytes (pS-*Miz-1*).

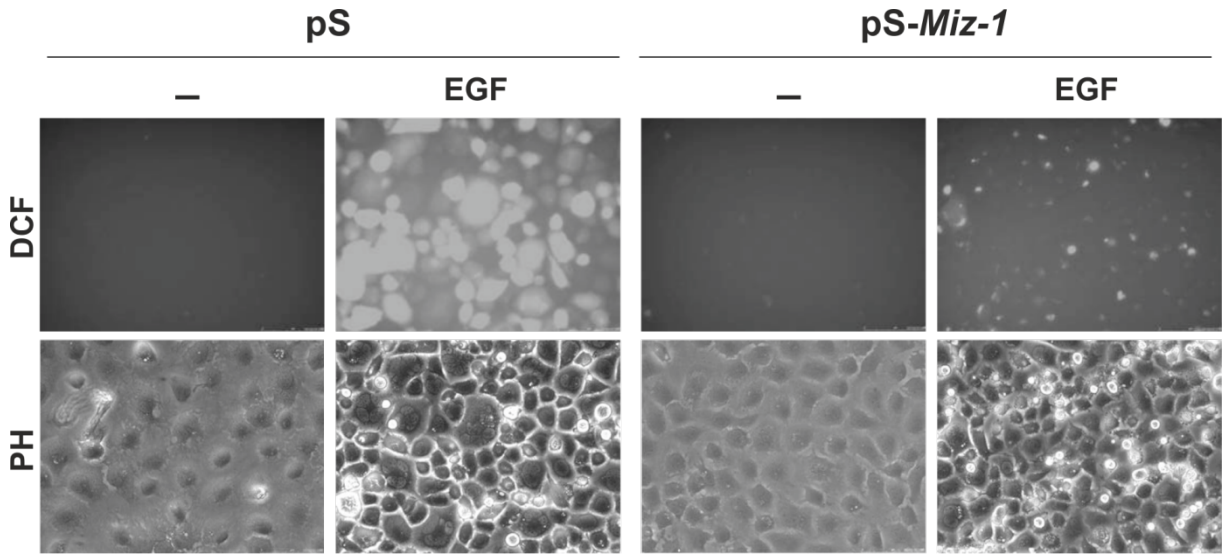

Figure 39: *Miz-1* knockdown counteracts HERmrk-induced ROS
DCF staining images (200-fold magnification; DCF) of Hm^{hi} cells stably transfected with an empty control vector (pS) or the *Miz-1* knockdown plasmid (pS-Miz-1) upon 10 days in culture. Where indicated, cells were cultured in starving medium alone (-) or stimulated with EGF. Corresponding phase contrast images (PH) are shown.

To test whether the ROS levels correlated with the DNA damage extent, I performed comet assays in alkaline conditions (*Figure 40*). Even though a background level of DNA damage was observed regardless of *Miz-1* expression status upon 14 days in starving medium (-), it became obvious that *Miz-1* knockdown limited the DNA damage effect upon EGF stimulation and subsequent HERmrk activation.

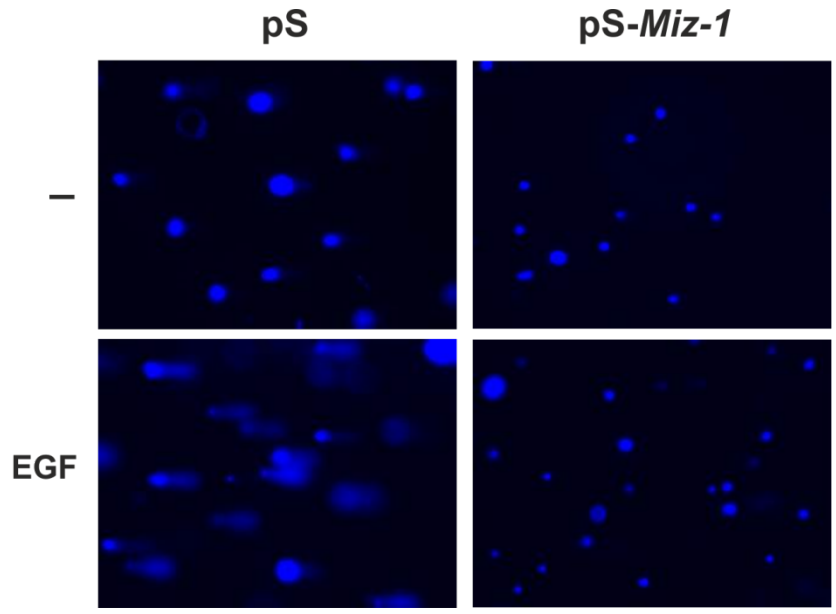

Figure 40: *Miz-1* knockdown counteracts HERmrk-induced DNA damage
Comet assay images (100-fold magnification) of Hm^{hi} cells stably transfected with an empty control vector (pS) or the *Miz-1* knockdown plasmid (pS-Miz-1) upon 14 days in culture. Where indicated, cells were cultured in starving medium alone (-) or stimulated with EGF. DNA was visualized using Hoechst 33342.

To identify the molecular mediators of senescence prevention upon Miz-1 knockdown, I performed Western blot analyses of the well-established MIZ-1 targets and senescence inducers $p15^{Ink4b}$, $p16^{Ink4a}$, $p19^{Arf}$ and $p21^{Cip1/Waf1}$ as well as the DNA damage markers P-p53, P-Chk1 and P-Chk2 and overall p53 as well as pRb protein (*Figure 41*). Surprisingly, I found equal or even higher protein levels of senescence inducers and their regulators upon Miz-1 knockdown (pS-*Miz-1*) in Hm^{hi} cells compared to the control (pS) within the first week of treatment. The only exception was hypophosphorylated, active pRb, whose level was lower in *Miz-1* knockdown cells. Moreover, upon 14 days of treatment, no more p21 could be detected regardless of *Miz-1* expression status. Besides, the protein levels of the DNA damage markers P-p53 and P-Chk2 as well as pRb levels were lower in *Miz-1* knockdown melanocytes.

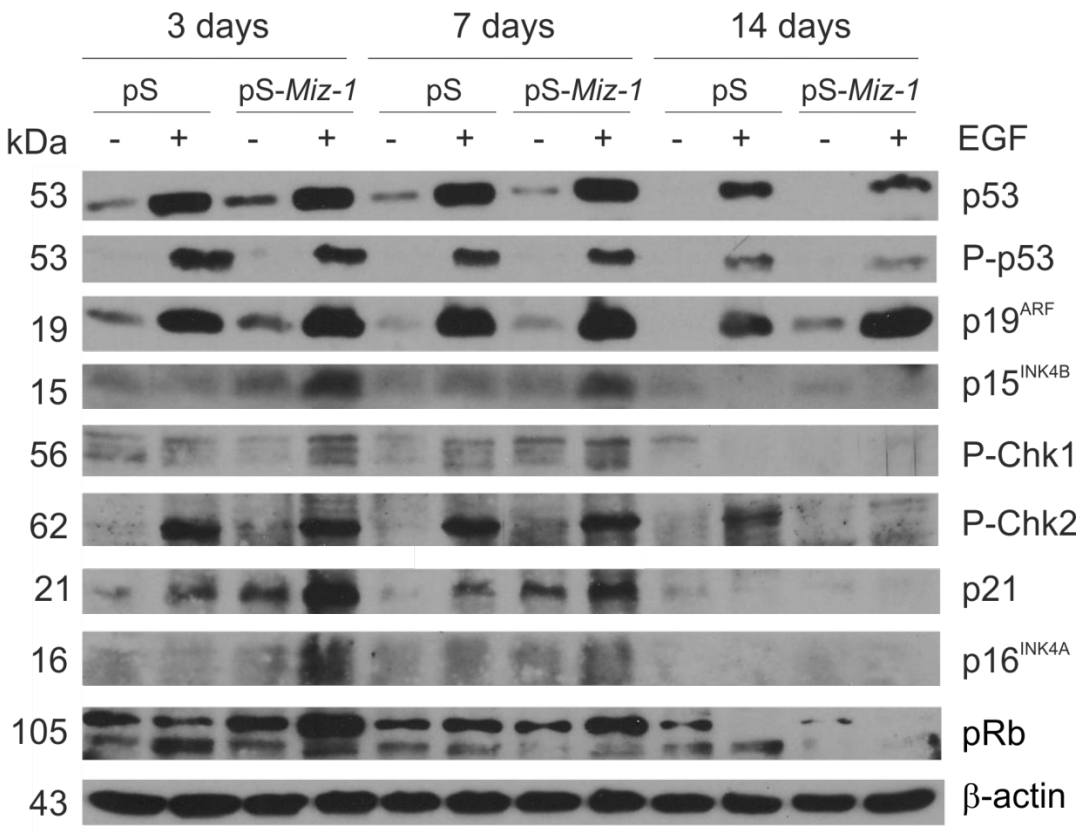

Figure 41: *Miz-1* knockdown does not diminish the protein levels of senescence inducers
Western blot analyses of Hm^{hi} cells stably transfected with an empty control vector (pS) or the *Miz-1* knockdown plasmid (pS-Miz-1) upon 3, 7 and 14 days in culture. Where indicated, cells were cultured in starving medium alone (-) or stimulated with EGF (EGF). Cells were harvested at indicated time points and whole cell lysates were separated using 10% SDS gels. Protein weights are indicated in kDa. β-actin served as loading control.

Taken together, *Miz-1* knockdown was not only found to diminish HERmrk-induced senescence, but also significantly enhanced the proliferation potential as well as the *in vitro* tumourigenic capacity of Hm^{hi} melanocytes. In accordance with these findings, *Miz-1* knockdown also limited ROS levels and DNA damage extent upon HERmrk activation. This was mirrored by the decreased amount of DNA damage markers P-p53 and P-Chk2 after 14 days of EGF stimulation. However, none of the classic MIZ-1 targets such as $p15^{Ink4b}$ or $p21^{Cip1/Waf1}$ went along with the senescence-protective effect of *Miz-1* knockdown in Hm^{hi} cells. Instead, protein expression levels of the monitored MIZ-1 targets were even higher upon *Miz-1* knockdown in Hm^{hi} melanocytes.

7.12 The impact of MYC overexpression and *Miz-1* knockdown on N-RAS*-induced melanocyte senescence

Since Xmrk was not the only oncogene we had shown to induce senescence in our melanocyte model, I was wondering whether N-RAS*-mediated senescence could also be influenced by MYC overexpression or *Miz-1* knockdown. Unfortunately, I could not use the melan a-N-RAS* cells we had analysed previously due to antibiotics resistance overlaps. Hence, I first transfected melan a cells with a doxycycline-inducible pTetON vector followed by a transfection with either the empty pTRE2hyg (ø) vector or pTRE2hyg-N-RAS^{61K}-flag (N-RAS*). Upon antibiotic selection, these cell lines were either transfected with pBabe (ctrl.) or pBabe-MYC-TA (MYC-TA) to investigate the influence of MYC overexpression (*Figure 42*) or with pRS (ctrl.) or pRS-sh*Miz-1* (sh*Miz-1*) to check for a possible role of *Miz-1* knockdown on N-RAS*-induced melanocyte senescence (*Figure 43*).

A long-term senescence assay revealed MYC-TA overexpression to strongly enhance melanocyte proliferation as well as pigmentation, the latter of which was abolished upon N-RAS* expression. Unfortunately, N-RAS* expression was not restricted to but could be increased by doxycycline (Dox) treatment as in presence of Dox cell density of N-RAS*-MYC-TA melanocytes was higher than in their starved (-) counterparts. Furthermore, N-RAS* melanocytes became multinucleated and SA-β-Gal-positive and cell density was much lower than in ø-cells. Nevertheless, some multinucleated cells remained when MYC-TA was overexpressed.

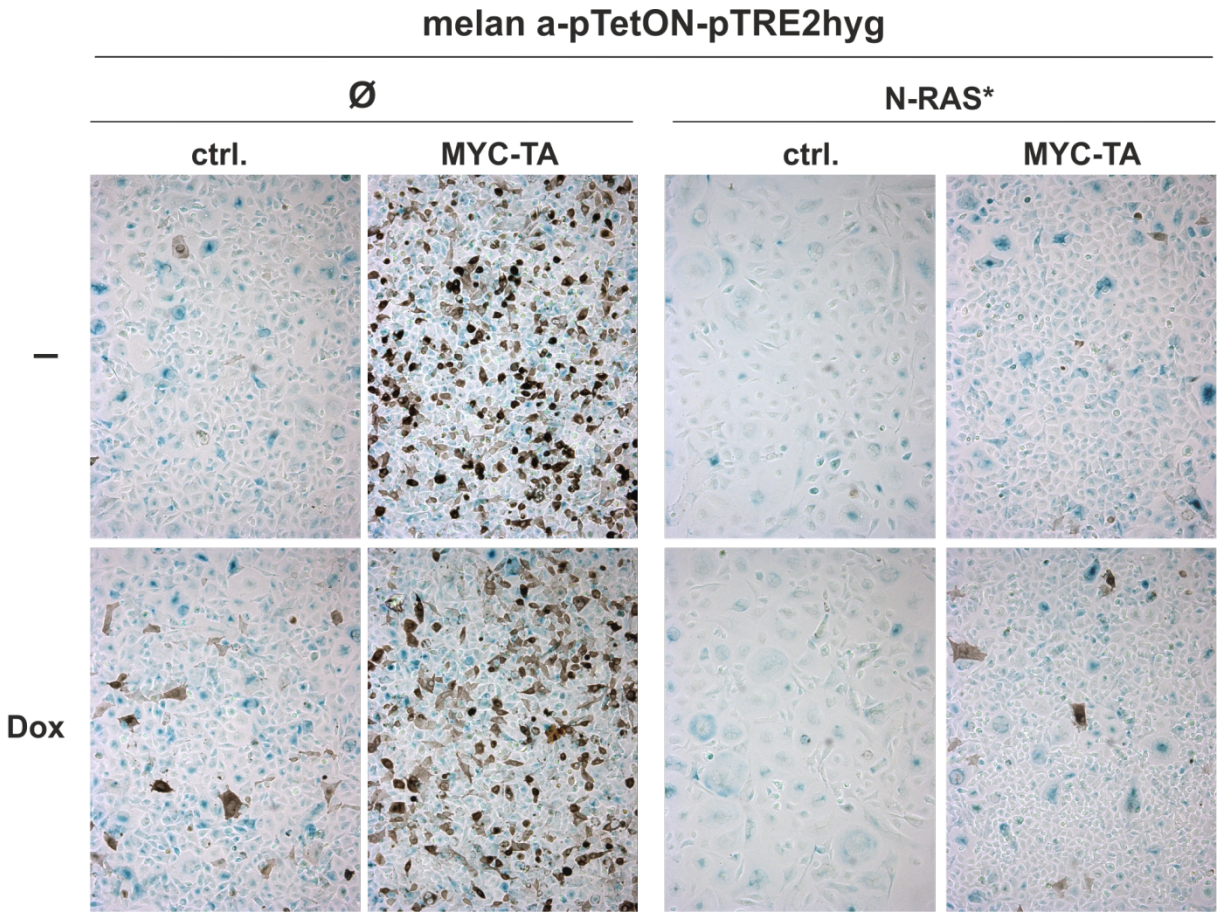

Figure 42: MYC overexpression counteracts N-RAS*-induced melanocyte senescence
Brightfield images (100-fold magnification) of SA-β-Gal-stained melan a-pTetON-pTRE2hyg and melan a-pTetON-pTRE2hyg-N-RAS* cells stably transfected with an empty control vector (ctrl.) or the MYC-TA overexpression plasmid (MYC-TA) upon 14 days in culture. Where indicated, cells were cultured in starving medium alone (-) or stimulated with doxycycline (Dox).

Hence, MYC overexpression counteracts N-RAS*-induced melanocyte senescence, while strongly enhancing the proliferation potential.

Similar to MYC-TA overexpression, did I find *Miz-1* knockdown to enhance melanocyte proliferation, but only when N-RAS* was expressed. Unfortunately, N-RAS* expression was once again not restricted to, but could be increased by doxycycline (Dox) treatment as in presence of Dox the number of multinucleated, SA-β-Gal-positive N-RAS*-ctrl melanocytes was higher than in their starved (-) counterparts. This N-RAS*-induced, multinucleated phenotype was diminished upon *Miz-1* knockdown.

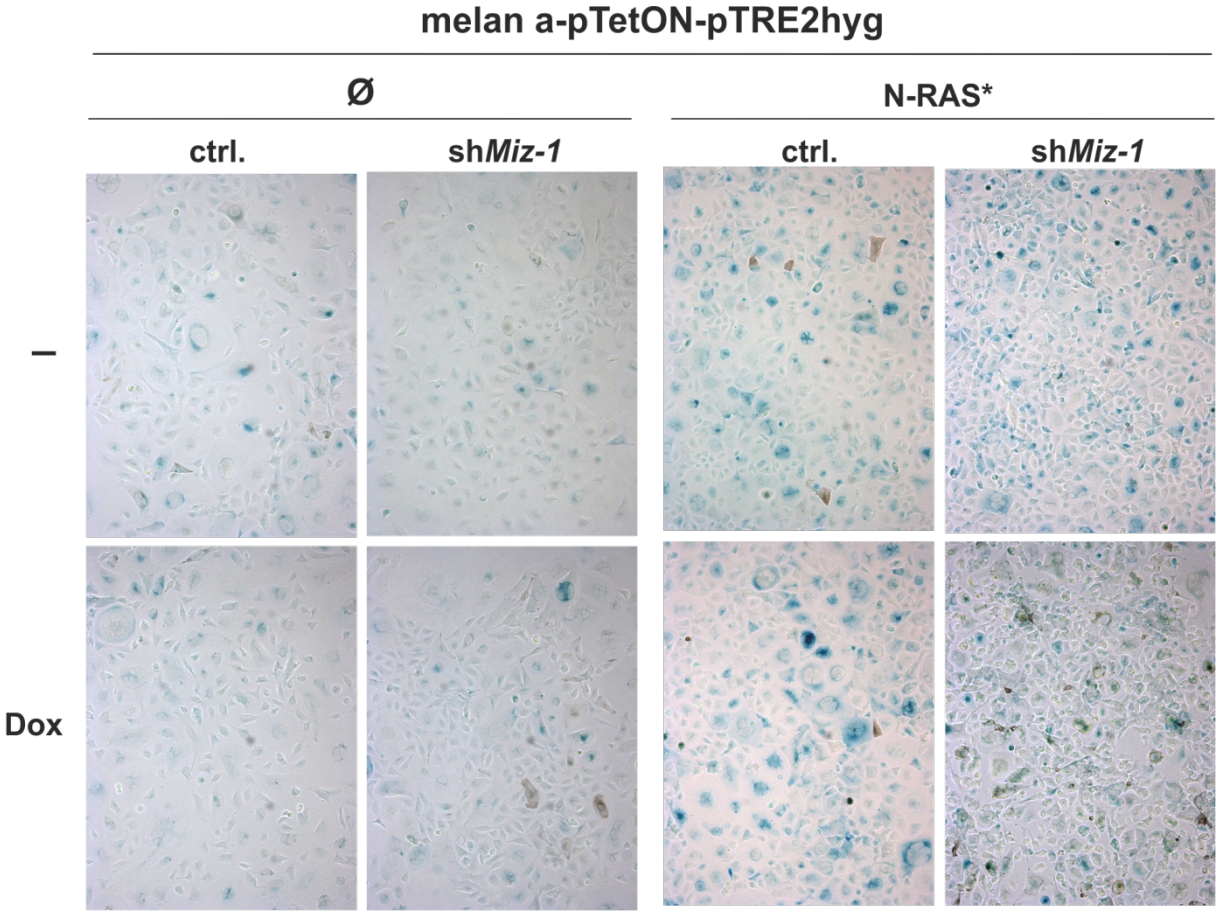

Figure 43: *Miz-1* knockdown counteracts N-RAS*-induced melanocyte senescence
Brightfield images (100-fold magnification) of SA-β-Gal-stained melan a-pTetON-pTRE2hyg and melan a-pTetON-pTRE2hyg-N-RAS* cells stably transfected with an empty control vector (ctrl.) or the *Miz-1* knockdown plasmid (shMiz-1) upon 14 days in culture. Where indicated, cells were cultured in starving medium alone (-) or stimulated with doxycycline (Dox).

Hence, *Miz-1* knockdown counteracts N-RAS*-induced melanocyte senescence, while enhancing the proliferation potential. Taken together, similar to our findings for Xmrk-induced senescence in Hm^{hi} cells, both MYC overexpression and *Miz-1* knockdown limit N-RAS*-induced senescence in melan a cells. However, the senescence extent in the melan-a-N-RAS* clones used for these experiments was much lower than in EGF-stimulated Hm^{hi} cells and quantification data is lacking.

7.13 CTH as a possible mediator of senescence-protective effect of MYC overexpression and Miz-1 knockdown in Hm^{hi} melanocytes

Having determined that MYC and MIZ-1 are regulators of senescence, we wanted to identify the molecular players underlying this phenomenon. To expand further analyses to a genome-wide level, an mRNA expression microarray was performed by Susanne Kneitz [Microarray Core Unit, IZKF (Interdisciplinary Center for Clinical Research), University of Wuerzburg, Wuerzburg, Germany], who compared unstimulated Hm^{hi} cells, Hm^{hi} cells + EGF, Hm^{hi}-MYC-TA cells + EGF, and Hm^{hi}-pS-*Miz1* cells + EGF. The mRNA samples used were prepared after 14 days of treatment, when EGF stimulation had already initiated senescence in Hm^{hi} cells. Six genes, represented by 7 Affymetrix Ids, were commonly upregulated by Miz1 knockdown or MYC-TA overexpression in comparison to the senescent controls. In literature, most of them are described to be associated with cancer progression (*Table 1*).

Table 1: Genes co-regulated by MIZ-1 and MYC in EGF-stimulated Hm^{hi} cells

Gene product	Features
S100A6	Ca^{2+} binding protein; high affinity to proteins of the p53 family; previously associated with senescence [261,262]
MAL **(myelin and lymphocyte protein)**	Proteolipid involved in membrane microdomains´ stabilization, transport machinery and signal transduction; aberrant expression in various cancer types (e.g. lymphomas, head and neck squamous cell carcinoma, breast, ovary) [263,264]
MSLN **(mesothelin)**	Cell surface antigen expressed on mesothelial cells; Aberrant expression in various cancer types (e.g. mesotheliomas, pancreas, ovary) [263,265]
TC1 **(thyroid cancer 1)**	highly expressed in thyroid cancer [266]; induced by heat shock, oxidative and other stresses [267]
GLIPR1 **(glioma pathogenesis-related 1)**	Secreted protein; matrix-interacting; tumour suppressive in prostate cancer [268]
CTH **(cystationase)**	Enzyme; synthesis of cysteine from methionine (transsulfuration pathway) [269]

To elucidate the roles of all these genes in preventing senescence, it will be necessary to perform in-depth biochemical studies.

Interestingly, *CTH* was the gene with the highest mRNA fold change found upon both MYC overexpression and *Miz-1* knockdown compared to EGF-stimulated Hm^{hi} cells. Moreover, reports state CTH to be crucial for the supply of cellular glutathione and taurine [270], thus contributing to ROS detoxification. Since we have identified ROS to be a crucial senescence mediator in our model [230] and ROS levels were found to be diminished upon MYC overexpression and *Miz-1* knockdown, *CTH* regulation by MYC and *Miz-1* might be linked to senescence.

7.14 CTH overexpression suppresses HERmrk-induced senescence and decreases melanocyte pigmentation

Thus, I transfected the parental cell line melan a as well as Hm^{hi} cells with either an empty pBabe control vector (ctrl.) or pBabe-*CTH* resulting in CTH overexpression before performing a long-term stimulation assay (*Figure 44*). Interestingly, CTH overexpression seemed to enhance the proliferation potential of melan a as well as Hm^{hi} cells after 14 days in culture regardless of EGF treatment. In addition, CTH overexpression suppressed the HERmrk-induced, multinucleated phenotype observed for EGF-stimulated Hm^{hi}-ctrl. cells. While a large proportion of Hm^{hi}-ctrl. cells had become enlarged and multinucleated upon 7 days of EGF treatment, only sporadic multinucleated melanocytes were observed when CTH was overexpressed.

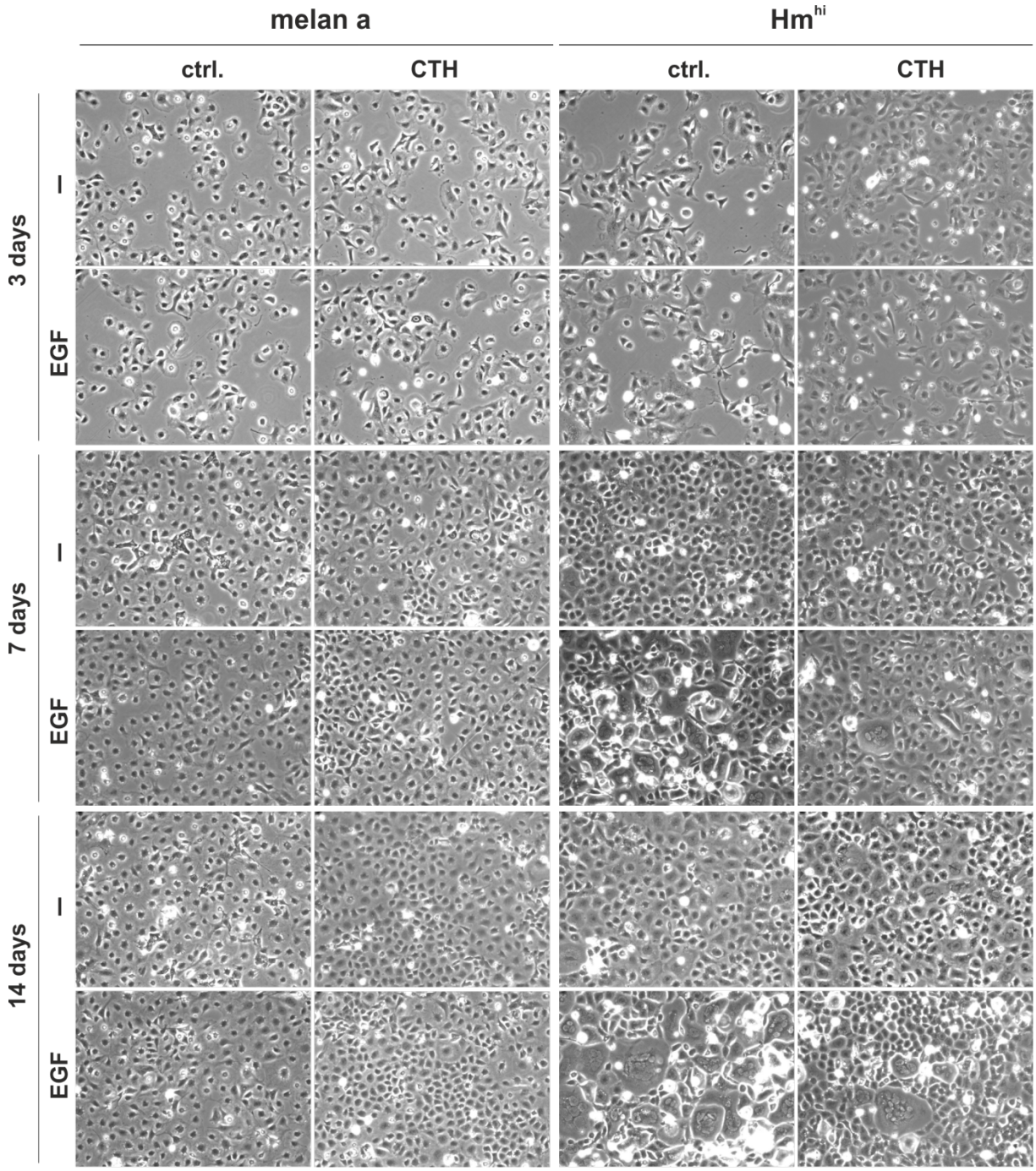

Figure 44: CTH overexpression suppresses Xmrk-induced melanocyte senescence
Phase contrast images (100-fold magnification) of melan a and Hm^{hi} cells stably transfected with an empty pBabe control vector (ctrl.) or the CTH overexpression plasmid pBabe-CTH (CTH) upon 3, 7 and 14 days in culture. Where indicated, cells were cultured in starving medium alone (-) or stimulated with EGF (EGF).

Wanting to compare the senescence extent after 14 days in culture, I performed a long-term senescence assay. SA-β-Gal stainings showed that senescence was largly suppressed by CTH overexpression in EGF-treated Hm^{hi} cells (*Figure 45a*). Hm^{hi} control (ctrl.) cells became multinucleated and SA-β-Gal-positive upon long-term EGF stimulation, while concurrent CTH

overexpression limited the multinucleated phenotype. Besides, no SA-β-Gal staining was detected in serum-starved (-) Hm^{hi} cells regardless of CTH's expression status.

Interestingly, CTH overexpression decreased the pigmentation of melan a cells in both absence and presence of EGF (*Figure 45b*). Since Hm^{hi} cells show hardly any pigmentation when cultured in starving medium, no difference in pigmentation intensity upon CTH overexpression became evident (data not shown).

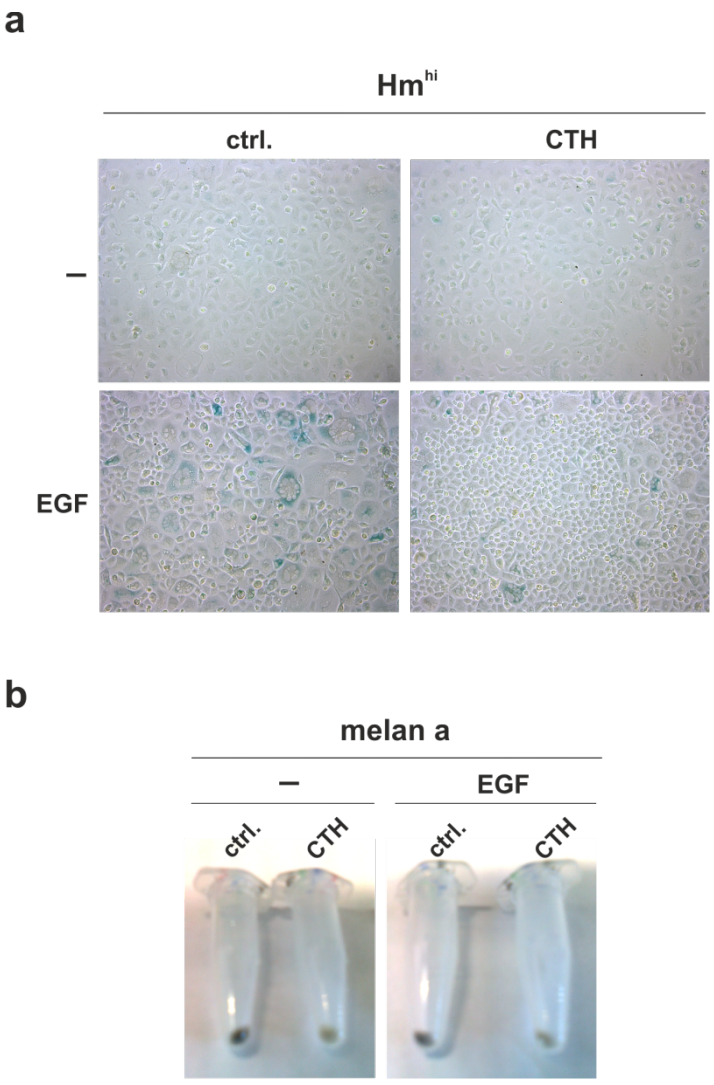

Figure 45: CTH overexpression suppresses HERmrk-induced melanocyte senescence and decreases melanocyte pigmentation

(a) Brightfield images (100-fold magnification) of SA-β-Gal-stained Hm^{hi} cells stably transfected with an empty pBabe control vector (ctrl.) or the CTH overexpression plasmid pBabe-CTH (CTH) upon 14 days in culture. Where indicated, cells were cultured in starving medium alone (-) or stimulated with EGF. (b) Pellets of melan a cells stably transfected with an empty pBabe control vector (ctrl.) or the CTH overexpression plasmid pBabe-CTH (CTH) upon 14 days in culture. Where indicated, cells were cultured in starving medium alone (-) or stimulated with EGF (EGF).

Taken together, it is safe to attribute CTH an important role in preventing ROS-induced senescence of Hm^{hi} cells.

7.15 HERmrk-induced senescent melanocytes are a source for highly proliferative, anoikis-resistant cells

Senescence is considered to be a tumour-protective mechanism and some groups even aim at senescence induction as a therapeutic target [271–273]. However, one should not neglect the fact that senescent cells secrete factors that promote the tumourigenic effect of neighbouring cells and cause inflammation [274–277].

The interesting and at the same time surprising part of my observations described in the first part of my thesis is the fact that I had found low and medium levels of the oncogene HERmrk to result in enhanced proliferation and tumourigenic potential of melanocytes, whereas high expression levels forced cells into senescence. However, *in vivo* the Xmrk expression level directly correlates with malignancy and melanoma progression [278]. These differences could either be attributed to *in vitro-in vivo* discrepancies or tackled in a scientific manner. I decided on the latter and investigated the effects of even longer oncogene activation on melanocytes (*Figure 46*). As expected, EGF-treated Hm^{hi} cells became multinucleated and SA-β-Gal-positive within 14 days of stimulation (*Figure 46a*). However, upon sustained EGF treatment, I observed nest-like structures consisting of small cells, which divided rapidly, overgrew the dish and finally formed 3D-structures (*Figure 46b*). Interestingly, it seemed that nests were found to arise predominantly in close proximity to a multinucleated cell (data not shown).

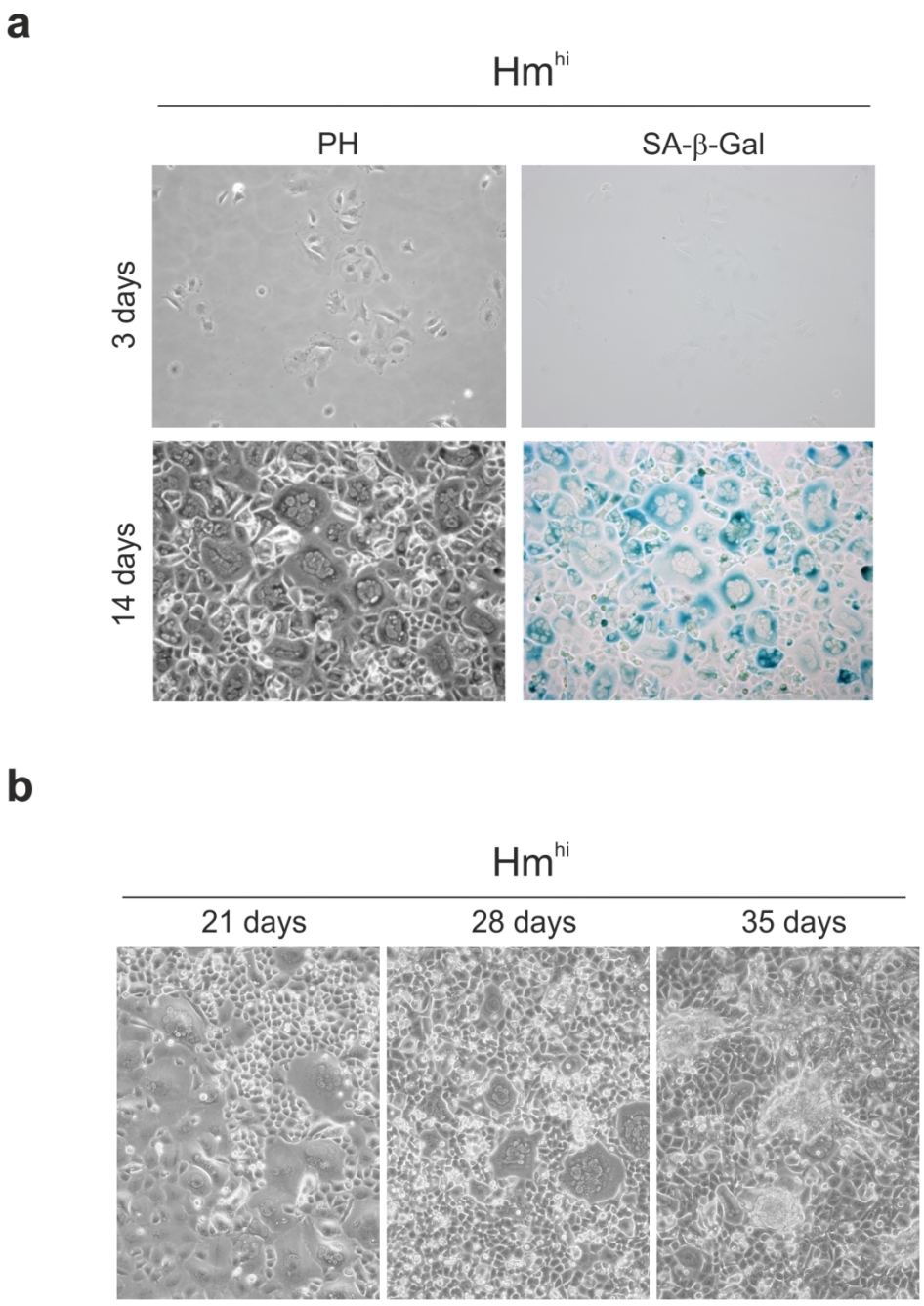

Figure 46: Sustained EGF treatment of multinucleated Hm^{hi} cells results in "nest" formation
(a) Phase contrast (PH) and brightfield images (100-fold magnification) of SA-β-Gal-stained Hm^{hi} cells stimulated with EGF upon 3 and 14 days in culture. (b) Phase contrast images of EGF-treated Hm^{hi} cells (100-fold magnification) at indicated time points.

7.16 Oncogene activation is the prerequisite for nest formation of Hm^{hi} melanocytes

To investigate whether long-term cultivation in starving medium alone is sufficient for the emergence of these nests, I performed further long-term assays comparing EGF-treated and starved Hm^{hi} cells (*Figure 47*). In starved Hm^{hi} cells, neither nest formation nor the appearance of small cells could be observed. Upon EGF stimulation, however, Hm^{hi} cells first became multinucleated before nests emerged. Even though multinucleated cells were still visible after 32 days in culture, the number and size of the nests steadily increased.

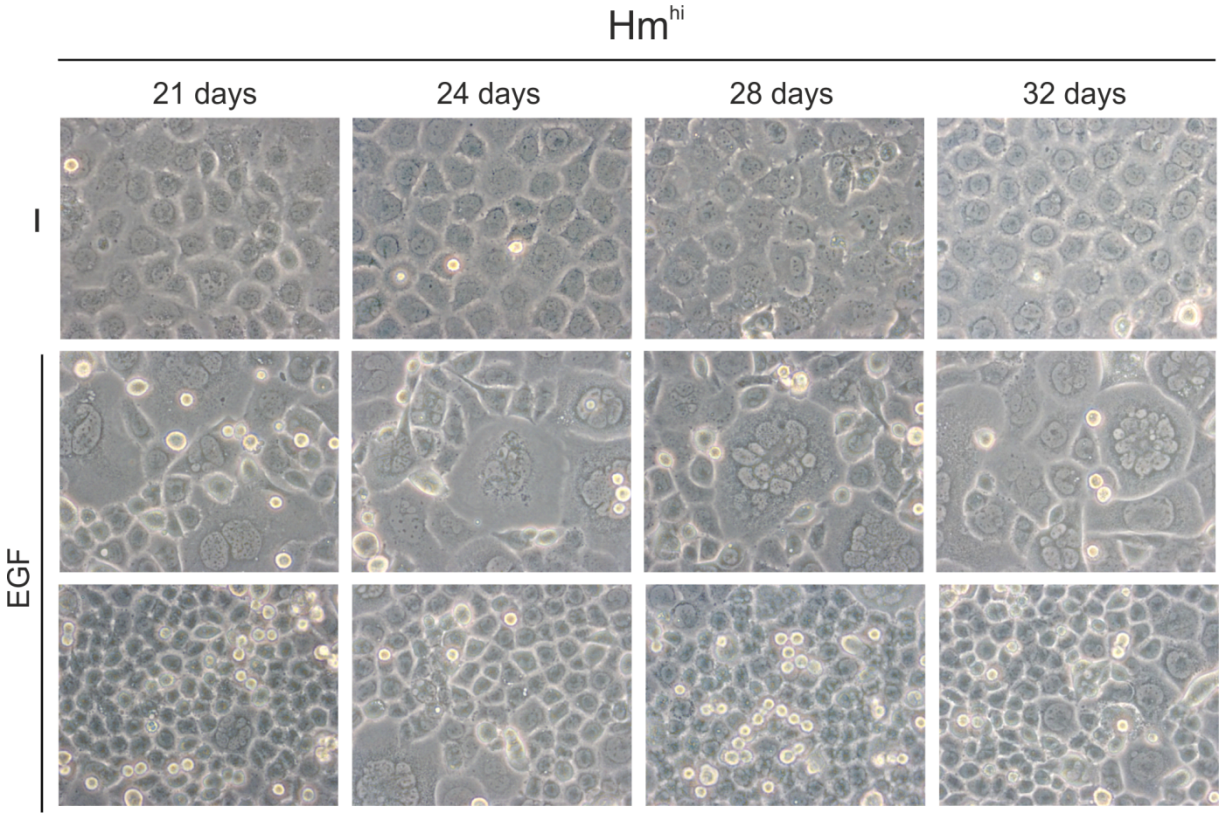

Figure 47: Appearance of "nest"-Hm^{hi} cells
Phase contrast images (320-fold magnification) of Hm^{hi} cells in a long-term senescence assay upon 21, 24, 28 and 32 days in culture. Where indicated, cells were cultured in starving medium alone (-) or stimulated with EGF (EGF). The upper EGF panel shows multinucleated Hm^{hi} cells and the lower one the smaller nest cells.

Taken together, HERmrk activation followed by multinucleation seems to be the prerequisite for nest formation.

7.17 *In vitro* transformation potential of Hm^{hi}-Neo cells

Since I wanted to further characterize these small, emerging cells, I picked different, large nests and transferred them into a 48-well plate using a pipette tip. I cultured these cells (Hm^{hi}-Neo-Pool) in complete medium before generating and raising single cell clones. The cells picked from a single nest were termed Hm^{hi}-Neo-Pool, single cell clones were numbered consecutively and the ones growing best in culture were chosen for further experiments. To compare the transformation potential of Hm^{hi}-Neo cells *in vitro*, soft agar assays were performed. Since Hm^{hi} cells showed no or only limited colony forming capacity in starving medium alone or supplemented with EGF, respectively, assays were performed in complete medium containing the growth stimulus TPA. Even though Hm^{hi} cells formed colonies in complete medium, the ones observed for the Hm^{hi}-Neo-Pools and the single cell clones were not only bigger but also more numerous (*Figure 48*).

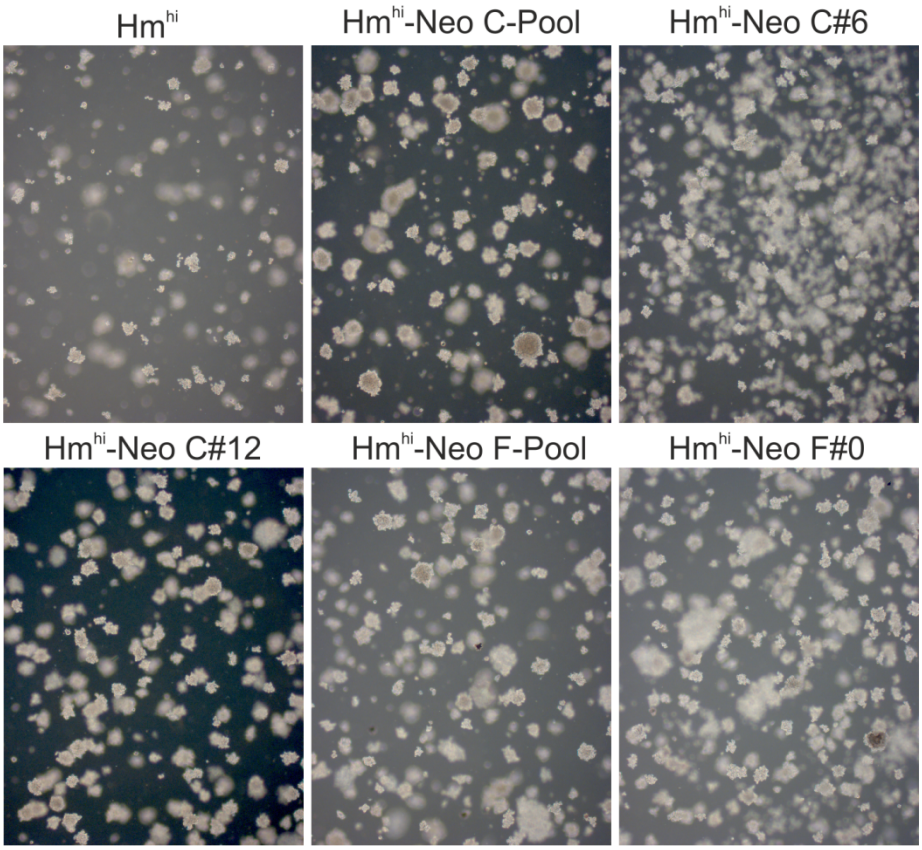

Figure 48: Hm^{hi}-Neo cells bear a higher transformation potential than Hm^{hi} cells in TPA-containing complete medium

Phase contrast images (25-fold magnification) of Hm^{hi} and Hm^{hi}-Neo cells upon 14 days in soft agar (complete medium).

7.18 Colony forming capacity in relation to culture media

Since Hm^{hi}-Neo cells seem to bear a higher transformation potential than Hm^{hi} cells in TPA-containing complete medium, I wanted to compare soft agar assays with serum-starved cells (*Figure 49*). To check whether colony formation was also possible without any growth stimulus, I performed assays using both starving medium and medium lacking TPA (D10). Notably, starving medium was supplemented with 10% dialyzed FCS, whereas D10 contains 10% FCS. Compared to FCS, dialyzed FCS contains significantly lower amounts of small molecules like amino acids, cytokines and hormones. The colony forming capacity of two Hm^{hi}-Neo clones was compared to Hm^{hi} and B16-F1 cells, a highly tumourigenic and metastatic melanoma cell line ^{279280}, was used as positive control.

None of the analysed cell lines formed colonies in starving medium. Besides, even though EGF treatment enabled colony formation in Hm^{hi} and Hm^{hi}-Neo cells, both number and size of the colonies observed was similar. When cells were cultured in D10-soft agar lacking TPA, colony formation was limited and no differences in colony number or size were observed comparing Hm^{hi} cells and the Hm^{hi}-Neo clones. Notably, the highly tumourigenic B16-F1 cells formed surprisingly few colonies in both D10 and complete medium even though B16-F1 cells can be cultured in either medium. However, Hm^{hi}-Neo F#8 cells showed many large colonies in complete medium, whereas clone E#8 formed fewer colonies than Hm^{hi} cells.

Taken together, soft agar assays indicated that Hm^{hi}-Neo cells are not able to form colonies in absence of growth stimuli. However, Hm^{hi}-Neo F#8 cells appear to be more tumourigenic than Hm^{hi} cells. Interestingly, the highly tumourigenic B16-F1 melanoma cells formed hardly any colonies.

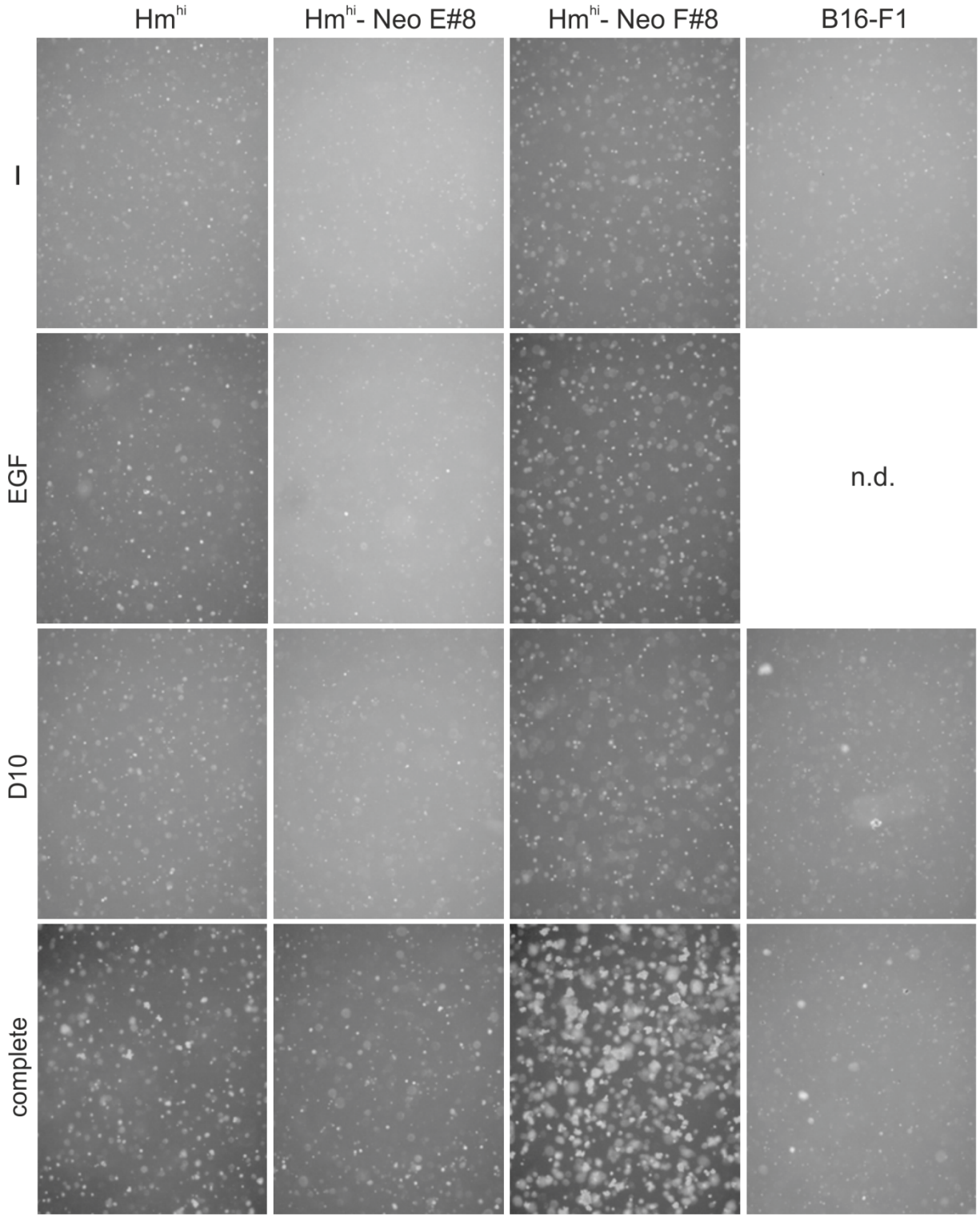

Figure 49: Increased transformation potential of Hm^{hi}-Neo compared to Hm^{hi} cells

Phase contrast images (25-fold magnification) of Hm^{hi}, Hm^{hi}-Neo E#8 and Hm^{hi}-Neo F#8 cells upon 14 days in soft agar. B16-F1 melanoma cells served as positive control. Where indicated cells were either cultured in starving medium alone (-) or supplemented with EGF (EGF) or with 10% FCS in absence (D10) or presence (complete) of TPA.

7.19 Features of Hm^{hi}-Neo clones in culture

Apart from the difference in cell size compared to Hm^{hi} cells, Hm^{hi}-Neo single cell clones also varied in shape and growth behaviour in culture (*Figure 50a*). Some clones had roundish cells (e.g. Hm^{hi}-Neo C#2 and Hm^{hi}-Neo E#9), others were spindle-shaped (e.g. Hm^{hi}-Neo F#5) and some grew in an extremely dense manner while cell borders became undistinguishable (Hm^{hi}-Neo E#8). Besides, most clones grew in an island-like manner (e.g. Hm^{hi}-Neo C#2 or Hm^{hi}-Neo E#8) whereby islands expanded outwards while island borders were rather even.

An even more fascinating observation was the rafts, an aggregate of two to several hundred viable cells, floating on the surface of the culture medium of Hm^{hi}-Neo clones (*Figure 50b*). These rafts came in different shapes and sizes and were found in all Neo clones. Interestingly, the rafts did not rely on high cell density on the dish, but were observed even when cell confluency on the main dish had not even reached 50%. Notably, these rafts could be replated and cultured.

Since Hm^{hi}-Neo C#6 cells grew rapidly in an island-like manner in complete culture medium while forming 3D-structures (*Figure 50c*) and rafts, I decided to use this cell clone to further scrutinize the cellular features of Hm^{hi}-Neo cells. Hence, from now on Hm^{hi}-Neo C#6 was termed Hm^{hi}-AR (anoikis resistant) and used for further experiments.

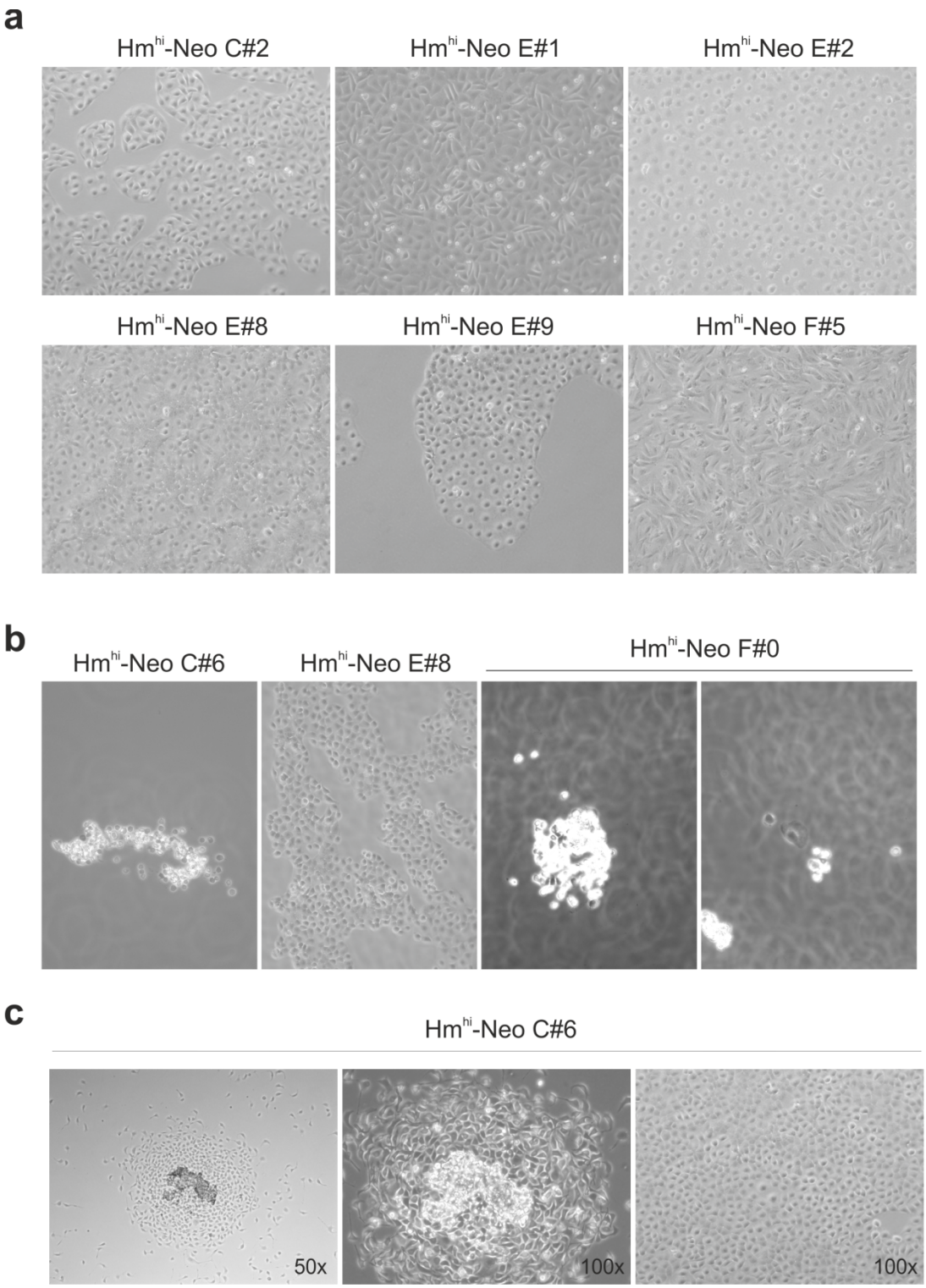

Figure 50: Hm^{hi}-Neo clones come in different shapes and generate cell rafts

(a) Phase contrast images (100-fold magnification) of different Hm^{hi}-Neo clones cultured in complete medium and (b) of cell rafts floating on the surface. (c) Phase contrast images (50- and 100-fold magnification) of Hm^{hi}-Neo C#6 cells cultured in complete medium.

7.20 Hm^{hi}-AR cells do not senesce upon oncogene activation

To check whether Hm^{hi}-AR cells still senesce when the HERmrk receptor is activated, I performed a long-term stimulation assay comparing melan a cells to Hm^{hi} and Hm^{hi}-AR cells. As expected, both control cell lines that were carried through the full long-term assay behaved as expected: melan a cells were indifferent to EGF treatment and Hm^{hi} cells became multinucleated. In clear contrast to these controls, Hm^{hi}-AR cells (*Figure 51*) showed enhanced proliferation upon EGF stimulation, but no large, multinucleated cells were observed. In addition, Hm^{hi}-AR cells also seemed to grow to a higher density than Hm^{hi} cells when cultured in starving medium alone (-).

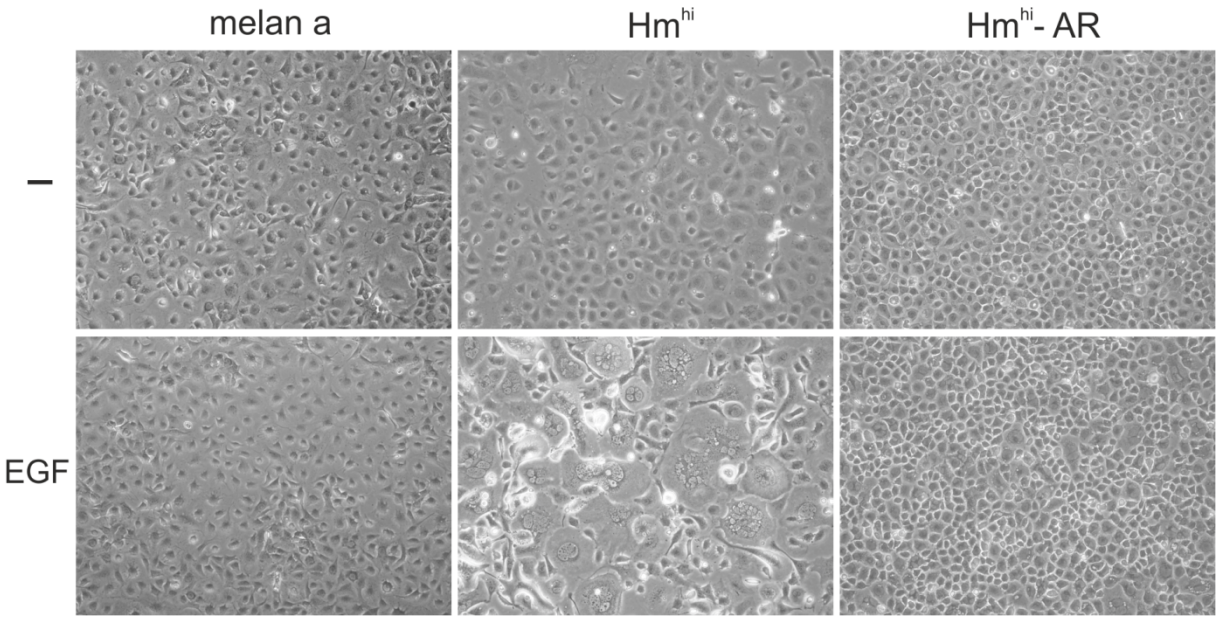

Figure 51: Hm^{hi}-AR cells do not form multinucleated cells upon EGF treatment
Phase contrast images (100-fold magnification) of melan a, Hm^{hi} and Hm^{hi}-AR cells upon 14 days in culture. Where indicated, cells were either cultured in starving medium alone (-) or supplemented with EGF (EGF).

Hence, in contrast to Hm^{hi} cells Hm^{hi}-AR cells do not seem to become multinucleated upon EGF treatment.

7.21 Lack of multinucleation for Hm^{hi}-AR cells cannot be overcome by sustained oncogene stimulation

To check whether the lack of large, multinucleated cells was just a matter of stimulation time, I continued the long-term stimulation assay comparing Hm^{hi} and Hm^{hi}-AR cells for up to 35 days (*Figure 52*). To illustrate the progression of cell growth behaviour throughout the complete assay, the images shown in *Figure 51* were included in the time-series shown in *Figure 52*. Clearly, there were no senescing Hm^{hi}-AR cells even upon long-term EGF treatment. Instead, Hm^{hi}-AR cells seemed to steadily increase the cell density on the dish in presence of EGF throughout the experiment, while their potential to grow in starving medium alone (-) appeared to be limited. Nevertheless, cell density seemed to be higher for starved Hm^{hi}-AR cells compared to their Hm^{hi} counterpart. EGF-treated Hm^{hi} cells once again became multinucleated upon EGF stimulation (14 days) before nests (21 days) followed by 3D-structures (35 days) were formed.

Taken together, Hm^{hi}-AR cells did not become multinucleated upon EGF treatment, but instead seemed to divide much faster than Hm^{hi} cells. The lack of multinucleated cells suggests that Hm^{hi}-AR cells do not undergo senescence.

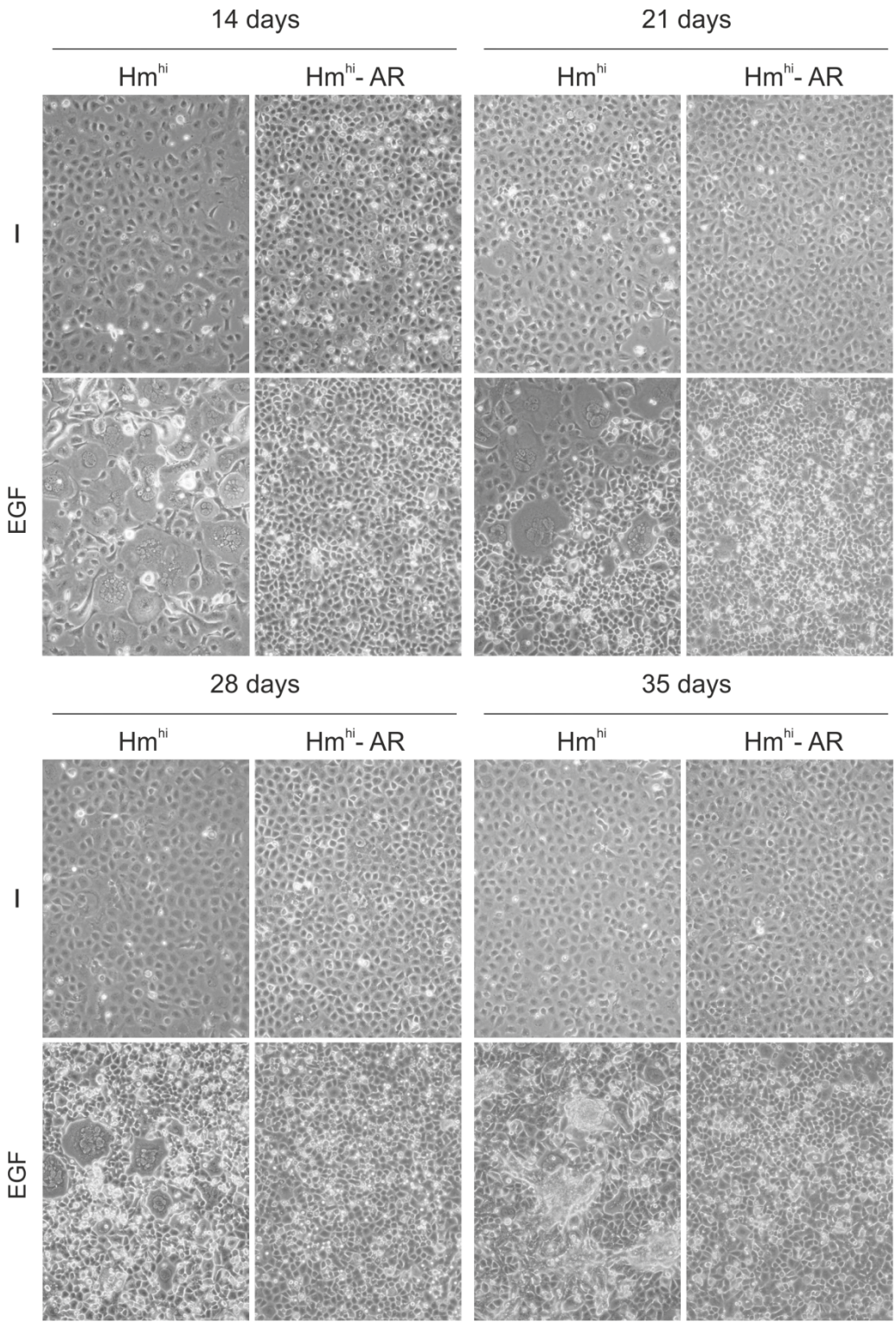

Figure 52: Hm^{hi}-AR cells do not form multinucleated cells upon long-term EGF treatment

Phase contrast images (100-fold magnification) of Hm^{hi} and Hm^{hi}-AR cells upon 14, 21, 28 and 35 days in culture. Where indicated, cells were either cultured in starving medium alone (-) or supplemented with EGF (EGF).

7.22 Hm^{hi}-AR cells show marker expression and nuclear-cytoplasmic ratios similar to those of stem cells

As the shape and size of Hm^{hi}-AR cells seemed to differ from that of Hm^{hi} cells, I wanted to quantify this phenomenon. Therefore, Dr. Toni Wagner (Department of Physiological Chemistry I, University of Wuerzburg, Wuerzburg, Germany) performed 3D confocal scans thereby determining the total cell volume and the nuclear volume, which enabled me to generate graphs and make the following figure (*Figure 53*). Even though in 2D images both cytoplasm and nucleus appeared smaller in Hm^{hi}-AR compared to Hm^{hi} cells (*Figure 53a*), measuring the compartment volumes disproved this assumption (*Figure 53b*). Interestingly, only cell and cytoplasm volume differed significantly when comparing Hm^{hi} to Hm^{hi}-AR cells, whereas the nuclear volumes of both cell lines were found to be very similar (*Figure 53b*). This fact results in a highly significant difference in the nuclear-cytoplasmic ratios of both cell clones, where Hm^{hi}-AR cells reached a 50% increase compared to Hm^{hi} cells (*Figure 53c*). Furthermore, we found Hm^{hi}-AR nuclei to be dome-shaped compared to the rather flat Hm^{hi} nuclei (*Figure 53d*). This finding explains the discrepancy between the apparently smaller nuclei of Hm^{hi}-AR compared to Hm^{hi} cells according to the 2D pictures (*Figure 53a*) and the actual, highly similar nuclear volumes depicted in the compartment graph (*Figure 53b*).

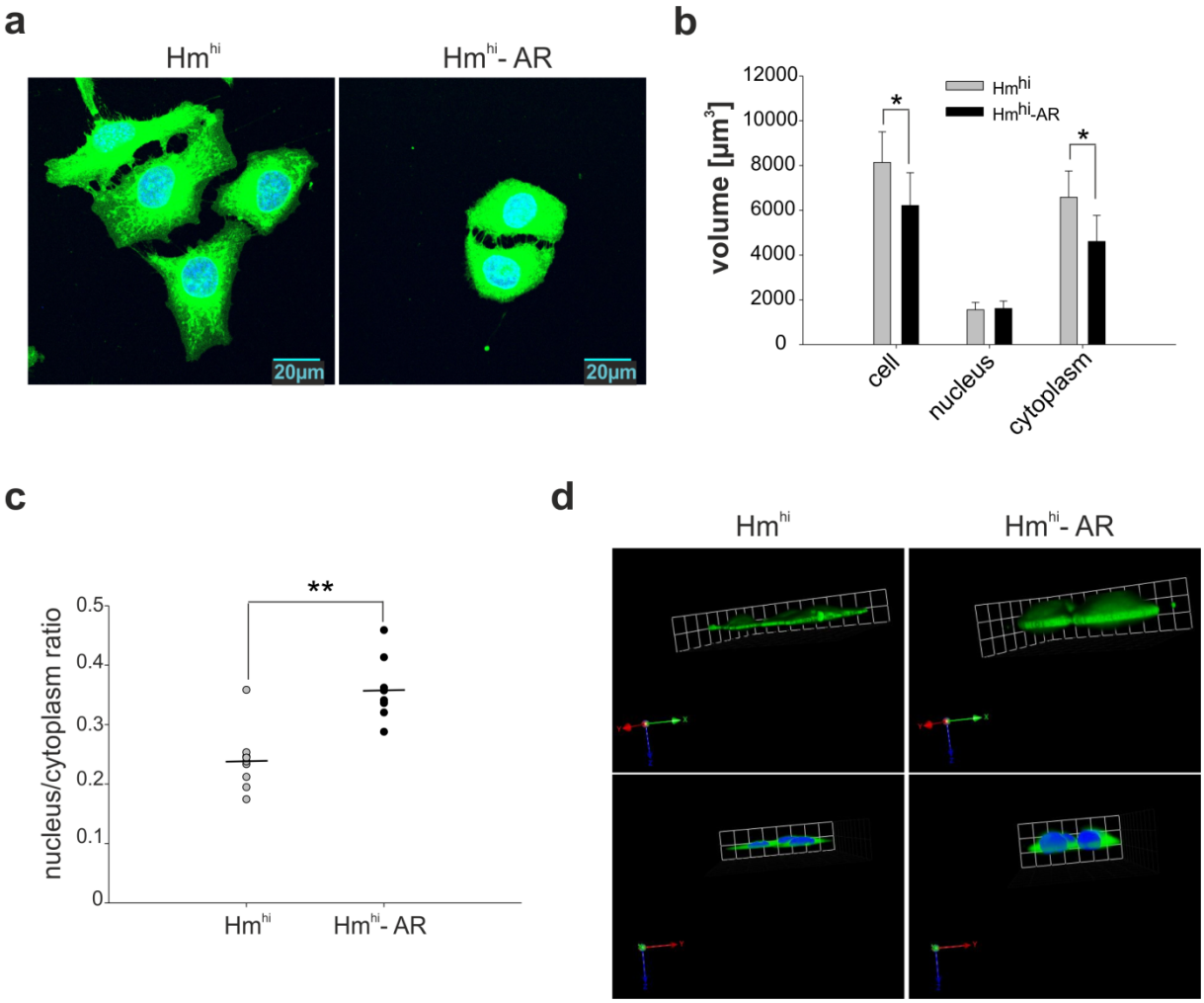

Figure 53: Hm^{hi}-AR cells are smaller and have a higher nuclear-cytoplasmic ratio than Hm^{hi} cells
(a) False colour 2D confocal snapshots (600-fold magnification) of Hm^{hi} and Hm^{hi}-AR cells plated onto glass cover slips and cultured in complete medium. The cytoplasm was stained with cell mask deep red and DNA was counterstained using Hoechst 33342. (b) Bars display the mean compartment volumes of 9 Hm^{hi} and Hm^{hi}-AR cells each. Standard deviations are shown. Where indicated, statistical significance determined by Student´s t-test (paired, two-tailed) was reached (*p<0.05). (c) Scatter plot displaying the nuclear-cytoplasmic ratios for all 9 single cells analysed for both Hm^{hi} and Hm^{hi}-AR. Vertical bars represent the mean values. Statistical significance determined by Student´s t-test (paired, two-tailed) was reached (**p<0.01). (d) Equally cropped false colour 3D stack images comparing the shape of Hm^{hi} and Hm^{hi}-AR cells. Upper and lower panels show cells at the same rotation point. Axes are shown in the lower left corner (x: green, y: red, z: blue).

Since high nuclear-cytoplasmic ratios are not only a prominent feature for aggressive tumour cells [281–283], but also a hallmark of stem cells [284–286], I was wondering whether Hm^{hi}-AR cells expressed stem cell markers. Thus, I transiently transfected both Hm^{hi} and Hm^{hi}-AR cells with the Nanog-driven PL-SIN-EOS-S(4+)-eGFP vector [287], a gift from James Ellis (University of Toronto, Canada) kindly provided by Dr. Toni Wagner (Department of Physiological Chemistry I, University of Wuerzburg, Biocenter, Am Hubland, Wuerzburg, Germany). I found Hm^{hi} cells to lack Nanog expression, whereas a large fraction of Hm^{hi}-AR cells expressed functional Nanog protein (*Figure 54a*). Applying the antibiotic puromycin, I could even select

and expand Nanog-expressing Hm^{hi}-AR (Hm^{hi}-AR-EOS) cells (*Figure 54b*), while Hm^{hi} cells did not survive the selection procedure. Western blot analyses revealed that Hm^{hi}-AR clones also expressed, apart from Nanog, the stem cell markers C-Myc and Oct4 at different levels, whereas Hm^{hi} cells lacked both Nanog and Oct4 protein expression while showing low levels of C-Myc. Hm^{hi}-AR-EOS cells expressed very high levels of C-Myc and Nanog, but Oct4 protein was hardly detectable (*Figure 54c*).

Nevertheless, it seems safe to conclude that Hm^{hi}-AR cells show marker expression and nuclear-cytoplasmic ratios similar to those of stem cells.

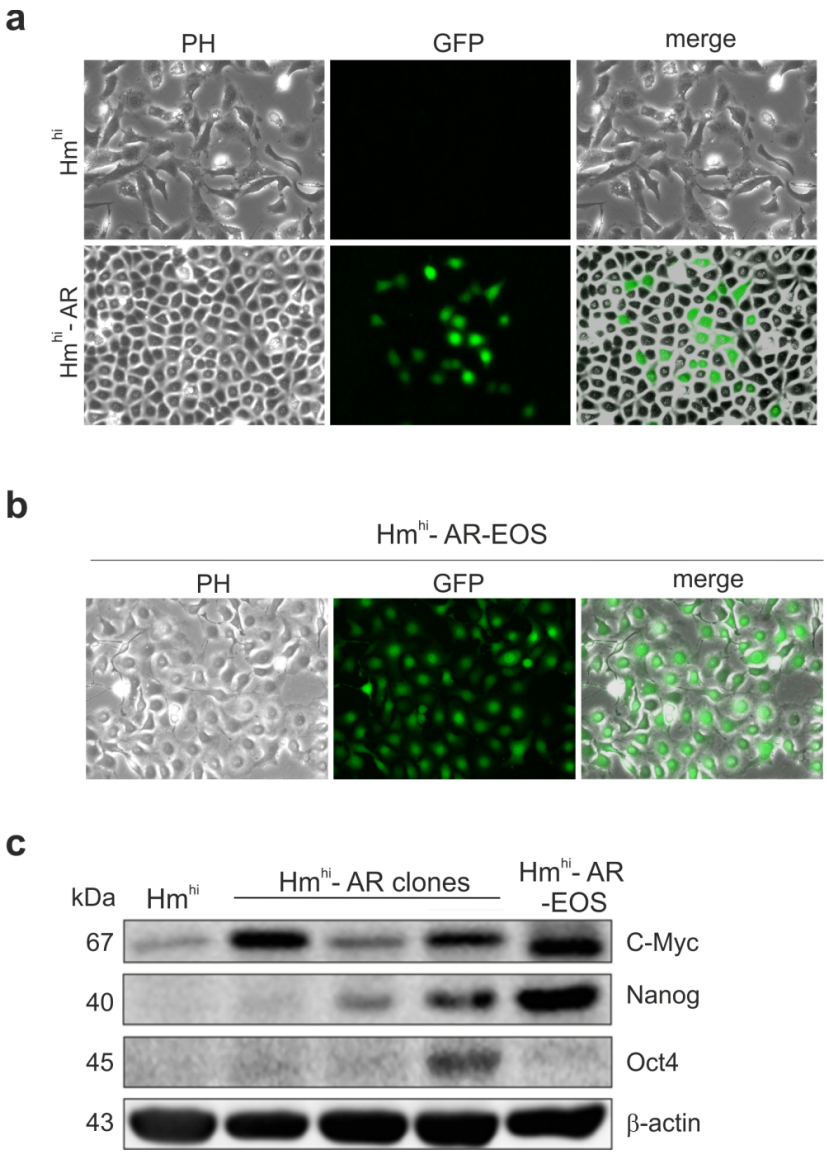

Figure 54: Hm^{hi}-AR cells express stem cell markers

(a) Phase contrast and fluorescence images (200-fold magnification) of Hm^{hi} and Hm^{hi}-AR cells transiently transfected with the Nanog-driven PL-SIN-EOS-S(4+)-eGFP vector and (b) of Hm^{hi}-AR cells stably expressing the PL-SIN-EOS-S(4+)-eGFP vector and therefore termed Hm^{hi}-AR-EOS. (c) Western blot analyses of Hm^{hi}, three different Hm^{hi}-AR clones and Hm^{hi}-AR-EOS cells cultured in complete medium. Cells were harvested and whole cell lysates were separated on 10-12% SDS gels. Protein weights are indicated in kDa. β-actin served as loading control.

7.23 HERmrk receptor and DNA damage level in Hm^{hi}-AR clones

To investigate whether the HERmrk receptor level correlates with the enhanced proliferation observed for Hm^{hi}-AR compared to Hm^{hi} cells, I performed Western blot analyses (*Figure 55*). I found some Hm^{hi}-AR clones to express extremely high Xmrk levels, whereas the third Hm^{hi}-AR clone showed a weaker protein band compared to Hm^{hi} cells (*Figure 55a*). Furthermore, for Hm^{hi}-AR-EOS cells, a medium Xmrk protein level could be detected (*Figure 55a*).

Interestingly, for the HERmrk high expressing Hm^{hi}-AR clones, the Xmrk expression level directly correlated with the detected protein level of the DNA damage markers P-p53 and P-Chk2 (*Figure 55b*). Notably, the protein levels of both DNA damage markers were higher in the Hm^{hi}-AR clone expressing low amounts of Xmrk compared to the DNA damage extent in Hm^{hi} control cells.

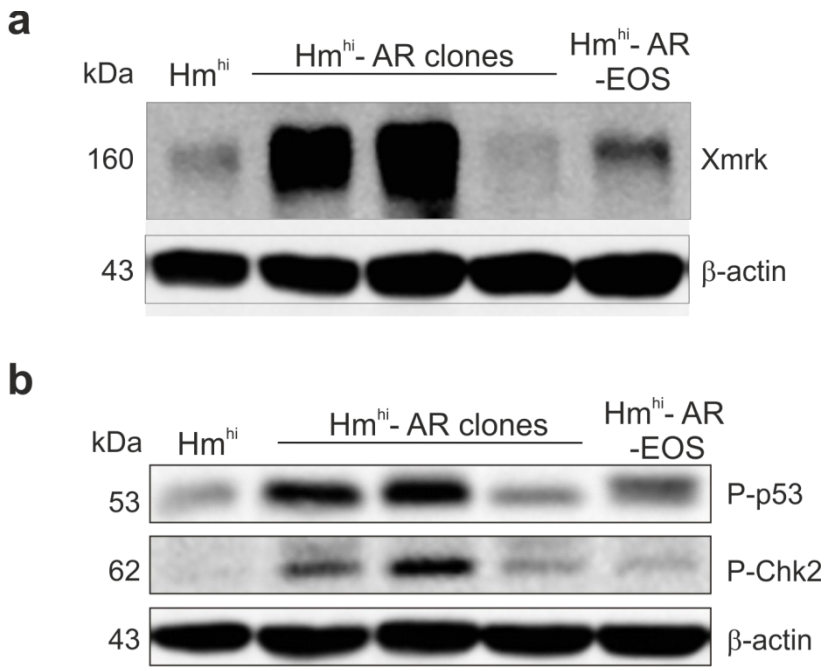

Figure 55: Hm^{hi}-AR clones express variable levels of HERmrk and DNA damage markers
Western blot analyses of (a) HERmrk expression levels and (b) the DNA damage markers P-p53 and P-Chk2 for Hm^{hi}, three different Hm^{hi}-AR clones and Hm^{hi}-AR-EOS cells cultured in complete medium. Cells were harvested and whole cell lysates were separated using 10% SDS gels. Protein weights are indicated in kDa. β-actin served as loading control.

Taken together, compared to Hm^{hi} cells, all Hm^{hi}-AR clones investigated expressed higher protein levels of DNA damage markers and most expressed very high HERmrk receptor levels.

7.24 *In vivo* transformation potential of Hm^{hi} and Hm^{hi}-AR cells

To see whether the enhanced proliferation and transformation capacity *in vitro* can be confirmed *in vivo*, we decided to inoculate Hm^{hi}-AR and melan a control cells into nude mice. Dr. Christoph Otto [Experimental Surgery, Experimental Transplantation Immunology, Clinic of General, Visceral, Vascular and Pediatric Surgery (Surgical Clinic I), University of Wuerzburg Hospital, Wuerzburg, Germany] and his technician Bettina Mühling performed the experiments using five animals each and subcutanously inoculating equal cell numbers in both flanks.

In melan a control (ctrl.) mice, the inoculated cells formed a nevus-like structure visible as a black dot at the site of inoculation (*Figure 56a*). However, neither visible nevus-like structures, nor tumours had been formed in Hm^{hi}-AR mice when the animals were sacrificed 71 days post inoculation (*Figure 56a*). Notably, in contrast to melan a control (ctrl.) cells, Hm^{hi}-AR cells showed no pigmentation. Nevertheless, within the final week prior to sacrifice, all five Hm^{hi}-AR mice suffered from significant weight loss (*Figure 56b*), showed a humpy back and wrinkled skin, most likely due to the loss of subcutaneous fat, while behaving normally [personal conversation with Bettina Mühling]. Interestingly, when Hm^{hi}-AR mice were opened up, we found the stomach of all animals to be strongly dilated (*Figure 56c*). Unfortunately, melan a control mice had already been sacrificed so we could only compare the stomach size to the ones of N-RAS* mice (N-RAS*) which had been kept in the absence of doxycycline and are discussed below (*Figure 56c*). The stomach of N-RAS* mice looked unsuspicious (*Figure 56c*).

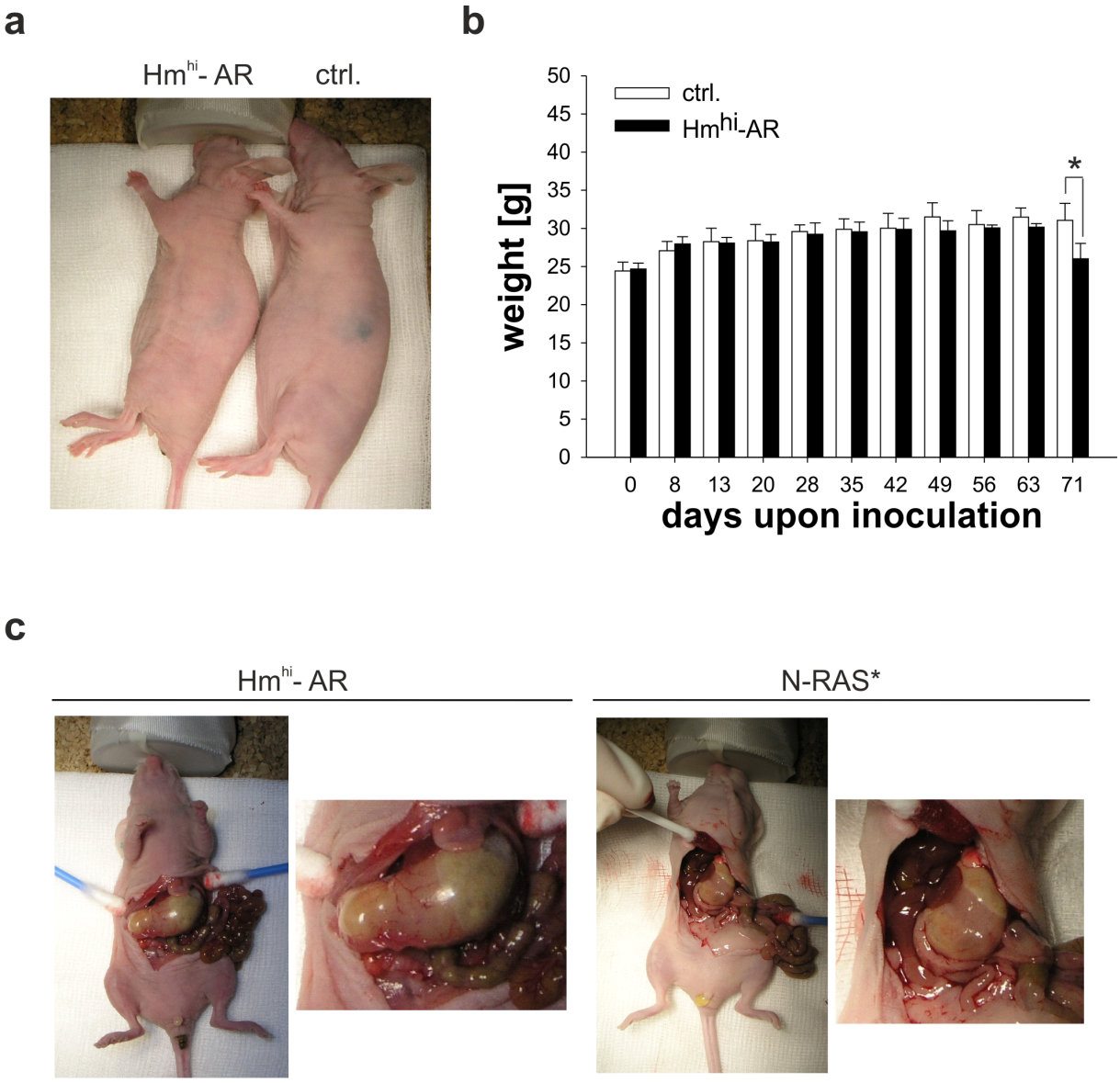

Figure 56: Hm^{hi}-AR cells do not induce rapid tumour growth in nude mice, but induce features of bad medical condition

(a) Comparison of nude mice either bearing melan a control (ctrl.) or Hm^{hi}-AR (Hm^{hi}-AR) cells 71 days upon inoculation. (b) Graph depicts the weight of melan a control (ctrl.) and Hm^{hi}-AR (Hm^{hi}-AR) mice over time. Bars represent the mean weight of five animals each. Standard deviations are shown. Statistical significance determined by Student´s t-test (paired, two-tailed) was reached 71 days upon inoculation (*$p<0.05$). (c) Comparison of nude mice stomachs 71 days upon inoculation of Hm^{hi}-AR (Hm^{hi}-AR) or N-RAS* (N-RAS*) cells. The N-RAS* mouse had been kept without doxycycline.

Taken together, melan a control (ctrl.) cells formed nevus-like structures upon inoculation into nude mice, while Hm^{hi}-AR cells led to a significant weight loss and unhealthy-looking mice even though no tumours were visible.

7.25 N-RAS*-induced senescent melanocytes are a source for highly proliferative, anoikis-resistant, tumourigenic and de-differentiated cells

Since apart from HERmrk, we had identified N-RAS* to induce senescence in melanocytes [230], I wanted to know whether sustained doxycycline treatment also resulted in overgrowth of senescent cells and nest formation. Hence, I performed a long-term stimulation assay using N-RAS* cells. As expected, just like EGF-stimulated Hm^{hi} cells, doxycycline-treated N-RAS* cells became multinucleated and SA-β-Gal-positive within 14 days of stimulation (*Figure 57a*). However, upon sustained doxycycline treatment, I observed nest-like structures consisting of small cells, which divided rapidly, overgrew the dish and finally formed 3D-structures (*Figure 57b*). Once again, all nests were found to arise in close proximity to a multinucleated cell. Importantly, in doxycycline-treated N-RAS* cells, nest formation occurred much more rapidly than in EGF-stimulated Hm^{hi} cells. Besides, the N-RAS* nest-forming cells appeared to be even smaller than Hm^{hi}-AR cells and the 3D structures overgrowing the dish were much more impressive compared to those observed in EGF-treated Hm^{hi} cells.

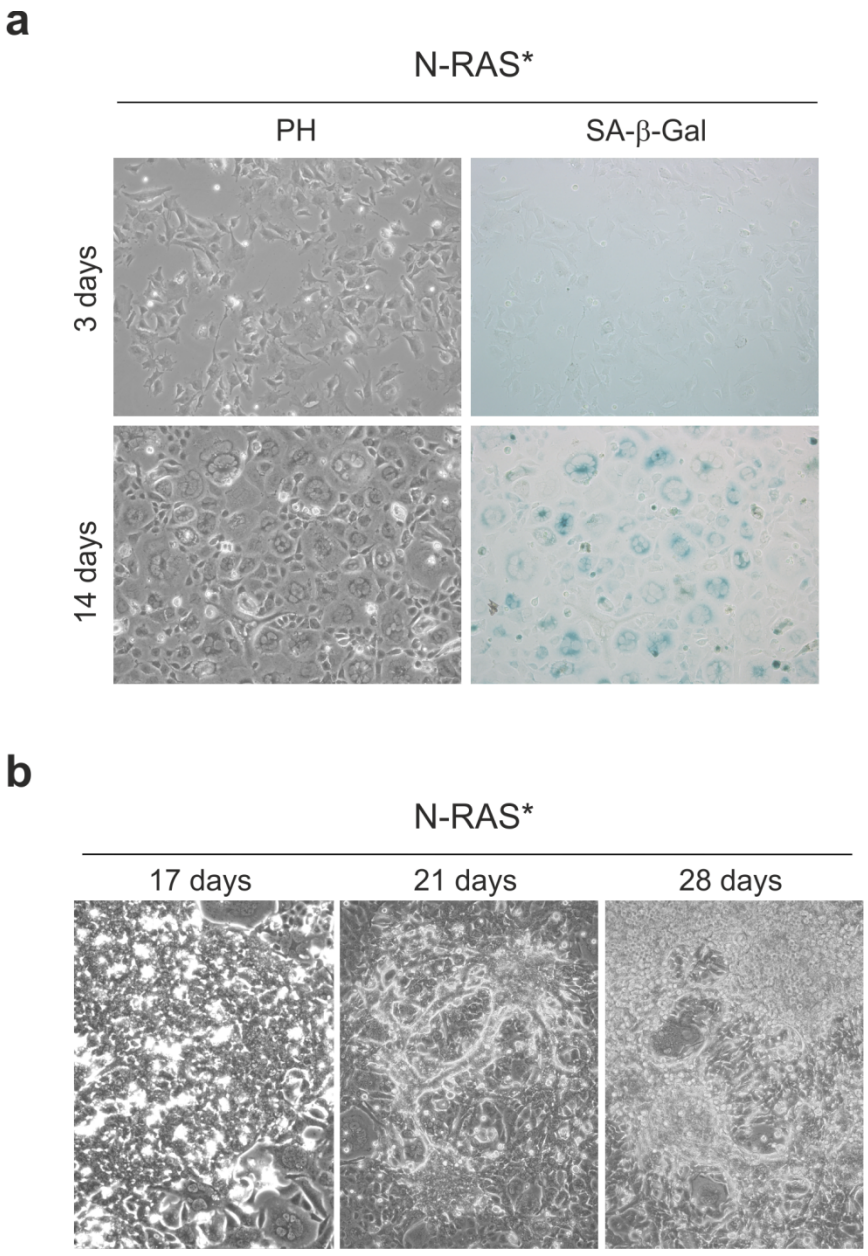

Figure 57: Sustained Dox treatment of multinucleated N-RAS* cells results in "nest" formation
(a) Phase contrast (PH) and brightfield images (100-fold magnification) of SA-β-Gal-stained N-RAS* cells stimulated with doxycycline (Dox) upon 3 and 14 days in culture. (b) Phase contrast images of doxycycline-treated N-RAS* cells (100-fold magnification) at indicated time points.

Since I wanted to further characterize these small, emerging cells, I once again picked different, large nests and transferred cells into a 48-well plate with the help of a pipette tip. I cultured these cells (N-RAS*-Neo-Pool) in complete medium before generating and raising single cell clones. The cells picked from a single nest were termed N-RAS*-Neo-Pool, single cell clones were numbered consecutively and the ones growing best in culture were chosen for further experiments.

7.26 Features of N-RAS*-Neo single cell clones

These N-RAS*-Neo single cell clones either grew in an island-like manner (e.g. N-RAS*-Neo C#4 or N-RAS*-Neo D#1) or formed nest-like structures (e.g. N-RAS*-Neo E#2 or N-RAS*-Neo E#4) (*Figure 58a*).

As N-RAS*-Neo-Pool cells cultured in complete medium formed rafts similar to those observed for Hm^{hi}-Neo cells, I replated the supernatant cells, expanded them and termed the cells N-RAS*-AR-Pool (for anoikis resistant) (*Figure 58b*). N-RAS*-AR-Pool cells again formed rafts, cell clumps and single cells were floating in the supernatant. Once again, I replated these cells, termed them supernatant of N-RAS*-AR-Pool and cultured them in complete medium (*Figure 58b*). I generated single cell clones, which were termed N-RAS*-AR#1-#4. The ones growing best, namely N-RAS*-AR#2 and N-RAS*-AR#3 (*Figure 58b*), were chosen for further experiments. Notably, the supernatant cells seemed to become smaller and increased their proliferation potential with every replating procedure. Moreover, N-RAS-AR single cell clones again formed rafts even though the cell density on the culture dish was low (*Figure 58c*).

Taken together, sustained doxycycline treatment of multinucleated N-RAS* melanocytes resulted in nest formation followed by appearance of cell-rafts and generation of 3D structures. The small, nest-generating cells could be replated before forming rafts, which again were viable and highly proliferative.

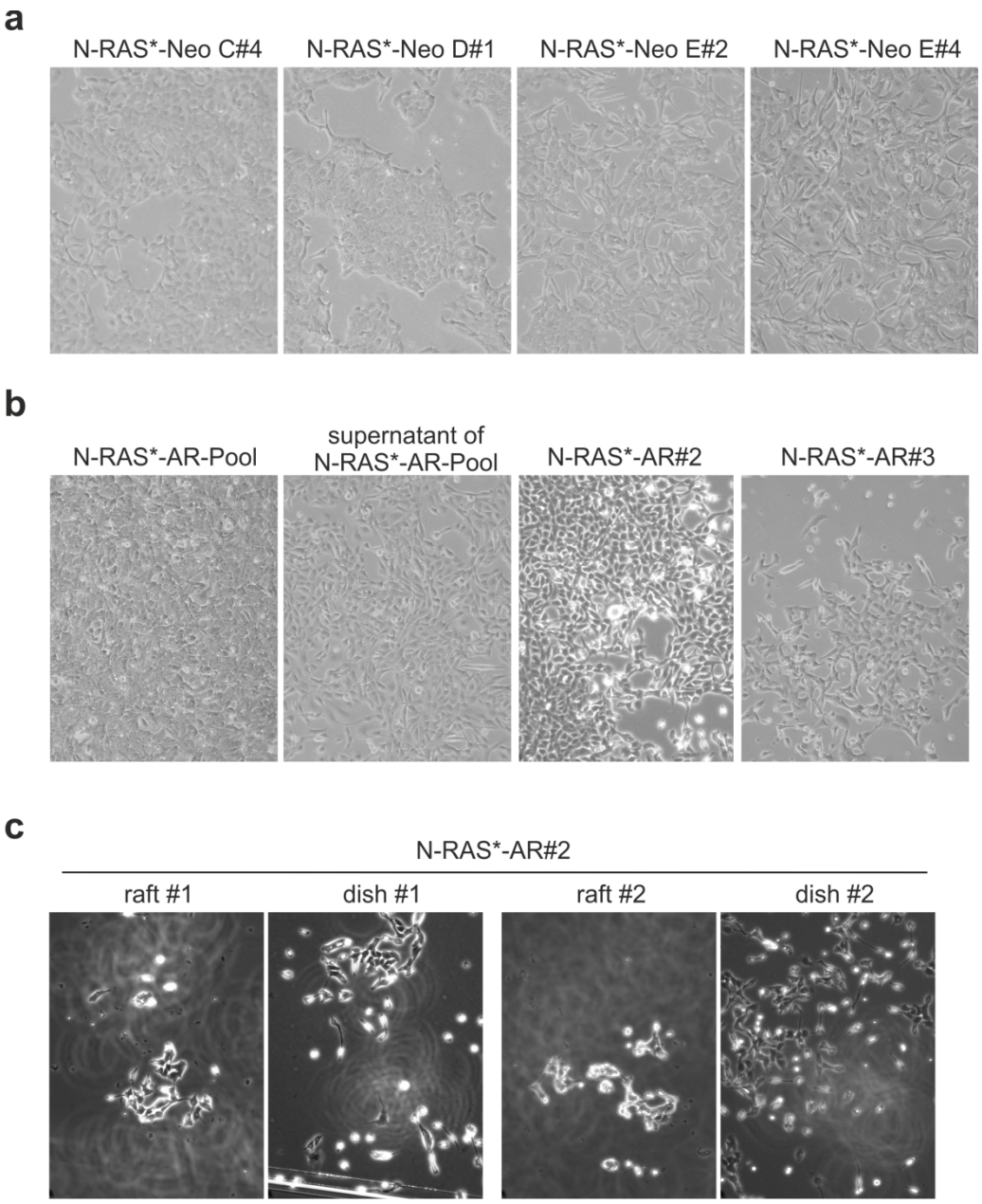

Figure 58: N-RAS*-Neo cells generate rafts

(a) Phase contrast images (100-fold magnification) of N-RAS*-Neo single cell clones and (b) N-RAS*-AR lines cultured in complete medium. (c) Phase contrast images (100-fold magnification of two rafts in the focus level (raft) generated by N-RAS*-AR#2 cells. The corresponding pictures of the attached cells in the focus level of the culture dish (dish) were taken at the site of the respective raft.

7.27 *In vitro* tumourigenic potential of N-RAS*-Neo-AR-Pool cells

To investigate the transformation potential of N-RAS*-Neo-AR-Pool cells *in vitro*, soft agar assays were performed (*Figure 59*). I found N-RAS*-AR-Pool cells to form fairly large and numerous colonies in starving medium. Upon additional doxycycline treatment, the colonies observed were larger and similar to those observed when N-RAS*-AR-Pool cells were

supplied with 10% serum (D10). Notably, cells had not been serum-starved prior to the experiment.

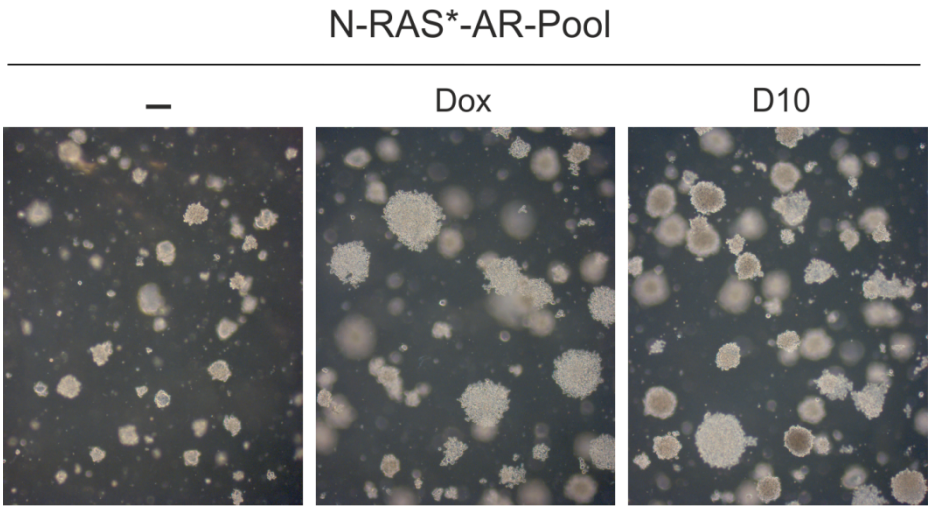

Figure 59: N-RAS*-AR-Pool cells bear in vitro transformation potential
Phase contrast images (25-fold magnification) of N-RAS*-AR-Pool cells upon 14 days in soft agar. Where indicated, cells were kept in starving medium alone (-) or supplemented with doxycycline (Dox) or agar was supplied with 10% serum (D10).

7.28 *In vitro* tumourigenic potential of melan a control, N-RAS* and N-RAS*-AR clones

Since N-RAS*-AR-Pool cells proved to be tumourigenic *in vitro*, I wanted to compare the transformation potential of serum-starved N-RAS*-AR#2 and N-RAS*-AR#3 to those of melan a control (ctrl.) and N-RAS* melanocytes. Therefore, soft agar assays using different media were performed (*Figure 60*). Upon 14 days in soft agar I found melan a control cells (ctrl.) to lack colony forming capacity regardless of culture conditions. Furthermore, N-RAS* cells only formed very few small colonies in presence of doxycycline (Dox). N-RAS*-AR#2 and N-RAS*#3 cells however, formed colonies irrespective of medium supply. Interestingly, even though complete medium contained TPA in addition to the 10% serum in D10, the N-RAS*-AR#2 and #3 colonies observed upon culture in complete medium were much smaller than those observed in D10. Notably, the number and size of N-RAS*-AR#2 and #3 colonies observed in starving medium (-) were not altered in presence of doxycycline (Dox), while #3 generally formed larger colonies.

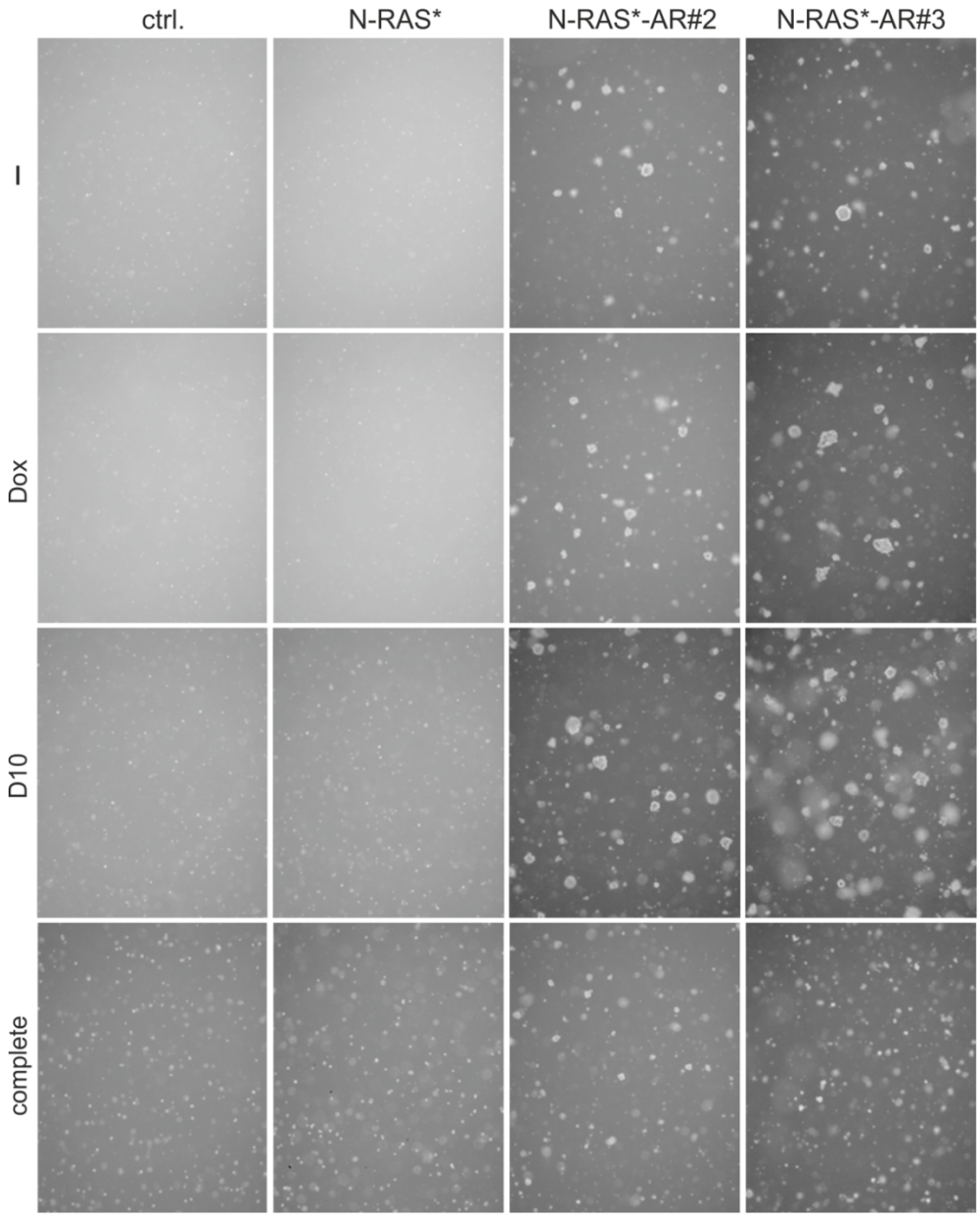

Figure 60: N-RAS*-AR#2 and #3 cells bear in vitro transformation potential

Phase contrast images (25-fold magnification) of melan a control (ctrl.), N-RAS*, N-RAS*-AR#2 and #3 cells upon 14 days in soft agar. Where indicated, cells were kept in starving medium alone (-) or supplemented with doxycycline (Dox) or agar was supplied with 10% serum in absence (D10) or presence of TPA (complete).

Taken together, serum-starved N-RAS*-AR#2 and #3 cells showed a very high *in vitro* transformation potential regardless of culture conditions, whereas N-RAS* melanocytes relied on doxycycline treatment to form very few, extremely small colonies, while melan a control cells completely lacked transformation capacity.

Since serum-starved N-RAS*-AR#3 cells formed the largest and most numerous colonies in soft agar and proliferated extremely well when cultured in complete medium, I decided to

use this single cell clone to further scrutinize the features of N-RAS*-AR cells. Hence, I termed N-RAS*-AR#3 cells N-RAS*-AR and used them for further experiments.

7.29 N-RAS*-AR cells do not senesce, but proliferate

First of all, I wanted to check whether N-RAS*-AR cells still senesce. Therefore, I performed a long-term stimulation assay comparing melan a cells to Hm^{hi} and Hm^{hi}-AR cells (*Figure 61a*). While melan a cells were indifferent to EGF treatment, N-RAS* cells became multinucleated as usual. N-RAS*-AR cells however, showed enhanced cell density upon doxycycline (Dox) treatment, but no large, multinucleated cells were observed. In addition, N-RAS*-AR cells grew to a much higher density than N-RAS*melanocytes when cultured in starving medium alone (-). Notably, there was only a minor difference in cell density when comparing starved (-) and doxycycline-treated (Dox) N-RAS*-AR cells.

This difference in cell density already became obvious when looking at the culture medium in the 6-well plate used for the assay (*Figure 61b*). While the red colour of the medium remained throughout the experiment for melan a control (ctrl.) cells, N-RAS* cells seemed to have consumed more nutrients as indicated by the decrease in medium pH, which led to the observed change of colour. Intriguingly, N-RAS*-AR cells appeared to have completely metabolized and acidified the medium, which had turned yellow prior to the end of the experiment.

To visualize the difference in proliferation as well as the 3D structures formed upon doxycycline treatment in N-RAS* and N-RAS*-AR cells, I stained the cells with crystal violet (Figure 61c). While melan a control (ctrl.) cells showed only a very weak violet staining, the 3D structures in N-RAS* cells stained dark purple. The colour intensity was even higher in the densely packed N-RAS*-AR cells.

Taken together, in contrast to N-RAS* melanocytes N-RAS*-AR cells do not become multinucleated upon doxycycline treatment. Instead, N-RAS*-AR cells seem to bear an increased, doxycycline-independent proliferation potential.

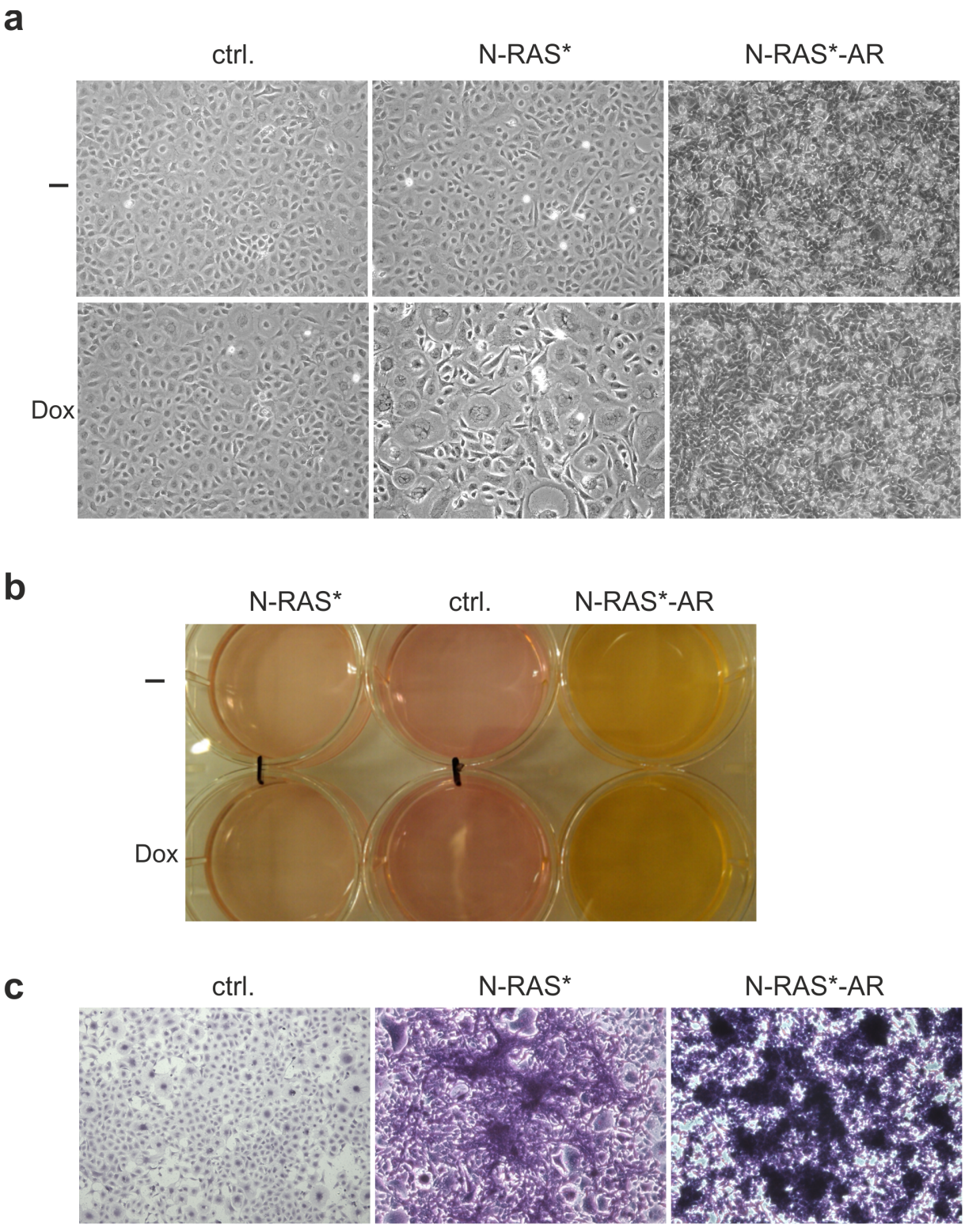

Figure 61: N-RAS*-AR cells do not form multinucleated cells upon doxycycline treatment
(a) Phase contrast images (100-fold magnification) of melan a control (ctrl.), N-RAS* and N-RAS*-AR cells upon 14 days in culture. Where indicated, cells were either cultured in starving medium alone (-) or supplemented with doxycycline (Dox). (b) Equally cropped images of the 6-wells used for the senescence assay upon 14 days in culture. Where indicated, cells were either cultured in starving medium alone (-) or supplemented with doxycycline (Dox). (c) Brightfield images (100-fold magnification) of crystal violet-stained melan a control (ctrl.), N-RAS* and N-RAS*-AR cells upon 14 days in culture.

7.30 N-RAS*-AR cells seem to proliferate in a Dox-independent manner and lack density-induced growth inhibition

Thus, I repeated the long-term stimulation assay and also cultured the cells in medium supplemented with 10% serum (D10) (*Figure 62*). I found melan a control (ctrl.) cells to behave indifferent to culture conditions. N-RAS* cells senesced upon doxycycline (Dox) treatment and D10 did not seem to enhance their proliferation potential compared to the level observed in starving medium (-). In contrast, N-RAS*-AR cells appeared to proliferate equally well in all three culture conditions analysed. Strikingly, illustrated by the phase contrast images, no density-induced growth inhibition occured in N-RAS*-AR cells, while the other cell lines kept flat, extended cell shapes. In stark contrast, N-RAS*-AR cells formed cell clumps and continued to grow in a 3-dimensional fashion.

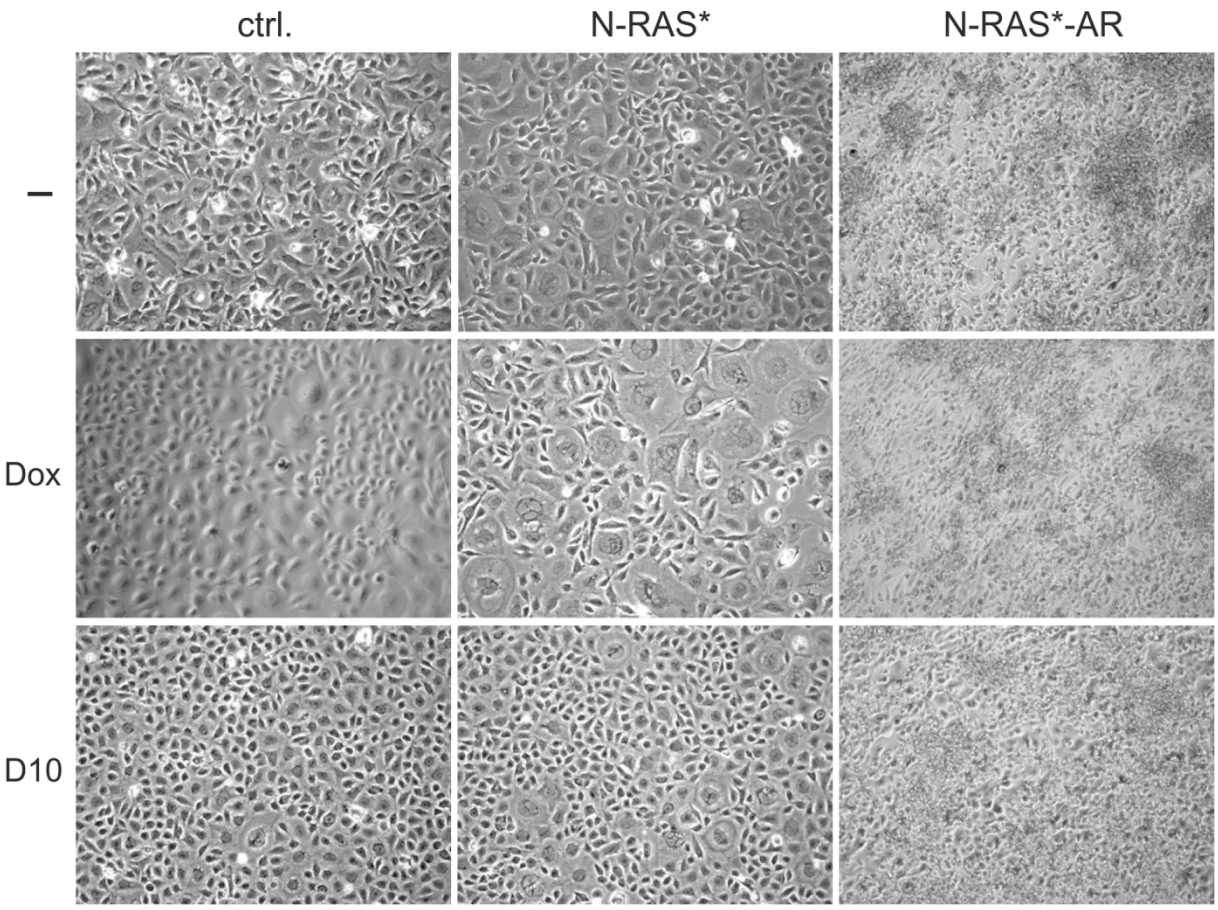

Figure 62: N-RAS*-AR cells seem to proliferate in a doxycycline-independent manner
Phase contrast images (100-fold magnification) of melan a control (ctrl.), N-RAS* and N-RAS*-AR cells upon 14 days in culture. Where indicated, cells were either cultured in starving medium alone (-) or supplemented with doxycycline (Dox) or in medium containing 10% FCS (D10).

7.31 N-RAS*-AR cells grow regardless of culture conditions

Since N-RAS*-AR cells seemed to proliferate in a doxycycline-independent manner and much better than their N-RAS* counterparts, I wanted to quantify this phenomenon. Hence, proliferation assays using different culture conditions were performed to compare the proliferation potential of melan a control (ctrl.), N-RAS* and N-RAS*-AR cells (*Figure 63*).

I found melan a control (ctrl.) cells to lack proliferation capacity when cultured in DMEM supplemented with only 2.5% dialyzed serum (-) (*Figure 63a*). As expected, doxycycline (Dox) treatment could not induce proliferation of melan a control cells (ctrl.) (*Figure 63a*). N-RAS* cells however, slightly proliferated after an initial proliferation lag in medium containing 2.5% dialyzed FCS even though stimulation with doxycycline did not alter the total cell number (*Figure 63a*). Unfortunately, N-RAS* expression was found to be leaky resulting in increased N-RAS* protein levels compared to empty vector control melanocytes (Figure 65a). Interestingly, N-RAS*-AR cells only needed a 3 day period to recover their proliferation capacity from the pre-experiment-starvation and replating in medium containing only 2.5% dialyzed FCS: N-RAS*-AR cells proliferated equally well in absence (-) or presence of Dox finally exceeding N-RAS* cell numbers by a factor of 4 at day 10 (*Figure 63a*). The results were similar when cells were cultured in DMEM supplemented with 10% dialyzed FCS (*Figure 63b*). Melan a control (ctrl.) cells hardly proliferated irrespective of doxycycline status, while N-RAS* melanocytes responded to Dox stimulation reaching higher total cell numbers despite multinucleation compared to cells cultured in starving medium alone (-). In addition, N-RAS*-AR cells proliferated about 10 times faster than Dox-treated N-RAS* melanocytes and similarly well in absence and presence of Dox with total numbers being slightly higher when cells were stimulated with Dox. Total cell numbers increased once again when cells were cultured in DMEM containing 10% FCS in absence (-) or presence of TPA (TPA) (*Figure 63c*). While melan a control (ctrl.) cells hardly and N-RAS* cells only slightly proliferated in absence of TPA (-), N-RAS*-AR cells proliferated really well with total cell numbers increasing by about 40% compared to Dox-stimulated cells in medium containing 10% of dialyzed FCS. Interestingly, the addition of TPA did not alter N-RAS*-AR cell number. However, only in presence of TPA and 10% FCS did melan a control (ctrl.) cells proliferate, even though total cell number was higher for N-RAS* cells. Nevertheless, melan a control (ctrl.) and N-RAS* cells only reached about 30% and 60% of the total N-RAS*-AR cell number in complete medium in presence of TPA.

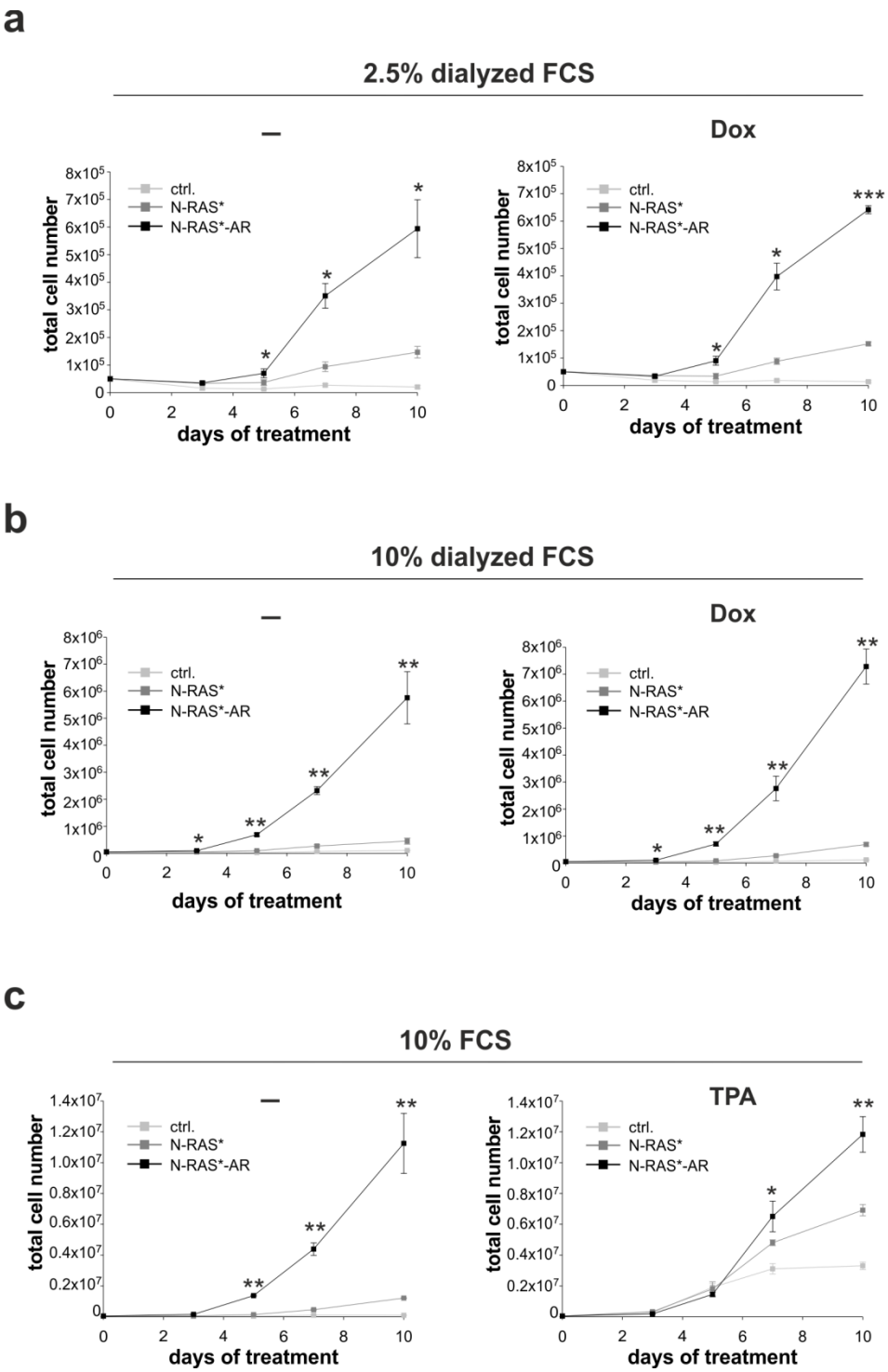

Figure 63: N-RAS*-AR cells bear an increased proliferation potential independent of TPA

Graphs depict the total cell number (mean values of three independent experiments) of melan a control (ctrl.), N-RAS* and N-RAS*-AR cells over time in DMEM containing (a) 2.5% dialyzed FCS, (b) 10% dialyzed FCS or (c) 10% FCS in absence (-) or presence of doxycycline (Dox) and TPA (TPA). Standard deviations are shown. Student´s t-test (paired, 2-tailed) revealed statistical significance comparing N-RAS* and N-RAS*-AR cells at each time point indicated by asterisks (*p<0.05, **p<0.01, ***p<0.001).

Taken together, N-RAS*-AR cells grow regardless of culture conditions as they proliferate best in presence of 10% FCS, but also in starving medium supplemented with either 2.5% or 10% dialyzed FCS.

7.32 Lack of multinucleation for N-RAS*-AR cells cannot be overcome by sustained oncogene stimulation

In the following, I wanted to exclude both, a possible delayed onset of raft formation for melan a and N-RAS* cells as well as multinucleation for N-RAS*-AR cells. Thus, I performed a long-term stimulation assay comparing melan a control (ctrl.), N-RAS* and N-RAS*-AR cells for up to 28 days (*Figure 64*) instead of the usual 14 days. I did not find N-RAS*-AR cells to senesce upon long-term doxycycline (Dox) treatment. Instead, N-RAS*-AR cells steadily proliferated throughout the experiment irrespective of doxycycline (Dox) status. Intriguingly, N-RAS*-AR cells even detached from the culture dish after cell density had become too high prior to the end of the experiment. N-RAS* cells first became multinucleated (14 days) before the appearance of nests and 3D structures (21 days) upon doxycycline (Dox) treatment. Notably, N-RAS* cells also became multinucleated and formed nests and 3D structures when cultured in starving medium alone (-), even though the onset was delayed compared to Dox-stimulated cells. This observation indicates leaky N-RAS* expression. Importantly, melan a control (ctrl.) melanocytes neither formed nests, nor rafts nor 3D structures irrespective of doxycycline status.

Taken together, N-RAS*-AR cells do not senesce upon sustained doxycycline treatment and melan a control cells did neither form nests nor rafts nor 3D structures within 28 days in culture.

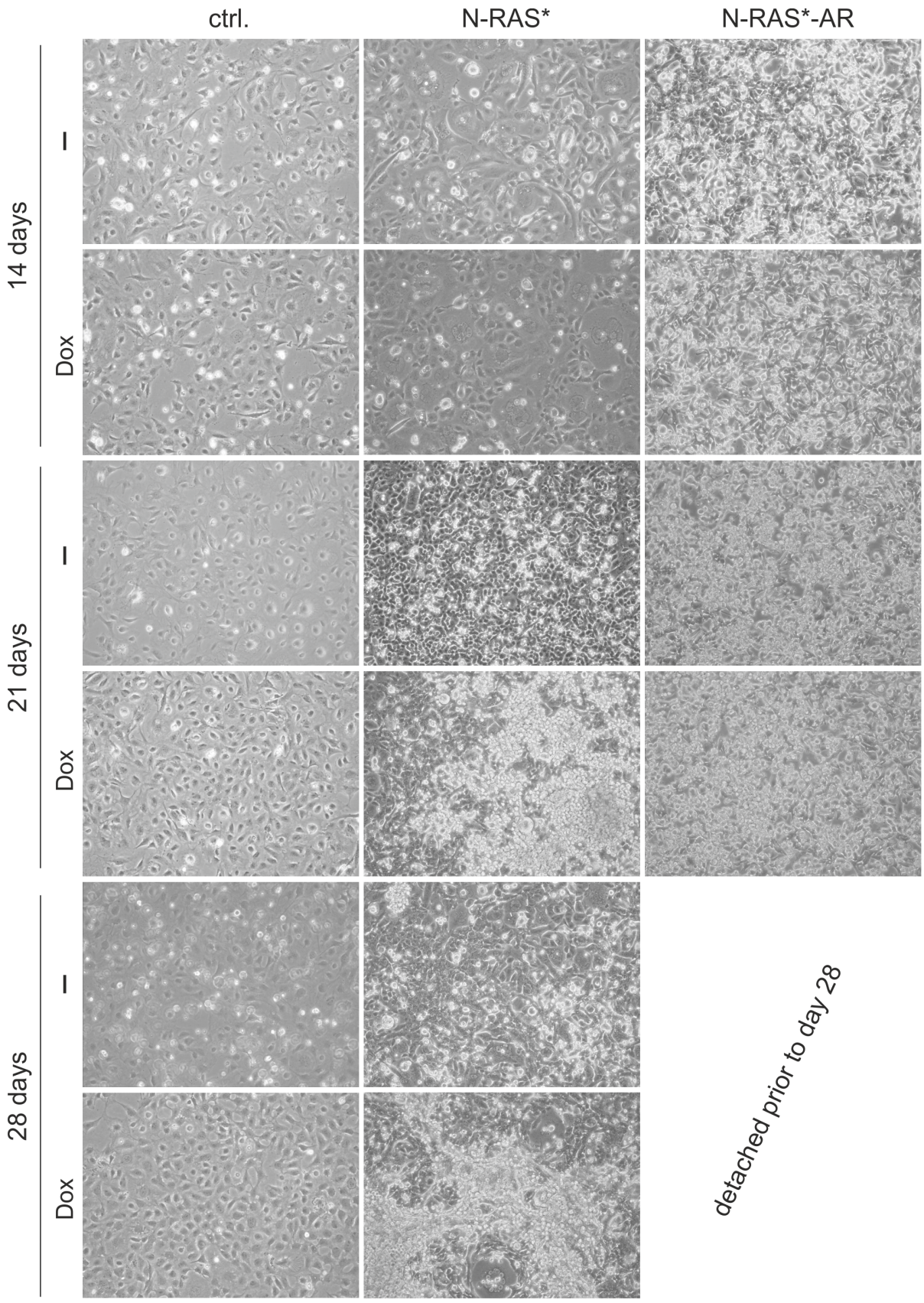

Figure 64: N-RAS*-AR cells´ lack of senescence cannot be overcome by sustained doxycycline treatment
Phase contrast images (100-fold magnification) of melan a control (ctrl.), N-RAS* and N-RAS*-AR cells upon 14, 21 and 28 days in culture. Where indicated, cells were either cultured in starving medium alone (-) or supplemented with doxycycline (Dox).

7.33 N-RAS*-AR clones express high levels of N-Ras and show DNA damage

To investigate whether the N-Ras expression level correlates with the enhanced proliferation observed for N-RAS*-AR compared to N-RAS* cells, I performed Western blot analyses of cells cultured in complete medium (*Figure 65*). I found all N-RAS*-AR clones investigated to express enhanced N-Ras protein levels compared to those of N-RAS* cells (*Figure 65a*). Furthermore, only a faint N-Ras band was detected for melan a control (ctrl.) melanocytes.

Interestingly, the N-Ras expression level directly correlated with the detected protein level of the DNA damage markers P-p53 and P-Chk2 (*Figure 65b*). Notably, the P-p53 protein levels were very low in melan a control (ctrl.) and N-RAS* cells while P-Chk2 was undetectable in either cell line (*Figure 65b*).

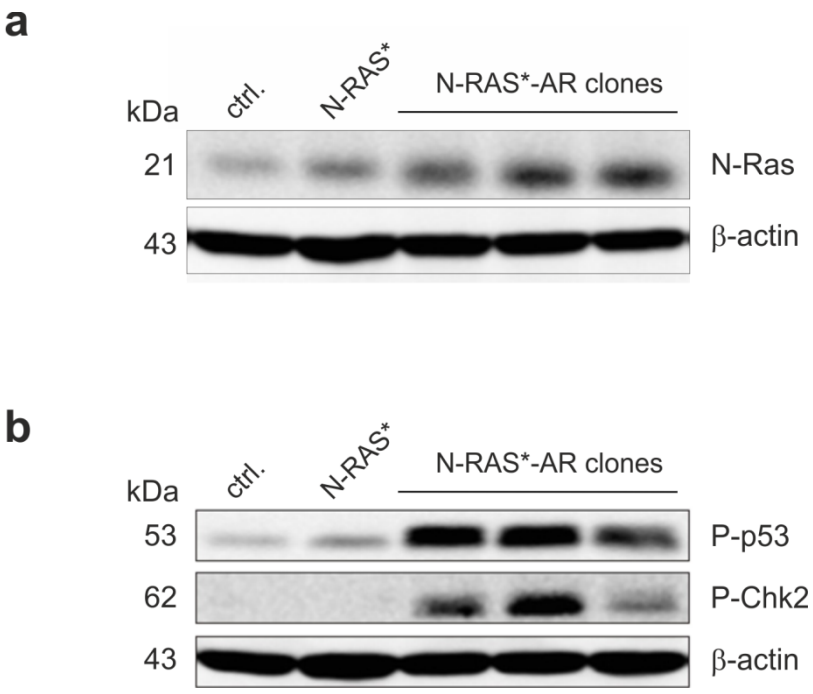

Figure 65: N-RAS*-AR clones express high levels of N-Ras and DNA damage markers
Western blot analyses of (a) N-Ras expression levels and (b) the DNA damage markers P-p53 and P-Chk2 for melan a control (ctrl.), N-RAS* cells and three different N-RAS*-AR clones cultured in complete medium. Cells were harvested and whole cell lysates were separated using 10% SDS gels. Protein weights are indicated in kDa. β-actin served as loading control.

Taken together, N-RAS*-AR clones not only express higher N-Ras protein levels than N-RAS* cells but also bear an enhanced DNA damage level.

7.34 N-RAS*-AR cells show higher *in vitro* transformation potential than B16-F1 melanoma cells

Prior to planned *in vivo* assays analyzing the tumour-forming potential of N-RAS* and N-RAS*-AR cells, I wanted to compare their *in vitro* transformation potential to that of the highly metastatic B16-F1 melanoma cell line frequently used as positive control in nude mice assays. I found N-RAS*-AR cells to form much more and larger colonies in agar supplemented with 10% FCS than B16-F1 cells. As previously observed (*Figure 60*), N-RAS* cells were unable to form colonies.

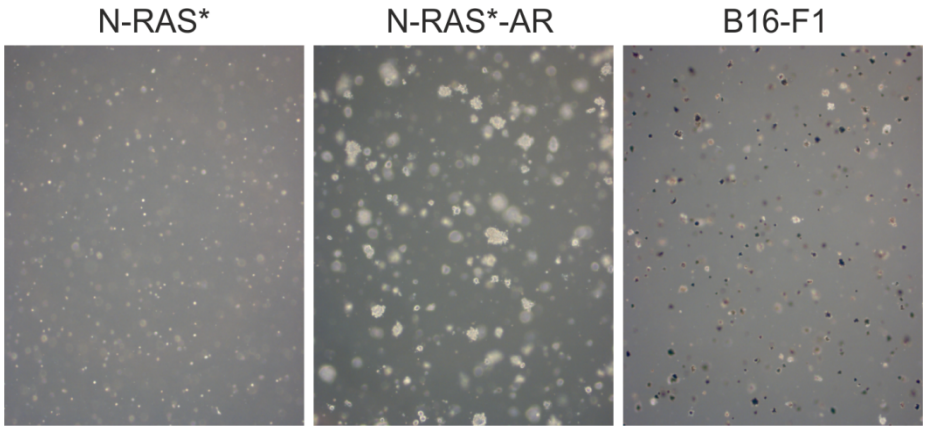

Figure 66: N-RAS*-AR cells bear a higher in vitro transformation potential than B16-F1 cells
Phase contrast images (25-fold magnification) of N-RAS*, N-RAS*-AR melanocytes and the highly metastatic B16-F1 melanoma cells upon 14 days in soft agar. Agar was supplied with 10% FCS.

7.35 *In vivo* transformation potential of melan a control, N-RAS* and N-RAS*-AR cells

Since N-RAS*-AR cells demonstrated a high transformation potential *in vitro*, we were wondering whether these cells could also be tumourigenic *in vivo*. Hence, Dr. Christoph Otto [Experimental Surgery, Experimental Transplantation Immunology, Clinic of General, Visceral, Vascular and Pediatric Surgery (Surgical Clinic I), University of Wuerzburg Hospital, Wuerzburg, Germany] and his technician Bettina Mühling inoculated nude mice with melan a control (ctrl.), N-RAS* or N-RAS*-AR cells. Upon subcutaneous cell application into both flanks, N-RAS* mice were either supplied with common drinking water (-) or with water supplemented with doxycycline (Dox).

7.36 N-RAS*-AR cells induce rapid tumour growth in nude mice

As already described (*Figure 56*), melan a control (ctrl.) cells formed black, nevus-like structures upon inoculation in nude mice (*Figure 67a*). These nevus-like structures formed at every single injection site and were limited to the skin. In some mice the duct generated by the injection needle was found to be colonized (*Figure 67a*). Interestingly, N-RAS* cells formed highly similar black, nevus-like structures in both absence (-) and presence (Dox) of doxycycline. Notably, the nevus-like structures generated by N-RAS* cells did neither differ in size nor in shape and appearance from those formed by melan a control (ctrl.) melanocytes (*Figure 67a*). All melan a control (ctrl.) and N-RAS* mice behaved normally throughout the experiment [personal conversation with Bettina Mühling] and seemed to be healthy when sacrificed 71 days upon inoculation.

In contrast to melan a control (ctrl.) and N-RAS* melanocytes, N-RAS*-AR cells formed large and aggressive tumours in absence of doxycycline (*Figure 67b*) at all injection sites within one week upon inoculation. The tumours grew so rapidly (*Figure 67c*) that N-RAS*-AR mice had to be sacrificed at day 28 due to extensive tumour load (*Figure 67b*). Notably, N-RAS*-AR cells had already metastasized to the lung (data not shown).

Importantly, in contrast to Hm^{hi}-AR mice (*Figure 56*), weight development was not altered over the course of the experiment when comparing all three cell lines inoculated (*Figure 67d*).

Taken together, in contrast to melan a control (ctrl.) and N-RAS* melanocytes, N-RAS*-AR cells proved to be highly tumourigenic *in vivo* inducing very aggressive, fast-growing and metastasizing tumours at every injection site.

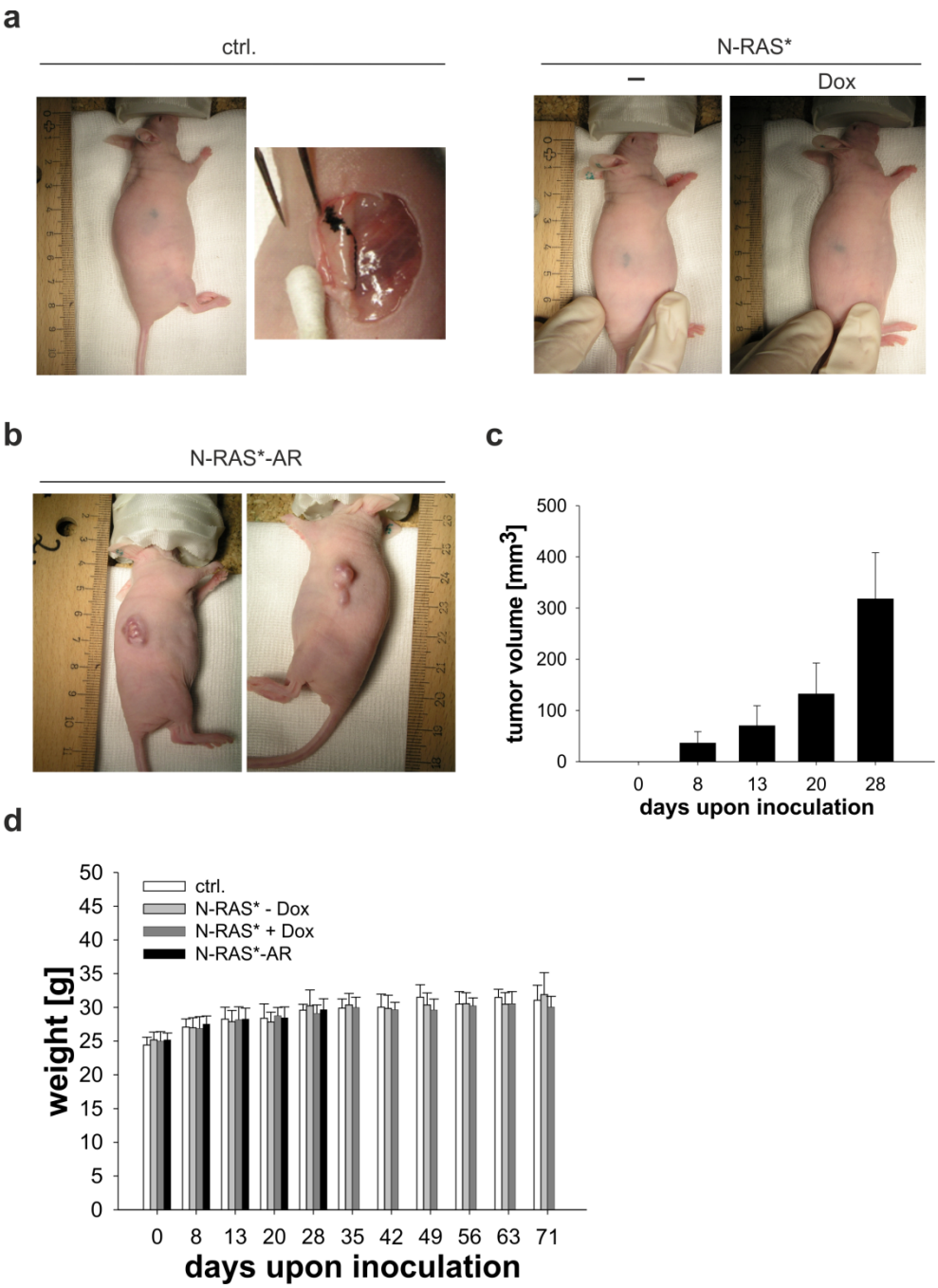

Figure 67: N-RAS*-AR cells induce rapid tumour growth in nude mice

(a) Comparison of nude mice either bearing melan a control (ctrl.) or N-RAS* cells in absence (-) or presence of doxycycline (Dox) 71 days upon inoculation. (b) Representative nude mouse bearing N-RAS*-AR-induced tumours on both flanks 28 days upon inoculation. (c) Graph depicts the mean N-RAS*-AR tumour weight per flank over time. Standard deviations are shown. (d) Graph depicts the weight of melan a control (ctrl.), N-RAS*-AR and N-RAS* mice in absence (-) or presence (Dox) of doxycycline over time. Bars represent the mean weight of five animals each. Standard deviations are shown.

7.37 N-RAS*-AR cells show increased nuclear-cytoplasmic ratio

Since the highly tumourigenic N-RAS*-AR cells also seemed to be much smaller than N-RAS* cells, I again quantified the phenomenon with help from Dr. Toni Wagner (Department of

Physiological Chemistry I, University of Wuerzburg, Wuerzburg, Germany) who performed 3D confocal scans thereby determining the total cell volume and the nuclear volume (*Figure 68, 3D pictograms 68d by Dr. Toni Wagner, figure by Claudia Leikam*). Even though in 2D images both cytoplasm and nucleus seem to be smaller in N-RAS*-AR compared to N-RAS* cells (*Figure 68a*), measuring the compartment volumes disproved this assumption (*Figure 68b*). Interestingly, only cell and cytoplasm volume differed significantly when comparing N-RAS* to N-RAS*-AR cells, whereas the nuclear volumes of both cell lines were found to be highly similar (*Figure 68b*). Notably, N-RAS* cells were more than four times bigger than N-RAS*-AR cells and the cytoplasm differed by a factor of almost 6. These data resulted in a highly significant difference in the nuclear-cytoplasmic ratios of both cell clones, since N-RAS*-AR cells reached a 6-fold higher ratio compared to N-RAS* cells (*Figure 68c*). Furthermore, the 3D scans proved N-RAS*-AR nuclei to be dome-shaped compared to the rather flat N-RAS* nuclei (*Figure 68d*). This finding explains the discrepancy between the apparently smaller nuclei of N-RAS*-AR compared to N-RAS* cells according to the 2D pictures (*Figure 68a*) and the actual, highly similar nuclear volumes depicted in the compartment-volume graph (*Figure 68b*).

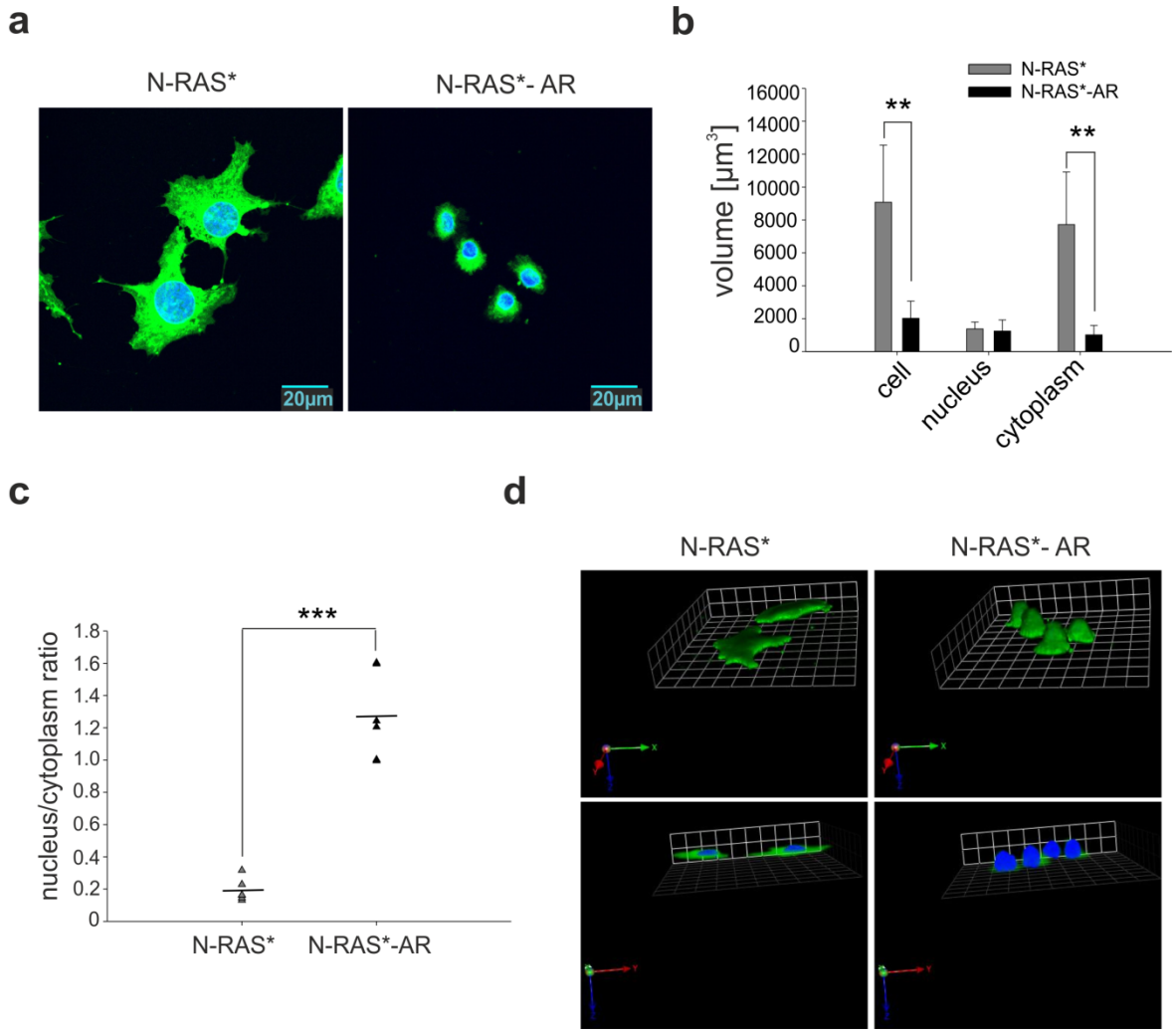

Figure 68: N-RAS*-AR cells are much smaller and have a significantly higher nuclear-cytoplasmic ratio than N-RAS* melanocytes

(a) False colour 2D confocal snapshots (600-fold magnification) of N-RAS* and N-RAS*-AR cells plated onto glass cover slips and cultured in complete medium. The cytoplasm was stained with cell mask deep red and DNA was counterstained using Hoechst. (b) Bars display the mean compartment volumes of 6 N-RAS* and N-RAS*-AR cells each. Standard deviations are shown. Where indicated, statistical significance determined by Student´s t-test (paired, two-tailed) was reached (**p<0.01). (c) Scatter plot displaying the nuclear-cytoplasmic ratios for all 6 single cells analysed for each cell line, N-RAS* and N-RAS*-AR. Vertical bars represent the mean values. Statistical significance determined by Student´s t-test (paired, two-tailed) was reached (***p<0.001). (d) Equally cropped false colour 3D stack images comparing the shape of N-RAS* and N-RAS*-AR cells. Upper and lower panel show cells at the same rotation point. Axes are shown in the lower left corner (x: green, y: red, z: blue).

7.38 Microarray analyses comparing Dox-treated N-RAS* and N-RAS*-AR cells

Wanting to further scrutinize the features of N-RAS*-AR cells to eventually identify the molecular players underlying the high tumourigenicity, an mRNA expression microarray was performed by Susanne Kneitz [Microarray Core Unit, IZKF (Interdisciplinary Center for Clinical

Research), University of Wuerzburg, Wuerzburg, Germany], who compared doxycycline-treated N-RAS* cells that had undergone senescence (6-14 days) before evading senescence (28 days) to N-RAS*-AR cells cultured in presence of doxycycline. Cells from a standard long-term senescence assay were harvested at indicated time points and pellets were stored at -80°C prior to mRNA preparation.

7.39 N-RAS*-AR cells express stem cell markers

We wanted to identify genes that were clearly regulated when comparing doxycycline-treated and multinucleated N-RAS* cells (6 days of doxycycline) to the intermediate state, when N-RAS* cells were multinucleated and SA-β-Gal-positive even though first nests were observed (14 days of doxycycline) and multinucleated N-RAS* melanocytes overgrown with small nest cells (28 days of doxycycline) and finally to anoikis-resistant and highly tumourigenic N-RAS*-AR cells (*Figure 69a*). Since N-RAS*-AR cells showed a massively increased nuclear-cytoplasmic ratio and were so tiny while growing similarly well in any culture medium, the microarray data was filtered to only contain stem cell marker genes (*Figure 69a*). *Nanog*, *Pdpn* and *Abcb1* (mouse homologue of human *CD133*) mRNA levels were much higher in N-RAS*-AR cells than in doxyclycline-treated N-RAS* cells regardless of stimulation time. Notably, the pluripotency markers *Pdpn* and *Nanog* were exclusively expressed in N-RAS*-AR cells, whereas doxycycline-treated N-RAS* melanocytes did not express these genes at any time point investigated (*Figure 69a*).

Western blot analyses further supported the microarray data since N-RAS*-AR clones cultured in complete medium were found to express KLF4, C-Myc, Nanog and Oct4 protein. While C-Myc and Nanog protein levels were high, the Oct4 protein band was rather faint. Nevertheless, N-RAS* cells exclusively expressed low levels of C-Myc while the band observed for melan a control cells (ctrl.) was even weaker. None of the other stem cell markers investigated could be detected in either melan a control (ctrl.) or N-RAS* cells.

In accordance with these data were my observations upon transient transfection of both N-RAS* and N-RAS*-AR cells with the Nanog-driven PL-SIN-EOS-S(4+)-eGFP vector [287]. I found N-RAS* cells to lack Nanog expression, whereas a large fraction of N-RAS*-AR cells expressed functional Nanog protein (*Figure 69c*). Unfortunately, I could not select Nanog-expressing N-RAS*-AR cells as they were already puromycin-resistant prior to transfection with the Nanog-driven vector.

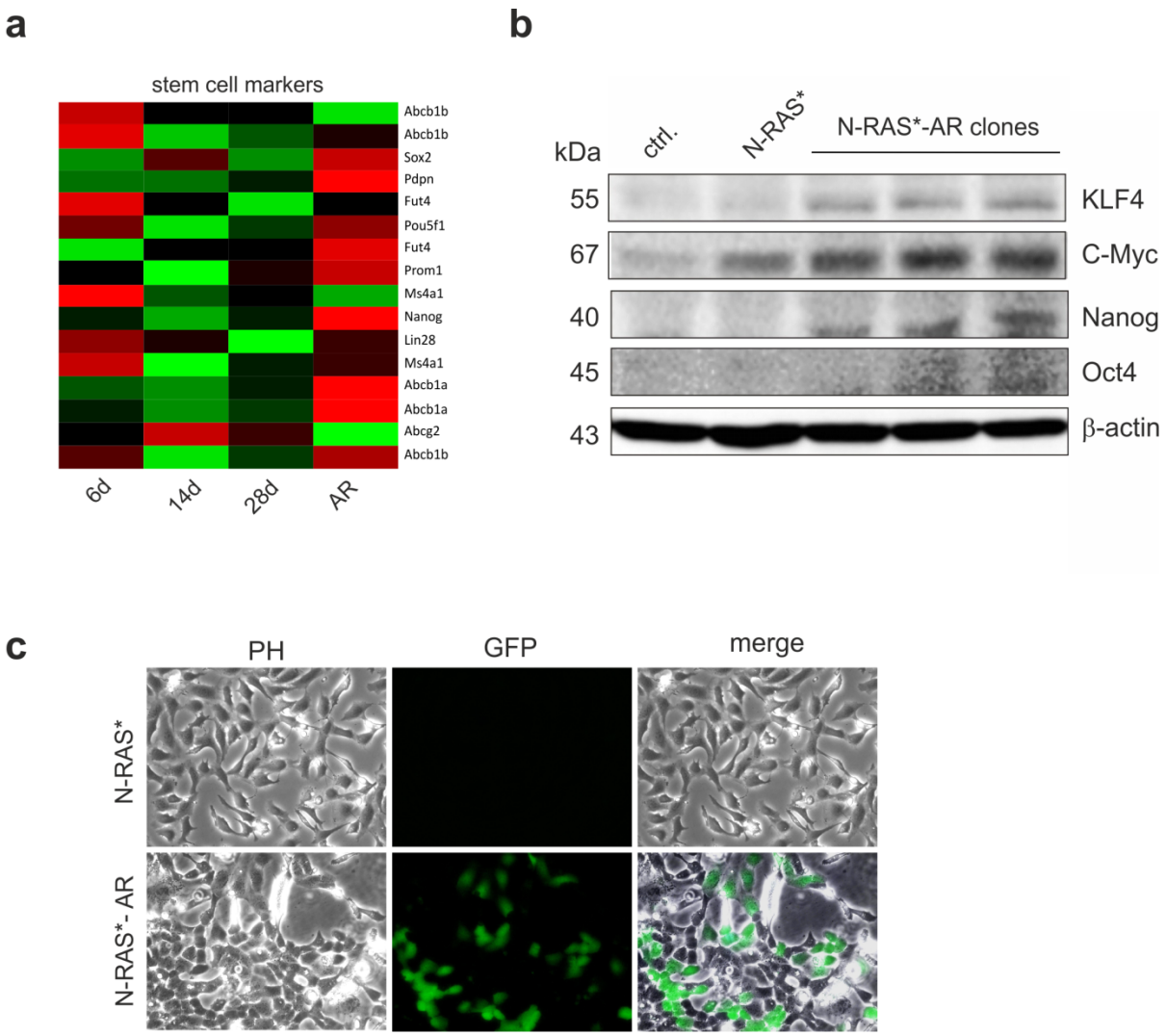

Figure 69: N-RAS*-AR cells express stem cell markers

(a) Heat plot illustrating the mRNA expression of various stem cell marker genes investigated. The color code ranges from green (not expressed) to red (highly expressed). (b) Western blot analyses of melan a control (ctrl.) melanocytes, N-RAS* cells and three different N-RAS*-AR clones cultured in complete medium. Cells were harvested and whole cell lysates were separated on 10-12% SDS gels. Protein weights are indicated in kDa. β-actin served as loading control. (c) Phase contrast and fluorescence images (200-fold magnification) of N-RAS* and N-RAS*-AR cells transiently transfected with the Nanog-driven PL-SIN-EOS-S(4+)-eGFP vector.

Taken together, in contrast to N-RAS* cells, N-RAS*-AR cells express several stem cell markers on RNA and protein level.

7.40 N-RAS*-AR cells lack melanocyte expression markers but show neuronally-expressed genes

Another interesting result obtained from the microarray analyses was the fact that N-RAS*-AR cells lacked melanocyte expression markers such as *Tyrp1*, *Mlana*, *Dct* and *Sox10* even though doxycycline-treated N-RAS* cells expressed these markers at any time point

investigated (Figure 70a). *Mitf* was the only melanocyte differentiation marker still expressed in N-RAS*-AR cells even though expression levels were not as high as in N-RAS* cells treated with doxycycline for 14 or 28 days. Notably, expression of melanocyte expression markers was highest in multinucleated N-RAS* melanocytes upon 14 days of doxycycline treatment (*Figure 70a*).

While melanocyte differentiation gene expression levels in N-RAS* cells decreased after 14 days of doxycycline treatment, neuronal markers were found to be up-regulated with mRNA levels peaking at day 28 (Figure 70b). Interestingly, even though most neuronal markers, e.g. Efna1, Nefl, Areg or Smarca1, were still induced in N-RAS*-AR cells, some seemed to have been silenced (e.g. Id4, Sema6a or Chl1) (Figure 70b).

Taken together, the lack of melanocyte differentiation marker expression and the up-regulation of neuronal genes further supports the de-differentiation process that N-RAS*-AR cells had apparently undergone.

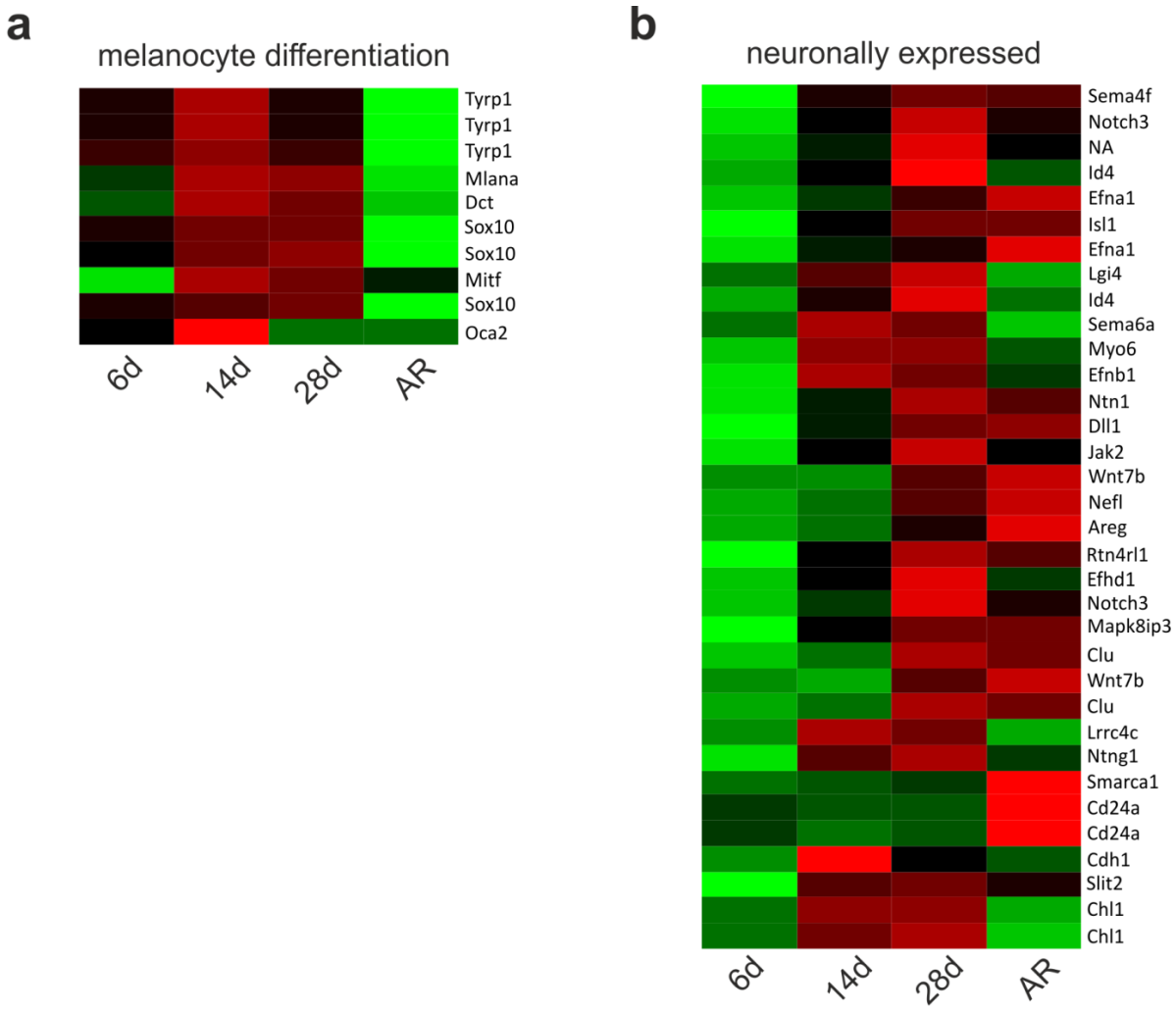

Figure 70: N-RAS*-AR cells lack melanocyte differentiation markers and express neuronally-expressed genes
Heat plots illustrating the mRNA expression of (a) the melanocyte differentiation markers and (b) neuronally expressed genes investigated. The color code ranges from green (not expressed) to red (highly expressed).

Another interesting gene set found to be up-regulated in our microarray analyses were proliferation markers. A broad range of positive regulators of proliferation including *Gli2*, *Btc*, *Ptgs2* and *Kitl* were induced in N-RAS*-AR cells, whereas their mRNA levels were low in N-RAS* melanocytes throughout the course of sustained doxycycline treatment (*Figure 71a*). This finding underscored and explained the enhanced proliferation potential of N-RAS*-AR compared to N-RAS* cells when cultured in different media (*Figure 63*).

Apart from the up-regulation of proliferation markers, the microarray analyses also identified several meiosis marker genes like *Cyp26b2*, *Tex15*, *Suv39h2* and *Spo11* to be highly expressed in N-RAS*-AR cells (*Figure 71b*).

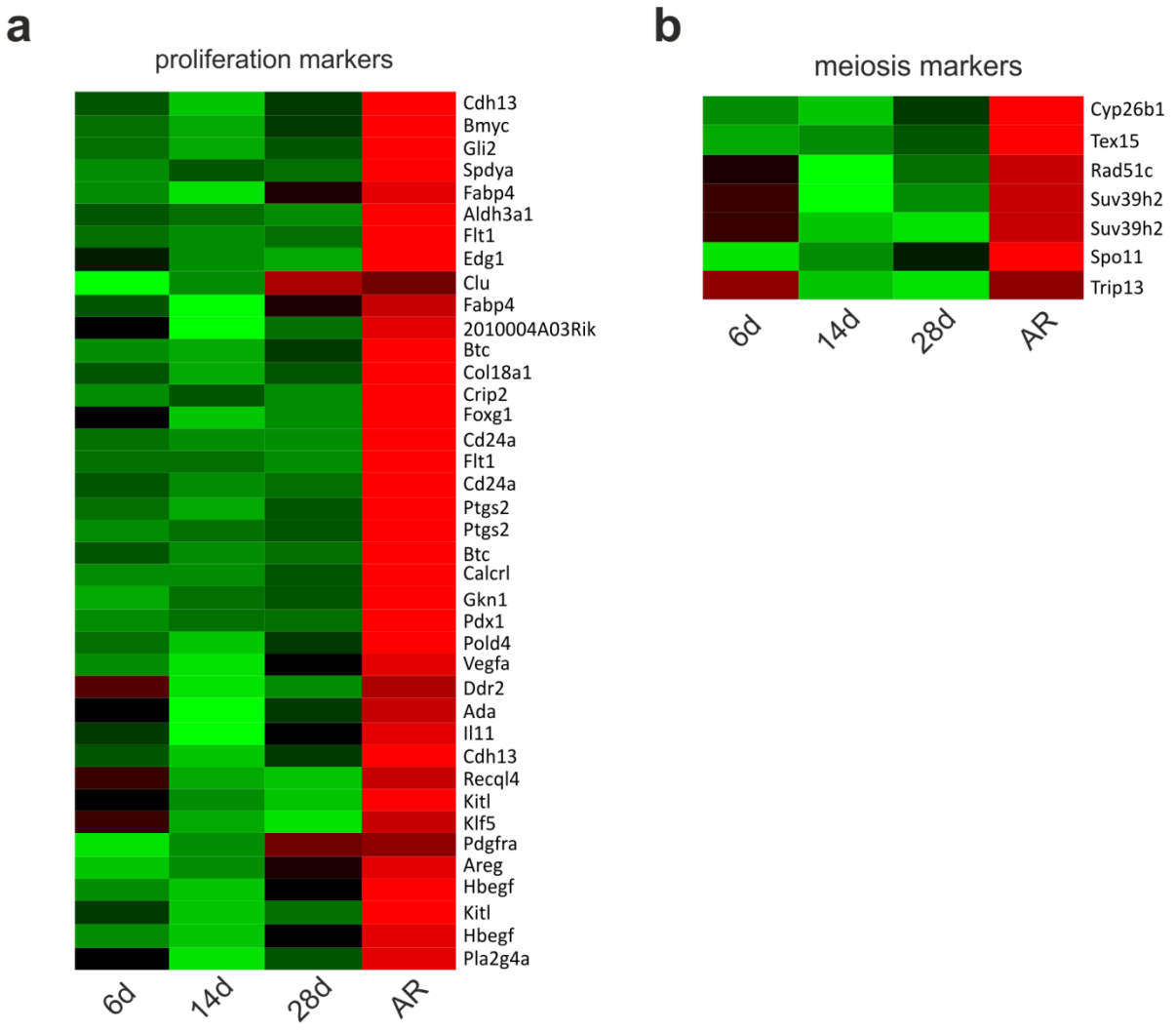

Figure 71: N-RAS*-AR cells express proliferation and meiosis markers
Heat plots illustrating the mRNA expression of (a) proliferation and (b) meiosis marker genes investigated. The color code ranges from green (not expressed) to red (highly expressed).

Taken together, microarray analyses revealed an induction of stem cell, neuronal, proliferation and meiosis markers in N-RAS*-AR cells while melanocyte differentiation markers were down-regulated.

7.41 Multinucleated N-RAS* melanocytes bud off tiny, viable cells

Having observed nests emerge upon sustained doxycycline treatment of multinucleated N-RAS* melanocytes, I was wondering where the tiny cells forming these structures originated from. Thus, I subcloned the MN [EF1a-red membrane and green nucleus]-2A sequence kindly provided by Dr. Toni Wagner into the pBabe vector before transiently transfecting N-RAS* cells with pBabe-MN [EF1a-red membrane and green nucleus]-2APuro, which labels cell membranes red and nuclei green. Upon long-term doxycycline treatment of these N-RAS* cells, time-lapse analyses were performed. I found N-RAS* cells to bud off tiny cells (*Figure 72*), while both the multinucleated mother and the newly-generated small cell were viable.

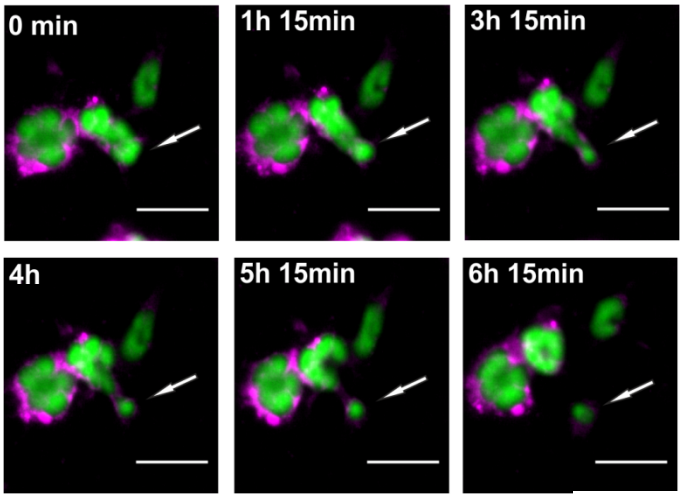

Figure 72: Multinucleated N-RAS* cells give rise to small cells
N-RAS* transiently transfected with pBabe-MN [EF1a-red membrane and green nucleus]-2APuro were plated onto glass cover-slips and cultured in starving medium supplemented with doxycycline. Upon 16 days of treatment, the glass cover slips were transferred into the heatable, CO_2-supplied incubation chamber built for this purpose and monitored at 100-fold magnification for 17 hours with pictures being taken every 15 minutes. Equally cropped images are shown and time points are indicated. Scale bars represent 50µm. A white arrow highlights the budding cell.

Importantly, the cells budded off by multinucleated N-RAS* cells were not only viable, but also capable of undergoing mitosis (Figure 73) as some of them quickly divided upon budding. I claim these cells to be N-RAS*-AR progenitors.

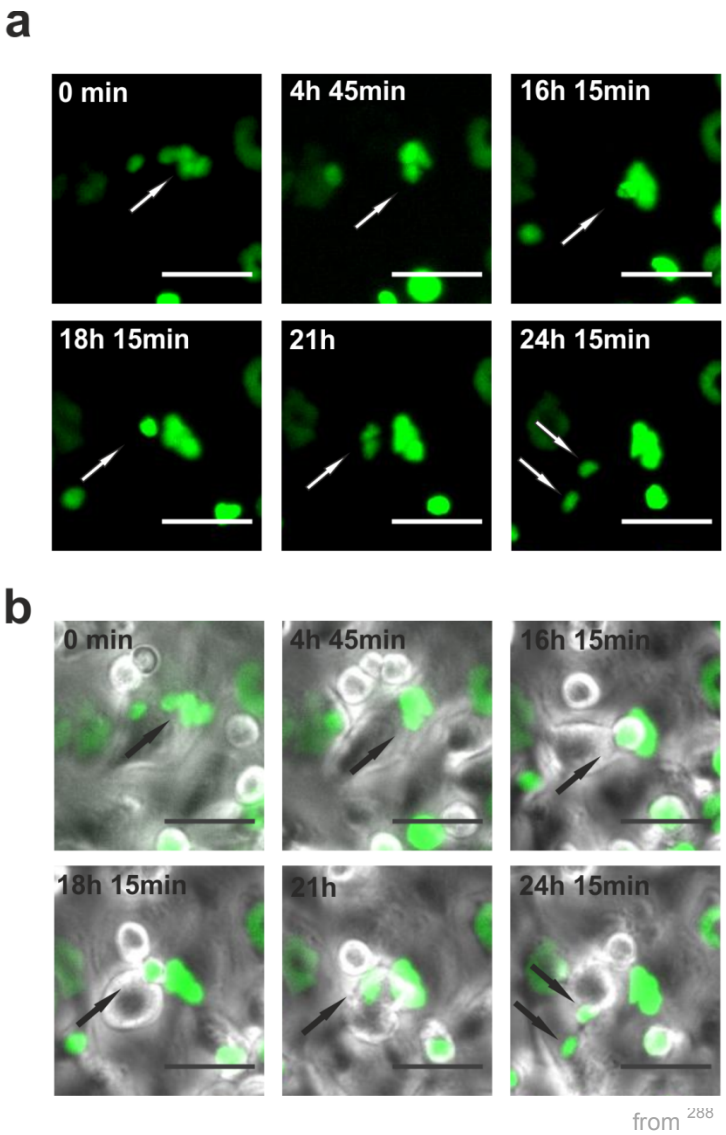

Figure 73: Multinucleated N-RAS* cells bud off small cells capable of dividing
N-RAS* cells were transiently transfected with pBabe-puro-H2-eGFP before being plated onto glass cover-slips. Upon 27 days of continuous doxycycline treatment, the cells were monitored for 28 hours at 100-fold magnification with pictures being taken every 15 minutes. Equally cropped (a) GFP fluorescence images alone or (b) merged with the phase contrast counterparts are shown and time points are indicated. Scale bars represent 50µm. (a) White or (b) dark grey arrows highlight the budding and dividing cell.

Taken together, sustained doxycycline treatment of senescent N-RAS* melanocytes enables multinucleated cells to bud off viable, small cells, which are anoikis-resistant, have lost addiction to their original oncogene, are highly tumourigenic *in vitro* and *in vivo* and bear stem-like features.

Having gained all this knowledge from a murine cell culture model, we were wondering whether our findings were species or even cell line specific or might also hold true in human melanocytes.

7.42 Long-term N-RAS* expression induces binucleation in human melanocytes, followed by the emergence of tiny, highly proliferative and anoikis-resistant cells

Thus, I analyzed normal human epidermal melanocyte (NHEM) cells which had been transfected with the pCDH-CMV-N-RAS^{61K}-EF1-copGFP vector (kind gift by Dr. Roland Houben, Department of Dermatology, University Hospital Wuerzburg, Wuerzburg, Germany) allowing constitutive expression of oncogenic N-RAS as well as GFP. Thanks to this N-RAS^{61K} expression plasmid, NHEM cells bearing the vector (NHEM-N-RAS* or GFP/N-RAS^{61K}) could easily be identified due to the concomitant, fluorescent GFP signal.

NHEM-N-RAS* cells were cultured at a very low cell density in standard growth medium. Upon one week in culture, I observed several enlarged NHEM cells, all of which were GFP-positive (data not shown). A few days later, I found several enlarged NHEM-N-RAS* cells containing multiple nuclei in the dish (*Figure 74a and b*). After three weeks in culture, nest-like, GFP-positive colonies were observed (*Figure 74c*) which rapidly grew in a three-dimensional (3D) manner (*Figure 74d*). Concomitantly, I found a steadily increasing number of floating, green-fluorescing NHEM-N-RAS* cell rafts on the surface of the culture medium (*Figure 74e*). Notably, these rafts could be replated and cultured (*Figure 74f*).

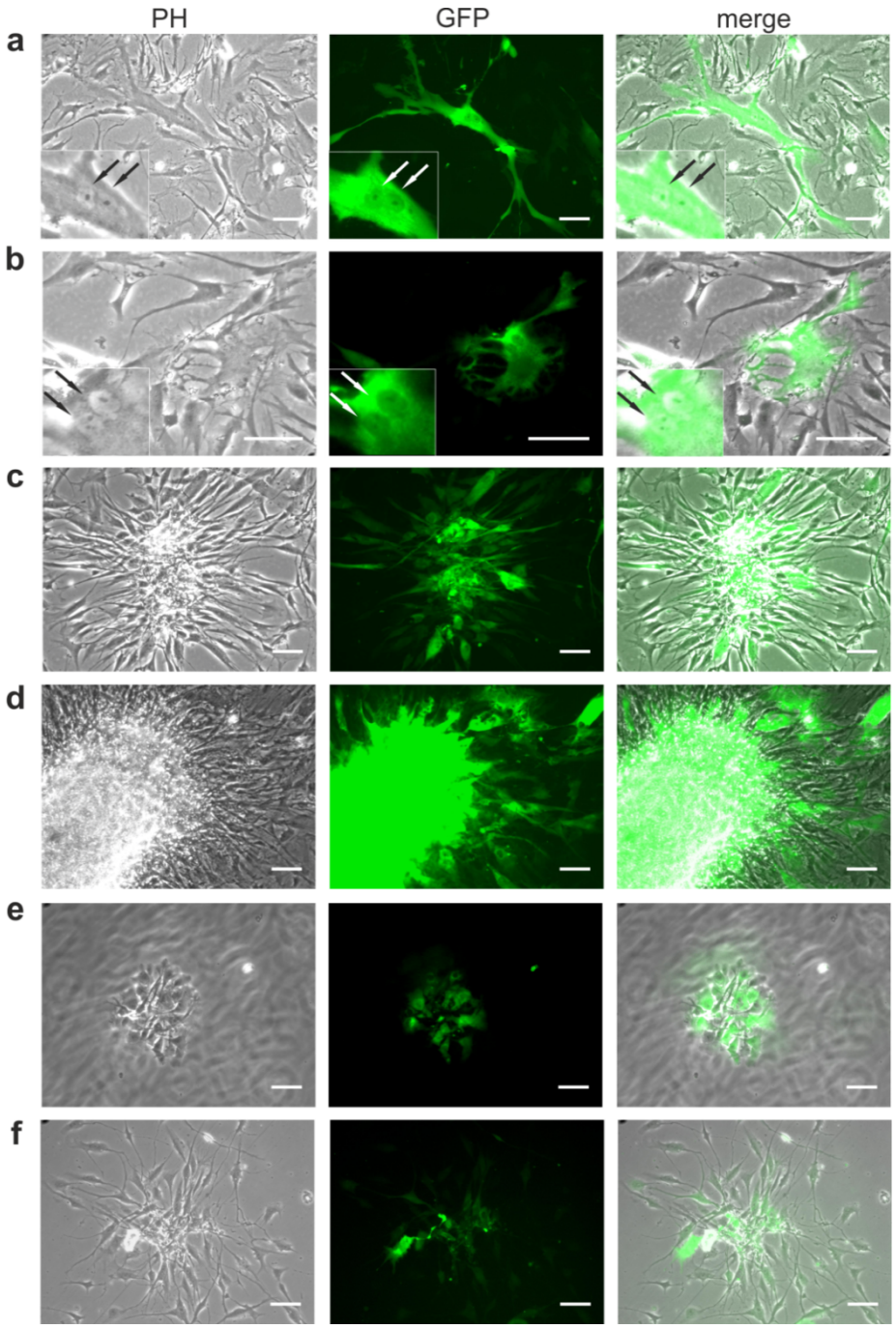

Figure 74: N-RAS^{61K} expression induces multinuclear cells and subsequent anoikis in human melanocytes
(a), (b) Prolonged N-RAS^{61K} expression in human NHEM melanocytes resulted in the appearance of enlarged, multinucleated cells. The white arrows highlight the two nuclei within a single GFP/N-RAS^{61K} positive cell. (c) Upon three weeks in culture, GFP/N-RAS^{61K} cells formed nest-like colonies which (d) grew rapidly into 3D structures. (e) Concomitantly, rafts of floating GFP/N-RAS^{61K} cells were observed. (f) These anoikis-resistant raft cells could be replated and cultured. Scale bars represent 100µm.

7.43 Nest variations observed for NHEM-N-RAS* melanocytes

The nest-like colonies observed upon sustained GFP/N-RAS^{61K} expression in human NHEM melanocytes came in various shapes and sizes (*Figure 75*). Notably, the cells forming these colonies seemed to be much smaller than normal NHEM-N-RAS* cells.

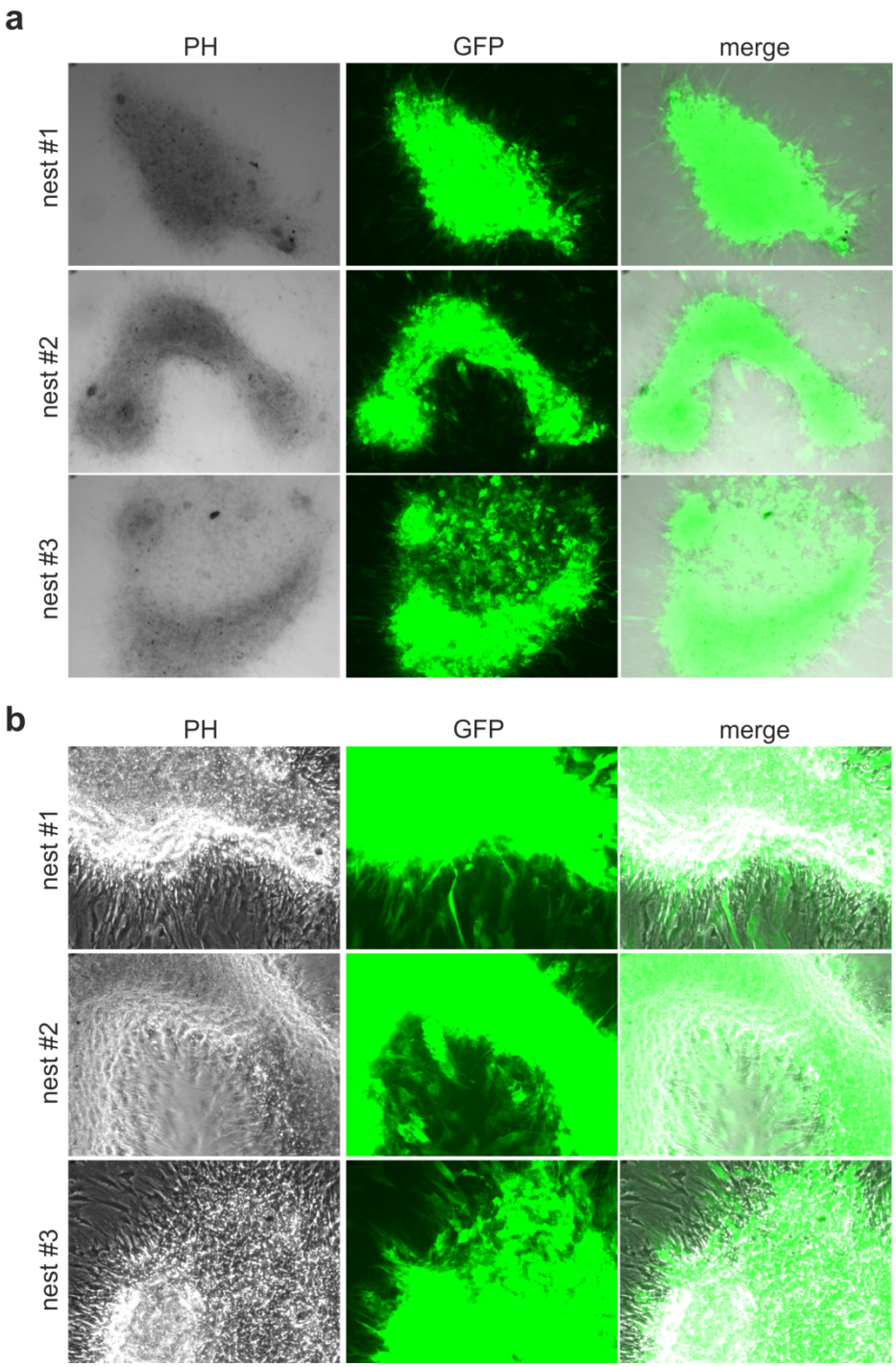

Figure 75: N-RAS^{61K}-expressing NHEM cells form nest-like 3D colonies
(a), (b) Images of three different 3D structures which arose from nests made of small cells in close proximity to multinucleated GFP/N-RAS^{61K}NHEM cells at (a) 50-fold and (b) 100-fold magnification.

7.44 NHEM-N-RAS* cells form 3-dimensional, anoikis-resistant and viable cell rafts

To this point, I had only proven that 2-dimensional rafts were viable when plated onto fresh dishes. However, NHEM-N-RAS* cells added another dimension to this phenomenon. They not only formed floating sheets of cells, but ball-like, 3-dimensional aggregates of cells that detached from the plastic surface and remained viable, as demonstrated by their ability to reattach and expand when replated into fresh, empty dishes (*Figure 76)*. I termed the replated cells NHEM-N-RAS*-AR as they were anoikis-resistant and appeared to have an increased proliferation potential compared to NHEM-N-RAS* cells.

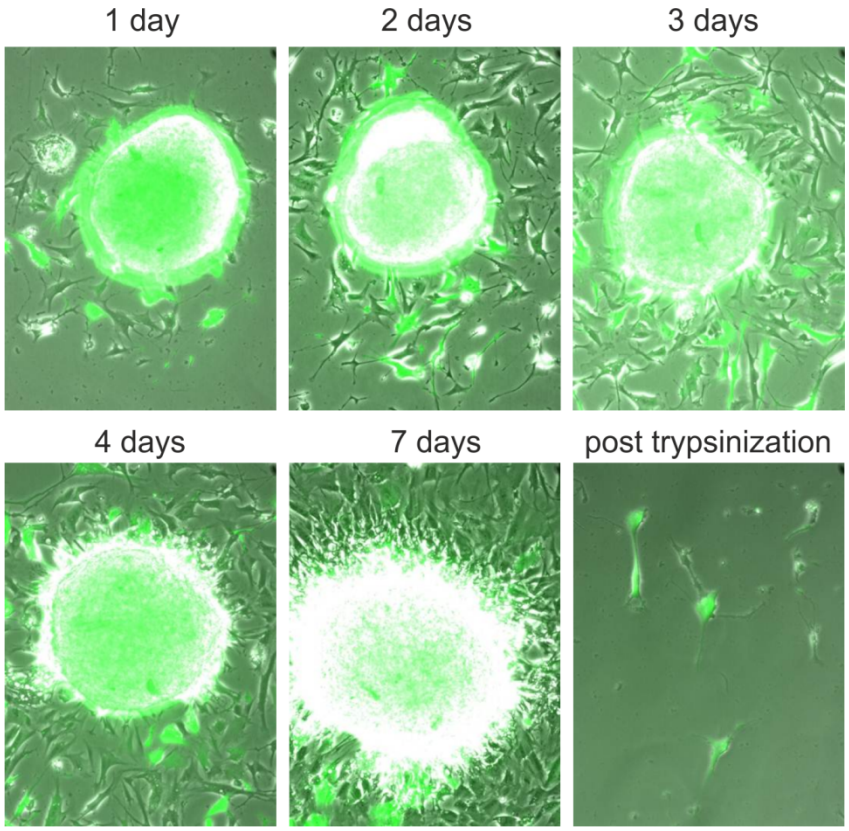

Figure 76: NHEM-N-RAS*-AR cells can be replated
Merge images (100-fold magnification) of replated NHEM-N-RAS*-AR melanocytes. Cells started to reattach and divide as soon as the aggregate had been transferred to a new well even though the colony also kept growing in a 3D manner. One day after trypsinization (post trypsinization) single cells remained and divided normally.

7.45 Similarities between murine N-RAS*-AR and human NHEM-N-RAS*-AR cells

Since murine N-RAS*-AR cells proved to be highly tumourigenic upon inoculation into nude mice, I was of course wondering about the impact human NHEM-N-RAS*-AR might have. However, due to lack of time, I only managed to compare their phenotypes, while including the respective parental cell line (*Figure 77*).

When comparing the cultured NHEM-N-RAS*-AR cells to N-RAS*-AR cells with murine origin, I noticed a similar cell shape and growth behavior. Both AR lines grew in a net-like manner when cultured in their respective complete medium. Furthermore, NHEM-N-RAS*-AR as well as N-RAS*-AR cells were found to be much smaller than NHEM or N-RAS* melanocytes, respectively.

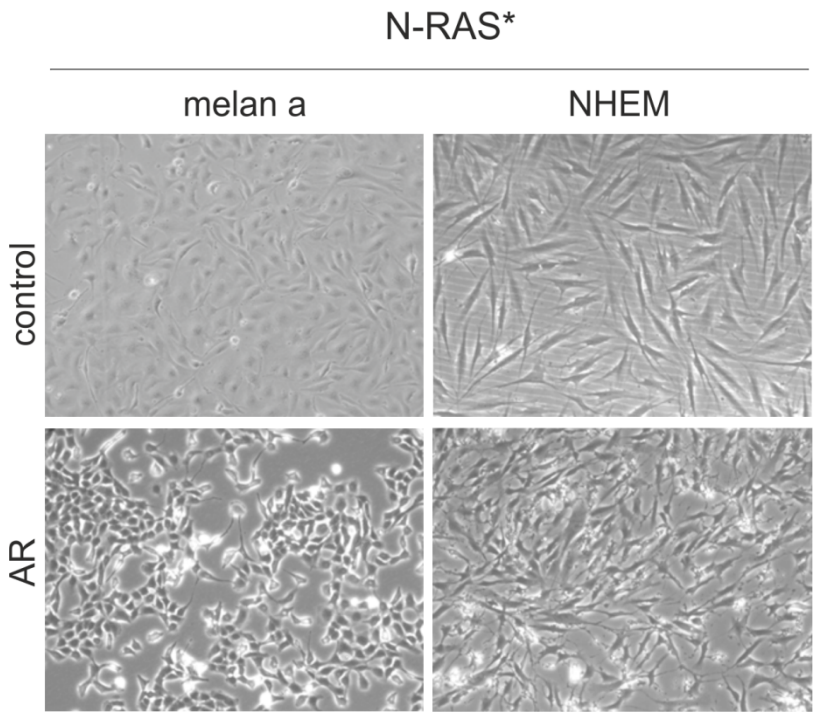

Figure 77: Similar features of N-RAS*-AR and NHEM-N-RAS*-AR cells in culture
Phase contrast images (100-fold magnification) of N-RAS* and NHEM-N-RAS* cells and their anoikis-resistant (AR) counterparts cultured in the respective complete medium

Unfortunately, due to lack of time, no further experiments could be performed to scrutinize the features of NHEM-N-RAS* cells.

In summary, oncogene-induced senescence followed by the generation of small, highly proliferative cells was not restricted to the murine cell culture model, but also holds true for the human melanocyte system.

8. Discussion

Nevi are common, benign, melanocytic lesions frequently harbouring the oncogenic $BRAF^{V600E}$ mutation [17], but rarely develop into malignancies [289]. Michaloglou et al. were the first to show that $BRAF^{V600E}$ expression initially enhanced melanocyte proliferation before cells arrested in a $p16^{INK4A}$-dependent manner and became SA-β-Gal-positive and therefore senescent [290]. Our cell culture model for oncogene-induced senescence was the first to explicitly recapitulate the occurrence of multinucleated cells, a well-known hallmark of human nevi [291,292]. Intriguingly, two independent oncogenes, namely HERmrk and $N\text{-}RAS^{61K}$, induced this multinucleated phenotype in the murine melanocyte cell line melan a. Notably, these multinucleated melanocytes had an increased cell size and were SA-β-Gal-positive. More importantly, the dosage-dependent response of murine melanocytes observed upon HERmrk activation states the first link between proliferation rates and oncogene expression level in this cell type: when low levels of the oncogene are expressed melanocytes proliferate well, whereas high oncogene expression levels limit proliferation and cells senesce.

Prior to our study, a dosage-dependent effect on proliferation and cell cycle arrest had been reported for B- and C-Raf expression in murine fibroblasts [293,294]. Furthermore, high $H\text{-}Ras^{GV12}$ expression in mice first led to hyperplasia followed by senescence [295]. Moreover, human primary melanocyte cultures only senesced at high $H\text{-}RAS^{G12V}$ expression levels, but the cellular features in a low oncogene dosage background has not been investigated [296]. Sometimes, oncogene expression levels directly correlate with proliferation potential and malignancy. C-Myc overexpression, for example, can alter the protein expression profiles of hamster ovary cells thereby enhancing their proliferation potential [297]. In accordance with these findings, proliferation of nasopharyngeal carcinoma cells is suppressed by microRNA let 7 via down-regulation of C-Myc expression [298]. Interestingly, oncogenes, such as PML/RARalpha and TEL/ABL, only efficiently induced leukemia in mice when expressed at a low level or close to pathophysiological level [299]. These studies together with our findings on HERmrk-induced senescence in melanocytes stress the importance of studying oncoprotein function in a dosage-dependent manner.

Most senescent cells have undergone a cell cycle block in G0 [300,301] or in G0-G1 [302,303], which prevents endomitosis and multinucleation. However, a G0 arrest can be excluded in our system, since multinucleation precedes the senescence phenotype. Previously, p21- or p53-mediated cell cycle blocks in G2 were observed in endothelial cells and fibroblasts [304–307] as well as in several yeast strains [308]. Besides, lung and bladder cancer cells were found to arrest in G2 upon overexpression of the mitotic kinase Nek6 [309]. However, the endomitosis observed for our senescent melanocytes rather suggests a cytokinesis failure. Rare cases of premature senescence, e.g. upon treatment of HT1080 fibrosracoma cells with the DNA-

damaging agent adriamycin, go along with multinucleation of the cells [310]. In addition, treatment of NIH3T3 fibroblasts with the histone deacetylase inhibitor sodium butyrate blocked cells in G0/G1, thereby featuring flat, enlarged, senescent-like cells some of which showed multiple nuclei [311]. Furthermore, polyamine depletion in MALME-3M melanoma cells led to a p21-dependent G1 arrest and polyamine inhibition release led to bi- or mutinucleation in 25% of the cells [312]. Moreover, mice bearing mutations in ERCC1, an endonuclease involved in nucleotide excision repair, show multinucleated, senescent liver and kidney cells [313]. Besides, inactivating the transgenic SV40 large T antigen drives human fibroblasts into ROS-mediated senescence with more than half the cells bearing two or more nuclei [314]. In these studies, elevated ROS levels activated protein kinase C δ, which in turn further increased ROS levels. This positive feedback loop finally resulted in cytokinesis failure and multinuclear cells [314]. In accordance with our findings, concomitant treatment with the ROS scavenger NAC rescued the senescence phenotype and allowed fibroblasts to proliferate normally [314]. Supporting these studies, both hepatocyte growth factor [315] and the neurotransmitter calcitonin gene-related peptide [316] limited the intracellular ROS levels and thus attenuated angiotensin-II-mediated senescence in endothelial progenitor cells. These data reinforce our finding of ROS being the crucial senescence-mediator in HERmrk-induced melanocyte senescence.

Hence, with multinuclear cells being a commonly observed feature of some human nevi [317,318], our data propose that HERmrk signalling might resemble the aberrant oncogene signal found in those nevi, thereby correlating the occurrence of multinuclear melanocytes with the senescence phenotype. However, due to a DNA content of more than 8n FACS analyses failed to ascertain in which phase of the cell cycle multinuclear Hm^{hi} cells finally arrest. Hence, introducing the FUCCI (fluorescent ubiquitination-based cell cycle indicator) construct into Hm^{hi} melanocytes would circumvent the DNA content problem as it allows colour-coded (red in G1, yellow/light green in S and green in G2/M) cell phase determination [319]. With pRB and p53, two major pathways are usually causative for the induction of senescence [78]. We found no difference in hyopohosphorylated, active RB protein levels, but instead a marked decrease in the ratio of hyper- to hypophosphorylated pRB and minor differences for the overall amount of p53, when comparing senescing Hm^{hi} cells with non-senescing Hm^{me} and Hm^{lo} melanocytes. In addition, we only observed a weak increase of $p16^{INK4A}$ and $p15^{INK4B}$ and no consistent increase of ARF in senescent versus non-senescent cells. Notably, the loss of $p16^{INK4A}$ and ARF was reported to be a prerequisite of most mouse melanocyte cell lines, including melan a [81]. However, these studies were performed under standard growth conditions. We found melan a cells to lack $p16^{INK4A}$ and ARF expression under standard culture conditions, but both proteins were expressed in starved cells. Since we found no mutation in the *Cdkn2a* cDNA, we concluded that melan a cells are capable of producing functional INK4A and ARF when stressed.

For human cells, it has been shown that neither $p16^{INK4A}$ nor $p14^{ARF}$ were necessary to induce senescence in human melanocytes upon N-RAS^{Q61K} expression [320]. Besides, oncogenic Raf-1 was shown to induce senescence in human mammary epithelial cells (HMEC), which is independent of $p16^{INK4A}$, $p21^{Cip1}$, $p14^{ARF}$, $p27^{Kip1}$ and $p57^{Kip2}$ [321]. One feature exclusively observed in senescing Hm^{hi} cells was the dramatic increase in protein levels of the DNA damage markers P-p53 (Ser18) and P-Chk2. Ser18-phosphorylated p53 is a target of ATR and ATM kinases. Interestingly, p53 stability remains unaffected in mice bearing a Ser18-Ala mutation thereby lacking phosphorylation of this residue [322]. Likewise, DNA damage-induced P-p53 (Ser15), the P-p53 (Ser18) equivalent in humans, leads to reduced interaction of p53 with its ubiquitin ligase MDM2 both *in vitro* and *in vivo* [323]. These data are in line with our observation that the protein levels of P-Ser18-p53 do not parallel the overall amount of p53. However, P-Ser15-p53 augments p53-mediated recruitment of CBP/p300 resulting in an increase in C-terminal p53 acetylation and enhanced target gene activation [324]. Thus, rather than comparing total p53 protein, we consider P-Ser18-p53 levels to be the gauge of choice as it nicely parallels the senescence extent in our melanocyte system.

Apart from the induction of DNA damage markers, we found ROS levels to correlate with the senescence extent observed in Hm cells. Even though both premature and replicative senescence have formerly been associated with increased ROS generation [325–327], the origin of oxidative stress observed upon oncogene activity remains a matter of extensive debate. The GTPases and HERmrk downstream effectors RAC1 and RAS [65] were reported to be essential for the generation of ROS in various cell culture models [328,329]. We found the treatment with the ROS scavenger NAC to limit the formation of multinuclear cells, while enhancing the proliferation potential of Hm^{hi} cells. Similar observations were made in primary rat hepatocytes, where oxidative stress in presence of growth factors resulted in polyploidy and decreased proliferation [330]. Furthermore, NAC treatment reversed H_2O_2-induced generation of polyploidy in human lymphoid cells [331].

Apart from activation of HERmrk, a positive regulator of the RAS/RAF/MAPK pathway, we determined oncogenic N-RAS to resemble ROS generation followed by the occurrence of multinuclear cells and SA-β-Gal activity when expressed in our melanocyte system. Nonetheless, whether this phenotype is also expression level-dependent has not been determined in our system. However, tumours progressing to higher grades of malignancy have been reported to increase RAS expression levels which in turn lead to senescence [295,332,333]. Besides, RAS-induced OIS has been attributed to either increased oxygen levels [328,334] or exertion of the DNA damage response pathway due to DNA double strand breaks [235,335], both of which were also observed in our model system. Besides, overexpression of MTH1, the cellular 8-oxodGTPase human MuT homolog 1, suppressed H-RAS^{V12}-induced senescence in BJ fibroblasts even though ROS levels were unaffected compared to senescing control cells only expressing H-RAS^{V12}. Further experiments revealed

that MTH1 overexpression conveyed its senescence-protective effect through limiting the RAS-mediated DNA damage extent. Hence, the guanine nucleotide pool was suggested to be a critical target for oncogenic RAS-induced ROS [336]. Another way to counteract RAS-induced senescence is to diminish ROS directly. RAS signalling was shown to activate superoxide radical-generating NADPH oxidases [337] including NOX4 [338]. The H-RAS^{V12}-mediated senescence response of non-tumoural thyroid cells could be limited by siRNA-knockdown of *NOX4* [338]. Furthermore, cells cultured in low oxygen conditions or in presence of the ROS scavenger NAC did not undergo RAS-mediated senescence [244]. Hence, in summary, our data provide evidence that oncogenic RAS-induced senescence in melanocytes relies on the generation of ROS followed by DNA damage.

Taken together, we established a model, which mimics the multinuclear phenotype of human nevus cells *in vitro* by overexpressing a powerful melanoma oncogene, namely either HERmrk or N-RAS^{61K}. As we proved for the HERmrk model, senescence induction relied on oncogene-dependent ROS generation, concomitant DNA damage and increased p53 activity. Our data for the first time adduce a connection between oxidative stress, multinucleation and senescence in melanocytes.

Intriguingly, I found the tumour marker *Survivin* to be exclusively up-regulated in the senescing melanocyte cell line Hm^{hi}, whereas no *Survivin* expression could be detected in the non-senescing, proliferating and more tumourigenic clones Hm^{me} and Hm^{lo}. This up-regulation in mRNA was paralleled by an increase in survivin protein in EGF-treated, multinuclear Hm^{hi} melanocytes. In addition, *Survivin* mRNA expression appeared to correlate with the proportion of multinuclear cells as levels went down upon NAC treatment. Interestingly, shRNA knockdown of *Survivin* expression was not followed by the expected decrease in survivin protein, but instead resulted in an increased survivin level even though multinuclear melanocytes were observed when cells were cultured in complete medium. The occurrence of multinuclear cells upon *Survivin* knockdown was not surprising as survivin enables correct cytokinesis [222,224] and its ablation was shown to result in polyploidy [224,226], while survivin expression is thought to play a role in endomitosis [225]. It might well be that shRNA knockdown of *Survivin* initially resulted in multinucleated Hm^{hi} cells, while activating counter-regulatory feedback mechanisms. Another explanation could be a stabilization of remaining survivin protein. Taken together, at first sight it seems contradictory that the prognostic tumour marker *Survivin*, which is associated with poor prognosis in several cancer types including melanoma [339–341], is highly expressed in our senescent melanocytes. However, survivin might play an important role in the budding of tiny, tumourigenic and de-differentiated cells from multinucleated Hm^{hi} cells. Unfortunately, I did not have the opportunity to investigate this possibility.

Even though I could not identify the molecular mediator crucial for senescence induction in our melanocyte system, two protective setups, namely MYC overexpression and *Miz-1*

knockdown, were validated. In addition to antioxidants such as N-acetylcysteine, I found both MYC overexpression and *Miz-1* knockdown to diminish ROS levels, multinucleation and senescence in Hm^{hi} cells, while enhancing their tumourigenic potential and proliferation capacity. Notably, all three MYC overexpression constructs (MYC-wt, MYC-VD and MYC-TA) were capable of suppressing HERmrk-induced senescence of Hm^{hi} cells while conveying tumourigenicity, but the effects were most impressive for the more stable MYC-TA form. This is not surprising as MYC is an unstable protein with a half-life of only 20-30 minutes, which has been reported to be stabilized in several tumour types including Burkitt´s lymphoma [342]. Interestingly, even though MYC overexpression slightly enhanced proliferation in starved Hm^{hi} cells, MYC´s impact became much more obvious when HERmrk was active in presence of EGF. Besides, the dramatic increase in soft agar growth of Hm^{hi} cells upon MYC overexpression exclusively occurred in presence of EGF. Hence, our data provide compelling evidence that MYC and HERmrk act synergistically. These findings are in accordance with the observation that MYC expression suppresses RAS- and RAF-induced senescence in melanoma cells [159]. Besides, MYC´s potential to de-differentiate cells and increase their proliferation capacity becomes evident when used for generating pluripotent cells from fully differentiated adult fibroblasts [314]. The expression of four transcription factors, namely MYC together with Oct3/4, Sox2 and Klf4 reprograms differentiated adult fibroblasts back to a pluripotent state [314]. The resulting induced pluripotent stem cells (iPSCs) resemble embryonic stem cells. Further analyses showed that three of these genes, Oct4, Sox2, and Klf4, are critical to the reprogramming process, but MYC enhances the reprogramming efficiency [343–345].

In addition, MYC also regulates several microRNAs [346,347]. MYC primes breast cancer cells for epithelial-mesenchymal transition (EMT) and stimulates angiogenesis by inducing miR-9 [348]. Moreover, MYC represses the expression of miR23a and miR23b allowing for enhanced glutaminase expression in lymphoma and prostate cancer cells [349]. Glutaminase converts glutamine to glutamate, which also serves as substrate for the synthesis of the antioxidant glutathione [350].

Hence, bearing all these MYC features in mind, it is not surprising that MYC is deregulated in the vast majority of human cancers [351,352]. Notably, MYC suppression induces senescence and tumour regression in several tumour types including lymphoma [154], osteosarcoma and hepatocellular carcinoma [353,354]. Besides, several years ago MYC overexpression was demonstrated to be prevalent in both primary and secondary malignant melanoma and hence suggested to be a prognostic marker [355]. More importantly, *MYC* knockdown in human $BRAF^{V600E}$ and $N\text{-}RAS^{Q61R}$ melanoma lines sensitized cells for oncogene-induced senescence, while MYC overexpression suppressed OIS induction in melanocytes [159]. Interestingly, senescence suppression was more efficient in a $BRAF^{V600E}$ background than in $N\text{-}RAS^{Q61R}$-expressing melanocytes [159]. This finding might explain why MYC overexpression diminished

senescence in Hm^{hi} cells and only limited the senescence extent in N-RAS^{61Q}-expressing melan a cells. In addition, down-regulation of MYC forced M14 melanoma cells into senescence and cellular crisis [157]. Interestingly, cells were not only enlarged and SA-β-Gal-positive, but also contained multiple nuclei, while an increase in reactive oxygen species accompanied by glutathione depletion was observed [157]. Besides, concurrent treatment of those M14 melanoma cells that were manipulated to express reduced levels of MYC with the ROS scavenger NAC (N-acteyl-cysteine) suppressed the growth arrest [157]. These data nicely go along with our findings that MYC overexpression diminished the presence of reactive oxygen species in EGF-treated Hm^{hi} cells. Hence, these data suggest MYC to counteract the intrinsic ROS levels, which are likely to be an important player in senescence induction of melanocytes and melanoma cells. In this context, the allocation of cysteine seems to be crucial for ROS suppression. In accordance with this finding, our microarray analysis identified a novel MYC target gene, *CTH*, which allows cysteine production via the transsulfuration pathway [269]. Cysteine is therefore required to synthesize cellular redox-controlling molecules like glutathione and taurine [270].

Intriguingly, MYC expression not only facilitates cells to overcome senescence, but can also induce senescence. In absence of cyclin-dependent kinase 2 (Cdk2) long-term activation of MYC led to senescence in mouse embryo fibroblasts [356]. Similarly, MYC overexpression upon depletion of *WRN*, the Werner Syndrome and DNA repair gene, in human fibroblasts rapidly induced senescence [357].

Thus, in a nutshell, MYC is on the one hand capable of exerting the senescence programme in a defined genetic background, but on the other hand suppresses oncogene-induced senescence in various cell lines and tumour types. The MYC-mediated OIS suppression in our model system is likely to be at least partly mediated by increased CTH expression thereby allowing for increased detoxification of intracellular stress. Furthermore, MYC and HERmrk act synergistically since both the proliferation potential and the *in vitro* tumourigenicity were greatly enhanced when both oncogenes were active. Likewise, MYC expression limited senescence and led to an increased proliferation capacity in N-RAS*-expressing melanocytes.

Apart from MYC overexpression, we also found *Miz-1* knockdown to diminish HERmrk-mediated ROS levels, DNA damage and senescence, while enhancing the proliferation potential and *in vitro* tumourigenicity, but to a lesser extent than MYC overexpression. Similarly, *Miz-1* knockdown limited the senescence extent and enhanced proliferation in N-RAS*-expressing melanocytes. When cells are stressed, MYC binds to Miz-1 thereby preventing induction of Miz-1 target genes like $p15^{INK4B}$ or *p21* [141]. Besides, only when MYC permanently represses Miz-1, lymphoma cells can be kept from undergoing TGFβ-mediated senescence [358]. Surprisingly, we found neither $p15^{INK4B}$ nor p21 protein levels to correlate with senescence suppression in Hm^{hi} cells upon *Miz-1* knockdown. However, microarray analysis also revealed Hm^{hi}-pS-*Miz-1* melanocytes to express slightly elevated *Cth* levels,

suggesting that the senescence-protective effect upon *Miz-1* knockdown also relies on enhanced ROS detoxification, probably via CTH.

The majority of cellular antioxidant systems, including GSH and taurine, require cysteine. Under normal conditions, most cells are able to accommodate their need for cysteine by importing extracellular cystine [359]. Cells with particularly high ROS loads, e.g. tumour cells, additionally rely on the CTH-dependent transsulfuration pathway for the biosynthesis of cysteine from methionine [270]. However, increased H_2S, a byproduct generated in a cysteine-degrading step also mediated by CTH, allows for antiproliferative effects when CTH is overexpressed [360,361]. Besides, CTH has been associated with tumour-protective activities since mutations decreasing CTH activity have been reported to cause cystathioninuria, hypercystathioninemia and increased risk of developing atherosclerosis and bladder cancer [362]. Moreover, treatment of gastric cancer cells with the H_2S donor and potential anti-cancer agent S-propargyl-cysteine suppressed proliferation and migration and reduced the tumour volume in nude mice. These phenomena could be attributed to enhanced CTH expression as concomitant treatment with the CTH inhibitor PAG reversed the effects [363]. Nevertheless, due to its cysteine-generating properties, only low CTH levels are detected in normal tissue, whereas expression is elevated in tumours (http://www.proteinatlas.org/ENSG00000116761). However, information on CTH regulation in tumours is scarce. Notably, the pro-tumourigenic functions of CTH are associated with high glutathione levels, which have been connected to different tumour types including melanoma [364–368]. Moreover, CTH expression was found to be vital for cancer cell survival since glutathione depletion in glioma cells up-regulated CTH [369] and so did butyrate expression in colon cancer cells [370], but the responsible transcription factors remain unidentified. Besides, our studies identified the first tumour-associated transcription factors, namely MYC and MIZ-1, which regulate CTH expression. Furthermore, the finding that CTH overexpression diminished HERmrk-induced senescence and enhanced proliferation in Hm^{hi} cells suggests a possible role for CTH in senescence evasion. Additionally, together with the enhanced proliferation potential, the loss of pigmentation in melan a cells upon CTH overexpression points to a possible dedifferentiation, which might go along with an increase in tumourigenicity. However, further experiments are necessary to test this hypothesis.

Interestingly, deregulation of CTH expression seems to have little effect on developmental processes. *Cth*$^{-/-}$ mice show normal development and only suffer from hypertension in adulthood [371]. Moreover, the inhibitory mechanisms of DL-propargylglycine (PAG) on CTH function is well-documented [372,373]. H_2S produced by CTH causes cardiovascular and nervous system-related diseases in mice, the symptoms of which are efficiently relieved applying PAG [374]. Nonetheless, due to PAG´s limited membrane permeability, designing improved inhibitors should be considered.

Taken together, we identified *CTH* as a novel MYC/MIZ-1 target gene, and thus provide the first direct link between tumour-associated transcription factors and CTH. Furthermore, our experiments proved that CTH is important for intracellular stress reduction, a vital feature of tumour cells. Hence, it is safe to attribute CTH the role of a possible player in the demonstrated senescence-protective effects upon MYC overexpression or *Miz-1* knockdown in Hm^{hi} cells.

Even though oncogene-induced senescence is considered a major barrier in cancer progression, we were surprised to find Hm^{hi} cells senesce while Hm^{lo} and Hm^{me} cells proliferated considering that high Xmrk expression levels are related to highly malignant melanoma in fish, while low Xmrk levels cause pigment spots and minor tumours [278].

Likewise, expression of oncogenic RAS in mice resulted in stimulated proliferation and mammary hyperplasia when H-RASV12 levels were low, while high RAS activity induced ARF-$p16^{INK4A}$-independent senescence [295]. Thus, a three step model for RAS-mediated tumour development was proposed: (1) an activating RAS mutation, (2) RAS overexpression (3) senescence evasion [295]. Occasionally melanomas develop from pre-existing nevi composed of senescent melanocytes [375,376]. However, information on senescence evasion on the cellular level is lacking.

I could show that sustained oncogene expression of either N-RAS* or HERmrk initially leads to OIS induction followed by the generation of nest-like colonies. Similar structures have previously been described to occur six weeks upon carcinogenic exposure of non-tumourigenic C3H10T1/2 mouse embryo cells with polycyclic hydrocarbons [377]. Notably, the small cells were only observed once the cell culture had reached confluency. The generation of clones isolated from these nests followed by inoculation led to late tumour formation in immunocompromised mice [377]. However, only 50-80% of mice showed tumours, which were observed after 2-6 months upon inoculation [377]. These findings are in line with our observations, but in our system N-RAS*-AR cells were highly tumourigenic and formed aggressive tumours at every single injection site within only one week post inoculation. Since the origin of the tumourigenic cells remained unclear [377] with a minimum of 13 passages upon carcinogenic treatment claimed to be necessary prior to neosis [378], Sundaram et al took out to perform time-lapse imaging [379]. They found irradiated and carcinogen-treated C3H10T1/2 mouse embryo fibroblasts to become multinucleated before tiny, mononucleated cells, capable of dividing, were generated, presumably from multinucleated mother cells. The mother cells were claimed to die due to mitotic crisis [379]. In addition, giant $p53^{-/-}$ mouse embryonic fibroblasts and human metastatic neuroblastoma-derived HTB11 have been shown to develop tiny daughter cells either spontaneously or after carcinogen treatment, respectively [379]. Even though the tiny daughter cells look similar to those observed in N-RAS* and HERmrk-expressing melanocytes upon long-term oncogenic stress, the actual budding process was discussed, but not shown. Thanks to nuclear and cytoplasmic

fluorescent labelling, our time-lapse analyses revealed multinucleated N-RAS* and Hm^{hi} cells to bud off tiny, mononucleated cells, which undergo mitosis while the mother cells survived. Notably, a large proportion of multinucleated melanocytes had undergone senescence by that time. In addition, microarray analyses demonstrated N-RAS*-AR cells to differ from multinucleated N-RAS* cells in their gene expression profile. Even though Sundaram et al found differences in autoradiograms of RT-PCR-differential display analyses comparing untreated C3H10T1/2 cells to etoposide-treated and neotic counterparts, gene names and further studies are lacking [379]. Our microarray data, however, proved N-RAS*-AR cells to have largely lost melanocyte differentiation markers, which had been induced during senescence initiation. *Mitf* was the only typical marker for mature melanocytes still found to be expressed at reasonable levels in N-RAS*-AR cells. Interestingly, MITF is not only important for melanocyte proliferation and survival, but is also sustained in human melanoma [380]. Nevertheless, in accordance with the gene expression signature of N-RAS*-AR cells, highly invasive melanoma cells have been shown to express lower levels of the MITF target genes *Tyrp1*, *Mlana* and *Dct*. These cells as well as N-RAS*-AR cells rather express members of the Wnt pathway as well as certain matrix components [56]. More importantly, inhibition of Mitf not only increased the tumourigenic potential of melanoma cells, but also up-regulated the stem cell markers *Oct4* and *Nanog* [381]. This finding supports the increased stem cell marker expression including Nanog on both mRNA and protein levels observed for Hm^{hi}-AR as well as N-RAS*-AR clones. Furthermore, both Hm^{hi}-AR and N-RAS*-AR cells exhibited a significantly higher nuclear/cytoplasmic ratio than Hm^{hi} and N-RAS* cells, respectively. High nuclear/cytoplasmic are a hallmark of stem cells [284–286] and a prominent feature of aggressive tumour cells [281–283]. Cells in malignant tumours usually have a nuclear/cytoplasmic ratio of about 0.5, whereas cells in benign lesions bear a close to normal ratio of 0.17 [283]. The ratios observed for Hm^{hi}-AR and N-RAS*-AR cells were 0.35 and 1.2, respectively, going along with the trend observed for cells with enhanced tumourigenicity and de-differentiation potential. Notably, 3D volume analyses of stem cell compartments to determine the nuclear/cytoplasmic ratio are lacking and figures referring to the ratio often only show 2D images [285,382], which is unfit to exactly and reliably determine the ratio [284,383].

Concurrent with the decrease of melanocyte differentiation markers and the increase in some pluripotency-associated genes, several neuronal markers were induced in N-RAS*-AR cells. Since melanocytes originate from the neural crest lineage, this change in gene expression points to a de-differentiation process, which might accompany N-RAS*-AR generation. Intriguingly, human melanoma cells have also been associated with neuronally-expressed genes [47,384]. In addition, melanoma cells often express high levels of meiosis-related genes and are susceptible to meiomitosis, an abnormal cell division through which cancer daughter cells inherit partially expressed meiotic machinery upon mitosis [385]. The budding observed in N-RAS*-AR cells bears resemblance to the asymmetric division

described to occur in tetra- or polyploid tumour cells. In a process termed depolyploidisation, aneuploid cancer cells give rise to para-diploid cells in order to re-enter a normal cell cycle. Depolyploidisation allows the cells to limit the risk of accumulating DNA damage, which might otherwise result in cell death [386,387]. A shared phenomenon between cells undergoing depolyploidisation and N-RAS*-AR cells is the up-regulation of meiotic genes such as *Spo11,* which is associated with depolyploidisation [387–389]. Apart from *Spo11*, depolyploidisation has been linked to re-expression of additional meiosis-related genes and the clonogenic re-growth of tumour cells after genotoxic treatment [388,390]. In addition, these tumour cells were found to up-regulate the key self-renewal transcription factors *OCT4*, *NANOG* and *SOX2* [391]. Interestingly, ploidy has been reported to be a valuable parameter in the assessment of cancers and for the majority of tumours aneuploidy was found to correlate with further-progressed tumour stage and poor prognosis [184,185,392]. Besides, mounting evidence suggests that polyploid cells are genetically unstable and can act as intermediates on the road to aneuploidy and, ultimately, cancer [178,181]. Further supporting this argument, genes involved in maintaining chromosome stability are frequently deregulated in human tumours [186].

Multinucleated so-called “starburst cells” were also found in the vast majority of lentigo maligna patient samples [393]. This melanoma type has been causally linked to chronic sun exposure [394,395]. This observation points to a connection between UV-induced DNA damage and the generation of starburst cells. Furthermore, not only melanoma samples exhibit polyploid cells, but multinuclear melanocytes are also found in premalignant nevi [396,397]. Notably, even though the majority of melanomas arises de novo, malignant lesions can also emerge from nevi [398–402]. Multinuclear cells are also found in other cancer types, e.g. in malignant mammary cancers. Here, only tetraploid $p53^{-/-}$ mouse mammary epithelial cells induced malignant tumours in nude mice, whereas their diploid counterparts did not [199]. Interestingly, a small fraction of tetraploid human IMR90 fibroblasts started to re-express Nanog and Oct4 together with DNA damage and senescence markers before some of them became octaploid and even divided prior to undergoing replicative senescence [403]. In addition, PROb rat colon carcinoma cells, which had adopted apolyploid and multinucleated senescence-like phenotype upon cisplatin treatment, have been observed to give rise to tiny, diploid, rapidly dividing and colony-forming cells [404]. Notably, both the appearance and endoreplication process generating the multinuclear cells described here as well as the features of the tiny, emerging cells [404] strongly resemble the emergence of N-RAS*-AR and Hm^{hi}-AR cells. However, experiments to scrutinize the gene and protein expression patterns and verify the origin of PROb-derived AR cells are lacking. Nevertheless, the high proliferation potential of PROb-AR cells is in line with that of N-RAS*-AR cells, which emphasizes their tumourigenic features. Our N-RAS*-AR microarray analysis revealed an induction of proliferation-associated genes such as the growth factors *Kitl*, *Vegfa*, *Btc* and

Areg and growth factor receptors like *Pdgfra* or *Flt1*as well as molecules involved in transmitting growth-promoting signals e.g. *Ptgs2* or *Fabp4*. In addition, we found N-RAS*-AR cells to proliferate very well under all tested culture conditions. Neither did N-RAS*-AR cells require the growth stimulus of TPA, nor normal FCS. More importantly, N-RAS*-AR cells proliferated equally well in absence and presence of doxycycline and formed aggressive, metastasizing tumours in absence of Dox in nude mice. Hence, N-RAS*-AR cells have lost their oncogene addiction. Besides, time-lapse imaging of longterm-activated N-RAS* cells clearly demonstrated the budding of N-RAS*-AR cells from multinucleated N-RAS* cells frequently followed by subsequent mitosis of N-RAS*-AR cells. Apart from HERmrk and N-RAS* in melan a mouse melanocytes, I also found N-RAS* expression in primary human NHEM melanocytes to induce the generation of giant, binuclear cells. In addition, the occurrence of bi-nucleated NHEM-N-RAS* cells was also followed by the emergence of three-dimensional cell nests made up of tiny cells that appeared to proliferate rapidly and generated floating cell rafts. These NHEM-N-RAS*-AR raft cells could be sub-cultured and cells showed no sign of senescence. Notably, the mono-nucleated, untransfected NHEM cells remaining on the dish either arrested or died. To my knowledge, binuclear cells accompanied by the emergence of highly proliferative offspring, have not been previously reported for NHEM cells, even though B-RAF^{V600E} expression was found to induce OIS in primary human melanocytes [233,405–407]. Hence, the budding of tiny, de-differentiated, highly-proliferative and aggressive tumour cells from bi- or multinucleated cells is likely to occur not only in murine, but also in human melanocytes. Nevertheless, further experiments need to be performed to verify this assumption.

Summarizing our data, which could be underpinned by a diversity of findings from fellow researchers, we suggest the following model for oncogene-induced, ROS-dependent senescence in melanocytes (*Figure 78*): Aberrant oncogene signalling, in our case caused by HERmrk or N-RAS*, leads to enhanced levels of reactive oxygen species (ROS), which in turn results in the accumulation of DNA damage as detected by an induction of P-Chk2 and P-p53. Melanocytes eventually become enlarged, multinucleated and SA-β-Gal-positive. Concurrent N-acetylcysteine (NAC) treatment of EGF-stimulated Hm^{hi} cells limited both ROS levels and senescence extent. Besides, MYC overexpression and *Miz-1* knockdown diminished the senescence extent in Hm^{hi} and limited that of melan a-N-RAS* cells, respectively, while enhancing the proliferation potential of both cell lines. Microarray analyses suggested *CTH* induction to be a factor involved in senescence prevention. This idea could be verified since CTH overexpression diminished the senescence extent in EGF-treated Hm^{hi} cells. Moreover, senescence appears not to be inert, because multinucleated Hm^{hi} and N-RAS* melanocytes budded off tiny, mononuclear cells, which were de-differentiated, anoikis-resistant, highly proliferative and induced early-metastasizing tumours in nude mice. Most likely, this finding is not restricted to murine melanocytes. Hence, our model might match melanoma

development from pre-existing senescent melanocytes and could possibly also hold true in other senescence models.

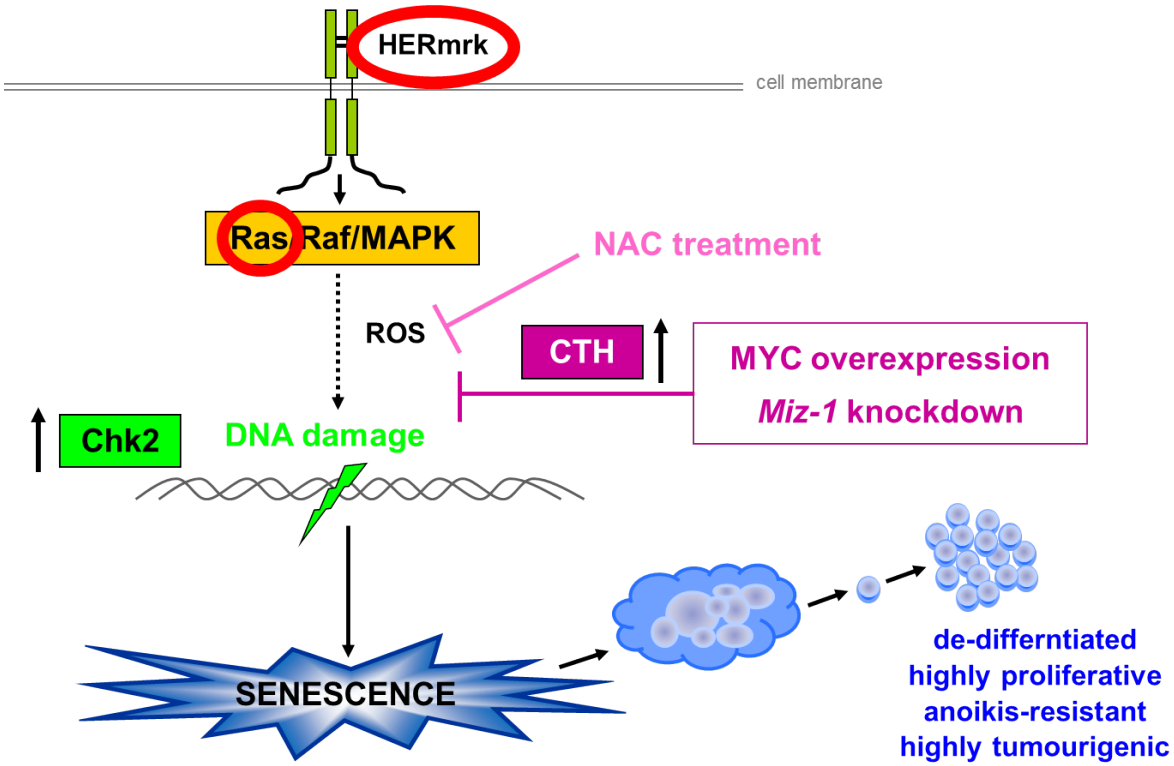

Figure 78: Proposed model for ROS-dependent oncogene-induced senescence in melanocytes
Prolonged HERmrk or N-RAS* expression in mouse melanocytes led to enhanced ROS levels and concurrent DNA damage, both of which could be limited by NAC treatment and diminished by MYC overexpression or *Miz-1* knockdown. Notably, CTH overexpression is likely to be a mediator for senescence suppression. The appearance of enlarged, multinucleated, senescent cells was followed by budding of tiny, mononucleated, highly proliferative, de-differentiated, anoikis-resistant and tumourigenic cells. The appearance of similar cells was also observed upon N-RAS* expression in human NHEM melanocytes.

The notion that induction of senescence is a prerequisite for tumour development seems paradoxical at first. However, several reports underpin our data. Mice expressing oncogenic RAS in their lungs develop malignant adenocarcinomas from benign and senescent adenomas [408]. In addition, p53 expression was found to correlate with previous UV exposure and invasion status of human melanoma [395]. With p53 being an important senescence mediator, this finding might point to a possible re-activation of the senescence programme in melanoma. Most importantly, we identified multinuclear, polyploid cells frequently observed in cancer as the source of the malignant offspring. Besides, senescent cells have been implicated in promoting cancer by secreting factors associated with senescence induction, inflammation (e.g. the chemokines IL-6 and IL-8) and tumour development. This

so-called senescence-associated phenotype (SASP) not only occurs in cultured cells, but also in vivo upon DNA-damage, e.g. chemotherapy [4,409,410]. The factors secreted by senescent cells include chemokines including the CXC family members usually involved in inflammation response signalling. CXCL-8 (also termed interleukin 8, IL-8) expression has been associated with enhanced migration, angiogenesis and tumour growth in melanoma and other malignancies [411–415]. Besides, CXCL-8 expression has been shown to positively correlate with melanoma progression [416,417]. Intriguingly, the expression of either CXCL-8 or its receptors CXCR1 and CXCR2 has been associated with melanoma aggressiveness [418]. In addition, the observation that knocking down the chemokine receptor *CXCR2* in primary human fibroblasts diminishes the DNA damage response and senescence extent [419], while CXCR1 and CXCR2 overexpression boosts the tumourigenic potential of human melanoma cells [420] further supports the dual role of SASP in senescence and cancer progression.

Intriguingly, even though chemotherapy frequently induces complete tumour regression, relapses months or years upon treatment are common and observed in more than half of all advanced cervical cancer patients [421]. Moreover, DNA damaging agents applied in tumour therapy either induce apoptosis or limit cancer cell proliferation via senescence induction [422–425] or drive cells into aberrant mitosis termed mitotic catastrophe [426–428]. More importantly, tumours formed upon inoculation of rat colon carcinoma cells in syngeneic rats regressed within ten days in response to short-term cisplatin treatment, but tumour growth resumed three weeks later. Intriguingly, regressed tumours displayed enlarged, SA-β-Gal-positive cells, whereas relapse malignancies contained an abundance of small, cohesive, SA-β-Gal-negative cells [404].

Taken together, even though senescence is considered a major barrier to tumour induction and has been proposed to be a favourable approach for the development of novel cancer therapeutics in general [429] and in melanoma in particular [430], our data prove that oncogene-induced, multinuclear, senescent melanocytes are not inert, but provide a source for highly malignant progeny. These daughter cells are characterized by a de-differentiated, proliferation-promoting gene expression pattern and an increased nuclear/cytoplasmic ratio accompanied by re-established NANOG protein levels. Intriguingly, the anoikis-resistant cells exhibit rapid, excessive tumour growth and metastasis in nude mice. Thus, chemotherapy-induced polyploidy and senescence might lead to the emergence of a tumour that is more aggressive than that initially subjected to DNA damaging agents.

9. Conclusion

For decades, senescence has been considered to be a potent barrier against tumour progression. The fact that cancer cells have maintained the ability to senesce *in vivo* has raised hope for novel cytostatic drugs. Temozolomide (TMZ), a DNA-alkylating agent and chemotherapeutic drug used to fight metastatic melanoma with a response rate of only 10-20%, induces a $p21^{CIP1}$-mediated G2/M arrest accompanied by senescence-like features in some melanoma cells [431]. Besides, a subset of human melanoma cell lines bearing activating BRAF or N-RAS mutations also adopt senescence-like phenotypes in response to the diterpene ester and anti-cancer agent PEP005 [432]. Treatment with PEP005 induces SA-β-Gal reactivity, Rb activation, $p21^{CIP1}$ up-regulation and induction of an irreversible G2/M cell cycle arrest in a MAPK-dependent manner [432]. Moreover, researchers and companies are screening for more senescence-inducing agents using various melanoma cell lines, because they consider senescence induction as the future melanoma therapy of choice. However, our data strongly argue against this idea. Even though senescence induction seems favourable at first sight, our observations of de-differentiated, highly tumourigenic and anoikis-resistant cells generated from senescent ones might be a possible and noteworthy side-effect. Furthermore, recent observations have demonstrated that, although growth stopped, senescent cells display secretory capacity known as the senescence-associated secretory phenotype (SASP). The SASP comprises metalloprotease (MMP1, MMP3 or MMP10), pro-inflammatory chemokines (CXCL2, IL6, IL8 and TGF-β) and growth factors (GROα, HGF, VEGF) with auto- and paracrine effects, which might favour tumourigenesis in nearby non-senescent cells [433,434]. Whether senescent melanoma cells develop a SASP is still unknown. Nevertheless, one should also consider the high level of heterogeneity in melanomas and the micro-environments of the tumours, both of which influence the features of tumour cells. In addition, in all studies mentioned, the senescence arrest has only been investigated over a one or two-week period. Thus, it remains unclear, whether this growth arrest is irreversible. Furthermore, the causal role and requirement of most of the biomarkers investigated in senescence induction remains to be elucidated in greater detail. The senescence-related data collected over the last decades suggest the existence of a complex and overlapping regulatory network of senescence-inducing stimuli. Thus, it remains to be elucidated how the senescence programmes induced by modulation of these factors are connected. Taken together, future insights gained from the molecular events of senescence induction and follow-up events in melanocytes and melanoma cells might help us identify potential drug targets, without considering senescence induction to be the way to go.

10. References

1. Parkin, D. M., Bray, F., Ferlay, J. & Pisani, P. Estimating the world cancer burden: Globocan 2000. *International journal of cancer* **94**, 153-6 (2001).

2. Garbe, C. & Leiter, U. Melanoma epidemiology and trends. *Clin. Dermatol.* **27**, 3-9

3. Parkin, D. M., Bray, F., Ferlay, J. & Pisani, P. Global cancer statistics, 2002. *CA Cancer J Clin* **55**, 74-108

4. Atzpodien, J., Terfloth, K., Fluck, M. & Reitz, M. Cisplatin, gemcitabine, and treosulfan in relapsed stage IV cutaneous malignant melanoma patients. *Br. J. Cancer* **97**, 1329-32 (2007).

5. Atzpodien, J., Terfloth, K., Fluck, M. & Reitz, M. Cisplatin, gemcitabine and treosulfan is effective in chemotherapy-pretreated relapsed stage IV uveal melanoma patients. *Cancer Chemother. Pharmacol.* **62**, 685-8 (2008).

6. Tauceri, F. *et al.* Surgery and adjuvant therapies in the treatment of stage IV melanoma: our experience in 84 patients. *Langenbeck's archives of surgery / Deutsche Gesellschaft für Chirurgie* **394**, 1079-84 (2009).

7. Haass, N. K. & Smalley, K. S. M. Melanoma biomarkers: current status and utility in diagnosis, prognosis, and response to therapy. *Mol Diagn Ther* **13**, 283-96 (2009).

8. Gray-schopfer, V., Wellbrock, C. & Marais, R. Melanoma biology and new targeted therapy. *Nature* **445**, 851-857 (2007).

9. Chin, L., Garraway, L. A. & Fisher, D. E. Malignant melanoma: genetics and therapeutics in the genomic era. *Genes Dev.* **20**, 2149-82 (2006).

10. Michaloglou, C. *et al.* BRAFE600-associated senescence-like cell cycle arrest of human naevi. *Nature* **436**, 720-724 (2005).

11. Gray-Schopfer, V. C. *et al.* Cellular senescence in naevi and immortalisation in melanoma: a role for p16? *Br. J. Cancer* **95**, 496-505 (2006).

12. Kuilman, T. *et al.* Oncogene-induced senescence relayed by an interleukin-dependent inflammatory network. *Cell* **133**, 1019-31 (2008).

13. Meier, F. *et al.* Molecular events in melanoma development and progression. *Front. Biosci.* **3**, D1005-10 (1998).

14. Maldonado, J. L. *et al.* Determinants of BRAF mutations in primary melanomas. *J. Natl. Cancer Inst.* **95**, 1878-90 (2003).

15. Curtin, J. A. *et al.* Distinct sets of genetic alterations in melanoma. *N. Engl. J. Med.* **353**, 2135-47 (2005).

16. Bennett, D. C. How to make a melanoma: what do we know of the primary clonal events? *Pigment Cell Melanoma Res* **21**, 27-38 (2008).

17. Pollock, P. M. *et al.* High frequency of BRAF mutations in nevi. *Nat. Genet.* **33**, 19-20 (2003).

18. Bauer, J., Curtin, J. A., Pinkel, D. & Bastian, B. C. Congenital melanocytic nevi frequently harbor NRAS mutations but no BRAF mutations. *J. Invest. Dermatol.* **127**, 179-82 (2007).

19. Demunter, A., Stas, M., Degreef, H., De Wolf-Peeters, C. & van den Oord, J. J. Analysis of N- and K-ras mutations in the distinctive tumor progression phases of melanoma. *J. Invest. Dermatol.* **117**, 1483-9 (2001).

20. Chin, L. *et al.* Cooperative effects of INK4a and ras in melanoma susceptibility in vivo. *Genes & Development* **11**, 2822-2834 (1997).

21. Bardeesy, N. *et al.* Dual inactivation of RB and p53 pathways in RAS-induced melanomas. *Mol. Cell. Biol.* **21**, 2144-2153 (2001).

22. Natali, P. G. *et al.* Expression of the c-Met/HGF receptor in human melanocytic neoplasms: demonstration of the relationship to malignant melanoma tumour progression. *Br. J. Cancer* **68**, 746-50 (1993).

23. Goding, C. R. Melanocyte development and malignant melanoma. *Forum (Genova)* **10**, 176-87

24. Li, G. *et al.* Downregulation of E-cadherin and Desmoglein 1 by autocrine hepatocyte growth factor during melanoma development. *Oncogene* **20**, 8125-35 (2001).

25. Gray-Schopfer, V. C., da Rocha Dias, S. & Marais, R. The role of B-RAF in melanoma. *Cancer Metastasis Rev.* **24**, 165-83 (2005).

26. Curtin, J. A., Busam, K., Pinkel, D. & Bastian, B. C. Somatic activation of KIT in distinct subtypes of melanoma. *J. Clin. Oncol.* **24**, 4340-6 (2006).

27. Bardeesy, N. *et al.* Role of epidermal growth factor receptor signaling in RAS-driven melanoma. *Mol. Cell. Biol.* **25**, 4176-88 (2005).

28. Wellbrock, C. & Schartl, M. Activation of phosphatidylinositol 3- kinase by a complex of p59fyn and the receptor tyrosine kinase Xmrk is involved in malignant transformation of pigment cells. *Eur. J. Biochem.* **267**, 3513-3522 (2000).

29. Geissinger, E., Weisser, C., Fischer, P., Schartl, M. & Wellbrock, C. Autocrine Stimulation by Osteopontin Contributes to Antiapoptotic Signalling of Melanocytes in Dermal Collagen Autocrine Stimulation by Osteopontin Contributes to Antiapoptotic Signalling of. *Cancer Research* 4820-4828 (2002).

30. Van Raamsdonk, C. D. *et al.* Frequent somatic mutations of GNAQ in uveal melanoma and blue naevi. *Nature* **457**, 599-602 (2009).

31. Kalinec, G., Nazarali, A. J., Hermouet, S., Xu, N. & Gutkind, J. S. Mutated alpha subunit of the Gq protein induces malignant transformation in NIH 3T3 cells. *Mol. Cell. Biol.* **12**, 4687-93 (1992).

32. Van Raamsdonk, C. D. *et al.* Mutations in GNA11 in Uveal Melanoma. *N. Engl. J. Med.* **363**, 2191-9 (2010).

33. Zhou, X. P. *et al.* Epigenetic PTEN silencing in malignant melanomas without PTEN mutation. *Am. J. Pathol.* **157**, 1123-8 (2000).

34. Stahl, J. M. *et al.* Deregulated Akt3 activity promotes development of malignant melanoma. *Cancer Res.* **64**, 7002-10 (2004).

35. Ford, D. *et al.* Risk of cutaneous melanoma associated with a family history of the disease. The International Melanoma Analysis Group (IMAGE). *Int. J. Cancer* **62**, 377-81 (1995).

36. Gandini, S. *et al.* Meta-analysis of risk factors for cutaneous melanoma: III. Family history, actinic damage and phenotypic factors. *Eur. J. Cancer* **41**, 2040-59 (2005).

37. Hussussian, C. J. *et al.* Germline p16 mutations in familial melanoma. *Nat. Genet.* **8**, 15-21 (1994).

38. Kamb, A. *et al.* Analysis of the p16 gene (CDKN2) as a candidate for the chromosome 9p melanoma susceptibility locus. *Nat. Genet.* **8**, 23-6 (1994).

39. Kamb, A. *et al.* A cell cycle regulator potentially involved in genesis of many tumor types. *Science* **264**, 436-40 (1994).

40. Nobori, T. *et al.* Deletions of the cyclin-dependent kinase-4 inhibitor gene in multiple human cancers. *Nature* **368**, 753-6 (1994).

41. Bartkova, J. *et al.* The p16-cyclin D/Cdk4-pRb pathway as a functional unit frequently altered in melanoma pathogenesis. *Cancer Res.* **56**, 5475-83 (1996).

42. Walker, G. J. *et al.* Virtually 100% of melanoma cell lines harbor alterations at the DNA level within CDKN2A, CDKN2B, or one of their downstream targets. *Genes Chromosomes Cancer* **22**, 157-63 (1998).

43. Gilchrest, B. A., Eller, M. S., Geller, A. C. & Yaar, M. The pathogenesis of melanoma induced by ultraviolet radiation. *N. Engl. J. Med.* **340**, 1341-8 (1999).

44. Gandini, S. *et al.* Meta-analysis of risk factors for cutaneous melanoma: I. Common and atypical naevi. *Eur. J. Cancer* **41**, 28-44 (2005).

45. Clarke, M. F. *et al.* Cancer stem cells--perspectives on current status and future directions: AACR Workshop on cancer stem cells. *Cancer Res.* **66**, 9339-44 (2006).

46. Schatton, T. *et al.* Identification of cells initiating human melanomas. *Nature* **451**, 345-9 (2008).

47. Boiko, A. D. *et al.* Human melanoma-initiating cells express neural crest nerve growth factor receptor CD271. *Nature* **466**, 133-137 (2010).

48. Roesch, A. *et al.* A Temporarily Distinct Subpopulation of Slow-Cycling Melanoma Cells Is Required for Continuous Tumor Growth. *Cell* **141**, 583-594 (2010).

49. Held, M. A. *et al.* Characterization of melanoma cells capable of propagating tumors from a single cell. *Cancer Res.* **70**, 388-97 (2010).

50. Quintana, E. *et al.* Phenotypic Heterogeneity among Tumorigenic Melanoma Cells from Patients that Is Reversible and Not Hierarchically Organized. *Cancer Cell* **18**, 510-523 (2010).

51. Quintana, E. *et al.* Efficient tumour formation by single human melanoma cells. *Nature* **456**, 593-8 (2008).

52. Danen, E. H. *et al.* E-cadherin expression in human melanoma. *Melanoma Res.* **6**, 127-31 (1996).

53. Thomas, A. J. & Erickson, C. A. The making of a melanocyte: the specification of melanoblasts from the neural crest. *Pigment Cell Melanoma Res* **21**, 598-610 (2008).

54. Seftor, E. A. *et al.* Epigenetic transdifferentiation of normal melanocytes by a metastatic melanoma microenvironment. *Cancer Res.* **65**, 10164-9 (2005).

55. Hoek, K. S. *et al.* Metastatic potential of melanomas defined by specific gene expression profiles with no BRAF signature. *Pigment Cell Res.* **19**, 290-302 (2006).

56. Hoek, K. S. *et al.* In vivo switching of human melanoma cells between proliferative and invasive states. *Cancer Res.* **68**, 650-6 (2008).

57. Pinner, S. *et al.* Intravital imaging reveals transient changes in pigment production and Brn2 expression during metastatic melanoma dissemination. *Cancer Res.* **69**, 7969-77 (2009).

58. Goodall, J. *et al.* Brn-2 represses microphthalmia-associated transcription factor expression and marks a distinct subpopulation of microphthalmia-associated transcription factor-negative melanoma cells. *Cancer Res.* **68**, 7788-94 (2008).

59. Wellbrock, C., Fischer, P. & Schartl, M. PI3-kinase is involved in mitogenic signaling by the oncogenic receptor tyrosine kinase Xiphophorus melanoma receptor kinase in fish melanoma. *Exp. Cell Res.* **251**, 340-349 (1999).

60. Meierjohann, S., Schartl, M. & Volff, J.-N. Genetic, biochemical and evolutionary facets of Xmrk-induced melanoma formation in the fish Xiphophorus. *Comp. Biochem. Physiol. C Toxicol. Pharmacol.* **138**, 281-9 (2004).

61. Wellbrock, C., Gomez, A. & Schartl, M. Signal transduction by the oncogenic receptor tyrosine kinase Xmrk in melanoma formation of Xiphophorus. *Pigment Cell Res* **10**, 34-40 (1997).

62. Teutschbein, J., Schartl, M. & Meierjohann, S. Interaction of Xiphophorus and murine Fyn with focal adhesion kinase. *Comp. Biochem. Physiol. C Toxicol. Pharmacol.* **149**, 168-74 (2009).

63. Meierjohann, S., Wende, E., Kraiss, A., Wellbrock, C. & Schartl, M. The oncogenic epidermal growth factor receptor variant Xiphophorus melanoma receptor kinase induces motility in melanocytes by modulation of focal adhesions. *Cancer Res.* **66**, 3145-52 (2006).

64. Morcinek, J. C., Weisser, C., Geissinger, E., Schartl, M. & Wellbrock, C. Activation of STAT5 triggers proliferation and contributes to anti-apoptotic signalling mediated by the oncogenic Xmrk kinase. *Oncogene* **21**, 1668-78 (2002).

65. Wellbrock, C. & Schartl, M. Multiple binding sites in the growth factor receptor Xmrk mediate binding to p59fyn, GRB2 and Shc. *Eur. J. Biochem.* **260**, 275-283 (1999).

66. Felding-Habermann, B., Mueller, B. M., Romerdahl, C. A. & Cheresh, D. A. Involvement of integrin alpha V gene expression in human melanoma tumorigenicity. *J. Clin. Invest.* **89**, 2018-22 (1992).

67. Seftor, R. E. Role of the beta3 integrin subunit in human primary melanoma progression: multifunctional activities associated with alpha(v)beta3 integrin expression. *Am. J. Pathol.* **153**, 1347-51 (1998).

68. Meierjohann, S. *et al.* MMP-13 mediates cell cycle progression in melanocytes and melanoma cells: in vitro studies of migration and proliferation. *Mol. Cancer* **9**, 201 (2010).

69. Meierjohann, S., Mueller, T., Schartl, M. & Buehner, M. A structural model of the extracellular domain of the oncogenic EGFR variant Xmrk. *Zebrafish* **3**, 359-69 (2006).

70. Gomez, A. Ligand-independent Dimerization and Activation of the Oncogenic Xmrk Receptor by Two Mutations in the Extracellular Domain. *Journal of Biological Chemistry* **276**, 3333-3340 (2000).

71. Bennett, D. C. *et al.* Cloned mouse melanocyte lines carrying the germline mutations albino and brown: complementation in culture. *Development* **105**, 379-85 (1989).

72. Wittbrodt, J., Lammers, R., Malitschek, B., Ullrich, A. & Schartl, M. The Xmrk receptor tyrosine kinase is activated in Xiphophorus malignant melanoma. *EMBO J.* **11**, 4239-46 (1992).

73. HAYFLICK, L. & MOORHEAD, P. S. The serial cultivation of human diploid cell strains. *Exp. Cell Res.* **25**, 585-621 (1961).

74. Bischof, O. Deconstructing PML-induced premature senescence. *EMBO J.* **21**, 3358-3369 (2002).

75. Marcotte, R. & Wang, E. Replicative senescence revisited. *J. Gerontol. A Biol. Sci. Med. Sci.* **57**, B257-69 (2002).

76. Serrano, M. & Blasco, M. A. Putting the stress on senescence. *Curr. Opin. Cell Biol.* **13**, 748-53 (2001).

77. Collado, M. & Serrano, M. The power and the promise of oncogene-induced senescence markers. *Nat. Rev. Cancer* **6**, 472-6 (2006).

78. Sharpless, N. E. & DePinho, R. A. Cancer: crime and punishment. *Nature* **436**, 636-7 (2005).

79. Haferkamp, S. *et al.* The relative contributions of the p53 and pRb pathways in oncogene-induced melanocyte senescence. *Aging (Albany NY)* **1**, 542-56 (2009).

80. Terzian, T. *et al.* p53 prevents progression of nevi to melanoma predominantly through cell cycle regulation. *Pigment Cell & Melanoma Research* **23**, 781-794 (2010).

81. Sviderskaya, E. V. *et al.* p16(Ink4a) in melanocyte senescence and differentiation. *J. Natl. Cancer Inst.* **94**, 446-54 (2002).

82. Quelle, D. E., Zindy, F., Ashmun, R. A. & Sherr, C. J. Alternative reading frames of the INK4a tumor suppressor gene encode two unrelated proteins capable of inducing cell cycle arrest. *Cell* **83**, 993-1000 (1995).

83. Serrano, M., Hannon, G. J. & Beach, D. A. new regulatory motif in cell-cycle control causing specific inhibition of cyclin D/CDK4. *Nature* **366**, 704-707 (1993).

84. Pomerantz, J. *et al.* The Ink4a tumor suppressor gene product, p19Arf, interacts with MDM2 and neutralizes MDM2's inhibition of p53. *Cell* **92**, 713-23 (1998).

85. Chin, L., Pomerantz, J. & DePinho, R. A. The INK4a/ARF tumor suppressor: one gene--two products--two pathways. *Trends Biochem. Sci.* **23**, 291-6 (1998).

86. Pavletich, N. P. Mechanisms of cyclin-dependent kinase regulation: structures of Cdks, their cyclin activators, and Cip and INK4 inhibitors. *J. Mol. Biol.* **287**, 821-8 (1999).

87. Serrano, M. The tumor suppressor protein p16INK4a. *Exp. Cell Res.* **237**, 7-13 (1997).

88. Malumbres, M. *et al.* Cellular response to oncogenic ras involves induction of the Cdk4 and Cdk6 inhibitor p15(INK4b). *Mol. Cell. Biol.* **20**, 2915-25 (2000).

89. Ortega, S., Malumbres, M. & Barbacid, M. Cyclin D-dependent kinases, INK4 inhibitors and cancer. *Biochim. Biophys. Acta* **1602**, 73-87 (2002).

90. Lowe, S. W. & Sherr, C. J. Tumor suppression by Ink4a-Arf: progress and puzzles. *Curr. Opin. Genet. Dev.* **13**, 77-83 (2003).

91. Passegué, E. & Wagner, E. F. JunB suppresses cell proliferation by transcriptional activation of p16(INK4a) expression. *EMBO J.* **19**, 2969-79 (2000).

92. Kamijo, T. *et al.* Tumor suppression at the mouse INK4a locus mediated by the alternative reading frame product p19ARF. *Cell* **91**, 649-659 (1997).

93. Sharpless, N. E. *et al.* Loss of p16Ink4a with retention of p19Arf predisposes mice to tumorigenesis. *Nature 413:86- Sharpless, N. E., K. Kannan, J. Xu, M. W. Bosenberg, and L. Chin* (2001).

94. Franklin, D. S. CDK inhibitors p18INK4c and p27kip1 mediate two separate pathways to collaboratively supppress pituitary tumorigenesis. *Genes & Development* (1998).at <http://www.ncbi.nlm.nih.gov/pmc/articles/PMC317173/pdf/x8.pdf>

95. Latres, E. *et al.* Limited overlapping roles of P15(INK4b) and P18(INK4c) cell cycle inhibitors in proliferation and tumorigenesis. *EMBO J.* **19**, 3496-3506 (2000).

96. Zindy, F., van Deursen, J., Grosveld, G., Sherr, C. J. & Roussel, M. F. INK4d-deficient mice are fertile despite testicular atrophy. *Mol. Cell. Biol.* **20**, 372-8 (2000).

97. Krimpenfort, P. *et al.* p15Ink4b is a critical tumour suppressor in the absence of p16Ink4a. *Nature* **448**, 943-6 (2007).

98. Ortega, S., Malumbres, M. & Barbacid, M. Cyclin D-dependent kinases, INK4 inhibitors and cancer. *Biochim. Biophys. Acta* **1602**, 73-87 (2002).

99. Bai, F., Pei, X.-H., Godfrey, V. L. & Xiong, Y. Haploinsufficiency of p18(INK4c) sensitizes mice to carcinogen-induced tumorigenesis. *Mol. Cell. Biol.* **23**, 1269-77 (2003).

100. Hossain, M. G. *et al.* Expression of p18(INK4C) is down-regulated in human pituitary adenomas. *Endocr. Pathol.* **20**, 114-21 (2009).

101. Sánchez-Aguilera, A. *et al.* Silencing of the p18INK4c gene by promoter hypermethylation in Reed-Sternberg cells in Hodgkin lymphomas. *Blood* **103**, 2351-7 (2004).

102. Uziel, T. *et al.* The tumor suppressors Ink4c and p53 collaborate independently with Patched to suppress medulloblastoma formation. *Genes Dev.* **19**, 2656-67 (2005).

103. Leone, P. E. *et al.* Deletions of CDKN2C in multiple myeloma: biological and clinical implications. *Clin. Cancer Res.* **14**, 6033-41 (2008).

104. Sherr, C. J. Cancer Cell Cycles. *Science (80-)* **3788**, (1996).

105. Pardee, a B. A restriction point for control of normal animal cell proliferation. *Proc. Natl. Acad. Sci. U.S.A.* **71**, 1286-90 (1974).

106. Eischen, C. M., Weber, J. D., Roussel, M. F., Sherr, C. J. & Cleveland, J. L. Disruption of the ARF-Mdm2-p53 tumor suppressor pathway in Myc-induced lymphomagenesis. *Genes Dev.* **13**, 2658-69 (1999).

107. Narita, M. *et al.* Rb-mediated heterochromatin formation and silencing of E2F target genes during cellular senescence. *Cell* **113**, 703-16 (2003).

108. Dannenberg, J. H., van Rossum, A., Schuijff, L. & te Riele, H. Ablation of the retinoblastoma gene family deregulates G(1) control causing immortalization and

increased cell turnover under growth-restricting conditions. *Genes Dev.* **14**, 3051-64 (2000).

109. Efeyan, A. & Serrano, M. p53: guardian of the genome and policeman of the oncogenes. *Cell Cycle* **6**, 1006-10 (2007).

110. Embry, M. R., Billiard, S. M. & Giulio, R. T. D. Lack of p53 induction in fish cells by model chemotherapeutics. *Oncogene* **2**, 2004-2010 (2010).

111. Schmitt, C. A. Senescence, apoptosis and therapy--cutting the lifelines of cancer. *Nat. Rev. Cancer* **3**, 286-95 (2003).

112. Harris, S. L. & Levine, A. J. The p53 pathway: positive and negative feedback loops. *Oncogene* **24**, 2899-908 (2005).

113. Lozano, G. The oncogenic roles of p53 mutants in mouse models. *Curr. Opin. Genet. Dev.* **17**, 66-70 (2007).

114. Brown, J. P. Bypass of Senescence After Disruption of p21CIP1/WAF1 Gene in Normal Diploid Human Fibroblasts. *Science (80-)* **277**, 831-834 (1997).

115. Pantoja, C. & Serrano, M. Murine fibroblasts lacking p21 undergo senescence and are resistant to transformation by oncogenic Ras. *Oncogene* **18**, 4974-82 (1999).

116. Dirac, A. M. G. & Bernards, R. Reversal of senescence in mouse fibroblasts through lentiviral suppression of p53. *J. Biol. Chem.* **278**, 11731-4 (2003).

117. Berghmans, S. *et al.* tp53 mutant zebrafish develop malignant peripheral nerve sheath tumors. *Proc. Natl. Acad. Sci. U.S.A.* **102**, 407-12 (2005).

118. Chen, S., Hong, Y., Scherer, S. J. & Schartl, M. Lack of ultraviolet-light inducibility of the medakafish (Oryzias latipes) tumor suppressor gene p53. *Gene* **264**, 197-203 (2001).

119. Oren, M. Regulation of the p53 Tumor Suppressor Protein. *Journal of Biological Chemistry* **274**, 36031-36034 (1999).

120. Barak, Y., Juven, T., Haffner, R. & Oren, M. Mdm2 Expression Is Induced By Wild Type P53 Activity. *EMBO J.* **12**, 461-8 (1993).

121. Wu, X., Bayle, J. H., Olson, D. & Levine, a J. The p53-mdm-2 autoregulatory feedback loop. *Genes & Development* **7**, 1126-1132 (1993).

122. Jones, S. N., Roe, a E., Donehower, L. a & Bradley, a Rescue of embryonic lethality in Mdm2-deficient mice by absence of p53. *Nature* **378**, 206-8 (1995).

123. Rescue of early embryonic lethality in Mdm2-deficient mice by deletion of p53.pdf.

124. Grandori, C., Cowley, S. M., James, L. P. & Eisenman, R. N. The Myc/Max/Mad network and the transcriptional control of cell behavior. *Annu. Rev. Cell Dev. Biol.* **16**, 653-99 (2000).

125. Baudino, T. A. *et al.* c-Myc is essential for vasculogenesis and angiogenesis during development and tumor progression. *Genes Dev.* **16**, 2530-43 (2002).

126. Arnold, I. & Watt, F. M. c-Myc activation in transgenic mouse epidermis results in mobilization of stem cells and differentiation of their progeny. *Curr. Biol.* **11**, 558-68 (2001).

127. Frye, M., Gardner, C., Li, E. R., Arnold, I. & Watt, F. M. Evidence that Myc activation depletes the epidermal stem cell compartment by modulating adhesive interactions with the local microenvironment. *Development* **130**, 2793-808 (2003).

128. Pelengaris, S., Khan, M. & Evan, G. I. Suppression of Myc-induced apoptosis in beta cells exposes multiple oncogenic properties of Myc and triggers carcinogenic progression. *Cell* **109**, 321-34 (2002).

129. Felsher, D. W. & Bishop, J. M. Transient excess of MYC activity can elicit genomic instability and tumorigenesis. *Proc. Natl. Acad. Sci. U.S.A.* **96**, 3940-4 (1999).

130. Blackwood, E. M. & Eisenman, R. N. Max: a helix-loop-helix zipper protein that forms a sequence-specific DNA-binding complex with Myc. *Science* **251**, 1211-7 (1991).

131. Amati, B. *et al.* Transcriptional activation by the human c-Myc oncoprotein in yeast requires interaction with Max. *Nature* **359**, 423-6 (1992).

132. Kretzner, L., Blackwood, E. M. & Eisenman, R. N. Myc and Max proteins possess distinct transcriptional activities. *Nature* **359**, 426-9 (1992).

133. Li, L. H., Nerlov, C., Prendergast, G., MacGregor, D. & Ziff, E. B. c-Myc represses transcription in vivo by a novel mechanism dependent on the initiator element and Myc box II. *EMBO J.* **13**, 4070-9 (1994).

134. Mao, D. Y. L. *et al.* Analysis of Myc bound loci identified by CpG island arrays shows that Max is essential for Myc-dependent repression. *Curr. Biol.* **13**, 882-6 (2003).

135. Steiger, D., Furrer, M., Schwinkendorf, D. & Gallant, P. Max-independent functions of Myc in Drosophila melanogaster. *Nat. Genet.* **40**, 1084-91 (2008).

136. Fernandez, P. C. *et al.* Genomic targets of the human c-Myc protein. *Genes Dev.* **17**, 1115-29 (2003).

137. Cowling, V. H. & Cole, M. D. Myc Regulation of mRNA Cap Methylation. *Genes Cancer* **1**, 576-579 (2010).

138. Davis, A. C., Wims, M., Spotts, G. D., Hann, S. R. & Bradley, A. A null c-myc mutation causes lethality before 10.5 days of gestation in homozygotes and reduced fertility in heterozygous female mice. *Genes & Development* **7**, 671-682 (1993).

139. Charron, J. *et al.* Embryonic lethality in mice homozygous for a targeted disruption of the N-myc gene. *Genes & Development* **6**, 2248-2257 (1992).

140. Seoane, J., Le, H.-V. & Massagué, J. Myc suppression of the p21(Cip1) Cdk inhibitor influences the outcome of the p53 response to DNA damage. *Nature* **419**, 729-34 (2002).

141. Herold, S. *et al.* Negative regulation of the mammalian UV response by Myc through association with Miz-1. *Mol. Cell* **10**, 509-21 (2002).

142. Kozar, K. *et al.* Mouse development and cell proliferation in the absence of D-cyclins. *Cell* **118**, 477-91 (2004).

143. Miliani de Marval, P. L. *et al.* Lack of cyclin-dependent kinase 4 inhibits c-myc tumorigenic activities in epithelial tissues. *Mol. Cell. Biol.* **24**, 7538-47 (2004).

144. Nesbit, C. E., Tersak, J. M. & Prochownik, E. V. MYC oncogenes and human neoplastic disease. *Oncogene* **18**, 3004-16 (1999).

145. Adhikary, S. & Eilers, M. Transcriptional regulation and transformation by Myc proteins. *Nat. Rev. Mol. Cell Biol.* **6**, 635-45 (2005).

146. Pelengaris, S. & Khan, M. The many faces of c-MYC. *Arch. Biochem. Biophys.* **416**, 129-36 (2003).

147. Schlagbauer-Wadl, H. *et al.* Influence of increased c-Myc expression on the growth characteristics of human melanoma. *J. Invest. Dermatol.* **112**, 332-6 (1999).

148. Tulley, P. N. *et al.* The relation between c-myc expression and interferon sensitivity in uveal melanoma. *Br J Ophthalmol* **88**, 1563-7 (2004).

149. Parrella, P., Caballero, O. L., Sidransky, D. & Merbs, S. L. Detection of c-myc amplification in uveal melanoma by fluorescent in situ hybridization. *Invest. Ophthalmol. Vis. Sci.* **42**, 1679-84 (2001).

150. Biroccio, A. *et al.* c-Myc down-regulation increases susceptibility to cisplatin through reactive oxygen species-mediated apoptosis in M14 human melanoma cells. *Mol. Pharmacol.* **60**, 174-82 (2001).

151. Bucci, B. *et al.* Myc down-regulation sensitizes melanoma cells to radiotherapy by inhibiting MLH1 and MSH2 mismatch repair proteins. *Clin. Cancer Res.* **11**, 2756-67 (2005).

152. Aziz, N., Cherwinski, H. & McMahon, M. Complementation of defective colony-stimulating factor 1 receptor signaling and mitogenesis by Raf and v-Src. *Mol. Cell. Biol.* **19**, 1101-15 (1999).

153. Whitwam, T. *et al.* Differential oncogenic potential of activated RAS isoforms in melanocytes. *Oncogene* **26**, 4563-70 (2007).

154. Karlsson, A. *et al.* Genomically complex lymphomas undergo sustained tumor regression upon MYC inactivation unless they acquire novel chromosomal translocations. *Blood* **101**, 2797-803 (2003).

155. Wu, C.-H. *et al.* Cellular senescence is an important mechanism of tumor regression upon c-Myc inactivation. *Proc. Natl. Acad. Sci. U.S.A.* **104**, 13028-33 (2007).

156. Mallette, F. a, Gaumont-Leclerc, M.-F., Huot, G. & Ferbeyre, G. Myc down-regulation as a mechanism to activate the Rb pathway in STAT5A-induced senescence. *J. Biol. Chem.* **282**, 34938-44 (2007).

157. Biroccio, A., Amodei, S., Antonelli, A., Benassi, B. & Zupi, G. Inhibition of c-Myc oncoprotein limits the growth of human melanoma cells by inducing cellular crisis. *J. Biol. Chem.* **278**, 35693-701 (2003).

158. Guney, I., Wu, S. & Sedivy, J. M. Reduced c-Myc signaling triggers telomere-independent senescence by regulating Bmi-1 and p16(INK4a). *Proc. Natl. Acad. Sci. U.S.A.* **103**, 3645-50 (2006).

159. Zhuang, D. *et al.* C-MYC overexpression is required for continuous suppression of oncogene-induced senescence in melanoma cells. *Oncogene* **27**, 6623-34 (2008).

160. Land, H., Parada, L. F. & Weinberg, R. A. Tumorigenic conversion of primary embryo fibroblasts requires at least two cooperating oncogenes. *Nature* **304**, 596-602

161. Drayton, S. *et al.* Tumor suppressor p16INK4a determines sensitivity of human cells to transformation by cooperating cellular oncogenes. *Cancer Cell* **4**, 301-10 (2003).

162. Murphy, D. *et al.* Distinct Thresholds Govern Myc's Biological Output In Vivo. *Cancer Cell* **14**, 447-457 (2008).

163. Hermeking, H. & Eick, D. Mediation of c-Myc-induced apoptosis by p53. *Science* **265**, 2091-3 (1994).

164. Wagner, A. J., Kokontis, J. M. & Hay, N. Myc-mediated apoptosis requires wild-type p53 in a manner independent of cell cycle arrest and the ability of p53 to induce p21waf1/cip1. *Genes Dev.* **8**, 2817-30 (1994).

165. Zindy, F. *et al.* Myc signaling via the ARF tumor suppressor regulates p53-dependent apoptosis and immortalization. *Genes Dev.* **12**, 2424-33 (1998).

166. Finch, A. *et al.* Bcl-xL gain of function and p19 ARF loss of function cooperate oncogenically with Myc in vivo by distinct mechanisms. *Cancer Cell* **10**, 113-20 (2006).

167. Ziegelbauer, J., Wei, J. & Tjian, R. Myc-interacting protein 1 target gene profile: a link to microtubules, extracellular signal-regulated kinase, and cell growth. *Proc. Natl. Acad. Sci. U.S.A.* **101**, 458-63 (2004).

168. Staller, P. *et al.* Repression of p15INK4b expression by Myc through association with Miz-1. *Nat. Cell Biol.* **3**, 392-9 (2001).

169. Kime, L. & Wright, S. C. Mad4 is regulated by a transcriptional repressor complex that contains Miz-1 and c-Myc. *Biochem. J.* **370**, 291-8 (2003).

170. Seoane, J. *et al.* TGFbeta influences Myc, Miz-1 and Smad to control the CDK inhibitor p15INK4b. *Nat. Cell Biol.* **3**, 400-8 (2001).

171. Peukert, K. *et al.* An alternative pathway for gene regulation by Myc. *EMBO J.* **16**, 5672-86 (1997).

172. Liu, Q., Basu, S., Qiu, Y., Tang, F. & Dong, F. A role of Miz-1 in Gfi-1-mediated transcriptional repression of CDKN1A. *Oncogene* **29**, 2843-52 (2010).

173. Vriz, S., Lemaitre, J. M., Leibovici, M., Thierry, N. & Méchali, M. Comparative analysis of the intracellular localization of c-Myc, c-Fos, and replicative proteins during cell cycle progression. *Mol. Cell. Biol.* **12**, 3548-55 (1992).

174. Ziegelbauer, J. *et al.* Transcription factor MIZ-1 is regulated via microtubule association. *Mol. Cell* **8**, 339-49 (2001).

175. Wanzel, M. *et al.* A ribosomal protein L23-nucleophosmin circuit coordinates Miz1 function with cell growth. *Nat. Cell Biol.* (2008).doi:10.1038/ncb1764

176. D'Agnano, I. *et al.* Myc down-regulation induces apoptosis in M14 melanoma cells by increasing p27(kip1) levels. *Oncogene* **20**, 2814-25 (2001).

177. Greco, C. *et al.* c-MYC deregulation is involved in melphalan resistance of multiple myeloma: role of PDGF-BB. *Int J Immunopathol Pharmacol* **19**, 67-79

178. Storchova, Z. & Pellman, D. From polyploidy to aneuploidy, genome instability and cancer. *Nat. Rev. Mol. Cell Biol.* **5**, 45-54 (2004).

179. Comai, L. The advantages and disadvantages of being polyploid. *Nat. Rev. Genet.* **6**, 836-46 (2005).

180. Kellis, M., Birren, B. W. & Lander, E. S. Proof and evolutionary analysis of ancient genome duplication in the yeast Saccharomyces cerevisiae. *Nature* **428**, 617-24 (2004).

181. Ganem, N. J., Storchova, Z. & Pellman, D. Tetraploidy, aneuploidy and cancer. *Curr. Opin. Genet. Dev.* **17**, 157-62 (2007).

182. Nowell, P. C. The clonal evolution of tumor cell populations. *Science* **194**, 23-8 (1976).

183. Lengauer, C., Kinzler, K. W. & Vogelstein, B. Genetic instabilities in human cancers. *Nature* **396**, 643-9 (1998).

184. Kronenwett, U. *et al.* Improved grading of breast adenocarcinomas based on genomic instability. *Cancer Res.* **64**, 904-9 (2004).

185. Carter, S. L., Eklund, A. C., Kohane, I. S., Harris, L. N. & Szallasi, Z. A signature of chromosomal instability inferred from gene expression profiles predicts clinical outcome in multiple human cancers. *Nat. Genet.* **38**, 1043-8 (2006).

186. Rhodes, D. R. *et al.* ONCOMINE: a cancer microarray database and integrated data-mining platform. *Neoplasia* **6**, 1-6

187. Zimmet, J. & Ravid, K. Polyploidy: occurrence in nature, mechanisms, and significance for the megakaryocyte-platelet system. *Exp. Hematol.* **28**, 3-16 (2000).

188. Eggert, U. S., Mitchison, T. J. & Field, C. M. Animal cytokinesis: from parts list to mechanisms. *Annu. Rev. Biochem.* **75**, 543-66 (2006).

189. Mullins, J. M. & Biesele, J. J. Cytokinetic activities in a human cell line: the midbody and intercellular bridge. *Tissue Cell* **5**, 47-61 (1973).

190. Norden, C. *et al.* The NoCut pathway links completion of cytokinesis to spindle midzone function to prevent chromosome breakage. *Cell* **125**, 85-98 (2006).

191. Shi, Q. & King, R. W. Chromosome nondisjunction yields tetraploid rather than aneuploid cells in human cell lines. *Nature* **437**, 1038-42 (2005).

192. Rieder, C. L. & Maiato, H. Stuck in division or passing through: what happens when cells cannot satisfy the spindle assembly checkpoint. *Dev. Cell* **7**, 637-51 (2004).

193. Ogle, B. M., Cascalho, M. & Platt, J. L. Biological implications of cell fusion. *Nat. Rev. Mol. Cell Biol.* **6**, 567-75 (2005).

194. Brito, D. a & Rieder, C. L. Mitotic checkpoint slippage in humans occurs via cyclin B destruction in the presence of an active checkpoint. *Curr. Biol.* **16**, 1194-200 (2006).

195. Brito, D. a, Yang, Z. & Rieder, C. L. Microtubules do not promote mitotic slippage when the spindle assembly checkpoint cannot be satisfied. *J. Cell Biol.* **182**, 623-9 (2008).

196. Olaharski, A. J. *et al.* Tetraploidy and chromosomal instability are early events during cervical carcinogenesis. *Carcinogenesis* **27**, 337-43 (2006).

197. Galipeau, P. C. *et al.* progression to aneuploidy in Barrett ' s esophagus. *Cell* **93**, 7081-7084 (1996).

198. Rajagopalan, H. & Lengauer, C. Aneuploidy and cancer. *Nature* **432**, 338-41 (2004).

199. Fujiwara, T. *et al.* Cytokinesis failure generating tetraploids promotes tumorigenesis in p53-null cells. *Nature* **437**, 1043-7 (2005).

200. Lam, E. W., Robinson, C. & Watson, R. J. Characterization and cell cycle-regulated expression of mouse B-myb. *Oncogene* **7**, 1885-90 (1992).

201. Santilli, G. *et al.* Temperature-dependent modification and activation of B-MYB: implications for cell survival. *J. Biol. Chem.* **280**, 15628-34 (2005).

202. Grassilli, E., Salomoni, P., Perrotti, D., Franceschi, C. & Calabretta, B. Resistance to apoptosis in CTLL-2 cells overexpressing B-Myb is associated with B-Myb-dependent bcl-2 induction. *Cancer Res.* **59**, 2451-6 (1999).

203. Sitzmann, J., Noben-Trauth, K., Kamano, H. & Klempnauer, K. H. Expression of B-Myb during mouse embryogenesis. *Oncogene* **12**, 1889-94 (1996).

204. Tanaka, Y., Patestos, N. P., Maekawa, T. & Ishii, S. B-myb is required for inner cell mass formation at an early stage of development. *J. Biol. Chem.* **274**, 28067-70 (1999).

205. Tarasov, K. V. *et al.* B-MYB is essential for normal cell cycle progression and chromosomal stability of embryonic stem cells. *PLoS ONE* **3**, e2478 (2008).

206. Fu, J., Bian, M., Jiang, Q. & Zhang, C. Roles of Aurora kinases in mitosis and tumorigenesis. *Mol. Cancer Res.* **5**, 1-10 (2007).

207. Klein, U. R., Nigg, E. A. & Gruneberg, U. Centromere targeting of the chromosomal passenger complex requires a ternary subcomplex of Borealin, Survivin, and the N-terminal domain of INCENP. *Mol. Biol. Cell* **17**, 2547-58 (2006).

208. Bischoff, J. R. *et al.* A homologue of Drosophila aurora kinase is oncogenic and amplified in human colorectal cancers. *EMBO J.* **17**, 3052-65 (1998).

209. Morgan, D. O. Cyclin-dependent kinases: engines, clocks, and microprocessors. *Annu. Rev. Cell Dev. Biol.* **13**, 261-91 (1997).

210. Sherr, C. J. & Roberts, J. M. CDK inhibitors: positive and negative regulators of G1-phase progression. *Genes Dev.* **13**, 1501-12 (1999).

211. Sherr, C. J. & Roberts, J. M. Living with or without cyclins and cyclin-dependent kinases. *Genes Dev.* **18**, 2699-711 (2004).

212. Riabowol, K., Draetta, G., Brizuela, L., Vandre, D. & Beach, D. The cdc2 kinase is a nuclear protein that is essential for mitosis in mammalian cells. *Cell* **57**, 393-401 (1989).

213. Butt, A. J. *et al.* Cell cycle machinery: links with genesis and treatment of breast cancer. *Adv. Exp. Med. Biol.* **630**, 189-205 (2008).

214. Zhang, W., Shields, J. M., Sogawa, K., Fujii-Kuriyama, Y. & Yang, V. W. The gut-enriched Krüppel-like factor suppresses the activity of the CYP1A1 promoter in an Sp1-dependent fashion. *J. Biol. Chem.* **273**, 17917-25 (1998).

215. Yoon, H. S., Chen, X. & Yang, V. W. Kruppel-like factor 4 mediates p53-dependent G1/S cell cycle arrest in response to DNA damage. *J. Biol. Chem.* **278**, 2101-5 (2003).

216. Yoon, H. S. & Yang, V. W. Requirement of Krüppel-like factor 4 in preventing entry into mitosis following DNA damage. *J. Biol. Chem.* **279**, 5035-41 (2004).

217. Ghaleb, A. M., Katz, J. P., Kaestner, K. H., Du, J. X. & Yang, V. W. Krüppel-like factor 4 exhibits antiapoptotic activity following gamma-radiation-induced DNA damage. *Oncogene* **26**, 2365-73 (2007).

218. Wei, Z. *et al.* Klf4 interacts directly with Oct4 and Sox2 to promote reprogramming. *Stem Cells* **27**, 2969-78 (2009).

219. Li, F. *et al.* Control of apoptosis and mitotic spindle checkpoint by survivin. *Nature* **396**, 580-4 (1998).

220. Altieri, D. C. Validating survivin as a cancer therapeutic target. *Nat. Rev. Cancer* **3**, 46-54 (2003).

221. Kelly, R. J., Lopez-Chavez, A., Citrin, D., Janik, J. E. & Morris, J. C. Impacting tumor cell-fate by targeting the inhibitor of apoptosis protein survivin. *Mol. Cancer* **10**, 35 (2011).

222. Uren, A. G. *et al.* Survivin and the inner centromere protein INCENP show similar cell-cycle localization and gene knockout phenotype. *Curr. Biol.* **10**, 1319-28 (2000).

223. Wheatley, S. P., Carvalho, A., Vagnarelli, P. & Earnshaw, W. C. INCENP is required for proper targeting of Survivin to the centromeres and the anaphase spindle during mitosis. *Curr. Biol.* **11**, 886-90 (2001).

224. Beltrami, E. Acute Ablation of Survivin Uncovers p53-dependent Mitotic Checkpoint Functions and Control of Mitochondrial Apoptosis. *Journal of Biological Chemistry* **279**, 2077-2084 (2003).

225. Zhang, Y. *et al.* Aberrant quantity and localization of Aurora-B/AIM-1 and survivin during megakaryocyte polyploidization and the consequences of Aurora-B/AIM-1-deregulated expression. *Blood* **103**, 3717-26 (2004).

226. Wen, Q. *et al.* Survivin is not required for the endomitotic cell cycle of megakaryocytes. *Blood* **114**, 153-6 (2009).

227. Pfaffl, M. W., Horgan, G. W. & Dempfle, L. Relative expression software tool (REST) for group-wise comparison and statistical analysis of relative expression results in real-time PCR. *Nucleic Acids Res* **30**, e36 (2002).

228. Wittbrodt, J., Lammers, R., Malitschek, B., Ullrich, A. & Schartl, M. The Xmrk receptor tyrosine kinase is activated in Xiphophorus malignant melanoma. *EMBO J.* **11**, 4239-46 (1992).

229. Krueger, C. *et al.* A gene regulation system with four distinct expression levels. *Journal of Gene Medicine, The* 1037-1047 (2006).doi:10.1002/jgm

230. Leikam, C., Hufnagel, A., Schartl, M. & Meierjohann, S. Oncogene activation in melanocytes links reactive oxygen to multinucleated phenotype and senescence. *Oncogene* **27**, 7070-82 (2008).

231. Collado, M., Blasco, M. A. & Serrano, M. Cellular senescence in cancer and aging. *Cell* **130**, 223-233 (2007).

232. Jones, C. J. *et al.* Evidence for a telomere-independent "clock" limiting RAS oncogene-driven proliferation of human thyroid epithelial cells. *Mol. Cell. Biol.* **20**, 5690-9 (2000).

233. Gray-Schopfer, V. C. *et al.* Cellular senescence in naevi and immortalisation in melanoma: a role for p16? *Br. J. Cancer* **95**, 496-505 (2006).

234. Bartkova, J. *et al.* Oncogene-induced senescence is part of the tumorigenesis barrier imposed by DNA damage checkpoints. *Nature* **444**, 633-7 (2006).

235. Mallette, F. A., Gaumont-Leclerc, M.-F. & Ferbeyre, G. The DNA damage signaling pathway is a critical mediator of oncogene-induced senescence. *Genes Dev.* **21**, 43-8 (2007).

236. Nuciforo, P. G., Luise, C., Capra, M., Pelosi, G. & d' Adda di Fagagna, F. Complex engagement of DNA damage response pathways in human cancer and in lung tumor progression. *Carcinogenesis* **28**, 2082-8 (2007).

237. Aliouat-Denis, C.-M. *et al.* p53-independent regulation of p21Waf1/Cip1 expression and senescence by Chk2. *Mol. Cancer Res.* **3**, 627-34 (2005).

238. Chen, C.-R. *et al.* Dual induction of apoptosis and senescence in cancer cells by Chk2 activation: checkpoint activation as a strategy against cancer. *Cancer Res.* **65**, 6017-21 (2005).

239. Hirose, Y., Katayama, M., Mirzoeva, O. K., Berger, M. S. & Pieper, R. O. Akt activation suppresses Chk2-mediated, methylating agent-induced G2 arrest and protects from temozolomide-induced mitotic catastrophe and cellular senescence. *Cancer Res.* **65**, 4861-9 (2005).

240. Liu, X., Miller, C. W., Koeffler, P. H. & Berk, a J. The p53 activation domain binds the TATA box-binding polypeptide in Holo-TFIID, and a neighboring p53 domain inhibits transcription. *Mol. Cell. Biol.* **13**, 3291-300 (1993).

241. Avantaggiati, M. L. *et al.* Recruitment of p300/CBP in p53-dependent signal pathways. *Cell* **89**, 1175-84 (1997).

242. Finkel, T. Intracellular redox regulation by the family of small GTPases. *Antioxid. Redox Signal.* **8**, 1857-63 (2006).

243. Kopnin, P. B., Agapova, L. S., Kopnin, B. P. & Chumakov, P. M. Repression of sestrin family genes contributes to oncogenic Ras-induced reactive oxygen species up-regulation and genetic instability. *Cancer Res.* **67**, 4671-8 (2007).

244. Lee, A. C. *et al.* Ras proteins induce senescence by altering the intracellular levels of reactive oxygen species. *J. Biol. Chem.* **274**, 7936-40 (1999).

245. Li, F. Survivin study: what is the next wave? *J. Cell. Physiol.* **197**, 8-29 (2003).

246. Duffy, M. J., O'Donovan, N., Brennan, D. J., Gallagher, W. M. & Ryan, B. M. Survivin: a promising tumor biomarker. *Cancer Lett.* **249**, 49-60 (2007).

247. Chi, S., Cao, H., Wang, Y. & McNiven, M. A. Recycling of the epidermal growth factor receptor is mediated by a novel form of the clathrin adaptor EPS15. *J. Biol. Chem.* **286**, 35196-208 (2011).

248. Platta, H. W. & Stenmark, H. Endocytosis and signaling. *Curr. Opin. Cell Biol.* **23**, 393-403 (2011).

249. Sorkin, A. Internalization of the epidermal growth factor receptor: role in signalling. *Biochem. Soc. Trans.* **29**, 480-4 (2001).

250. Ceresa, B. P. Regulation of EGFR endocytic trafficking by rab proteins. *Histol. Histopathol.* **21**, 987-93 (2006).

251. Sørensen, S., Ranheim, T., Bakken, K. S., Leren, T. P. & Kulseth, M. A. Retention of mutant low density lipoprotein receptor in endoplasmic reticulum (ER) leads to ER stress. *J. Biol. Chem.* **281**, 468-76 (2006).

252. Jortikka, L., Laitinen, M., Lindholm, T. S. & Marttinen, A. Internalization and intracellular processing of bone morphogenetic protein (BMP) in rat skeletal muscle myoblasts (L6). *Cell. Signal.* **9**, 47-51 (1997).

253. Guidolin, D. *et al.* Bioinformatics and mathematical modelling in the study of receptor-receptor interactions and receptor oligomerization: focus on adenosine receptors. *Biochim. Biophys. Acta* **1808**, 1267-83 (2011).

254. Kost, D. P. & Michalopoulos, G. K. Effect of epidermal growth factor on the expression of protooncogenes c-myc and c-Ha-ras in short-term primary hepatocyte culture. *J. Cell. Physiol.* **144**, 122-7 (1990).

255. Jamerson, M. H., Johnson, M. D. & Dickson, R. B. Dual regulation of proliferation and apoptosis: c-myc in bitransgenic murine mammary tumor models. *Oncogene* **19**, 1065-71 (2000).

256. Gebhardt, A. *et al.* Myc regulates keratinocyte adhesion and differentiation via complex formation with Miz1. *J. Cell Biol.* **172**, 139-49 (2006).

257. Yada, M. *et al.* Phosphorylation-dependent degradation of c-Myc is mediated by the F-box protein Fbw7. *EMBO J.* **23**, 2116-25 (2004).

258. Popov, N., Schülein, C., Jaenicke, L. A. & Eilers, M. Ubiquitylation of the amino terminus of Myc by SCF(β-TrCP) antagonizes SCF(Fbw7)-mediated turnover. *Nat. Cell Biol.* **12**, 973-81 (2010).

259. Wanzel, M. *et al.* Akt and 14-3-3eta regulate Miz1 to control cell-cycle arrest after DNA damage. *Nat. Cell Biol.* **7**, 30-41 (2005).

260. Leikam, C;Hufnagel, A; Walz, S;Keitz, S;Eilers, M;Schartl, M;Meierjohann, S. Cystathionase mediates senescence evasion in melanocytes and melanoma cells. *submitted to Oncogene* (2012).

261. van Dieck, J. *et al.* Posttranslational modifications affect the interaction of S100 proteins with tumor suppressor p53. *J. Mol. Biol.* **394**, 922-30 (2009).

262. Słomnicki, L. P. & Leśniak, W. S100A6 (calcyclin) deficiency induces senescence-like changes in cell cycle, morphology and functional characteristics of mouse NIH 3T3 fibroblasts. *J. Cell. Biochem.* **109**, 576-84 (2010).

263. Copie-Bergman, C. *et al.* MAL expression in lymphoid cells: further evidence for MAL as a distinct molecular marker of primary mediastinal large B-cell lymphomas. *Mod. Pathol.* **15**, 1172-80 (2002).

264. Cao, W. *et al.* Epigenetic silencing of MAL, a putative tumor suppressor gene, can contribute to human epithelium cell carcinoma. *Mol. Cancer* **9**, 296 (2010).

265. Uehara, N., Matsuoka, Y. & Tsubura, A. Mesothelin promotes anchorage-independent growth and prevents anoikis via extracellular signal-regulated kinase signaling pathway in human breast cancer cells. *Mol. Cancer Res.* **6**, 186-93 (2008).

266. Sunde, M. *et al.* TC-1 is a novel tumorigenic and natively disordered protein associated with thyroid cancer. *Cancer Res.* **64**, 2766-73 (2004).

267. Park, J. *et al.* TC1 (C8orf4) is upregulated by cellular stress and mediates heat shock response. *Biochem. Biophys. Res. Commun.* **360**, 447-52 (2007).

268. Thompson, T. C. Glioma pathogenesis-related protein 1: tumor-suppressor activities and therapeutic potential. *Yonsei Med. J.* **51**, 479-83 (2010).

269. Rao, A. M., Drake, M. R. & Stipanuk, M. H. Role of the transsulfuration pathway and of gamma-cystathionase activity in the formation of cysteine and sulfate from methionine in rat hepatocytes. *J. Nutr.* **120**, 837-45 (1990).

270. Rosado, J. O., Salvador, M. & Bonatto, D. Importance of the trans-sulfuration pathway in cancer prevention and promotion. *Mol. Cell. Biochem.* **301**, 1-12 (2007).

271. Ewald, J. A., Desotelle, J. A., Wilding, G. & Jarrard, D. F. Therapy-induced senescence in cancer. *J. Natl. Cancer Inst.* **102**, 1536-46 (2010).

272. Giuliano, S., Ohanna, M., Ballotti, R. & Bertolotto, C. Advances in melanoma senescence and potential clinical application. *Pigment Cell Melanoma Res* (2010).doi:10.1111/j.1755-148X.2010.00820.x

273. Leal, J. A., Feliciano, A. & Lleonart, M. E. Stem cell MicroRNAs in senescence and immortalization: novel players in cancer therapy. *Med Res Rev* (2011).doi:10.1002/med.20246

274. Roninson, I. B., Broude, E. V. & Chang, B. D. If not apoptosis, then what? Treatment-induced senescence and mitotic catastrophe in tumor cells. *Drug Resist. Updat.* **4**, 303-13 (2001).

275. Coppé, J.-P. *et al.* Senescence-associated secretory phenotypes reveal cell-nonautonomous functions of oncogenic RAS and the p53 tumor suppressor. *PLoS Biol.* **6**, 2853-68 (2008).

276. Fumagalli, M. sasPense and ddRama in cancer and ageing. **11**, 2008-2010 (2009).

277. Rodier, F. & Campisi, J. Four faces of cellular senescence. *The Journal of Cell Biology* **192**, 547-56 (2011).

278. Schartl, M. Platyfish and swordtails: a genetic system for the analysis of molecular mechanisms in tumor formation. *Trends Genet.* **11**, 185-9 (1995).

279. Fidler, I. J. Biological behavior of malignant melanoma cells correlated to their survival in vivo. *Cancer Res.* **35**, 218-24 (1975).

280. Yao, H. *et al.* Effective melanoma immunotherapy with interleukin-2 delivered by a novel polymeric nanoparticle. *Mol. Cancer Ther.* **10**, 1082-92 (2011).

281. Bongiovanni, M. *et al.* Cytomorphologic features of poorly differentiated thyroid carcinoma: a multi-institutional analysis of 40 cases. *Cancer* **117**, 185-94 (2009).

282. Sun, L. *et al.* High-grade neuroendocrine carcinoma of the lung: comparative clinicopathological study of large cell neuroendocrine carcinoma and small cell lung carcinoma. *Pathol. Int.* **59**, 522-9 (2009).

283. Jang, S. J., Gardner, J. M. & Ro, J. Y. Diagnostic approach and prognostic factors of cancers. *Adv Anat Pathol* **18**, 165-72 (2011).

284. Tani, H., Morris, R. J. & Kaur, P. Enrichment for murine keratinocyte stem cells based on cell surface phenotype. *Proc. Natl. Acad. Sci. U.S.A.* **97**, 10960-5 (2000).

285. Sato, N. *et al.* Molecular signature of human embryonic stem cells and its comparison with the mouse. *Dev. Biol.* **260**, 404-13 (2003).

286. Sato, N., Meijer, L., Skaltsounis, L., Greengard, P. & Brivanlou, A. H. Maintenance of pluripotency in human and mouse embryonic stem cells through activation of Wnt signaling by a pharmacological GSK-3-specific inhibitor. *Nat. Med.* **10**, 55-63 (2004).

287. Hotta, A. *et al.* Isolation of human iPS cells using EOS lentiviral vectors to select for pluripotency. *Nat. Methods* **6**, 370-6 (2009).

288. Leikam, C; Hufnagel, AL; Otto, C; Kneitz, S; Mühling, B; Murphy, DJ; Wagner, TU; Schartl, M; Meierjohann, S. Oncogenic RAS-induced senescent cells are a source for tumor-initiating cells. *submitted* (2012).

289. Kuwata, T., Kitagawa, M. & Kasuga, T. Proliferative activity of primary cutaneous melanocytic tumours. *Virchows Arch A Pathol Anat Histopathol* **423**, 359-64 (1993).

290. Michaloglou, C. *et al.* BRAFE600-associated senescence-like cell cycle arrest of human naevi. *Nature* **436**, 720-4 (2005).

291. Barnhill, R. L. *et al.* Atypical spitz nevi/tumors: Lack of consensus for diagnosis, discrimination from melanoma, and prediction of outcome. *Human Pathology* **30**, 513-520 (1999).

292. Gray-schopfer, V. C. Cellular senescence in naevi and immortalisation in melanoma: a role for p16. *Br. J. Cancer* **95**, 496-505 (2006).

293. Sewing, A., Wiseman, B., Lloyd, A. C. & Land, H. High-Intensity Raf Signal Causes Cell Cycle Arrest Mediated by p21 Cip1. *Microbiology* **17**, 5588-5597 (1997).

294. Woods, D. *et al.* Raf-Induced Proliferation or Cell Cycle Arrest Is Determined by the Level of Raf Activity with Arrest Mediated by p21 Cip1. *Microbiology* **17**, 5598-5611 (1997).

295. Sarkisian, C. J. *et al.* Dose-dependent oncogene-induced senescence in vivo and its evasion during mammary tumorigenesis. *Nat. Cell Biol.* **9**, 493-505 (2007).

296. Denoyelle, C. *et al.* Anti-oncogenic role of the endoplasmic reticulum differentially activated by mutations in the MAPK pathway. *Nat. Cell Biol.* **8**, 1053-63 (2006).

297. Kuystermans, D., Dunn, M. J. & Al-Rubeai, M. A proteomic study of cMyc improvement of CHO culture. *BMC Biotechnol.* **10**, 25 (2010).

298. Wong, T.-S. *et al.* MicroRNA let-7 suppresses nasopharyngeal carcinoma cells proliferation through downregulating c-Myc expression. *J. Cancer Res. Clin. Oncol.* **137**, 415-22 (2011).

299. Ren, R. Modeling the dosage effect of oncogenes in leukemogenesis. *Curr. Opin. Hematol.* **11**, 25-34 (2004).

300. Itahana, K. *et al.* A role for p53 in maintaining and establishing the quiescence growth arrest in human cells. *J. Biol. Chem.* **277**, 18206-14 (2002).

301. Blagosklonny, M. V. Cell senescence and hypermitogenic arrest. *EMBO Rep.* **4**, 358-62 (2003).

302. Kim, S. Y., Kang, H. T., Choi, H. R. & Park, S. C. Biliverdin reductase A in the prevention of cellular senescence against oxidative stress. *Exp. Mol. Med.* **43**, 15-23 (2011).

303. David-Watine, B. Silencing nuclear pore protein tpr elicits a senescent-like phenotype in cancer cells. *PLoS ONE* **6**, e22423 (2011).

304. Rincheval, V. *et al.* Bcl-2 can promote p53-dependent senescence versus apoptosis without affecting the G1/S transition. *Biochem. Biophys. Res. Commun.* **298**, 282-8 (2002).

305. Spyridopoulos, I., Isner, J. M. & Losordo, D. W. Oncogenic ras induces premature senescence in endothelial cells: role of p21(Cip1/Waf1). *Basic Res. Cardiol.* **97**, 117-24 (2002).

306. Shitikova, Z. V., Aksenov, N. D., Pospelov, V. A. & Pospelov, T. V. [Cell senescence induced by histone deacetylase inhibitor sodium butyrate in rodent transformed cells resistant to apoptosis]. *Tsitologiia* **53**, 277-84 (2011).

307. Cmielová, J. *et al.* DNA damage caused by ionizing radiation in embryonic diploid fibroblasts WI-38 induces both apoptosis and senescence. *Physiol Res* **60**, 667-77 (2011).

308. Cazzalini, O., Scovassi, A. I., Savio, M., Stivala, L. A. & Prosperi, E. Multiple roles of the cell cycle inhibitor p21(CDKN1A) in the DNA damage response. *Mutat. Res.* **704**, 12-20

309. Jee, H. J. *et al.* Nek6 suppresses the premature senescence of human cancer cells induced by camptothecin and doxorubicin treatment. *Biochem. Biophys. Res. Commun.* **408**, 669-73 (2011).

310. Vigneron, A., Roninson, I. B., Gamelin, E. & Coqueret, O. Src inhibits adriamycin-induced senescence and G2 checkpoint arrest by blocking the induction of p21waf1. *Cancer Res.* **65**, 8927-35 (2005).

311. Xiao, H., Hasegawa, T., Miyaishi, O., Ohkusu, K. & Isobe, K. i Sodium butyrate induces NIH3T3 cells to senescence-like state and enhances promoter activity of p21WAF/CIP1 in p53-independent manner. *Biochem. Biophys. Res. Commun.* **237**, 457-60 (1997).

312. Kramer, D. L. *et al.* Polyamine Depletion in Human Melanoma Cells Leads to G1 Arrest Associated with Induction of p21WAF1/CIP1/SDI1, Changes in the Expression of p21-regulated Genes, and a Senescence-like Phenotype. *Cancer Res.* **61**, 7754-7762 (2001).

313. Weeda, G. *et al.* Disruption of mouse ERCC1 results in a novel repair syndrome with growth failure, nuclear abnormalities and senescence. *Curr. Biol.* **7**, 427-39 (1997).

314. Takahashi, K. & Yamanaka, S. Induction of pluripotent stem cells from mouse embryonic and adult fibroblast cultures by defined factors. *Cell* **126**, 663-76 (2006).

315. Sanada, F. *et al.* Hepatocyte growth factor, but not vascular endothelial growth factor, attenuates angiotensin II-induced endothelial progenitor cell senescence. *Hypertension* **53**, 77-82 (2009).

316. Zhou, Z. *et al.* Calcitonin gene-related peptide inhibits angiotensin II-induced endothelial progenitor cells senescence through up-regulation of klotho expression. *Atherosclerosis* **213**, 92-101 (2010).

317. Leopold, J. G. & Richards, D. B. Cellular blue naevi. *J Pathol Bacteriol* **94**, 247-55 (1967).

318. Savchenko, I. I. [Endomitosis in pigmented neoplasms of human skin]. *TSitologiia i genetika* **22**, 20-4

319. Sakaue-Sawano, A. *et al.* Visualizing Spatiotemporal Dynamics of Multicellular Cell-Cycle Progression. *Cell* **132**, 487-498 (2008).

320. Haferkamp, S. *et al.* Oncogene-Induced Senescence Does Not Require the p16(INK4a) or p14ARF Melanoma Tumor Suppressors. *J. Invest. Dermatol.* (2009).doi:10.1038/jid.2009.5

321. Olsen, C. L., Gardie, B., Yaswen, P. & Stampfer, M. R. Raf-1-induced growth arrest in human mammary epithelial cells is p16-independent and is overcome in immortal cells during conversion. *Oncogene* **21**, 6328-39 (2002).

322. Chao, C. *et al.* Cell type- and promoter-specific roles of Ser18 phosphorylation in regulating p53 responses. *J. Biol. Chem.* **278**, 41028-33 (2003).

323. Shieh, S. Y., Ikeda, M., Taya, Y. & Prives, C. DNA damage-induced phosphorylation of p53 alleviates inhibition by MDM2. *Cell* **91**, 325-34 (1997).

324. Lambert, P. F., Kashanchi, F., Radonovich, M. F., Shiekhattar, R. & Brady, J. N. Phosphorylation of p53 serine 15 increases interaction with CBP. *J. Biol. Chem.* **273**, 33048-53 (1998).

325. Passos, J. F. & Von Zglinicki, T. Oxygen free radicals in cell senescence: are they signal transducers? *Free Radic. Res.* **40**, 1277-83 (2006).

326. Valko, M. *et al.* Free radicals and antioxidants in normal physiological functions and human disease. *Int. J. Biochem. Cell Biol.* **39**, 44-84 (2007).

327. Sedelnikova, O. A. *et al.* Role of oxidatively induced DNA lesions in human pathogenesis. *Mutat. Res.* **704**, 152-9

328. Irani, K. Mitogenic Signaling Mediated by Oxidants in Ras-Transformed Fibroblasts. *Science (80-)* **275**, 1649-1652 (1997).

329. Debidda, M., Williams, D. a & Zheng, Y. Rac1 GTPase regulates cell genomic stability and senescence. *J. Biol. Chem.* **281**, 38519-28 (2006).

330. Gorla, G. R., Malhi, H. & Gupta, S. Polyploidy associated with oxidative injury attenuates proliferative potential of cells. *J. Cell. Sci.* **114**, 2943-51 (2001).

331. Kurata, S. Selective activation of p38 MAPK cascade and mitotic arrest caused by low level oxidative stress. *J. Biol. Chem.* **275**, 23413-6 (2000).

332. Quintanilla, M., Brown, K., Ramsden, M. & Balmain, A. Carcinogen-specific mutation and amplification of Ha-ras during mouse skin carcinogenesis. *Nature* **322**, 78-80

333. Algarra, I., Perez, M., Serrano, M. J., Garrido, F. & Gaforio, J. J. c-K-ras overexpression is characteristic for metastases derived from a methylcholanthrene-induced fibrosarcoma. *Invasion Metastasis* **18**, 261-70

334. Lee, A. C. *et al.* Ras proteins induce senescence by altering the intracellular levels of reactive oxygen species. *J. Biol. Chem.* **274**, 7936-7940 (1999).

335. Dimicco, R., Fumagalli, M. & Daddadifagagna, F. Breaking news: high-speed race ends in arrest – how oncogenes induce senescence. *Trends in Cell Biology* (2007).doi:10.1016/j.tcb.2007.07.012

336. Rai, P. *et al.* Enhanced elimination of oxidized guanine nucleotides inhibits oncogenic RAS-induced DNA damage and premature senescence. *Oncogene* **30**, 1489-96 (2011).

337. Mitsushita, J., Lambeth, J. D. & Kamata, T. The superoxide-generating oxidase Nox1 is functionally required for Ras oncogene transformation. *Cancer Res.* **64**, 3580-5 (2004).

338. Weyemi, U. *et al.* ROS-generating NADPH oxidase NOX4 is a critical mediator in oncogenic H-Ras-induced DNA damage and subsequent senescence. *Oncogene* (2011).doi:10.1038/onc.2011.327

339. Zhu, H. *et al.* High expression of survivin predicts poor prognosis in esophageal squamous cell carcinoma following radiotherapy. *Tumour Biol.* (2011).doi:10.1007/s13277-011-0217-y

340. Xu, P., Xu, X.-L., Huang, Q., Zhang, Z.-H. & Zhang, Y.-B. CIP2A with survivin protein expressions in human non-small-cell lung cancer correlates with prognosis. *Med. Oncol.* (2011).doi:10.1007/s12032-011-0053-3

341. Schramm, S.-J. & Mann, G. J. Melanoma Prognosis: A REMARK-Based Systematic Review and Bioinformatic Analysis of Immunohistochemical and Gene Microarray Studies. *Mol. Cancer Ther.* **10**, 1520-8 (2011).

342. Gregory, M. A. & Hann, S. R. c-Myc proteolysis by the ubiquitin-proteasome pathway: stabilization of c-Myc in Burkitt's lymphoma cells. *Mol. Cell. Biol.* **20**, 2423-35 (2000).

343. Nakagawa, M. *et al.* Generation of induced pluripotent stem cells without Myc from mouse and human fibroblasts. *Nat. Biotechnol.* **26**, 101-6 (2008).

344. Wernig, M. *et al.* A drug-inducible transgenic system for direct reprogramming of multiple somatic cell types. *Nat. Biotechnol.* **26**, 916-24 (2008).

345. Feng, B., Ng, J.-H., Heng, J.-C. D. & Ng, H.-H. Molecules that promote or enhance reprogramming of somatic cells to induced pluripotent stem cells. *Cell Stem Cell* **4**, 301-12 (2009).

346. O'Donnell, K. A., Wentzel, E. A., Zeller, K. I., Dang, C. V. & Mendell, J. T. c-Myc-regulated microRNAs modulate E2F1 expression. *Nature* **435**, 839-43 (2005).

347. Chang, T.-C. *et al.* Widespread microRNA repression by Myc contributes to tumorigenesis. *Nat. Genet.* **40**, 43-50 (2008).

348. Ma, L. *et al.* miR-9, a MYC/MYCN-activated microRNA, regulates E-cadherin and cancer metastasis. *Nat. Cell Biol.* **12**, 247-56 (2010).

349. Gao, P. *et al.* c-Myc suppression of miR-23a/b enhances mitochondrial glutaminase expression and glutamine metabolism. *Nature* **458**, 762-5 (2009).

350. Yuneva, M., Zamboni, N., Oefner, P., Sachidanandam, R. & Lazebnik, Y. Deficiency in glutamine but not glucose induces MYC-dependent apoptosis in human cells. *J. Cell Biol.* **178**, 93-105 (2007).

351. Dang, C. V. *et al.* Function of the c-Myc oncogenic transcription factor. *Exp. Cell Res.* **253**, 63-77 (1999).

352. Albihn, A., Johnsen, J. I. & Henriksson, M. A. MYC in oncogenesis and as a target for cancer therapies. *Adv. Cancer Res.* **107**, 163-224 (2010).

353. Felsher, D. W. Cancer revoked: oncogenes as therapeutic targets. *Nat. Rev. Cancer* **3**, 375-80 (2003).

354. Wu, C.-H. *et al.* Cellular senescence is an important mechanism of tumor regression upon c-Myc inactivation. *Proc. Natl. Acad. Sci. U.S.A.* **104**, 13028-33 (2007).

355. Ross, D. A. & Wilson, G. D. Expression of c-myc oncoprotein represents a new prognostic marker in cutaneous melanoma. *Br J Surg* **85**, 46-51 (1998).

356. Campaner, S. *et al.* Cdk2 suppresses cellular senescence induced by the c-myc oncogene. *Nature Cell Biology* **12**, 54-59 (2010).

357. Grandori, C. *et al.* Werner syndrome protein limits MYC-induced cellular senescence. *Genes Dev.* **17**, 1569-74 (2003).

358. van Riggelen, J. *et al.* The interaction between Myc and Miz1 is required to antagonize TGFbeta-dependent autocrine signaling during lymphoma formation and maintenance. *Genes Dev.* **24**, 1281-94 (2010).

359. Conrad, M. & Sato, H. The oxidative stress-inducible cystine/glutamate antiporter, system x (c) (-) : cystine supplier and beyond. *Amino Acids* (2011).doi:10.1007/s00726-011-0867-5

360. Yang, G., Cao, K., Wu, L. & Wang, R. Cystathionine gamma-lyase overexpression inhibits cell proliferation via a H2S-dependent modulation of ERK1/2 phosphorylation and p21Cip/WAK-1. *J. Biol. Chem.* **279**, 49199-205 (2004).

361. Ishii, I. *et al.* Murine cystathionine gamma-lyase: complete cDNA and genomic sequences, promoter activity, tissue distribution and developmental expression. *Biochem. J.* **381**, 113-23 (2004).

362. Renga, B. Hydrogen sulfide generation in mammals: the molecular biology of cystathionine-β- synthase (CBS) and cystathionine-γ-lyase (CSE). *Inflamm Allergy Drug Targets* **10**, 85-91 (2011).

363. Ma, K. *et al.* H2S donor, S-propargyl-cysteine, increases CSE in SGC-7901 and cancer-induced mice: evidence for a novel anti-cancer effect of endogenous H2S? *PLoS ONE* **6**, e20525 (2011).

364. Perry, R. R., Mazetta, J. A., Levin, M. & Barranco, S. C. Glutathione levels and variability in breast tumors and normal tissue. *Cancer* **72**, 783-7 (1993).

365. Berger, S. J., Gosky, D., Zborowska, E., Willson, J. K. & Berger, N. A. Sensitive enzymatic cycling assay for glutathione: measurements of glutathione content and its

modulation by buthionine sulfoximine in vivo and in vitro in human colon cancer. *Cancer Res.* **54**, 4077-83 (1994).

366. Pendyala, L. *et al.* Translational studies of glutathione in bladder cancer cell lines and human specimens. *Clin. Cancer Res.* **3**, 793-8 (1997).

367. Carretero, J. *et al.* Growth-associated changes in glutathione content correlate with liver metastatic activity of B16 melanoma cells. *Clin. Exp. Metastasis* **17**, 567-74 (1999).

368. Honda, T. *et al.* GSH depletion enhances adenoviral bax-induced apoptosis in lung cancer cells. *Cancer Gene Ther.* **11**, 249-55 (2004).

369. Kandil, S., Brennan, L. & McBean, G. J. Glutathione depletion causes a JNK and p38MAPK-mediated increase in expression of cystathionine-gamma-lyase and upregulation of the transsulfuration pathway in C6 glioma cells. *Neurochem. Int.* **56**, 611-9 (2010).

370. Cao, Q., Zhang, L., Yang, G., Xu, C. & Wang, R. Butyrate-stimulated H2S production in colon cancer cells. *Antioxid. Redox Signal.* **12**, 1101-9 (2010).

371. Yang, G. *et al.* H2S as a physiologic vasorelaxant: hypertension in mice with deletion of cystathionine gamma-lyase. *Science* **322**, 587-90 (2008).

372. Sun, Q. *et al.* Structural basis for the inhibition mechanism of human cystathionine gamma-lyase, an enzyme responsible for the production of H(2)S. *J. Biol. Chem.* **284**, 3076-85 (2009).

373. Huang, S. *et al.* Site-directed mutagenesis on human cystathionine-gamma-lyase reveals insights into the modulation of H2S production. *J. Mol. Biol.* **396**, 708-18 (2010).

374. Szabó, C. Hydrogen sulphide and its therapeutic potential. *Nat Rev Drug Discov* **6**, 917-35 (2007).

375. Sober, A. J. *et al.* Early recognition of cutaneous melanoma. *JAMA* **242**, 2795-9 (1979).

376. Williams, M. L. & Sagebiel, R. W. Melanoma risk factors and atypical moles. *West. J. Med.* **160**, 343-50 (1994).

377. Reznikoff, C. A., Bertram, J. S., Brankow, D. W. & Heidelberger, C. Quantitative and qualitative studies of chemical transformation of cloned C3H mouse embryo cells sensitive to postconfluence inhibition of cell division. *Cancer Res.* **33**, 3239-49 (1973).

378. Kennedy, A. R., Murphy, G. & Little, J. B. Effect of time and duration of exposure to 12-O-tetradecanoylphorbol-13-acetate on x-ray transformation of C3H 10T 1/2 cells. *Cancer Res.* **40**, 1915-20 (1980).

379. Sundaram, M., Guernsey, D. L., Rajaraman, M. M. & Rajaraman, R. Neosis: a novel type of cell division in cancer. *Cancer Biol. Ther.* **3**, 207-18 (2004).

380. Levy, C., Khaled, M. & Fisher, D. E. MITF: master regulator of melanocyte development and melanoma oncogene. *Trends Mol Med* **12**, 406-14 (2006).

381. Cheli, Y. *et al.* Mitf is the key molecular switch between mouse or human melanoma initiating cells and their differentiated progeny. *Oncogene* **30**, 2390 (2011).

382. Kim, D.-S., Cho, H.-J., Choi, H.-R., Kwon, S.-B. & Park, K.-C. Isolation of human epidermal stem cells by adherence and the reconstruction of skin equivalents. *Cell. Mol. Life Sci.* **61**, 2774-81 (2004).

383. Redvers, R. P., Li, A. & Kaur, P. Side population in adult murine epidermis exhibits phenotypic and functional characteristics of keratinocyte stem cells. *Proc. Natl. Acad. Sci. U.S.A.* **103**, 13168-73 (2006).

384. Flørenes, V. A., Holm, R., Myklebost, O., Lendahl, U. & Fodstad, O. Expression of the neuroectodermal intermediate filament nestin in human melanomas. *Cancer Res.* **54**, 354-6 (1994).

385. Grichnik, J. M. Melanoma, nevogenesis, and stem cell biology. *J. Invest. Dermatol.* **128**, 2365-80 (2008).

386. Salmina, K. *et al.* Up-regulation of the embryonic self-renewal network through reversible polyploidy in irradiated p53-mutant tumour cells. *Exp. Cell Res.* **316**, 2099-112 (2010).

387. Vitale, I. *et al.* Multipolar mitosis of tetraploid cells: inhibition by p53 and dependency on Mos. *The EMBO Journal* **29**, 1272-1284 (2010).

388. Erenpreisa, J., Cragg, M. S., Salmina, K., Hausmann, M. & Scherthan, H. The role of meiotic cohesin REC8 in chromosome segregation in gamma irradiation-induced endopolyploid tumour cells. *Exp. Cell Res.* **315**, 2593-603 (2009).

389. Ianzini, F. *et al.* Activation of Meiosis-Specific Genes Is Associated with Depolyploidization of Human Tumor Cells following Radiation-Induced Mitotic Catastrophe. *Cancer Research* **69**, 2296-2304 (2009).

390. Kalejs, M. *et al.* Upregulation of meiosis-specific genes in lymphoma cell lines following genotoxic insult and induction of mitotic catastrophe. *BMC Cancer* **6**, 6 (2006).

391. Salmina, K. *et al.* Up-regulation of the embryonic self-renewal network through reversible polyploidy in irradiated p53-mutant tumour cells. *Experimental Cell Research* **316**, 2099-2112 (2010).

392. Friedlander, M. L., Hedley, D. W. & Taylor, I. W. Clinical and biological significance of aneuploidy in human tumours. *J. Clin. Pathol.* **37**, 961-74 (1984).

393. Cohen, L. M. The starburst giant cell is useful for distinguishing lentigo maligna from photodamaged skin. *J. Am. Acad. Dermatol.* **35**, 962-8 (1996).

394. Atillasoy, E. S. *et al.* UVB induces atypical melanocytic lesions and melanoma in human skin. *Am. J. Pathol.* **152**, 1179-86 (1998).

395. Purdue, M. P. *et al.* Etiologic factors associated with p53 immunostaining in cutaneousmalignant melanoma. *Int. J. Cancer* **117**, 486-93 (2005).

396. Stenzinger, W., Suter, L. & Schumann, J. DNA aneuploidy in congenital melanocytic nevi: suggestive evidence for premalignant changes. *J. Invest. Dermatol.* **82**, 569-72 (1984).

397. Pilch, H., Günzel, S., Schäffer, U., Tanner, B. & Heine, M. Evaluation of DNA ploidy and degree of DNA abnormality in benign and malignant melanocytic lesions of the skin using video imaging. *Cancer* **88**, 1370-7 (2000).

398. Clark, W. H. *et al.* A study of tumor progression: the precursor lesions of superficial spreading and nodular melanoma. *Hum. Pathol.* **15**, 1147-65 (1984).

399. Watt, A. J., Kotsis, S. V. & Chung, K. C. Risk of melanoma arising in large congenital melanocytic nevi: a systematic review. *Plast. Reconstr. Surg.* **113**, 1968-74 (2004).

400. Purdue, M. P. *et al.* Etiologic and other factors predicting nevus-associated cutaneous malignant melanoma. *Cancer Epidemiol. Biomarkers Prev.* **14**, 2015-22 (2005).

401. Chang, Yu-mei, Newton-Bishop Julia A, Bishop D Timothy, . . . A Pooled Analysis of Melanocytic Naevus Phenotype and the Risk of Cutaneous Melanoma at Different Latitudes. *Int J Cancer* **124**, 420-428 (2009).

402. Shah, K. N. The risk of melanoma and neurocutaneous melanosis associated with congenital melanocytic nevi. *Semin Cutan Med Surg* **29**, 159-64 (2010).

403. Huna, A. *et al.* Self-Renewal Signalling in Presenescent Tetraploid IMR90 Cells. *Journal of aging research* **2011**, 103253 (2011).

404. Puig, P.-E. *et al.* Tumor cells can escape DNA-damaging cisplatin through DNA endoreduplication and reversible polyploidy. *Cell Biol. Int.* **32**, 1031-43 (2008).

405. Michaloglou, C. *et al.* LETTERS BRAF E600 -associated senescence-like cell cycle arrest of human naevi. *Nature* **436**, (2005).

406. Wajapeyee, N., Serra, R. W., Zhu, X., Mahalingam, M. & Green, M. R. Oncogenic BRAF induces senescence and apoptosis through pathways mediated by the secreted protein IGFBP7. *Cell* **132**, 363-74 (2008).

407. Scurr, L. L. *et al.* IGFBP7 is not required for B-RAF-induced melanocyte senescence. *Cell* **141**, 717-27 (2010).

408. Collado, M. *et al.* Tumour biology: senescence in premalignant tumours. *Nature* **436**, 642 (2005).

409. Davalos, A. R., Coppe, J.-P., Campisi, J. & Desprez, P.-Y. Senescent cells as a source of inflammatory factors for tumor progression. *Cancer and Metastasis Reviews* **29**, 273-283 (2010).

410. Gorgoulis, V. G. & Halazonetis, T. D. Oncogene-induced senescence: the bright and dark side of the response. *Curr. Opin. Cell Biol.* **22**, 816-827 (2010).

411. Matsushima, K. & Oppenheim, J. J. Interleukin 8 and MCAF: novel inflammatory cytokines inducible by IL 1 and TNF. *Cytokine* **1**, 2-13 (1989).

412. Wang, J. M., Taraboletti, G., Matsushima, K., Van Damme, J. & Mantovani, A. Induction of haptotactic migration of melanoma cells by neutrophil activating protein/interleukin-8. *Biochem. Biophys. Res. Commun.* **169**, 165-70 (1990).

413. Schadendorf, D. *et al.* IL-8 produced by human malignant melanoma cells in vitro is an essential autocrine growth factor. *J. Immunol.* **151**, 2667-75 (1993).

414. Singh, R. K. & Varney, M. L. IL-8 expression in malignant melanoma: implications in growth and metastasis. *Histol. Histopathol.* **15**, 843-9 (2000).

415. Li, A., Dubey, S., Varney, M. L. & Singh, R. K. Interleukin-8-induced proliferation, survival, and MMP production in CXCR1 and CXCR2 expressing human umbilical vein endothelial cells. *Microvasc. Res.* **64**, 476-81 (2002).

416. Singh, R. K., Gutman, M., Radinsky, R., Bucana, C. D. & Fidler, I. J. Expression of interleukin 8 correlates with the metastatic potential of human melanoma cells in nude mice. *Cancer Res.* **54**, 3242-7 (1994).

417. Ugurel, S., Rappl, G., Tilgen, W. & Reinhold, U. Increased serum concentration of angiogenic factors in malignant melanoma patients correlates with tumor progression and survival. *J. Clin. Oncol.* **19**, 577-83 (2001).

418. Varney, M. L., Johansson, S. L. & Singh, R. K. Distinct expression of CXCL8 and its receptors CXCR1 and CXCR2 and their association with vessel density and aggressiveness in malignant melanoma. *Am. J. Clin. Pathol.* **125**, 209-16 (2006).

419. Acosta, J. C. *et al.* Chemokine signaling via the CXCR2 receptor reinforces senescence. *Cell* **133**, 1006-18 (2008).

420. Singh, S., Nannuru, K. C., Sadanandam, A., Varney, M. L. & Singh, R. K. CXCR1 and CXCR2 enhances human melanoma tumourigenesis, growth and invasion. *Br. J. Cancer* **100**, 1638-46 (2009).

421. Cannistra, S. A. Cancer of the ovary. *N. Engl. J. Med.* **351**, 2519-29 (2004).

422. Wang, X. *et al.* Evidence of cisplatin-induced senescent-like growth arrest in nasopharyngeal carcinoma cells. *Cancer Res.* **58**, 5019-22 (1998).

423. Chang, B. D. *et al.* A senescence-like phenotype distinguishes tumor cells that undergo terminal proliferation arrest after exposure to anticancer agents. *Cancer Res.* **59**, 3761-7 (1999).

424. Schmitt, C. A. *et al.* A senescence program controlled by p53 and p16INK4a contributes to the outcome of cancer therapy. *Cell* **109**, 335-46 (2002).

425. te Poele, R. H., Okorokov, A. L., Jardine, L., Cummings, J. & Joel, S. P. DNA damage is able to induce senescence in tumor cells in vitro and in vivo. *Cancer Res.* **62**, 1876-83 (2002).

426. Roninson, I. B., Broude, E. V. & Chang, B. D. If not apoptosis, then what? Treatment-induced senescence and mitotic catastrophe in tumor cells. *Drug Resist. Updat.* **4**, 303-13 (2001).

427. Nitta, M. *et al.* Spindle checkpoint function is required for mitotic catastrophe induced by DNA-damaging agents. *Oncogene* **23**, 6548-58 (2004).

428. Brown, J. M. & Attardi, L. D. The role of apoptosis in cancer development and treatment response. *Nat. Rev. Cancer* **5**, 231-7 (2005).

429. Lleonart, M. E., Artero-Castro, A. & Kondoh, H. Senescence induction; a possible cancer therapy. *Molecular Cancer* **8**, 3 (2009).

430. Giuliano, S., Ohanna, M., Ballotti, R. & Bertolotto, C. Advances in melanoma senescence and potential clinical application. *Pigment Cell & Melanoma Research* no-no (2011).doi:10.1111/j.1755-148X.2010.00820.x

431. Mhaidat, N. M. *et al.* Temozolomide induces senescence but not apoptosis in human melanoma cells. *Br. J. Cancer* **97**, 1225-33 (2007).

432. Cozzi, S.-J., Parsons, P. G., Ogbourne, S. M., Pedley, J. & Boyle, G. M. Induction of senescence in diterpene ester-treated melanoma cells via protein kinase C-dependent hyperactivation of the mitogen-activated protein kinase pathway. *Cancer Res.* **66**, 10083-91 (2006).

433. Coppé, J.-P., Desprez, P.-Y., Krtolica, A. & Campisi, J. The senescence-associated secretory phenotype: the dark side of tumor suppression. *Annu Rev Pathol* **5**, 99-118 (2010).

434. Freund, A., Orjalo, A. V., Desprez, P.-Y. & Campisi, J. Inflammatory networks during cellular senescence: causes and consequences. *Trends Mol Med* **16**, 238-46 (2010).

435. Chin, L. The genetics of malignant melanoma: lessons from mouse and man. *Nat. Rev. Cancer* **3**, 559-70 (2003).

11. Acknowledgements

First of all I would like to thank Professor Manfred Schartl for giving me the opportunity to work on this interesting topic. Even though I really sucked at biochemistry and almost quit studying biomedical sciences after only three semesters (maybe I should have...this would have kept us all from this disastrous ending...), Manfred believed in me and supported my work including crazy experiments (which in the end proofed not to be that crazy after all...) throughout. Thank you very much for all your help and support!

I want to thank Dr. Svenja Meierjohann for support and guidance in the beginning of my thesis as well as during the time I dealt with severe health issues. Besides, I would like to thank her and Professor Martin Eilers for supervising this thesis and most importantly teaching me vital lessons in how to try to become and be a successful scientist, respectively. I never dared to imagine what it takes an ambitious scientist to reach their goals.

I would like to thank Toni for all his support (anything ranging from vivid scientific discussions, experimental aid, being optimistic for no obvious reason, buying an expensive Adidas jacket to keep me motivated and kicking my ass and ...just being there).

Furthermore, I would like to thank my family and friends for all their support and help. Thanks for walking me to the list of biochemistry exam results. Thanks for putting up with me being extremely excited about something you couldn´t really understand but tried really hard. Thanks for comforting me when things did not work out the way I wanted them to. Thanks for believing in me at any time. And most of all, thanks for being there when my tiny, little world collapsed and I stopped believing in the good.

I would like to thank all my lab members and anyone working at the institute for any kind of help and advice received. I especially want to thank Anita for her support, her friendship and for sharing the best and the worst times of my thesis with me. I will definitely miss our 14 hour challenging but satisfying plating sessions and our quest to gain the manatee serenity level. I would also like to thank Max and Johannes for their friendship and for being scientists how I imagined true ones to be like.

Finally, I would like to thank the Graduate School of Life Sciences (GSLS) for the financial support and all the great soft skill courses without which I would not have been able to do this thesis.

12. Publications

12.1 Oncogene activation in melanocytes links reactive oxygen to multinucleated phenotype and senescence

Oncogene activation in melanocytes links reactive oxygen to multinucleated phenotype and senescence.

Leikam, C., Hufnagel, A., Schartl, M., Meierjohann, S.

(2008). Oncogene 56, 7070-82.

Link: http://www.ncbi.nlm.nih.gov/pubmed/18806824

DOI: 10.1038/onc.2008.323

Oncogene (2008), 1–13

www.nature.com/onc

ORIGINAL ARTICLE

Oncogene activation in melanocytes links reactive oxygen to multinucleated phenotype and senescence

C Leikam, A Hufnagel, M Schartl and S Meierjohann

Department of Physiological Chemistry I, Biocenter, Am Hubland, University of Wurzburg, Wurzburg, Germany

Contrary to malignant melanoma, nevi are a benign form of melanocytic hyperproliferation. They are frequently observed as precursor lesions of melanoma, but they also feature biochemical markers of senescence. In particular, evidence for oncogene-induced melanocyte senescence as natural means to prevent tumorigenesis has been obtained in nevi with mutated B-Raf^{V600E}. Here, we demonstrate that strong oncogenic growth factor receptor signalling drives melanocytes into senescence, whereas weaker signals keep them in the proliferative state. Activation of oncogene-induced senescence also produces multinucleated giant cells, a long known histological feature of nevus cells. The protein levels of the senescence mediators, p53 and pRB, and their upstream activators do not correlate with senescence. However, strong oncogene signalling leads to pronounced reactive oxygen stress, and scavenging of reactive oxygen species (ROS) efficiently prevents the formation of multinucleated cells and senescence. Similarly, expression of oncogenic N-RAS results in ROS generation, DNA damage and the same multinuclear senescent phenotype. Hence, we identified oncogenic signalling-dependent ROS production as critical mediator of the melanocytic multinuclear phenotype and senescence, both of them being hallmarks of human nevus cells.
Oncogene advance online publication, 22 September 2008; doi:10.1038/onc.2008.323

Keywords: ROS; melanoma; senescence; oncogene; N-RAS; melanocyte

Introduction

Oncogene-induced senescence is suggested to be a natural antitumorigenic means. It can counteract excessive growth stimulatory signals from activated oncogenes by restricting growth of the affected cells and retaining them in the premalignant state. Accordingly, acquired nevi with activating *B-RAF* mutations display classical hallmarks of senescence, such as cell cycle arrest and senescence-associated acidic β-Gal activity (Michaloglou *et al*., 2005).

INK4A (inhibitor of cyclin-dependent kinase 4A) induction in nevi is intriguing, as this might reflect the main difference between melanoma and premalignant skin lesions. Half of all vertical growth phase melanoma have lost *INK4A* expression, adding up to about 75% in metastatic melanoma (Straume *et al*., 2000). The tumour suppressors, *INK4A* and alternative reading frame (*ARF*), both encoded by the gene locus *CDKN2A* (cyclin-dependent kinase inhibitor 2A), are known to be involved in oncogene-induced senescence and are disabled in a variety of tumours, particularly in familial and non-familial melanoma (Chin, 2003). Besides, INK4A and ARF are upstream regulators of pRB and p53, respectively. Importantly, INK4A-pRB and ARF-p53 are the two tumour-suppressing pathways considered to be responsible for the execution of proliferative arrest that characterizes senescence (Collado and Serrano, 2006). In general, mutations in the *CDKN2A* locus often affect both gene products. Nevertheless, melanoma cases where the *CDKN2A* mutation only decreases the activity of one of either genes have been reported (Sharpless *et al*., 2001; Haluska *et al*., 2006). Although the dispensability of INK4A has been described for some nevus cells (Michaloglou *et al*., 2005), INK4A is discussed as main senescence mediator in human nevi (Bennett, 2003; Gray-Schopfer *et al*., 2006). Even though the link between oncogenic RAS or B-RAF and downstream senescence inducers in melanocytes is unclear, a connection between mitogen activated protein kinase (MAPK) activation and INK4A or ARF has been reported for other cell lines (Aguirre *et al*., 2003; Lachat *et al*., 2004; Michaloglou *et al*., 2005).

Apart from oncogenic mutations in *RAS* or *B-RAF*, the hyperactivation of upstream-acting receptor tyrosine kinases (RTKs) is observed in melanoma (Natali *et al*., 1993; Goding, 2000; Li *et al*., 2001; Gray-Schopfer *et al*., 2005; Curtin *et al*., 2006). In murine H-RAS^{V12}-driven melanoma, transcriptional induction of epidermal growth factor receptor (EGFR) ligands is observed, resulting in an autocrine EGFR-stimulating loop that is important for melanomagenesis (Bardeesy *et al*., 2005). The EGFR orthologue *Xiphophorus* melanoma receptor

Correspondence: Dr S Meierjohann, Department of Physiological Chemistry I, Biocenter, Am Hubland, University of Wurzburg, 97074 Wurzburg, Germany.
E-mail: svenja.meierjohann@biozentrum.uni-wuerzburg.de
Received 29 February 2008; revised 25 July 2008; accepted 11 August 2008

kinase (Xmrk) is a representative of such oncogenic RTKs (Meierjohann and Schartl, 2006). Its overexpression is causative for the development of melanoma in the *Xiphophorus* fish melanoma model, and when ectopically expressed in mammalian pigment cells it can induce the full neoplastic phenotype (Geissinger *et al*., 2002; Wellbrock *et al*., 2002; Meierjohann *et al*., 2006). Melanoma development by Xmrk shows many parallels to human melanoma development by RAS or B-RAF. The importance of MAPK activation in melanoma was first described in the Xmrk model, and only later this pathway was found to be crucial in human melanoma, too (Wellbrock and Schartl, 1999; Davies *et al*., 2002; Satyamoorthy *et al*., 2003). Similarly, the secretion of osteopontin (OPN) and activation of STAT5, both events going along with activation of Xmrk, were later detected to contribute to human melanoma maintenance, and meanwhile OPN is even considered a serum diagnostic marker for melanoma (Wellbrock *et al*., 1998, 2005; Geissinger *et al*., 2002; Mirmohammadsadegh *et al*., 2006; Hayashi *et al*., 2007; Rangel *et al*., 2008).

To better understand the events occurring in oncogene-induced pigment cell transformation and senescence, we have established a melanocyte culture model with cell lines expressing different levels of RTK, represented by inducible Xmrk. We found that high proliferative capacity and soft agar growth went along only with low and intermediate expression levels, whereas high expression levels reduced these effects owing to the induction of senescence. The senescence phenotype was featured by multinucleation, which made the cells resemble nevus cells. We could demonstrate that the generation of these cells is dependent on reactive oxygen species (ROS) that are exclusively produced in melanocytes with a very high level of active RTK. Thus, one crucial difference between the RTK downstream signalling in low and high expressers is the production of ROS, which causes senescence and multinucleation of melanocytes. Interestingly, ROS production and multinuclear senescent cells are also observed in melanocytes expressing N-RAS^{61K}.

Results

Low and intermediate levels of receptor tyrosine kinase expression lead to melanocyte proliferation and transformation

For the analysis of RTK transformation capacity, we chose three clones derived from the parental melan a cells expressing different levels of the EGF-inducible version of the oncogenic EGFR orthologue Xmrk ('HERmrk' or shortly 'Hm'). According to the RTK expression levels, these cell lines were termed Hm^{lo}, Hm^{me} and Hm^{hi} (Figure 1a). To check if different Hm expression levels correspond to downstream signalling capacity, we monitored activation of the PI3 kinase pathway by western blot (Supplementary Figure S1A). We also monitored RNA expression of *Egr1* that is induced in response to HERmrk-dependent STAT5 activation (unpublished results), and *Opn*, which is a downstream target of the MAPK pathway (Geissinger *et al*., 2002), by performing quantitative real-time PCR (Supplementary Figure S1B). The data demonstrate Hm expression levels to parallel the signalling capacity.

In proliferation experiments, all three pigment cell clones responded to EGF and started to proliferate under long-term EGF treatment, whereas the parental cell line melan a was indifferent to EGF stimulation (Figure 1b). Hm^{lo} and Hm^{me} grew almost equally well. On the contrary, clone Hm^{hi} had a threefold lower proliferative potential (Figure 1b). To monitor for clonogenic growth, soft agar assays were performed. They also revealed a significant negative correlation between receptor expression level and growth ($P<0.05$) (Figure 1c).

High-level HERmrk expression results in melanocyte senescence

As the lack of proliferation in Hm^{hi} might be the result of a terminal cellular arrest, a senescence-associated β-galactosidase assay was performed. After long-term cultivation in starving medium, a slight increase in β-Gal-stained cells was observed for all three cell clones. However, these cells never exceeded 1.2% of the total cell population (Figure 2a). Upon receptor stimulation, Hm^{lo} and Hm^{me} cells exhibited only a slight increase in senescent cells. Contrastingly, clone Hm^{hi} displayed a rapid increase in senescent cells between 7 and 14 days of EGF stimulation adding up to 15% of the total cell population after 14 days (Figure 2a).

Taken together, high levels of oncogenic Hm signalling prevented the potentially tumorigenic effects of low-to-intermediate Hm levels.

Multinuclear melanocytes are senescent and are generated by endomitosis and fusion

A remarkable feature of all Hm cells was the occurrence of highly multinucleated cells during the course of EGF treatment (Figure 2b). Senescence-associated β-galactosidase staining revealed that a large majority of these cells were senescent, whereas mononuclear cells usually showed no staining. The appearance of multinuclear cells slightly preceded the positive β-Gal signal, suggesting a causative relationship. Taken together, in Hm^{hi} cells, the number of multinuclear senescent cells accumulated up to 15%, whereas almost no such cells were found in the other two cell clones. Specifically, senescence of melanocytes appeared to be connected to a multinucleated phenotype.

To clarify how the multinuclear senescent cells were generated, we performed a time-lapse analysis of EGF-stimulated Hm^{hi} cells (Figure 3 and Supplementary Figure S1). It revealed that in most cases, nuclear division without subsequent cytokinesis occurred (Supplementary movie S1, highlighted in black). Surprisingly, fusion of cells could also be observed occasionally (Supplementary movie S2, highlighted in black). Yet, even in case of fusion, endomitosis occurred in one of

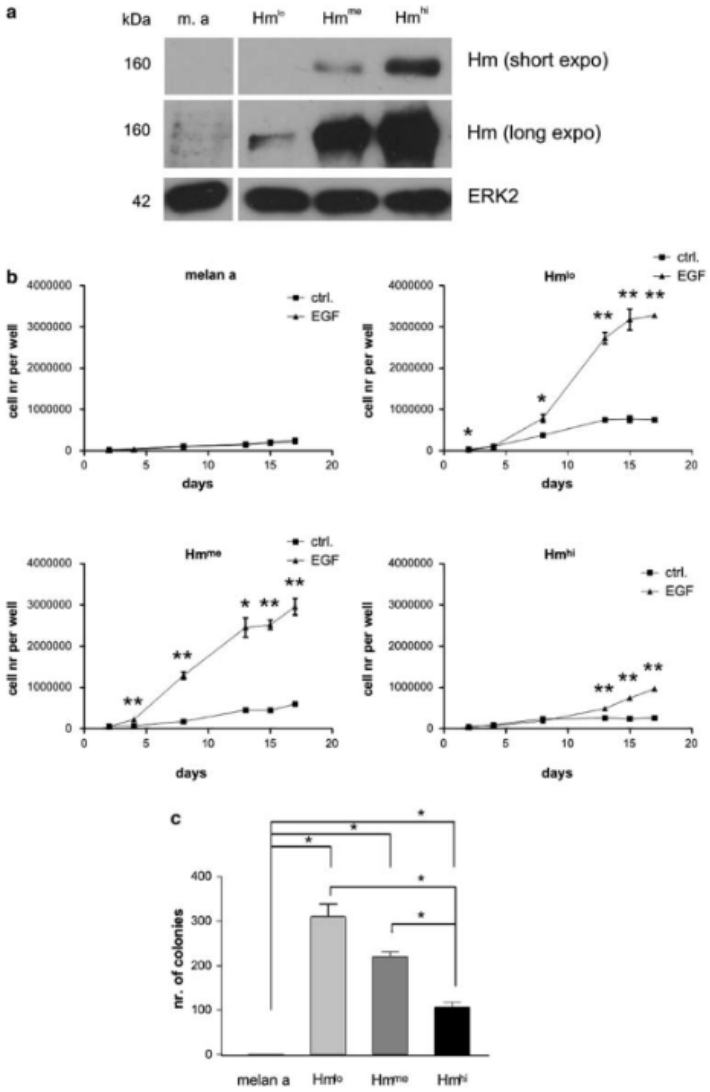

Figure 1 Proliferation and transformation potential determined by Hm receptor levels of melanocytes. (**a**) Western blot analysis of whole-cell lysates of melan a and the melan a Hm cell clones Hm^{lo}, Hm^{me} and Hm^{hi}. Protein (35 μg) was blotted and probed against the C-terminal part of Xmrk and ERK2 (loading control). (**b**) Cell proliferation assay of melan a and the melan a Hm cell clones Hm^{lo}, Hm^{me} and Hm^{hi} in the absence or presence of EGF. The graphs depict the mean values of three independent assays. Bars indicate standard deviations (in some cases too small to be seen). Student's *t*-test (two-tailed, unpaired) revealed statistical significance highlighted by asterisks (*$P<0.05$; **$P<0.01$). To perform the *t*-test, the values of the control samples at each time point were compared to the EGF-stimulated samples at the same time point. (**c**) Soft agar growth of melan a and the melan a Hm cell clones Hm^{lo}, Hm^{me} and Hm^{hi} in the presence of EGF. The number of colonies per well of a six-well plate was counted after 14 days of incubation. The graph shows the mean values of three independent assays. Bars indicate standard deviations (in case of melan a too small to be seen). Students' *t*-test (two-tailed, paired) revealed statistical significance highlighted by asterisks (*$P<0.05$). EGF, epidermal growth factor.

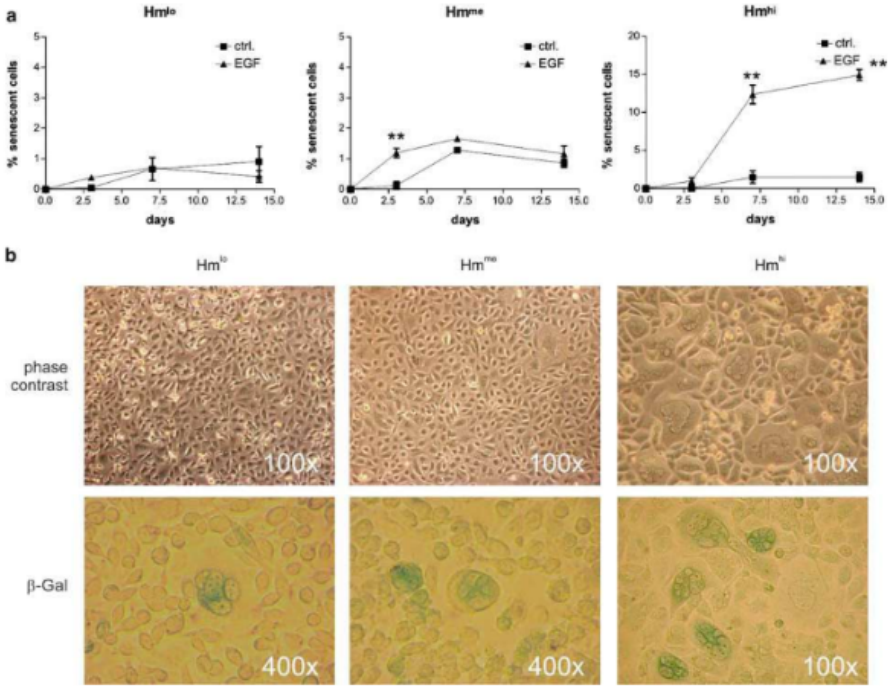

Figure 2 Senescence induction by high levels of the RTK Hm. (**a**) Quantification of senescent cells in the three cell clones Hm^{lo}, Hm^{me} and Hm^{hi} depicted in percentage of senescent cells per total cell number. Cells were counted under the microscope and the assay was repeated at least three times. Bars indicate standard deviations (in some cases too small to be seen). Where indicated, statistical significance, calculated by Student's *t*-test (two-tailed, unpaired), was reached (*$P<0.05$ (not present here); **$P<0.01$). To perform the *t*-test, the values of the control samples at each time point were compared with the EGF-stimulated samples at the same time point. (**b**) Images of unstained and SA-β-gal-stained cell clones. The images show cells from independent assays. Phase contrast pictures (100-fold magnification) illustrate the cells after 2 weeks of EGF treatment. In case of SA-β-gal staining for Hm^{lo} and Hm^{me}, a 400-fold magnification was chosen to demonstrate the occasional occurrence of blue, senescent cells. EGF, epidermal growth factor; RTK, receptor tyrosine kinase; SA-β-gal, senescence-associated β-galactosidase.

the cells. Both effects eventually led to the multinuclear state.

pRB and p53 are induced by HERmrk

With pRB and p53, two major pathways are usually causative for the induction of senescence. By means of quantitative real-time PCR and protein blots, we monitored the upstream activators of both pathways, namely $p19^{ARF}$ (*Arf*) and the cyclin-dependent kinase inhibitors $p16^{INK4A}$ (*Ink4a*), $p15^{INK4B}$ (inhibitor of cyclin-dependent kinase 4B, *Ink4b*), $p21^{WAF}$ (*p21*) and $p27^{KIP1}$ (*p27*). These genes are crucial mediators of senescence and are often upregulated in response to oncogenic stress (Collado and Serrano, 2006). We examined the transcript as well as the protein levels of these senescence marker genes.

Quantitative real-time PCR experiments revealed an induction of *Arf* in both senescent Hm^{hi} cells and the non-senescent Hm^{lo} cells, particularly after 14 days of stimulation (Figure 4). On protein level (Figures 5a and c), Hm^{lo} and Hm^{hi} cells also displayed an upregulation at all time points. For Hm^{me} cells, only a faint upregulation of *Arf* transcript was visible. However, ARF protein was slightly induced in response to EGF (probably the induction is underestimated, as the β-actin control shows lower loading of EGF-stimulated lysate compared to the unstimulated control at days 7 and 14). Corresponding to the level of *Arf* induction, p53, the effective downstream target of ARF, was stabilized in all cell clones in response to EGF throughout the experiment. The degree of p53 protein increase correlated with the ARF protein level (Figures 5a–c) and was most prominent in the senescent cell clone Hm^{hi}.

From the group of cyclin-dependent kinase inhibitor genes, *Ink4a* was slightly induced at transcript level in all three cell lines, whereas an increase in protein was

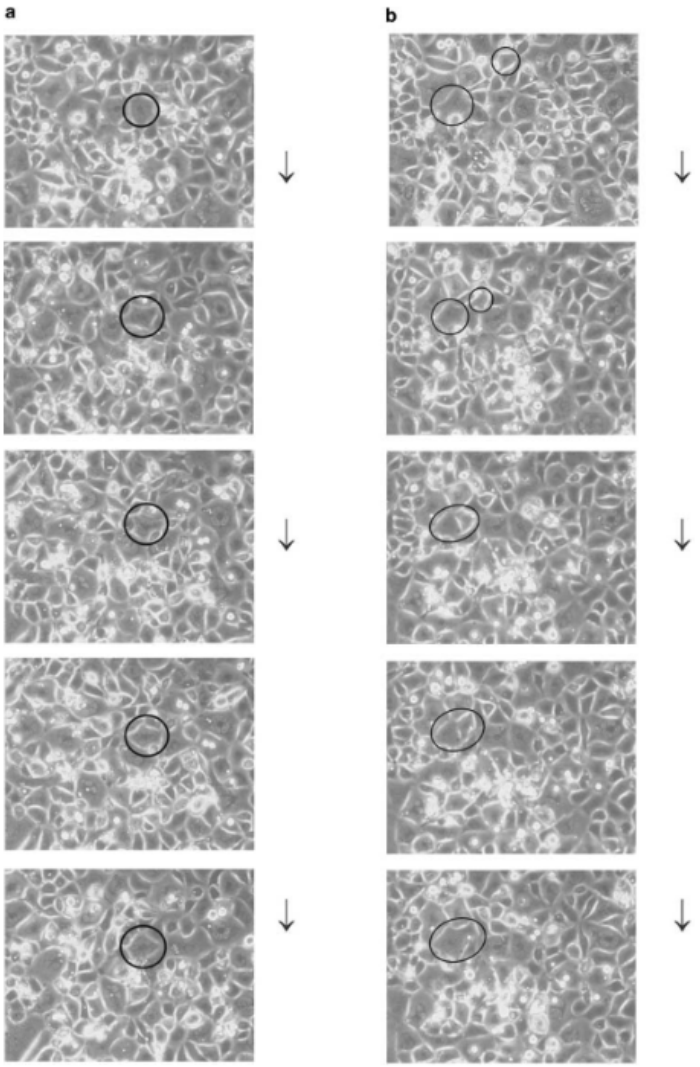

Figure 3 Generation of multinucleated melanocytes by endomitosis and fusion. After 7 days of EGF treatment, melan a Hm^{si} cells were monitored for 17 h. Pictures were taken every 20 min (200-fold magnification). **(a)** Endomitosis and **(b)** cell–cell fusion events are illustrated. EGF, epidermal growth factor.

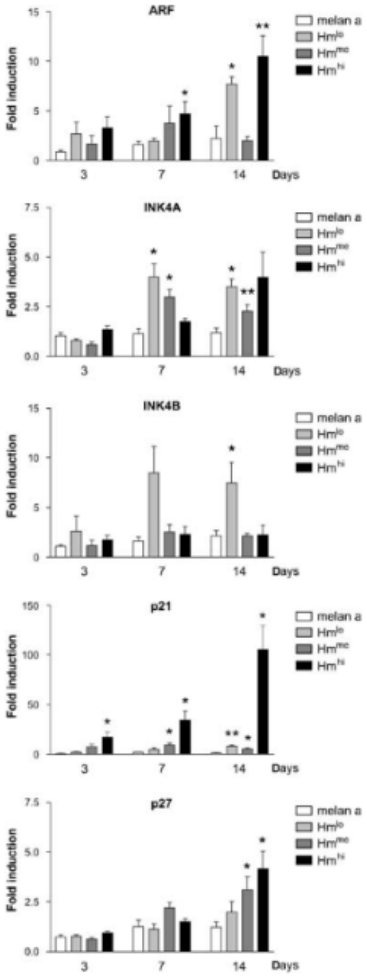

Figure 4 Upregulation of *Arf* and CKI mRNA levels in senescent and non-senescent melan a Hm cells. Quantitative real-time PCR analyses of *Arf*, *Ink4a*, *Ink4b*, *p21* and *p27* transcripts in EGF-stimulated parental cell line melan a and melan a Hm clones Hm^{lo}, Hm^{me} and Hm^{hi}. Data were normalized to *Hprt* and fold induction is referred to the control of each cell clone, kept in starving medium without EGF. Graphs display the mean values of at least six independent experiments. Bars indicate standard deviations. Students' *t*-test (two-tailed, paired) revealed statistical significant differences referring to the EGF-treated melan a control cells, highlighted by one ($*P<0.05$) or two asterisks ($**P<0.001$). ARF, alternative reading frame; CKI, cyclin-dependent kinase inhibitor; HPRT, hypoxanthine-guanine phosphoribosyltransferase; INK4, inhibitor of cyclin-dependent kinase 4.

exclusively observed in Hm^{hi} cells (Figures 4 and 5). For *Ink4b*, transcript induction was only found in Hm^{lo} cells, but not in any of the other cell lines. Contrastingly, its protein product accumulated to some extent at late time points in Hm^{hi} cells. Both *p21* and *p27* were most strongly upregulated at RNA level in the senescent cell line Hm^{hi}, whereas only a slight increase in p21 protein and no increase in p27 were visible in these cells. In case of the downstream effector pRB, the inactive, hyperphosphorylated form of the protein disappeared from Hm^{hi} cells at late time points. However, the active, hypophosphorylated form of the protein accumulated to a similar extent in all three cell lines.

Earlier, Sviderskaya *et al*. (2002) reported that most mouse melanocyte cell lines, including melan a, have lost INK4A and ARF protein expression under normal culture conditions. This loss is discussed to be a prerequisite for the maintenance of melanocyte lines. We have performed a comparative western blot with melan a and melan a Hm^{hi} cells revealing that under standard growth conditions, expression of these genes is usually prevented, whereas oncogenic conditions or serum starvation as used in our experimental settings relieve this suppression (data not shown, available on request). In addition, we sequenced the *Cdkn2a* cDNA from EGF-induced melan a Hm cells and found no mutation (data not shown). Thus, these cells are capable of producing functional INK4A and ARF, but without oncogenic stress, their promoter is presumably silenced.

DNA damage response is activated in cells bearing high levels of active HERmrk

As the p53 pathway is strongly induced in Hm^{hi} cells, we took a closer look at p53 regulation. DNA damage response pathways have a major function in mediating p53 function and senescence (Bartkova *et al*., 2006; Mallette *et al*., 2007; Nuciforo *et al*., 2007). DNA damage response combines signals resulting from various DNA-damaging events, including oxidative stress. Ataxia telangiectasia mutated (ATM) belongs to the primarily activated components of these pathways that are recruited to the sites of DNA damage. Checkpoint kinase 2 (CHK2) is a target of ATM, controlling the cell cycle upon DNA damage induction. In many cell culture models, it is described to be sufficient and necessary for senescence (Aliouat-Denis *et al*., 2005; Chen *et al*., 2005; Hirose *et al*., 2005), but so far its implication in melanocyte senescence has not been studied. p53 is a direct target of ATM and ataxia telangiectasia and Rad3 related (ATR), which phosphorylate the protein at Ser15 (human) or Ser18 (mouse). This phosphorylation promotes interactions of p53 with important transcriptional coactivators and can thus be considered an activating modification (Liu *et al*., 1993; Avantaggiati *et al*., 1997).

To investigate the involvement of DNA damage response in Hm-mediated senescence, we monitored phosphorylation of mouse CHK2 Thr77 (=human Thr68) and p53 Ser18 in the different cell clones. In

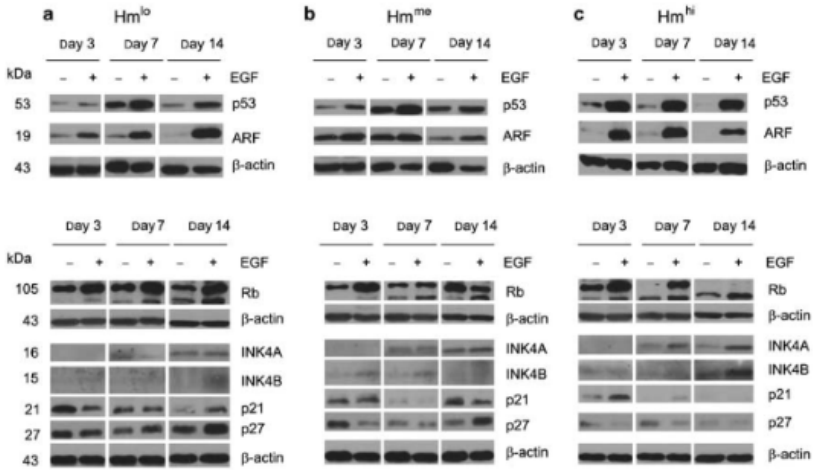

Figure 5 Upregulation of p53 and pRB and pathway proteins in senescent and non-senescent melan a Hm cells. Western blot analyses of ARF, p53, pRB, INK4A, INK4B, p21 and p27 for melan a Hm clones Hm^{lo} (**a**), Hm^{me} (**b**) and Hm^{hi} (**c**). β-actin served as loading control. The respective protein size is indicated in kDa. In case of pRB, an upper, hyperphosphorylated and a lower, hypophosphorylated form of the protein were detected. ARF, alternative reading frame; INK4, inhibitor of cyclin-dependent kinase 4.

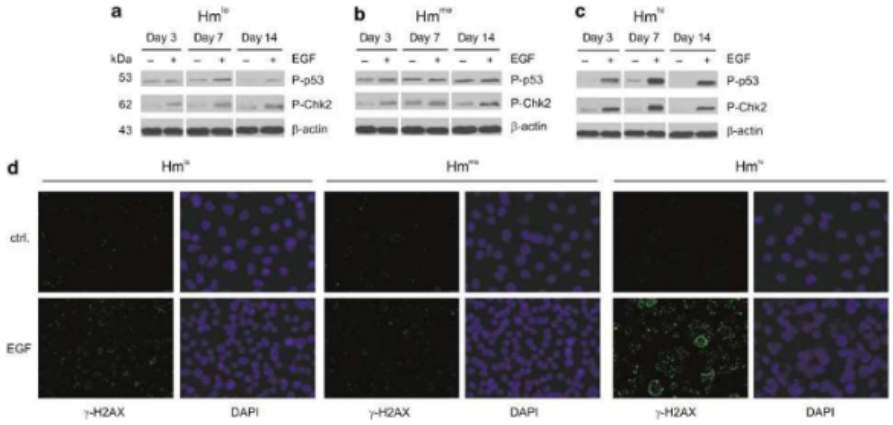

Figure 6 Strong activation of DNA damage response in senescent melan a Hm cells. Western blot analyses of P-p53 (Ser18) and P-Chk2 (Thr 77) for melan a Hm clones Hm^{lo} (**a**), Hm^{me} (**b**) and Hm^{hi} (**c**). β-actin served as loading control. The respective protein size is indicated in kDa. (**d**) Immunofluorescence of γH2AX (Ser139) in Hm^{lo}, Hm^{me} and Hm^{hi} cells, starved or EGF-stimulated for 14 days (400-fold magnification). Cells were counterstained with DAPI. DAPI, 4',6-diamidino-2-phenylindole; EGF, epidermal growth factor.

Hm^{hi} cells, a clear increase in phosphorylation of both proteins was observed upon EGF stimulation (Figure 6c). Contrastingly, cell lines Hm^{lo} and Hm^{me} displayed only a very modest increase of P-CHK2 and no clear increase of P-p53 at either time point (Figures 6a and b).

This is in stark contrast to the overall protein amount of p53 that was also remarkably increased in Hm^{lo} cells, even though no P-p53 signal could be detected here (Figure 5a). Thus, the fraction of Ser18-phosphorylated p53 was much higher in the senescent cell clone Hm^{hi}. To scrutinize this further, we performed an immunofluor-

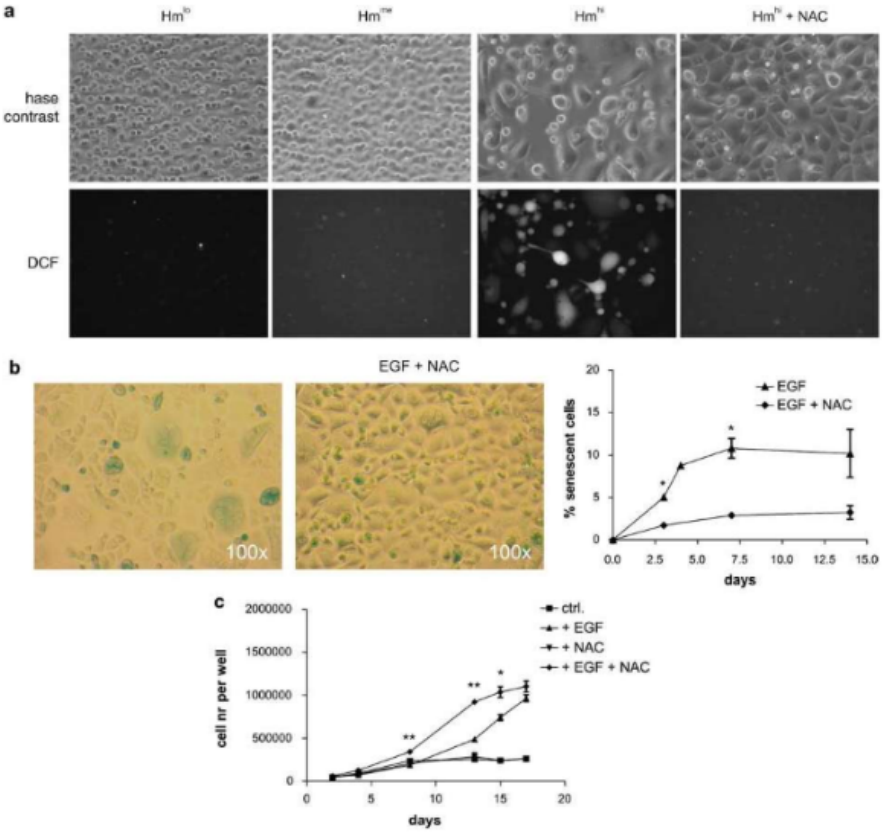

Figure 7 Prevention of Hm-mediated senescence by *N*-acetylcysteine. (**a**) Phase contrast and DCF fluorescence images from the same area upon 8 days of EGF stimulation of Hm^{lo}, Hm^{me} and Hm^{hi} cells. Additional NAC treatment of Hm^{hi} cells abolished the DCF signal (100-fold magnification). (**b**) Representative brightfield images of β-Gal-stained Hm^{hi} cells upon 14 days of EGF treatment in the absence or presence of NAC and quantification of senescent Hm^{hi} cells. Cells were counted under the microscope and the assay was repeated at least three times. Where indicated, statistical significance, calculated by Student's *t*-test (two-tailed, unpaired), was reached ($^*P<0.05$). To perform the *t*-test, values of the EGF-stimulated samples at each time point were compared to the EGF- and NAC-stimulated samples at the same time point. The *P*-value for day 14 was 0.072. (**c**) Cell proliferation assay of Hm^{lo} cells left untreated or treated with EGF, NAC or both. Graphs display the mean values of three independent experiments. Bars from (**b**) and (**c**) indicate standard deviations (in some cases too small to be seen). Where indicated, statistical significance, calculated by Student's *t*-test (two-tailed, unpaired), was reached ($^*P<0.05$; $^{**}P<0.01$). To perform the *t*-test, values of the EGF-stimulated samples at each time point were compared to the EGF- and NAC-stimulated samples at the same time point. EGF, epidermal growth factor; DCF, 2′,7′-dichlorofluorescein; NAC, *N*-acetylcysteine.

escence staining using an antibody recognizing phosphohistone 2A.X (Ser139) (γH2AX). γH2AX recognizes double-strand breaks, accumulating at sites of DNA damage in a characteristic punctate pattern (Figure 6d). Although some degree of DNA damage was observed in starved cells of all cell lines analysed, it is obvious that EGF stimulation increased γH2AX only in Hm^{hi} cells, where it was massively present, particularly in multinucleated cells.

Reactive oxygen species mediate the senescence response

A possible cause for the induction of DNA damage in Hm^{hi} cells is the generation of ROS. ROS often go along with aberrant RAS signalling, either caused by oncogenic forms of the protein or by strong upstream growth factor signalling through the RAS/RAF/MAPK pathway (Finkel, 2006; Kopnin *et al*., 2007). In fibroblasts, RAS-induced ROS are causative for senescence (Lee *et al*., 1999; Bischof *et al*., 2002). We performed EGF-

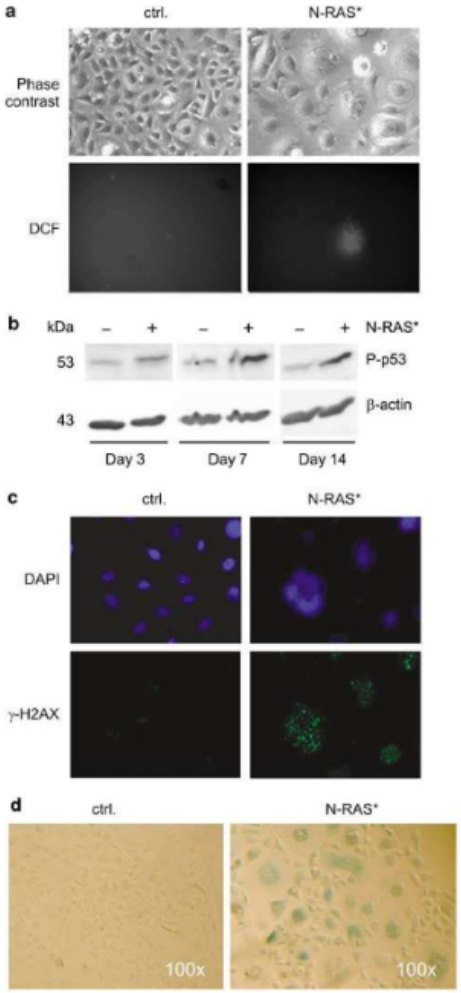

Figure 8 Oncogenic N-RAS causes ROS, DNA damage response and a multinuclear senescent phenotype. (**a**) Phase contrast and DCF fluorescence images from the same area upon 14 days of doxycyclin treatment (400-fold magnification). (**b**) Western blot analyses of P-p53 (Ser18) for melan a ctrl and melan a N-RAS* after indicated times of doxycyclin stimulation. β-actin served as loading control. The respective protein size is indicated in kDa. (**c**) Immunofluorescence of γH2AX (Ser139) in melan a ctrl or melan a N-RAS* cells treated with doxycyclin for 14 days (400-fold magnification). Cells were counterstained with DAPI. (**d**) Images of unstained and SA-β-gal-stained melan a ctrl and melan a N-RAS* cells after 14 days of doxycyclin treatment (100-fold magnification). DAPI, 4',6-diamidino-2-phenylindole; DCF, 2',7'-dichlorofluorescein; ROS, reactive oxygen species; SA-β-gal, senescence-associated β-galactosidase.

stimulated senescence assays and monitored ROS production using 2′,7′-dichlorodihydrofluorescein diacetate (DCF-DA). At time points of senescence onset in Hm^{hi}, the presence of ROS was exclusively detectable in EGF-stimulated Hm^{hi} cells and was maintained throughout the assay period (Figure 7a).

To examine the impact of ROS on senescence, Hm^{hi} cells were stimulated with EGF in the presence or absence of the ROS scavenger *N*-acetylcysteine (NAC). The presence of NAC reduced the proportion of senescent cells to about one-third (Figure 7b), whereas cell proliferation was induced (Figure 7c). The number of senescent and multinuclear cells declined accordingly. We conclude that Xmrk mediates the appearance of both effects mainly through the generation of ROS.

Oncogenic N-RAS induces a similar multinuclear senescent phenotype

To find out if oncogenic RAS can lead to a phenotype similar to Hm in melanocytes, we generated melan a cells with inducible expression of the human melanoma oncogene $N\text{-}RAS^{61K}$ ('N-RAS*', Supplementary Figure S2A and B). We measured ROS level, DNA damage and senescence of N-RAS* cells compared to their controls. N-RAS* induced increased ROS levels in these cells, though at a lower rate compared to Hm^{hi} cells (Figure 8a). However, this was sufficient to generate a DNA damage response, as visualized by P-p53 immunoblot and γH2AX immunofluorescence (Figures 8b and c). Similar to Hm^{hi} cells, N-RAS*-expressing cells also became multinuclear and senescent (Figure 8d).

Discussion

Here, we present an *in vitro* melanocyte model of oncogene-induced senescence that for the first time shares the characteristic multinucleated phenotype with *in vivo* occurring nevi. We demonstrate that the expression level of RTKs, exemplarily presented by the inducible version of Xmrk, called HERmrk, determines whether melanocytes proliferate or undergo senescence. In the expression ranges investigated, the RTK level negatively correlates with proliferation rates and soft agar growth, but only Hm^{hi} cells with particularly high RTK levels became senescent. This is the first time that an oncogene dosage effect with high proliferation rates at low dosages and senescence at high dosages was observed in melanocytes. A dosage-dependent effect on proliferation and cell cycle arrest has previously been reported for B- and C-Raf, but so far only in murine fibroblasts (Sewing *et al*., 1997; Woods *et al*., 1997). *In vivo*, mice expressing inducible $H\text{-}Ras^{GV12}$ in the mammary gland develop an increasingly severe initial hyperplasia in response to graded RAS activation. Yet, later on in mammary development, an inhibition of ductal elongation, going along with senescence, occurred in mice expressing high RAS levels (Sarkisian *et al*., 2007). In human primary melanocyte cultures, senescence caused by lentiviral $H\text{-}RAS^{G12V}$ was observed

only at high oncogene expression levels, but the proliferation at low oncogene levels has not been addressed (Denoyelle *et al*., 2006).

A very remarkable feature of the senescent Hm^{hi} cells was the appearance of multinuclear cells, which occurred in addition to the usually observed features such as flattened cell shape, increased cell size and β-Gal staining. Most senescent cells described in the literature are blocked in G0, thereby preventing endomitosis and the appearance of multiple nuclei (Itahana *et al*., 2002; Blagosklonny, 2003). However, the appearance of multiple nuclei in our cells rules out a block in G0. Occasionally, a cell cycle block in G2, mediated by p21 or p53, has been observed in endothelial cells and fibroblasts (Rincheval *et al*., 2002; Spyridopoulos *et al*., 2002). Yet, the endomitosis observed here for the senescent melanocytes points to a block or deficiency in cytokinesis. In single cases, premature senescence, for example induced by the DNA-damaging agent adriamycin, has been described to be accompanied by multiple intracellular nuclei (Vigneron *et al*., 2005). In addition, senescence in human fibroblasts, caused by the inactivation of the transgenic SV40 large T antigen, leads to the appearance of cells with more than two nuclei (Takahashi *et al*., 2006). In those experiments, ROS levels were also increased and further enhanced by protein kinase Cδ signalling, leading to a block in cytokinesis. This situation is well comparable to our own observations, and the link between HERmrk activation, ROS generation and cytokinesis in melanocytes is a subject of future studies. Interestingly, multinuclear cells are very common in human nevi that are considered to consist of senescent melanocytes (Leopold and Richards, 1967; Savchenko, 1988). Our data suggest that HERmrk mimics the situation of aberrant oncogenic signalling in human nevi and connects the multinuclear phenotype to the process of melanocyte senescence.

The molecular events accompanying senescence in the melanocytes revealed no significant differences in the levels of hypophosphorylated pRB between the three examined cell lines. In case of overall protein amount of p53, only minor quantitative differences were detected. Compared to other systems characterized by premature senescence, the changes we observed in cyclin-dependent kinase inhibitor expression were only modest (Jones *et al*., 2000; Malumbres *et al*., 2000; Denoyelle *et al*., 2006; Gray-Schopfer *et al*., 2006). Neither pRB status nor p53 expression levels correlated with Hm expression levels. Thus, the more robust ARF and p53 inductions might make the difference between Hm^{lo} and Hm^{hi} cells if expressed above a certain threshold level.

Interestingly, there is evidence for p53-independent functions of ARF, particularly in melanocytes. Genetic deficiency of ARF, but not p53, increases melanoma development in mice (Ha *et al*., 2007). Recently, pRB has been demonstrated to be another target of the ubiquitin ligase MDM2 with ARF preventing their interaction, subsequently leading to the accumulation of pRB (Chang *et al*., 2007). Thus, it is possible that ARF is responsible for the stabilization of both p53 and pRB. However, as we did not see an enhanced stabilization of pRB in the cell clone Hm^{hi} that displayed the highest amount of ARF, this possibility is rendered unlikely in our cell system.

One of the features that was exclusively observed in the senescent Hm^{hi} cells was the phosphorylation of p53 at residue Ser18, which is a target of ATR and ATM kinases. In mice bearing the Ser18→Ala missense mutation, the lacking phosphorylation of this residue does not affect the stability of p53 (Chao *et al*., 2003). Accordingly, the human equivalent P-Ser15 has no effect on the interaction between human p53 and its ubiquitin ligase HDM2 (Dumaz and Meek, 1999). This might explain why the amount of P-Ser18-p53 did not correlate with the overall amount of p53 in our non-senescent cell lines. In humans, P-Ser15 enhances the ability of p53 to recruit CBP/p300, followed by an increase of C-terminal p53 acetylation and increased DNA-binding activity (Lambert *et al*., 1998). Hence, the increase of P-Ser18-p53, which is observed in Hm^{hi} cells only, is a better indicator for p53 activity than the overall amount of p53 and correlates well with senescence in this melanocyte system.

A second very prominent observation was the strong production of ROS exclusively found in the senescent Hm^{hi} cells. Premature as well as replicative senescence have previously been connected to enhanced ROS generation (Passos and von Zglinicki, 2006). However, the origin of oxidative stress in response to oncogene activation is still controversially discussed. In terms of signal transduction molecules, the GTPases RAC1 and RAS are known to be necessary for ROS induction in several cell systems (Irani *et al*., 1997; Debidda *et al*., 2006). Both of them are downstream effectors of Xmrk (Wellbrock and Schartl, 1999 and unpublished results).

Here, we demonstrate that the inhibition of ROS by NAC strongly reduces the generation of multinuclear cells and increases replicative capacity of Hm^{hi} cells. This is in accordance with the observations by Gorla *et al*. (2001), where generation of oxidative stress in a mitogenic setting induced polyploidy and reduced proliferation of mouse hepatocytes. Likewise, H_2O_2 treatment of human lymphoid cells resulted in the formation of polyploid nuclei, which was reversed by NAC treatment (Kurata, 2000). HERmrk is an upstream activator of the RAS/RAF/MAPK pathway. We could demonstrate that oncogenic N-RAS alone also leads to increased ROS levels, DNA damage and a multinuclear and senescent phenotype that resembles the situation observed in Hm^{hi} cells. However, whether this effect depends on the expression level of $N\text{-}Ras^{61K}$ in melan a cells will be determined in future studies.

Taken together, using two potent melanoma oncogenes, we provide compelling evidence to suggest that a long-known phenomenon of human nevi, namely the multinucleated phenotype, can be recapitulated *in vitro* by oncogene-dependent ROS production accompanied by enhanced DNA damage and p53 activation. These findings yield the first link between oxidative stress, multinucleated phenotype and senescence in melanocytes.

Materials and methods

Cell culture

The EGF-inducible version of the oncogenic EGFR orthologue Xmrk ('HERmrk' or shortly 'Hm'), consisting of the extracellular domain of the human EGF receptor ('HER') and the intracellular part of Xmrk ('mrk'), was used to establish stable cell lines of the mouse melanocyte cell line melan a (Bennett *et al*., 1989; Wittbrodt *et al*., 1992). Three cell clones with different expression levels were chosen for further analysis. In accordance with RTK expression levels, cell lines were termed Hm^{lo}, Hm^{me} and Hm^{hi} melan a. All cells were cultured as described earlier (Meierjohann *et al*., 2006). For senescence assays, cells were cultured in starving medium (Dulbecco's Modified Eagle's Medium with 10% dialysed foetal calf serum (Gibco/Invitrogen, Karlsruhe, Germany)) for 3 days before the assay was started. Where indicated, 100 ng/ml human EGF (Tebu-bio, Offenbach, Germany), 2 mM NAC or 1 μg/ml doxycyclin (Sigma-Aldrich, Munich, Germany) was added. Medium was renewed every 4 days, and EGF or NAC were freshly supplied every second day. After 3, 7 and 14 days, cells were analysed as described below.

Construction of an inducible expression plasmid for N-RAS^{Q61R}

N-RAS^{Q61K} was PCR-amplified from the Addgene plasmid 12543 (Khosravi-Far *et al*., 1996). The PCR product was cloned into *Bam*HI/*Eco*RV-digested pTREhyg2 vector (BD Biosciences, Clontech, Heidelberg, Germany), thus obtaining pTRE2hyg2-*N-RAS^{Q61K}*.

Generation of Dox-inducible N-RAS^{Q61R} melan a cells

Cells were transfected with pWHE459 vector allowing the expression of the doxycyclin-inducible reverse transactivator (Krueger *et al*., 2006), using Gene Juice transfection reagent (Novagen/Merck, Schwalbach, Germany). Cells were selected applying 2 μg/ml puromycin for 14 days. pTRE2hyg2-*N-RAS^{Q61K}* was transfected into melan a –pWHE459 cells using Gene Juice reagent. After hygromycin selection (350 μg/ml) for 3 weeks, cells were used for further analyses.

Senescence-associated β-galactosidase staining

Cells (4×10^4 per well) were seeded onto 12-well dishes and cultured for 3 days in starving medium. Melan a Hm cells were either left untreated or stimulated with 100 ng/ml EGF, whereas melan a pTRE2hyg (called melan a ctrl) or melan a N-RAS^{Q61K} cells (called melan a N-RAS*) were left untreated or stimulated by the addition of 1 μg/ml doxycyclin. After 3, 7 and 14 days, cells were washed with phosphate-buffered saline (PBS) (pH 7.2) and fixed with ice-cold 0.5% glutardialdehyde in PBS (pH 7.2) for 10 min at room temperature. After rinsing the cells with PBS (pH 7.2, 1 mM $MgCl_2$), they were stained in the dark for 3.5 h at 37 °C (using PBS pH 6.0, 1 mg/ml X-Gal, 0.12 mM $K_3Fe(CN)_6$, 0.12 mM $K_4Fe(CN)_6$ and 1 mM $MgCl_2$). Cells were then washed with PBS (pH 7.2) and examined by light microscopy.

Cell lysis and immunoblot analysis

Cells were cultured for 3 days in starving medium before being stimulated with 100 ng/ml EGF, 1 μg/ml doxycyclin or left untreated for 3, 7 and 14 days, followed by harvesting. Cells were then rinsed twice with PBS and lysed in lysis buffer (20 mM 4-(2-hydroxyethyl)-1-piperazineethanesulphonic acid (pH 7.8), 500 mM NaCl, 5 mM $MgCl_2$, 5 mM KCl, 0.1% deoxycholate, 0.5% Nonidet-P40, 10 μg/ml aprotinin, 10 μg/ml leupeptin, 200 μM Na_3VO_4, 1 mM phenylmethanesulphonylfluoride and 100 mM NaF). Protein (35 μg (pRB and p53 western blots) or 80 μg (all other western blots)) was resolved by SDS–polyacrylamide gel electrophoresis and analysed by immunoblotting. Polyclonal anti-mrk recognizing the C-terminal part of Xmrk ('pep-mrk') was generated by Biogenes (Berlin, Germany). Anti-β-actin (C-4), anti-pRB (C-15), anti-p15 (M-20), anti-p16 (M-156), anti-p21 (N-20) and anti-p27 (F8) antibodies were purchased from Santa Cruz Biotechnology (Heidelberg, Germany). p53 antibody was derived from mouse hybridoma supernatant (clone PAB 122), and anti-p19^{ARF} antibody was obtained from Abcam (Cambridge, UK). Anti-P-p53 (Ser15), anti-P-CHK2 (Thr 68) and anti-P-AKT (Ser473) were purchased from Cell Signaling Technology (New England Biolabs, Frankfurt, Germany).

Immunofluorescence

Cells (1×10^5) were seeded on glass cover slips, starved for 3 days in Dulbecco's Modified Eagle's Medium with 10% dialysed foetal calf serum and treated as indicated. Immunofluorescence was performed as described before (Meierjohann *et al*., 2006). Anti-γH2AX antibody (1:100; Cell Signalling) and CY3-conjugated goat-anti-rabbit (Jackson ImmunoResearch Laboratories, Newmarket, Suffolk, UK) were used.

RNA isolation and real-time PCR

Cells were starved and EGF-treated as described and RNA isolation was performed with TrIR solution (ABGene, Hamburg, Germany). Whole RNA (4 μg) was reversely transcribed using the RevertAidTM First Strand cDNA Synthesis Kit (Fermentas, Leon-Rot, Germany). Fluorescence-based quantitative real-time PCR was performed using the iCycler (Bio-Rad, Munich, Germany). See Supplementary information (Supplementary Table S1) for oligonucleotides used. Gene expression was normalized to hypoxanthine-guanine phosphoribosyltransferase. Relative expression levels were calculated applying REST software (Pfaffl *et al*., 2002).

Cell proliferation assay

Cells (5×10^4 per well) were seeded onto a six-well plate and either treated with 100 ng/ml EGF and/or 2 mM NAC as indicated, or left untreated. Cells were harvested by trypsinization after 2, 4, 8, 13, 15 and 17 days, pelleted, resolved in PBS and counted under the microscope.

Soft agar growth assay

One millilitre of 1.2% agar was mixed with 1 ml 2 × Dulbecco's Modified Eagle's Medium and plated onto six-well plates. Upon polymerization, the solid agar was overlain with an equal amount of soft agar mix (0.6% agar) containing 4×10^4 cells per well. The polymerized soft agar was supplied with 100 μl of starving media for the controls and the same amount of starving media including EGF (final concentration per well: 100 ng/ml). This solution was added every second day. After 14 days of growth, the number of cell colonies was counted, with 'colony' being defined as more than eight cells per spot.

Reactive oxygen species detection assay

Cells were starved and treated as described for the β-Gal assay. At times indicated, 20 μM 2′,7′-dichlorofluorescein diacetate was added to the medium and cells were stained for 5 min before being washed with PBS and overlain with starving medium. Cells were analysed microscopically for the presence of ROS-induced dichlorofluorescein (excitation 488 nm).

Abbreviations

ATM, ataxia telangiectasia mutated; ARF, alternative reading frame; CDKN2A, cyclin-dependent kinase inhibitor 2A; Chk2, checkpoint kinase 2; CKI, cyclin-dependent kinase inhibitor; DCF, 2′,7′-dichlorofluorescein; EGF, epidermal growth factor; EGFR, epidermal growth factor receptor; Hm, HERmrk; INK4A, inhibitor of cyclin-dependent kinase 4A; INK4B, inhibitor of cyclin-dependent kinase 4B; NAC, *N*-acetylcysteine; ROS, reactive oxygen species; RTK, receptor tyrosine kinase; SA-β-gal, senescence-associated β-galactosidase; Xmrk, *Xiphophorus* melanoma receptor kinase.

Acknowledgements

We thank Dr Thorsten Stiewe for kindly providing the PAB 122 hybridoma supernatant and Professor Jürgen Hoppe for his help with the time lapse experiment. In addition, we thank Johannes Haydn for generating the melan a pWHE459 cell lines and Toni Wagner for great technical support. This work was supported by the Deutsche Forschungsgesellschaft, Transregio 17 ('RAS-dependent pathways in human cancer'). CL was supported by a grant of the German Excellence Initiative to the Graduate School of Life Sciences, University of Wurzburg.

References

Aguirre AJ, Bardeesy N, Sinha M, Lopez L, Tuveson DA, Horner J *et al*. (2003). Activated Kras and Ink4a/Arf deficiency cooperate to produce metastatic pancreatic ductal adenocarcinoma. *Genes Dev* **17**: 3112–3126.

Aliouat-Denis CM, Dendouga N, Van den Wyngaert I, Goehlmann H, Steller U, van de Weyer I *et al*. (2005). P53-independent regulation of p21Waf1/Cip1 expression and senescence by Chk2. *Mol Cancer Res* **3**: 627–634.

Avantaggiati ML, Ogryzko V, Gardner K, Giordano A, Levine AS, Kelly K. (1997). Recruitment of p300/CBP in p53-dependent signal pathways. *Cell* **89**: 1175–1184.

Bardeesy N, Kim M, Xu J, Kim RS, Shen Q, Bosenberg MW *et al*. (2005). Role of epidermal growth factor receptor signaling in RAS-driven melanoma. *Mol Cell Biol* **25**: 4176–4188.

Bartkova J, Rezaei N, Liontos M, Karakaidos P, Kletsas D, Issaeva N *et al*. (2006). Oncogene-induced senescence is part of the tumorigenesis barrier imposed by DNA damage checkpoints. *Nature* **444**: 633–637.

Bennett DC. (2003). Human melanocyte senescence and melanoma susceptibility genes. *Oncogene* **22**: 3063–3069.

Bennett DC, Cooper PJ, Dexter TJ, Devlin LM, Haesman J, Nester B. (1989). Cloned mouse melanocyte lines carrying the germline mutations albino and brown: complementation in culture. *Development* **105**: 379–385.

Bischof O, Kirsh O, Pearson M, Itahana K, Pelicci PG, Dejean A. (2002). Deconstructing PML-induced premature senescence. *EMBO J* **1**: 3358–3369.

Blagosklonny M. (2003). Cell senescence and hypermitogenic arrest. *EMBO Rep* **4**: 358–362.

Chang DL, Qui W, Ying H, Zhang Y, Chen CY, Xiao ZX. (2007). ARF promotes accumulation of retinoblastoma protein through inhibition of MDM2. *Oncogene* **26**: 4627–4634.

Chao C, Hergenhahn M, Kaeser MD, Wu Z, Saito S, Iggo R *et al*. (2003). Cell type- and promoter-specific roles of Ser18 phosphorylation in regulating p53 responses. *J Biol Chem* **248**: 41028–41033.

Chen CR, Wang W, Rogoff HA, Li X, Li CJ. (2005). Dual induction of apoptosis and senescence in cancer cells by Chk2 activation: checkpoint activation is a strategy against cancer. *Cancer Res* **65**: 6017–6021.

Chin L. (2003). The genetics of malignant melanoma: lessons from mouse and man. *Nat Rev Cancer* **3**: 559–570.

Collado M, Serrano M. (2006). The power and the promise of oncogene-induced senescence markers. *Nat Rev Cancer* **6**: 472–476.

Curtin JA, Busam K, Pinkel D, Bastian BC. (2006). Somatic activation of KIT in distinct subtypes of melanoma. *J Clin Oncol* **24**: 4340–4346.

Davies H, Bignell GR, Cox C, Stephens P, Edkins S, Clegg S *et al*. (2002). Mutations of the BRAF gene in human cancer. *Nature* **417**: 949–954.

Debidda M, Williams DA, Zheng Y. (2006). Rac1 GTPase regulates cell genomic stability and senescence. *J Biol Chem* **281**: 38519–38528.

Denoyelle C, Abou-Rjaily G, Bezrookove V, Verhaegen M, Johnson TM, Fullen DR *et al*. (2006). Anti-oncogenic role of the endoplasmic reticulum differentially activated by mutations in the MAPK pathway. *Nat Cell Biol* **8**: 1053–1063.

Dumaz N, Meek DW. (1999). Serine 15 phosphorylation stimulates p53 transactivation but does not directly influence interaction with HDM2. *EMBO J* **18**: 7002–7010.

Finkel T. (2006). Intracellular redox regulation by the family of small GTPases. *Antioxid Redox Signal* **8**: 1857–1863.

Geissinger E, Weisser C, Fischer P, Schartl M. (2002). Autocrine stimulation by osteopontin contributes to antiapoptotic signalling of melanocytes in dermal collagen. *Cancer Res* **62**: 4820–4828.

Goding CR. (2000). Melanocyte development and malignant melanoma. *Forum (Genova)* **10**: 176–187.

Gorla GR, Malhi H, Gupta S. (2001). Polyploidy associated with oxidative injury attenuates proliferative potential of cells. *J Cell Sci* **114**: 2943–2951.

Gray-Schopfer VC, Cheong SC, Chong H, Chow J, Moss T, Abdel-Malek Z *et al*. (2006). Cellular senescence in naevi and immortalisation in melanoma: a role for p16? *Br J Cancer* **95**: 496–505.

Gray-Schopfer VC, da Rocha Dias S, Marais R. (2005). The role of B-Raf in melanoma. *Cancer Metastasis Rev* **24**: 165–183.

Ha L, Ichikawa T, Anyer M, Dickins R, Lowe S, Sharpless NE *et al*. (2007). ARF functions as a melanoma tumor suppressor by inducing p53-independent senescence. *Proc Natl Acad Sci USA* **104**: 10968–10973.

Haluska FG, Tsao H, Wu H, Haluska FS, Lazar A, Goel V. (2006). Genetic alterations in signaling pathways in melanoma. *Clin Cancer Res* **12**: 2301s–2307s.

Hayashi C, Rittling S, Hayata T, Amagasa T, Denhardt D, Ezura Y *et al*. (2007). Serum osteopontin, an enhancer of tumor metastasis to bone, promotes B16 melanoma cell migration. *J Cell Biochem* **101**: 979–986.

Hirose Y, Katayama M, Mirzoeva OK, Berger MS, Pieper RO. (2005). Akt activation suppresses Chk2-mediated, methylating agent-induced G2 arrest and protects from temozolomide-induced mitotic catastrophe and cellular senescence. *Cancer Res* **65**: 4861–4869.

Irani K, Xia Y, Zweier JL, Sollott SJ, Der CJ, Fearon ER *et al*. (1997). Mitogenic signaling mediated by oxidants in Ras-transformed fibroblasts. *Science* **275**: 1649–1652.

Itahana K, Dimri GP, Hara E, Itahana Y, Zou Y, Desprez PY *et al*. (2002). A role for p53 in maintaining and establishing the quiescence growth arrest in human cells. *J Biol Chem* **277**: 18206–18214.

Jones CJ, Kipling D, Morris M, Hepburn P, Skinner J, Bounacer A *et al*. (2000). Evidence for a telomere-independent 'clock' limiting RAS oncogene-driven proliferation of human thyroid epithelial cells. *Mol Cell Biol* **20**: 5690–5699.

Khosravi-Far R, White MA, Westwick JK, Solski PA, Chrzanowska-Wodnicka M, Van Aelst L *et al*. (1996). Oncogenic RAS activation of Raf/mitogen-activated protein kinase-independent pathways is sufficient to cause tumorigenic transformation. *Mol Cell Biol* **16**: 3923–3933.

Kopnin PB, Agapova LS, Kopnin BP, Chumakov PM. (2007). Repression of sestrin family genes contributes to oncogenic Ras-induced reactive oxygen species up-regulation and genetic instability. *Cancer Res* **67**: 4671–4678.

Krueger C, Danke C, Pfleiderer K, Schuh W, Jäck HM, Lochner S *et al*. (2006). A gene regulation system with four distinct expression levels. *J Gene Med* **8**: 1037–1047.

Kurata S. (2000). Selective activation of p38 MAPK cascade and mitotic arrest caused by low level oxidative stress. *J Biol Chem* **275**: 23413–23416.

Lachat Y, Diserens AC, Nozaki M, Kobayashi H, Hamou MF, Godard S *et al*. (2004). INK4a/Arf is required for suppression of EGFR/DeltaEGFR(2–7)-dependent ERK activation in mouse astrocytes and glioma. *Oncogene* **23**: 6854–6863.

Lambert PF, Kashanchi F, Radonovich MF, Shickhattar R, Brady JN. (1998). Phosphorylation of p53 serine 15 increases interaction with CBP. *J Biol Chem* **273**: 33048–33053.

Lee AC, Fenster BE, Ito H, Takeda K, Bae NS, Hirai T *et al*. (1999). Ras proteins induce senescence by altering the intracellular levels of reactive oxygen species. *J Biol Chem* **274**: 7936–7940.

Leopold JG, Richards DB. (1967). Cellular blue neavi. *J Pathol Bacteriol* **94**: 247–255.

Li G, Schaider H, Satyamoorthy K, Hanakawa Y, Hashimoto K, Herlyn M. (2001). Downregulation of E-cadherin and Desmoglein 1 by autocrine hepatocyte growth factor during melanoma development. *Oncogene* **20**: 8125–8135.

Liu X, Miller CW, Koeffler PH, Berk AJ. (1993). The p53 activation domain binds the TATA box-binding polypeptide in Holo-TFIID, and a neighboring p53 domain inhibits transcription. *Mol Cell Biol* **13**: 3291–3300.

Mallette FA, Gaumont-Leclerk MF, Ferbeyre G. (2007). The DNA damage signaling pathway is a critical mediator of oncogene-induced senescence. *Genes Dev* **21**: 43–48.

Malumbres M, Pérez De Castro I, Hernández MI, Jiménez M, Corral T, Pellicer A. (2000). Cellular response to oncogenic ras involves induction of the Cdk4 and Cdk6 inhibitor p15 (INK4b). *Mol Cell Biol* **20**: 2915–2925.

Meierjohann S, Schartl M. (2006). From Mendelian to molecular genetics: the *Xiphophorus* melanoma model. *Trends Genet* **22**: 654–661.

Meierjohann S, Wende E, Kraiss A, Wellbrock C, Schartl M. (2006). The oncogenic epidermal growth factor receptor variant *Xiphophorus* melanoma receptor kinase induces motility in melanocytes by modulation of focal adhesions. *Cancer Res* **66**: 3145–3152.

Michaloglou C, Vredeveld LC, Soengas MS, Denoyelle C, Kuilman T, van der Horst CM *et al*. (2005). BRAFE600-associated senescence-like cell cycle arrest of human naevi. *Nature* **436**: 636–637.

Mirmohammadsadegh A, Hassan M, Bardenheuer W, Marini A, Gustrau A, Nambiar S *et al*. (2006). STAT5 phosphorylation in malignant melanoma is important for survival and is mediated through SRC and JAK1 kinases. *J Investig Dermatol* **126**: 2272–2280.

Natali PG, Nicotra MR, Di Renzo MF, Prat M, Bigotti A, Cavaliere R *et al*. (1993). Expression of the c-Met/HGF receptor in human melanocytic neoplasms: demonstration of the relationship to malignant melanoma tumor progression. *Br J Cancer* **68**: 746–750.

Nuciforo PG, Luise C, Capra M, Pelosi G, di Fagagna FD. (2007). Complex engagement of DNA-damage response pathways in human cancer and in lung tumor progression. *Carcinogenesis* **28**: 2082–2088.

Passos JF, von Zglinicki T. (2006). Oxygen free redicals in cell senescence: are they signal transducers? *Free Rad Res* **40**: 1277–1283.

Pfaffl MW, Horgan GW, Dempfle L. (2002). Relative expression software tool (REST) for group-wise comparison and statistical analysis of relative expression results in real-time PCR. *Nucleic Acids Res* **30**: e36.

Rangel J, Nosrati M, Torabian S, Shaikh L, Leong SP, Haqq C *et al*. (2008). Osteopontin as a molecular prognostic marker for melanoma. *Cancer* **112**: 144–150.

Rincheval V, Renaud F, Lemaire C, Godefroy N, Trotot P, Boulo V *et al*. (2002). Bcl-2 can promote p53-dependent senescence versus apoptosis without affecting the G1/S transition. *Biochem Biophys Res Commun* **298**: 282–288.

Sarkisian CJ, Keister BA, Stairs DB, Boxer RB, Moody SE, Chodosh LA. (2007). Dose-dependent oncogene-induced senescence *in vivo* and its evasion during mammary tumorigenesis. *Nat Cell Biol* **9**: 483–485.

Satyamoorthy K, Li G, Gerrero MR, Brose MS, Volpe P, Weber BL *et al*. (2003). Constitutive mitogen-activated protein kinase activation in melanoma is mediated by both BRAF mutations and autocrine growth factor stimulation. *Cancer Res* **63**: 756–759.

Savchenko I. (1988). Endomitosis in pigmented neoplasms of human skin. *TSitologiia i Genetika* **22**: 20–24.

Sewing A, Wiseman B, Lloyd AC, Land H. (1997). High-intensity Raf signal causes cell cycle arrest mediated by p21Cip1. *Mol Cell Biol* **17**: 5588–5597.

Sharpless NE, Bardeesy N, Lee KH, Carrasco D, Castrillon DH, Aguirre AJ *et al*. (2001). Loss of p16Ink4a with retention of p19Arf predisposes mice to tumorigenesis. *Nature* **413**: 86–91.

Spyridopoulos I, Isner JM, Losordo DW. (2002). Oncogenic ras induces premature senescence in endothelial cells: role of p21 (Cip1/Waf1). *Basic Res Cardiol* **97**: 117–124.

Straume O, Sviland L, Akslen LA. (2000). Loss of nuclear p16 protein expression correlates with increased tumor cell proliferation (Ki-67) and poor prognosis in patients with vertical growth phase melanoma. *Clin Cancer Res* **6**: 1845–1853.

Sviderskaya EV, Hill SP, Evans-Whipp TJ, Chin L, Orlow SJ, Easty DJ *et al*. (2002). p16(Ink4a) in melanocyte senescence and differentiation. *J Natl Cancer Inst* **94**: 446–454.

Takahashi A, Ohtani N, Yamakoshi K, Iida S, Tahara H, Nakayama K *et al*. (2006). Mitogenic signalling and the p16INK4a-Rb pathway cooperate to enforce irreversible cellular senescence. *Nat Cell Biol* **8**: 1291–1297.

Vigneron A, Roninson IB, Gamelin E, Coqueret O. (2005). Src inhibits adriamycin-induced senescence and G2 checkpoint arrest by blocking induction of p21 waf1. *Cancer Res* **65**: 8927–8935.

Wellbrock C, Geissinger E, Gómez A, Fischer P, Friedrich K, Schartl M. (1998). Signalling by the oncogenic receptor tyrosine kinase Xmrk leads to activation of STAT5 in *Xiphophorus* melanoma. *Oncogene* **16**: 3047–3056.

Wellbrock C, Schartl M. (1999). Multiple binding sites in the growth factor receptor Xmrk mediate binding to p59fyn, GRB2 and Shc. *Eur J Biochem* **260**: 275–283.

Wellbrock C, Weisser C, Geissinger E, Troppmair J, Schartl M. (2002). Activation of p59(Fyn) leads to melanocyte dedifferentiation by influencing MKP-1-regulated mitogen-activated protein kinase signaling. *J Biol Chem* **277**: 6443–6454.

Wellbrock C, Weisser C, Hassel JC, Fischer P, Becker J, Vetter CS *et al*. (2005). STAT5 contributes to interferon resistance of melanoma cells. *Curr Biol* **15**: 1629–1639.

Wittbrodt J, Lammers R, Malitschek B, Ullrich A, Schartl M. (1992). The Xmrk receptor tyrosine kinase is activated in *Xiphophorus* malignant melanoma. *EMBO J* **11**: 4239–4246.

Woods D, Parry D, Cherwinski H, Bosch E, Lees E, McMahon M. (1997). Raf-induced proliferation or cell cycle arrest is determined by the level of Raf activity with arrest mediated by p21Cip1. *Mol Cell Biol* **17**: 5598–5611.

Supplementary Information accompanies the paper on the Oncogene website (http://www.nature.com/onc)

12.2 Cystathionase mediates senescence evasion in melanocytes and melanoma cells

Cystathionase mediates senescence evasion in melanocytes and melanoma cells. Leikam, C;Hufnagel, A; Walz, S;Keitz, S;Eilers, M;Schartl, M;Meierjohann, S. (2012).

Re-submitted to Oncogene (July 2012).

Cystathionase mediates senescence evasion in melanocytes and melanoma cells

Claudia Leikam[1*], Anita Hufnagel[1*], Susanne Walz[2], Susanne Kneitz[1], Agnes Fekete[3], Martin J. Müller[3], Martin Eilers[2], Manfred Schartl[1], and Svenja Meierjohann[1]

[1]Department of Physiological Chemistry I, Biocenter, University of Wurzburg, Wurzburg, Germany

[2]Department of Biochemistry and Molecular Biology, Biocenter, University of Wurzburg, Wurzburg, Germany

[3]Department of Pharmaceutical Biology, Julius-von-Sachs Institute for Biological Sciences, University of Wurzburg, Wurzburg, Germany

*These authors contributed equally to this work.

To whom correspondence should be addressed:
Dr. Svenja Meierjohann
Department of Physiological Chemistry I
Biocenter
Am Hubland
University of Wurzburg
97074 Wurzburg
Germany
Tel.: 0049-931-3181348
Fax: 0049-931-3184150
E-mail: svenja.meierjohann@biozentrum.uni-wuerzburg.de

Running title: Cystathionase prevents pigment cell senescence

Abstract

The development of malignant melanoma is a highly complex process which is still poorly understood. A majority of human melanomas are found to express a few oncogenic proteins, such as mutant RAS and BRAF variants. However, these oncogenes are also found in nevi, and it is now a well-accepted fact that their expression alone leads to senescence. This renders the understanding of senescence escape mechanisms an important point to understand tumor development.

Here, we approached the question of senescence evasion by expressing the transcription factor MYC, which is known to act synergistically with many oncogenes, in melanocytes. We observed that MYC drives the evasion of reactive oxygen stress-induced melanocyte senescence, caused by activated receptor tyrosine kinase signalling. Conversely, MIZ1, the growth suppressing interaction partner of MYC, is involved in mediating melanocyte senescence. Both, MYC overexpression and *Miz1* knockdown led to a strong reduction of endogenous reactive oxygen species (ROS), DNA damage and senescence. We identified the cystathionase (CTH) gene product as mediator of the ROS-related MYC and MIZ1 effects. Blocking CTH enzymatic activity in MYC-overexpressing and *Miz1* knockdown cells increased intracellular stress and senescence. Importantly, pharmacological inhibition of cystathionase in human melanoma cells also reconstituted senescence in the majority of cell lines, and *CTH* knockdown reduced tumorigenic effects such as proliferation, H_2O_2 resistance and soft agar growth. Thus, we identified cystathionase as new MYC target gene with an important function in senescence evasion.

Keywords: ROS/melanoma/melanocyte/transsulfuration

Introduction

Melanomas are characterized by the presence of distinct genetic lesions, such as N-RAS^{Q61K}, BRAF^{V600E}, or GNAQ^{Q209L}, the latter being found in uveal melanoma (1, 2). At least N-RAS and BRAF possess the capacity to induce the potentially oncogenic transcription factor c-MYC (3, 4), and amplifications of c-MYC are commonly observed in uveal melanoma (5). c-MYC fulfills several pro-tumorigenic functions. A high *c-MYC* expression enhances aggressive melanoma growth in SCID mice (6) and goes along with IFNα resistance in human melanoma (7). c-MYC downregulation can sensitize melanoma cells to chemo- and radiotherapy (8, 9).

Many human oncogenes do not lead to tumorigenic cell transformation when expressed in an otherwise non-tumorigenic cellular background, but instead cause oncogene-induced senescence (OIS). However, overexpression of c-MYC in presence of senescence inducers such as constitutively active BRAF or STAT5A can prevent senescence and allow cell growth (10, 11).

Part of the pro-tumorigenic function of c-MYC is attributed to its interaction with the transcription factor MIZ1. In absence of c-MYC, cellular stress such as UV exposure induces binding of MIZ1 to the promoters of $p21^{CIP/WAF1}$ and $p15^{INK4B}$, thereby leading to enhanced gene expression and eventually to cell cycle arrest (12) (13, 14). Furthermore, MIZ1 is directly involved in the UV-mediated DNA damage response by promoting the activity of ATR. C-MYC can counteract these effects by forming a complex with MIZ1, thereby blocking its interaction with other proteins, which affects both transcriptional activity and signalling activity of MIZ1 (12, 15).

We previously described that activation of an oncogenic receptor tyrosine kinase in murine melanocytes leads to reactive-oxygen species (ROS)-dependent senescence when expressed at high levels (16). Here, we are using this melanocyte model to investigate the mechanism of senescence prevention by c-MYC and its interaction partner MIZ1. We show that both proteins affect senescence by modulating intracellular stress levels. Using microarray and ChIp analyses, we found that the cysteine-generating enzyme cystathionase (CTH) is regulated by both proteins. Interestingly, CTH is also strongly expressed in melanoma cell lines, mostly in a MYC-dependent manner, and is required for the prevention of DNA damage and senescence.

Results

To contribute to a better understanding of melanocyte senescence in response to cellular

oncogenic stress, we use a system that allows senescence induction in a tightly controlled way. The "HERmrk" melan-a cells are mouse melanocytes expressing a human EGF receptor ("HER") whose intracellular domain has been replaced by the corresponding part of Xmrk ("mrk"), a naturally occuring oncogenic version of the *Xiphophorus* EGF receptor. HERmrk activates many pathways simultaneously in an otherwise untransformed melanocytic background, including MAP kinase and PI3 kinase pathways (17).

MYC acts synergistically with HERmrk in conveying tumorigenic features to melanocytes

c-Myc, from now on simply termed *Myc*, is a well-established target gene of mammalian EGFR and mediates pro-proliferative and pro-survival effects of this receptor (18, 19). We tested *Myc* expression in cells expressing intermediate HERmrk levels (Hm^{me}) and high HERmrk levels (Hm^{hi}) (Figure S1A and B). In both cases, *Myc* was equally induced and peaked after 2 hours of stimulation. On protein level, Hm^{hi} cells displayed a basal amount of MYC, which, however, could not be further induced by EGF treatment. In Hm^{me} cells MYC was weakly expressed in the unstimulated state, but protein levels strongly increased after EGF addition. We reported previously that the expression level of HERmrk is crucial for determining the outcome in response to EGF stimulation: whereas Hm^{me} cells proliferate due to receptor activation, Hm^{hi} cells become senescent (16). As MYC has been associated with senescence prevention (20) (10), we were interested in the effect of MYC overexpression on Hm^{hi} cells. We transfected Hm^{hi} cells with expression plasmids encoding wildtype human MYC (MYC-wt) or the mutant MYC^{T58A} (MYC-TA, Figure 1A), the latter being more stable than its wildtype counterpart due to a lacking docking site for the ubiquitin ligase Fbw7 (21, 22). Control Hm^{hi} cells did not grow in absence of EGF and became multinuclear and senescent in presence of EGF, thereby blocking proliferation (Figure 1B and 2A). Hm^{hi}-MYC-TA and Hm^{hi}–MYC-wt cells, on the other hand, showed a slight, but quickly exhausting background proliferation in absence of HERmrk stimulation, and a strong proliferation in presence of EGF. To investigate colony-forming capacity of single cells, we performed soft agar growth assays and found that neither HERmrk nor MYC alone induced soft agar growth. However, both MYC constructs only enabled colony formation in presence of activated HERmrk (Figure 1C). Intriguingly, the colonies were much larger in cells expressing the stabilized MYC-TA mutant. These data indicate that HERmrk and MYC act synergistically in conveying neoplastic potential to melanocytes.

MYC prevents oncogene-induced ROS, DNA damage and senescence

Induction of senescence is the reason for the observed lack of efficient Hm^{hi} cell growth after EGF stimulation (Figure 1B and (16)). Accordingly, senescence was prevented in the highly proliferative cells overexpressing MYC-wt and MYC-TA (Figure 2A). As Hm^{hi} MYC-TA cells consistently exhibited a stronger effect than Hm^{hi}-MYC-wt cells, they were chosen for further experiments.

We previously reported that senescence of Hm^{hi} cells is caused by aberrant ROS, which lead to DNA damage and p53 activation (16). Accumulation of ROS can be visualized by the fluorescein derivative DCF-DA, which is converted to its fluorescent form only in presence of ROS. Interestingly, expression of MYC-TA prevented ROS accumulation upon EGF treatment (Figure 2B) as well as the concomitant DNA damage, as determined by DNA comet assay (Figure 2C).

To investigate the genes associated with the senescence-preventing effect, we performed comparative real-time-PCR of selected cell cycle-related MYC target genes from Hm^{hi} and Hm^{hi}-MYC-TA cells. The highest induction upon EGF stimulation was observed for *p21Cip1/Waf1*, which was induced more than 35-fold in Hm^{hi} cells after 14 days, i.e. when the cells were already senescent (Figure S2). In presence of MYC-TA, induction of *p21Cip1/Waf1* was significantly lower. This was not observed for any of the other investigated genes.

Endogenous MIZ1 mediates HERmrk-induced senescence

A reduced expression of *p21Cip1/Waf1* might be explained by an inhibitory effect of MYC on its interaction partner MIZ1, which is a known inducer of *p21Cip1/Waf1* in response to DNA damage (23). Interestingly, senescent Hm^{hi} cells expressed higher levels of *Miz1* RNA and protein than non-senescent Hm^{me} cells after 2 weeks of EGF exposure, i.e. when senescence was established in Hm^{hi} cells (Figure S3). To test if MIZ1 participates in senescence induction, Hm^{hi} cells were stably transfected with a *Miz1* knockdown vector (Hm^{hi}-pS-*Miz1*) or the corresponding control (Hm^{hi}-pS, Figure 3A). Hm^{hi}-pS-*Miz1* cells were resistant to EGF-induced senescence (Figure 3B) and displayed a lack of ROS accumulation and DNA damage (Figure 3C, D). The experiment was repeated with an independent *Miz1* knockdown construct, and similar results were obtained (Figure S4A-B). However, *Miz1* knockdown did not show the transforming effects that were observed upon MYC-TA expression: proliferation and soft agar growth were just marginally enhanced in Hm^{hi}-pS-*Miz1* knockdown cells compared to Hm^{hi}-pS cells (Fig. 3E, F). We then monitored protein expression of the well-established MIZ1 targets $p15^{Ink4a}$ and $p21^{Cip1/Waf1}$, which mediate cell cycle arrest and

senescence. Rather than the expected decrease, we found an increase of both proteins in response to *Miz1* knockdown during the first week of treatment, while p21 was undetectable after 2 weeks (Figure S5).

Thus, we concluded that p21-dependent cell cycle control is not the reason for MIZ1-dependent senescence mediation in this model.

CTH is a target gene of MYC and MIZ1

As MYC-TA expression and MIZ1 knockdown inhibit ROS-induced senescence, it is possible that ROS detoxification genes are affected by these transcription factors. We examined the expression of the classical antioxidant genes heme oxygenase (*Hmox1*), glutathione peroxidase (*Gpx1*) and peroxiredoxin (*Prdx1*). *Hmox1* was already induced by EGF (Figure S6A-C). None of the genes were upregulated by MYC expression or MIZ1 knockdown, but instead, MYC caused a slight but significant downregulation of *Hmox1* and *Gpx1* (Figure S6A,B). However, with the exception of *Prdx1* these genes were not regulated by oxidative stress, as incubation of HERmrk melanocytes with a glutathione ester caused no (*Hmox1*, *Gpx1*) or only slight (*Prdx1*) decrease of these antioxidant genes (Figure S6C).

To identify molecular players that might be causally linked to MYC- and MIZ1-regulated senescence, we performed an mRNA expression microarray analysis. We focused on genes that were upregulated in MYC-TA overexpressing and *Miz1* knockdown cells in comparison to the senescent Hm^{hi} cells. Only six genes, represented by 7 Affymetrix IDs, were commonly regulated (Figure 4A) and could be confirmed by real-time-PCR (Figure S7). Most of them are associated with cancer progression. In particular, cystathionase (*CTH*) encodes an enzyme involved in the synthesis of cysteine from methionine, the so-called transsulfuration pathway (TSP) (24). Importantly, MYC and MIZ1 also bind to the human *CTH* promoter, as we could demonstrate for HeLa cells using ChIp analysis (Figure 4B).

CTH inhibition recovers senescence in MYC-overexpressing and Miz1-depleted cells

The shared regulation of CTH by MYC and MIZ1 may be the reason for the reduced oxidative stress, DNA damage and senescence, which are observed in response to MYC-TA overexpression and *Miz1* knockdown. Interestingly, Hm^{hi} cells expressed very low levels of CTH protein irrespective of the stimulation state (Figure 4C). *Miz1* knockdown led to a faint induction of CTH protein in presence of EGF, which was consistent with low transcriptional upregulation. In contrast, MYC-TA strongly induced CTH protein, but only in cooperation with activated HERmrk (Figure 4C). Cystathionine-β-synthase (CBS) is the other enzyme

required for transsulfuration. It catalyzes the step preceding cystathionase, namely the generation of cystathionine from homocysteine (25), and its transcription is affected by cysteine availability (26). However, the levels of CBS protein were similar in Hm^{hi} cells irrespective of EGF stimulation and MYC or MIZ1 expression (Figure 4D). Similarly, RNA expression of methylene tetrahydrofolate reductase (MTHFR), a component of the TSP-associated remethylation pathway, was unchanged under the different conditions tested (Figure 4E). These data indicate that regulation of the transsulfuration pathway occurs on the level of CTH. Apart from CTH, cellular cysteine supply is also provided by the cystine-glutamate antiporter xCT (also named SLC7A11) (27). Whereas *Slc7a11* expression was strongly induced by HERmrk activation, it was not affected by MYC or MIZ1 (Figure 4F).

The enzymatic activity of CTH can be blocked by propargylglycine (PAG, (28)). When we applied PAG to EGF-stimulated Hm^{hi}–MYC-TA and Hm^{hi}-pS-Miz1 cells, we observed an increase of senescent cells (Figure 5A). Importantly, the overexpression of CTH in Hm^{hi} cells prevented senescence induction (Figure 5B).

OIS, e.g. induced by oncogenic RAS, was previously reported to go along with endoplasmic reticulum (ER) stress (29). Interestingly, increased homocysteine levels, which can be the result from a non-functional TSP, can induce ER stress and may thus affect senescence. Furthermore, it can lead to ATF4-dependent induction of CTH (30). We investigated whether homocysteine levels discriminated senescent Hm^{hi} from non-senescent CTH-overexpressing Hm^{hi} cells. We found no differences in homocysteine, but an increase in total glutathione in Hm^{hi}-CTH cells (Table S1). This indicates that homocysteine levels are most likely not causative for the stress-induced senescence in this pigment cell model. However, as ATF4 is a known inducer of cellular redox proteins and CTH, we tested if MYC and MIZ1 might regulate this transcription factor. Figure S8 demonstrates that *Atf4* is induced by EGF, but not by MYC expression or *Miz1* knockdown.

Melanoma cells are sensitive to CTH inhibition

To test CTH regulation and its role in ROS protection in human pigment cells, we transfected normal human epidermal melanocytes (NHEM) with the MYC overexpression vector pBabe-puro-MYC-TA (Figure S9). This resulted in a strong expression of CTH (Figure S9A). We also generated NHEM cells overexpressing CTH to examine the influence of CTH on ROS sensitivity in primary melanocytes. CTH-transgenic NHEM cells became more resistant to H_2O_2-induced DNA damage (Figure S9B) and growth inhibition (Figure S9C). In conclusion, MYC-induced CTH expression is also a feature of human melanocytes.

Human melanoma cells are also subject to high levels of ROS, which need to be tightly controlled to allow tumor propagation (31). In addition, they usually depend on endogenous MYC (10). We found that most human melanoma cell lines expressed high levels of MYC and intermediate or high levels of CTH (Figure 6A). The control human melanocyte cell line Hermes 3a, however, showed no MYC expression and only weak CTH expression. When we knocked down *MYC* in HeLa cells and five human melanoma cell lines, we found that CTH expression was reduced in four out of six tumor cell lines, confirming the MYC-dependent CTH regulation in these cells (Figure S9D). To test if CTH is also important for limiting DNA damage in melanoma cells and thereby contributes to senescence prevention, we treated different melanoma cell lines with increasing concentration of PAG. This resulted in increased DNA damage in all cell lines, as the DNA damage markers γ-H2AX or P-p53 were strongly induced (Figure 6B and Figure S10A). In most melanoma cell lines, PAG treatment also led to senescence (Figure 6C and S10B). To find out whether the effect of the inhibitor was CTH-specific, we knocked down *CTH* in four melanoma cell lines using siRNA and again observed an increase in DNA damage signalling in all cases (Figure 7A). Besides, proliferation was markedly reduced in response to *CTH* knockdown, while SA-β-Gal positive cells with high contents of heterochromatin accumulated (Figure 7B, C, Figure S11). Notably, the cell line UACC-62, harbouring an activated AKT pathway due to PTEN mutation, was particularly sensitive to *CTH* knockdown. When we supplied additional cystine to the medium of melanoma cells treated with CTH-specific siRNA, the growth was restored (Figure S12A). Importantly, H_2O_2 sensitivity was dramatically enhanced upon CTH reduction (Figure 7D), which could be explained by the high requirement for glutathione under stress conditions. While control cells increased their levels of total glutathione in response to H_2O_2, cells with reduced *CTH* were not capable of inducing this adaptive response (Figure 7E).

CTH can compensate for defective cystine import

Murine melanocytes depend on a functional cystine glutamate antiporter, as melan-a sut cells - murine pigment cells harbouring deficient *Slc7a11* - rely on the addition of the antioxidant β-mercaptoethanol to allow proliferation (32). Interestingly, CTH overexpression in melan-a sut cells was able to compensate for *Slc7a11* knockout and had an almost similar growth-promoting effect as β-mercaptoethanol (Fig. S12B). In human melanoma cells, we observed that cultivation in cystine-free medium strongly upregulated CTH, which explains their cellular tolerance towards cystine withdrawal (Figure S12C). Altogether, these data demonstrate the potency of the transsulfuration pathway in cysteine provision.

Taken together, we identified *CTH* as a novel MYC/MIZ1 target gene which proved to be important for intracellular stress reduction, thereby fulfilling a vital function for melanoma cells. Importantly, the specific CTH inhibitor PAG as well as information on its binding characteristics to the active site are already available, allowing for preclinical elucidation of CTH as possible target in melanoma therapy.

Discussion

The search for the reasons behind oncogene-induced senescence evasion and thus the detection of the tumor`s Achilles` heel is essential in order to identify druggable surrogate targets for cancer therapy. Many oncogenes induce senescence, and for some of these, factors that bypass this effect and thereby allow tumor growth have been identified. Similar to HERmrk, oncogenic RAS proteins induce high amounts of ROS, leading to senescence (33-35). If the accumulation of ROS-induced damage is prevented, as e.g. by enforced elimination of oxidized guanine nucleotides, senescence can be inhibited (36). To keep the ROS levels under control, ROS-induced countermeasures such as the induction of FOXM1 are active in many cells. FOXM1 stimulates the expression of superoxide dismutase (SOD), catalase and peroxiredoxins and thus contributes to senescence evasion of human fibroblasts (37, 38). Interestingly, FOXM1 is a target gene of c-MYC (39). Furthermore, the transcription factor NRF2 is induced by MYC, leading to the elevation of antioxidant enzymes and thereby lowering the intracellular amount of ROS (40). These data show that MYC counteracts oxidative stress on multiple levels.

We found that MYC acts synergistically with HERmrk, as it was able to transform EGF-stimulated Hm^{hi} cells. Similar effects occur when MYC is expressed together with oncogenic RAF or RAS, which alone would induce senescence (10). The potency of MYC to enhance proliferation and induce dedifferentiation is reflected by its role in generating pluripotent stem cells from differentiated adult cells (41). However, data describing the role of MYC in OIS evasion are only starting to accumulate. Intriguingly, MYC can exert a substantial level of sublethal cellular stress and can thus, under appropriate conditions, lead to OIS itself. As a consequence from aberrant DNA synthesis, MYC induces DNA damage (42) and even senescence in cells lacking the DNA repair protein WRN (43, 44). Recently, CDK2 was identified as another crucial component required to prevent MYC-induced senescence, and *Cdk2* knockdown in mice can substantially delay the onset of lymphoma (20, 45). On the one hand, these data indicate that MYC has the capacity to prevent accumulation of intrinsic cellular stress, which would otherwise result in senescence. On the other hand, they show that

the senescence program is latently present in some tumor types and can be reactivated. Melanoma cells usually express high levels of MYC, but can be driven into senescence and cellular crisis when the transcription factor is knocked down (10). Interestingly, the levels of glutathione (GSH) were reported to drop when MYC is inhibited in M14 melanoma cells, resulting in increased ROS levels (46). Supplementation with the cell permeable cysteine derivative N-acetylcysteine relieved this effect. This reveals two phenomena that are in accordance with our observations: 1) melanoma cells contain an intrinsic source of ROS that can be counteracted, e.g. by MYC, 2) the cellular cysteine supply is critical for growth and survival. It has previously been shown for melanoma and other cell types that the genes encoding the rate-limiting enzyme for glutathione (GSH) synthesis, γ-GCS, are induced by MYC (47, 48). Although γ-GCS levels were not affected by MYC in our model system (see Figure S2), we could identify the new target gene *CTH,* whose gene product is rate limiting for the production of cysteine in the transsulfuration pathway (24).

Through an interaction with MIZ1, MYC can prevent stress-induced induction of cell cycle regulatory genes such as *p21CIP1/WAF1* and *p15INK4B* and thereby translates DNA damage signals into cell cycle arrest (13, 49). We observed a higher amount of MIZ1 in senescent Hm^{hi} cells compared to Hm^{me} cells, and knockdown of *Miz1* largely prevented senescence. However, this was not accompanied by reduced levels of *p21Cip1/Waf1* and *p15Ink4B*, but instead by an increased amount of *Cth* transcript. Still, CTH increase was barely seen on protein level, suggesting that CTH is only partly responsible for the senescence-evading effect of *Miz1* knockdown in these cells.

Sufficient cysteine levels are the prerequisite for most cellular antioxidant systems, including GSH and taurine. Most cells meet their need for cysteine by importing extracellular cystine via the xCT cystine-glutamate antiporter (27). However, the corresponding gene *Slc7a11* was not regulated by MYC or MIZ1, and we showed that CTH expression can compensate for functional loss of *Slc7a11*. In line with these observations, it was reported that inhibition of xCT only affects viability of melanoma cells if GSH synthesis is blocked simultaneously (50). It is well known that the transsulfuration pathway, which converts methionine to cysteine, becomes important for cells with particularly strong ROS load (51). Accordingly, CTH expression is weak in normal tissue, but increased in tumor cells (http://www.proteinatlas.org/ENSG00000116761). Although an antiproliferative effect of the protein, caused by the increased production of H_2S, was reported (52), CTH has pro-tumorigenic functions (51). Still, only little is known about CTH regulation in tumors. Glutathione depletion and butyrate can stimulate CTH expression in glioma and colon cancer

cells, respectively (53, 54). Furthermore, it was recently demonstrated that the transcription factor ATF4 induces CTH expression in MEF cells exposed to ER stress (30). As ATF4 plays an important role in chemoresistance and hypoxia tolerance of tumor cells (55), it might also be involved in tumor-associated CTH expression. However, MYC is the first tumor-associated transcription factor directly demonstrated to regulate CTH expression.

Importantly, CTH plays no essential role in organismal development, as *Cth*-/- mice develop normally and only adult mice only suffer from hypertension (56). Besides, the mechanism by which DL-propargylglycine (PAG) inhibits CTH is well-characterized (28, 57). PAG is applied in mouse models for cardiovascular and nervous system-related diseases associated with H_2S produced by CTH, and efficiently relieves associated syndromes (58). However, PAG displays limited membrane permeability, and the development of improved inhibitors is required.

Taken together, CTH is an important cytoprotective protein, which is regulated by the concerted action of MYC and receptor tyrosine kinases such as HERmrk. In melanoma, CTH inhibition increases intracellular stress and thereby reinstalls the senescence pathway, rendering it a promising candidate for pharmacological intervention and combination melanoma therapy.

Materials and Methods

Cell culture – The EGF-inducible version of the oncogenic EGFR orthologue Xmrk ("HERmrk" or shortly "Hm") was described before (59). For senescence assays, cells were cultured in starving medium (DMEM with 10% dialyzed FCS (Gibco) for three days before the assay was started. Where indicated, 100 ng/ml human epidermal growth factor (EGF) (Tebubio) or 10 mM D,L-propargylglycine (PAG) was added. Medium was renewed every second day. Human melanoma cell lines A375, Bro, DX-3, LT5.1, Mel Im, Mel Ho, SK-MEL-3, SK-MEL-28, MeWo, and WM-35 as well as HeLa cells were cultivated in DMEM supplemented with 10% FCS, penicillin (100 U/ml, Gibco), and streptomycin (100 µg/ml, Gibco). The human melanocyte cell line Hermes 3a was cultivated as described (60).

Expression vectors –pSuper-*Miz1* (23) and pBabe-puro-MYC or -MYC^{T58A} (61) were described previously. For generation of pBabe-puro-CTH, murine *CTH* was amplified by PCR, digested with BamHI and SalI and cloned into the pBabe-puro expression vector.

siRNA transfection - Commercially available control siRNA and siRNA against human *MYC* or *CTH* (Smart Pool On Target Plus, Thermo Scientific) was transfected using X-treme gene transfection reagent (Roche), according to the manufacturer's

recommendations. Cells were analyzed three days after transfection, if not indicated otherwise. CTH-specific shRNA (Santa Cruz Biotechnology) was delivered to the cells by lentiviral infection as recommended. Cells were selected with 1 µg/ml puromycin before being used for further analyses.

SA-β-Gal staining - Cells were cultured in starving medium for three days before they were either left untreated or stimulated with 100 ng/ml EGF every second day. At indicated time points, cells were washed with PBS (pH 7.2) and fixed with 3.7% formaldehyde in PBS for 5 min at room temperature. After washing, they were stained in the dark for 12 h at 37°C (using 1 mg/mL X-Gal, 40 mM citric acid/sodium phosphate buffer (pH 6.0), 5 mM potassium ferricyanide, 5 mM potassium ferrocyanide, 150 mM NaCl, and 2 mM $MgCl_2$). Cells were then washed with PBS and were examined by light microscopy.

Cell lysis and immunoblot analysis – Lysis and blotting procedures were performed as described previously (16). The following antibodies were used: Anti-β-actin (C-4), anti-p15 (M-20), anti-p21 (N-20), anti-c-Myc (N-262), and anti-CTH (K-20) antibodies were from Santa Cruz Biotechnology. Anti-Phospho-p53 (Ser15) and anti-phospho-histone H2A.X (Ser139) were obtained from Cell Signaling. Anti-α-tubulin was purchased from Sigma-Aldrich. Miz1 antibody was derived from mouse hybridoma supernatant (clone 10E2).

RNA isolation and real-time-PCR –RNA isolation was performed with TrIR solution (ABGene). 4 µg of whole RNA was reversely transcribed using the RevertAidTM First Strand cDNA Synthesis Kit (Fermentas). Fluorescence-based quantitative real-time PCR was performed using the iCycler (Bio-Rad). Gene expression was normalized to hypoxanthine-guanine phosphoribosyltransferase (*Hprt*). Relative expression levels were calculated applying REST software (62). All oligonucleotides are displayed in table S2.

Cell proliferation assay – Cells were seeded at equal density onto wells of a 6-well plate and were either left untreated or stimulated with 100 ng/ml EGF and further addditives, as stated in the respective figure legends. Cells were harvested by trypsinization at indicated time points, pelleted, resolved in PBS and enumerated manually.

Soft agar growth assay – 1 ml of 1.2% agar was mixed with 1 ml 2x DMEM and plated onto 6-well plates. Upon polymerization, the solid agar was overlain with an equal amount of soft agar mix (0.3% agar) containing $4x10^4$ cells per well. The polymerized soft agar was supplied with 200 µl of starving media for the controls and the same amount of starving media supplemented with EGF (final concentration per well: 100 ng/ml). This solution was added every second day. After 14 days of cultivation, the number of cell colonies was counted, with "colony" being defined as more than eight cells per spot.

Reactive oxygen species detection assay – Cells were starved and treated as described for the β-Gal assay. At times indicated, 20 µM DCF-DA was added to the medium and cells were stained for 5 min before being washed with PBS and overlain with starving medium. Cells were analyzed microscopically for the presence of ROS-induced DCF (excitation 488 nm).

Comet assay – Cells were pre-starved for three days before being either left untreated or stimulated with 100 ng/ml EGF for 14 days. Cells were then trypsinized and used for the assay. Shortly, $2x10^4$ cells were mixed with 140 µl of 1% LMP agarose in PBS at 37°C. The mixture was then transferred as two equal drops to slides pre-coated with 1% standard agarose in H_2O. Upon polymerization, the slides were put into lysis solution (2.5M NaCl, 0.1M EDTA, 10mM Tris, 1% Triton X-100) for 1 hour at 4°C. Afterwards, the slides were washed three times in enzyme reaction buffer (40 mM HEPES, 0.1 M KCl, 0.5 mM EDTA, 0.2 mg/ml BSA, pH 8.0) before treatment with enzyme solution (0.5 mg/ml proteinase K in enzyme reaction buffer) in a moist box for 1 hour at 37°C followed by alkaline treatment in electrophoresis solution (0.3M NaOH, 1mM EDTA) for 40 minutes at 4°C. Subsequent electrophoresis was performed at 25 V for 30 minutes. Slides were then washed in neutralising solution (0.4 M Tris, pH 7.5) before cells were stained with 5µg/ml Hoechst 33258 in H_2O.

Glutathione detection assay – Cells were cultivated for three days in presence of 0, 25 or 50 µM H_2O_2. Intracellular glutathione was determined according to Tietze (63).

Chromatin immunoprecipitation (ChIP) – The analysis was performed as described previously (64). The following antibodies were used: Myc (N262, Santa Cruz) and Miz-1 (M. Teichmann, Bordeaux). Precipitated DNA was amplified with specific primers by real-time PCR. The oligonucleotides are displayed in table S2.

Conflict of interest

The authors declare no conflict of interest.

Acknowledgements

We thank Dorothy Bennett, St. George`s, University of London (Wellcome Trust Functional Genomics Cell Bank) for providing the cell lines Hermes 3a and melan-a sut. This work was supported by the Deutsche Forschungsgesellschaft, Transregio 17 ("RAS-dependent pathways in human cancer"). C.L. was supported by a grant of the German Excellence Initiative to the Graduate School of Life Sciences, University of Wurzburg.

References

1. Onken MD, Worley LA, Long MD, Duan S, Council ML, Bowcock AM, et al. Oncogenic mutations in GNAQ occur early in uveal melanoma. *Invest Ophthalmol Vis Sci*. 2008;**49**:5230-5234.

2. Van Raamsdonk CD, Bezrookove V, Green G, Bauer J, Gaugler L, O'Brien JM, et al. Frequent somatic mutations of GNAQ in uveal melanoma and blue naevi. *Nature*. 2009;**457**:599-602.

3. Whitwam T, Vanbrocklin MW, Russo ME, Haak PT, Bilgili D, Resau JH, et al. Differential oncogenic potential of activated RAS isoforms in melanocytes. *Oncogene*. 2007;**26**:4563-4570.

4. Aziz N, Cherwinski H, McMahon M. Complementation of defective colony-stimulating factor 1 receptor signaling and mitogenesis by Raf and v-Src. *Mol Cell Biol*. 1999;**19**:1101-1115.

5. Parrella P, Caballero OL, Sidransky D, Merbs SL. Detection of c-myc amplification in uveal melanoma by fluorescent in situ hybridization. *Invest Ophthalmol Vis Sci*. 2001;**42**:1679-1684.

6. Schlagbauer-Wadl H, Griffioen M, van Elsas A, Schrier PI, Pustelnik T, Eichler HG, et al. Influence of increased c-Myc expression on the growth characteristics of human melanoma. *J Invest Dermatol*. 1999;**112**:332-336.

7. Tulley PN, Neale M, Jackson D, Chana JS, Grover R, Cree I, et al. The relation between c-myc expression and interferon sensitivity in uveal melanoma. *Br J Ophthalmol*. 2004;**88**:1563-1567.

8. Biroccio A, Benassi B, Amodei S, Gabellini C, Del Bufalo D, Zupi G. c-Myc down-regulation increases susceptibility to cisplatin through reactive oxygen species-mediated apoptosis in M14 human melanoma cells. *Mol Pharmacol*. 2001;**60**:174-182.

9. Bucci B, D'Agnano I, Amendola D, Citti A, Raza GH, Miceli R, et al. Myc down-regulation sensitizes melanoma cells to radiotherapy by inhibiting MLH1 and MSH2 mismatch repair proteins. *Clin Cancer Res*. 2005;**11**:2756-2767.

10. Zhuang D, Mannava S, Grachtchouk V, Tang WH, Patil S, Wawrzyniak JA, et al. C-MYC overexpression is required for continuous suppression of oncogene-induced senescence in melanoma cells. *Oncogene*. 2008;**27**:6623-6634.

11. Mallette FA, Gaumont-Leclerc MF, Huot G, Ferbeyre G. Myc down-regulation as a mechanism to activate the Rb pathway in STAT5A-induced senescence. *J Biol Chem*. 2007;**282**:34938-34944.

12. Herold S, Hock A, Herkert B, Berns K, Mullenders J, Beijersbergen R, et al. Miz1 and HectH9 regulate the stability of the checkpoint protein, TopBP1. *EMBO J*. 2008;**27**:2851-2861.

13. Herold S, Wanzel M, Beuger V, Frohme C, Beul D, Hillukkala T, et al. Negative regulation of the mammalian UV response by Myc through association with Miz-1. *Mol Cell*. 2002;**10**:509-521.

14. Staller P, Peukert K, Kiermaier A, Seoane J, Lukas J, Karsunky H, et al. Repression of p15INK4b expression by Myc through association with Miz-1. *Nat Cell Biol*. 2001;**3**:392-399.

15. Wanzel M, Herold S, Eilers M. Transcriptional repression by Myc. *Trends Cell Biol*. 2003;**13**:146-150.

16. Leikam C, Hufnagel A, Schartl M, Meierjohann S. Oncogene activation in melanocytes links reactive oxygen to multinucleated phenotype and senescence. *Oncogene*. 2008;**27**:7070-7082.

17. Meierjohann S, Schartl M. From Mendelian to molecular genetics: the Xiphophorus melanoma model. *Trends Genet*. 2006;**22**:654-661.

18. Jamerson MH, Johnson MD, Dickson RB. Dual regulation of proliferation and

apoptosis: c-myc in bitransgenic murine mammary tumor models. *Oncogene*. 2000;**19**:1065-1071.

19. Kost DP, Michalopoulos GK. Effect of epidermal growth factor on the expression of protooncogenes c-myc and c-Ha-ras in short-term primary hepatocyte culture. *J Cell Physiol*. 1990;**144**:122-127.

20. Campaner S, Doni M, Hydbring P, Verrecchia A, Bianchi L, Sardella D, et al. Cdk2 suppresses cellular senescence induced by the c-myc oncogene. *Nat Cell Biol*. 2010;**12**:54-59; sup pp 51-14.

21. Popov N, Schulein C, Jaenicke LA, Eilers M. Ubiquitylation of the amino terminus of Myc by SCF(beta-TrCP) antagonizes SCF(Fbw7)-mediated turnover. *Nat Cell Biol*. 2010;**12**:973-981.

22. Yada M, Hatakeyama S, Kamura T, Nishiyama M, Tsunematsu R, Imaki H, et al. Phosphorylation-dependent degradation of c-Myc is mediated by the F-box protein Fbw7. *EMBO J*. 2004;**23**:2116-2125.

23. Wanzel M, Kleine-Kohlbrecher D, Herold S, Hock A, Berns K, Park J, et al. Akt and 14-3-3eta regulate Miz1 to control cell-cycle arrest after DNA damage. *Nat Cell Biol*. 2005;**7**:30-41.

24. Rao AM, Drake MR, Stipanuk MH. Role of the transsulfuration pathway and of gamma-cystathionase activity in the formation of cysteine and sulfate from methionine in rat hepatocytes. *J Nutr*. 1990;**120**:837-845.

25. Jhee KH, Kruger WD. The role of cystathionine beta-synthase in homocysteine metabolism. *Antioxid Redox Signal*. 2005;**7**:813-822.

26. Yamamoto N, Tanaka T, Noguchi T. Effect of cysteine on expression of cystathionine beta-synthase in the rat liver. *J Nutr Sci Vitaminol (Tokyo)*. 1995;**41**:197-205.

27. Conrad M, Sato H. The oxidative stress-inducible cystine/glutamate antiporter, system x (c) (-) : cystine supplier and beyond. *Amino Acids*. 2011.

28. Sun Q, Collins R, Huang S, Holmberg-Schiavone L, Anand GS, Tan CH, et al. Structural basis for the inhibition mechanism of human cystathionine gamma-lyase, an enzyme responsible for the production of H(2)S. *J Biol Chem*. 2009;**284**:3076-3085.

29. Denoyelle C, Abou-Rjaily G, Bezrookove V, Verhaegen M, Johnson TM, Fullen DR, et al. Anti-oncogenic role of the endoplasmic reticulum differentially activated by mutations in the MAPK pathway. *Nat Cell Biol*. 2006;**8**:1053-1063.

30. Dickhout JG, Carlisle RE, Jerome DE, Mohammed-Ali Z, Jiang H, Yang G, et al. Integrated stress response modulates cellular redox state via induction of cystathionine gamma-lyase: cross-talk between integrated stress response and thiol metabolism. *J Biol Chem*. 2012;**287**:7603-7614.

31. Fried L, Arbiser JL. The reactive oxygen-driven tumor: relevance to melanoma. *Pigment Cell Melanoma Res*. 2008;**21**:117-122.

32. Chintala S, Li W, Lamoreux ML, Ito S, Wakamatsu K, Sviderskaya EV, et al. Slc7a11 gene controls production of pheomelanin pigment and proliferation of cultured cells. *Proc Natl Acad Sci U S A*. 2005;**102**:10964-10969.

33. Nogueira V, Park Y, Chen CC, Xu PZ, Chen ML, Tonic I, et al. Akt determines replicative senescence and oxidative or oncogenic premature senescence and sensitizes cells to oxidative apoptosis. *Cancer Cell*. 2008;**14**:458-470.

34. Bischof O, Kirsh O, Pearson M, Itahana K, Pelicci PG, Dejean A. Deconstructing PML-induced premature senescence. *EMBO J*. 2002;**21**:3358-3369.

35. Lee AC, Fenster BE, Ito H, Takeda K, Bae NS, Hirai T, et al. Ras proteins induce senescence by altering the intracellular levels of reactive oxygen species. *J Biol Chem*. 1999;**274**:7936-7940.

36. Rai P, Young JJ, Burton DG, Giribaldi MG, Onder TT, Weinberg RA. Enhanced elimination of oxidized guanine nucleotides inhibits oncogenic RAS-induced DNA damage and premature senescence. *Oncogene*. 2010.

37. Park J, Jung Y, Kim J, Kim KY, Ahn SG, Song K, et al. TC1 (C8orf4) is upregulated by cellular stress and mediates heat shock response. *Biochem Biophys Res Commun*. 2007;**360**:447-452.

38. Li SK, Smith DK, Leung WY, Cheung AM, Lam EW, Dimri GP, et al. FoxM1c counteracts oxidative stress-induced senescence and stimulates Bmi-1 expression. *J Biol Chem*. 2008;**283**:16545-16553.

39. Blanco-Bose WE, Murphy MJ, Ehninger A, Offner S, Dubey C, Huang W, et al. C-Myc and its target FoxM1 are critical downstream effectors of constitutive androstane receptor (CAR) mediated direct liver hyperplasia. *Hepatology*. 2008;**48**:1302-1311.

40. DeNicola GM, Karreth FA, Humpton TJ, Gopinathan A, Wei C, Frese K, et al. Oncogene-induced Nrf2 transcription promotes ROS detoxification and tumorigenesis. *Nature*. 2011;**475**:106-109.

41. Takahashi K, Yamanaka S. Induction of pluripotent stem cells from mouse embryonic and adult fibroblast cultures by defined factors. *Cell*. 2006;**126**:663-676.

42. Sankar N, Kadeppagari RK, Thimmapaya B. c-Myc-induced aberrant DNA synthesis and activation of DNA damage response in p300 knockdown cells. *J Biol Chem*. 2009;**284**:15193-15205.

43. Robinson K, Asawachaicharn N, Galloway DA, Grandori C. c-Myc accelerates S-Phase and requires WRN to avoid replication stress. *PLoS One*. 2009;**4**:e5951.

44. Grandori C, Wu KJ, Fernandez P, Ngouenet C, Grim J, Clurman BE, et al. Werner syndrome protein limits MYC-induced cellular senescence. *Genes Dev*. 2003;**17**:1569-1574.

45. Hydbring P, Bahram F, Su Y, Tronnersjo S, Hogstrand K, von der Lehr N, et al. Phosphorylation by Cdk2 is required for Myc to repress Ras-induced senescence in cotransformation. *Proc Natl Acad Sci U S A*. 2010;**107**:58-63.

46. Biroccio A, Amodei S, Antonelli A, Benassi B, Zupi G. Inhibition of c-Myc oncoprotein limits the growth of human melanoma cells by inducing cellular crisis. *J Biol*

Chem. 2003;**278**:35693-35701.

47. Benassi B, Fanciulli M, Fiorentino F, Porrello A, Chiorino G, Loda M, et al. c-Myc phosphorylation is required for cellular response to oxidative stress. *Mol Cell*. 2006;**21**:509-519.

48. Benassi B, Zupi G, Biroccio A. Gamma-glutamylcysteine synthetase mediates the c-Myc-dependent response to antineoplastic agents in melanoma cells. *Mol Pharmacol*. 2007;**72**:1015-1023.

49. van Riggelen J, Muller J, Otto T, Beuger V, Yetil A, Choi PS, et al. The interaction between Myc and Miz1 is required to antagonize TGFbeta-dependent autocrine signaling during lymphoma formation and maintenance. *Genes Dev*. 2010;**24**:1281-1294.

50. Vene R, Castellani P, Delfino L, Lucibello M, Ciriolo MR, Rubartelli A. The Cystine/Cysteine Cycle and GSH Are Independent and Crucial Antioxidant Systems in Malignant Melanoma Cells and Represent Druggable Targets. *Antioxid Redox Signal*. 2011.

51. Rosado JO, Salvador M, Bonatto D. Importance of the trans-sulfuration pathway in cancer prevention and promotion. *Mol Cell Biochem*. 2007;**301**:1-12.

52. Yang G, Cao K, Wu L, Wang R. Cystathionine gamma-lyase overexpression inhibits cell proliferation via a H2S-dependent modulation of ERK1/2 phosphorylation and p21Cip/WAK-1. *J Biol Chem*. 2004;**279**:49199-49205.

53. Kandil S, Brennan L, McBean GJ. Glutathione depletion causes a JNK and p38MAPK-mediated increase in expression of cystathionine-gamma-lyase and upregulation of the transsulfuration pathway in C6 glioma cells. *Neurochem Int*. 2010;**56**:611-619.

54. Cao Q, Zhang L, Yang G, Xu C, Wang R. Butyrate-stimulated H2S production in colon cancer cells. *Antioxid Redox Signal*. 2010;**12**:1101-1109.

55. Rzymski T, Milani M, Singleton DC, Harris AL. Role of ATF4 in regulation of autophagy and resistance to drugs and hypoxia. *Cell Cycle*. 2009;**8**:3838-3847.

56. Yang G, Wu L, Jiang B, Yang W, Qi J, Cao K, et al. H2S as a physiologic

vasorelaxant: hypertension in mice with deletion of cystathionine gamma-lyase. *Science*. 2008;**322**:587-590.

57. Huang S, Chua JH, Yew WS, Sivaraman J, Moore PK, Tan CH, et al. Site-directed mutagenesis on human cystathionine-gamma-lyase reveals insights into the modulation of H2S production. *J Mol Biol*. 2010;**396**:708-718.

58. Szabo C. Hydrogen sulphide and its therapeutic potential. *Nat Rev Drug Discov*. 2007;**6**:917-935.

59. Meierjohann S, Wende E, Kraiss A, Wellbrock C, Schartl M. The oncogenic epidermal growth factor receptor variant Xiphophorus melanoma receptor kinase induces motility in melanocytes by modulation of focal adhesions. *Cancer Res*. 2006;**66**:3145-3152.

60. Gray-Schopfer VC, Cheong SC, Chong H, Chow J, Moss T, Abdel-Malek ZA, et al. Cellular senescence in naevi and immortalisation in melanoma: a role for p16? *Br J Cancer*. 2006;**95**:496-505.

61. Popov N, Herold S, Llamazares M, Schulein C, Eilers M. Fbw7 and Usp28 regulate myc protein stability in response to DNA damage. *Cell Cycle*. 2007;**6**:2327-2331.

62. Pfaffl MW, Horgan GW, Dempfle L. Relative expression software tool (REST) for group-wise comparison and statistical analysis of relative expression results in real-time PCR. *Nucleic Acids Res*. 2002;**30**:e36.

63. Tietze F. Enzymic method for quantitative determination of nanogram amounts of total and oxidized glutathione: applications to mammalian blood and other tissues. *Anal Biochem*. 1969;**27**:502-522.

64. Kress TR, Cannell IG, Brenkman AB, Samans B, Gaestel M, Roepman P, et al. The MK5/PRAK kinase and Myc form a negative feedback loop that is disrupted during colorectal tumorigenesis. *Mol Cell*. 2011;**41**:445-457.

Figure legends:

Figure 1: MYC acts synergistically with activated HERmrk.

A: Western blot of control Hm^{hi} cells and Hm^{hi} cells overexpressing human MYC-TA or MYC-wt. β-actin served as loading control. **B**: Proliferation of control Hm^{hi}, Hm^{hi}-MYC-TA and Hm^{hi}-MYC-wt cells. Where indicated, 100 ng/ml EGF was added. Data represent mean values of three independent experiments. **C**: Soft agar growth of control Hm^{hi} cells, Hm^{hi}-MYC-TA or Hm^{hi}-MYC-wt cells. Pictures were taken after 14 days of cultivation. Where indicated, 100 ng/ml EGF was added. *: $p<0.05$; **: $p<0.01$ (Student`s t-test, unpaired, two-tailed).

Figure 2: MYC prevents senescence, ROS and DNA damage.

A: Senescence-associated β-galactosidase staining of Hm^{hi} control and Hm^{hi}-MYC-TA cells upon 14 days of EGF stimulation. Left panel: brightfield images. Right panel: Quantification displaying the percentage of senescent cells. **B**: DCF fluorescence and phase contrast images of the same section upon 14 days of EGF stimulation in Hm^{hi} or Hm^{hi}-MYC-TA cells. In presence of MYC-TA, ROS induction through HERmrk was prevented. **C**: Comet assay of untreated or EGF-stimulated Hm^{hi} or Hm^{hi}-MYC-TA cells upon 14 days of treatment. *: $p<0.05$; **: $p<0.01$ (Student`s t-test, unpaired, two-tailed). Scale bar = 100 µm.

Figure 3: MIZ1 mediates ROS-induced senescence.

A: Knockdown of endogenous *Miz1* RNA levels by pSuper-*Miz1* expression in Hm^{hi} cells. Downregulation was assayed by real-time-PCR. Expression levels were normalized to *Hprt*. **B**: SA-β-Gal staining of control Hm^{hi} cells (Hm^{hi}-pS) and Hm^{hi}-pSuper-*Miz1* cells upon 14 days of EGF treatment. Left panel: brightfield images. Right panel: Quantification displaying the percentage of senescent cells. **C:** DCF fluorescence and phase contrast images of the same section upon 14 days of EGF stimulation in Hm^{hi}-pS and Hm^{hi}-pS-*Miz1* cells. When *Miz1* was knocked down, ROS induction through HERmrk was prevented. **D**: Comet assay of untreated and EGF-stimulated Hm^{hi}–pS or Hm^{hi}-pS-*Miz1* cells upon 14 days of treatment. **E**: Proliferation of Hm^{hi}–pS and Hm^{hi}-pS-*Miz1* cells. Where indicated, 100 ng/ml EGF was added. Data represent mean values of three independent experiments +/- SE. The p values only depict the difference between Hm^{hi} –pS and Hm^{hi}-pS-*Miz1* in presence of EGF. **F**: Soft agar growth of Hm^{hi}–pS and Hm^{hi}-pS-*Miz1* cells. Pictures were taken upon 14 days of cultivation. Where indicated, 100 ng/ml EGF was added. The right panel indicates the relative

increase of colonies (cell clumps consisting of at least eight cells) in Hm^{hi}-pS-*Miz1* cells compared to Hm^{hi}-pS cells. *: $p<0.05$; **: $p<0.01$; ***: $p<0.001$ (Student`s t-test, unpaired, two-tailed). Scale bar = 100 µm.

Figure 4: Genes conjointly regulated due to MYC overexpression and *Miz1* knockdown.
A: Venn diagram displaying all transcripts up-regulated in Hm^{hi}-MYC-TA cells compared to Hm^{hi} cells and in Hm^{hi}-pS-*Miz1* cells compared to Hm^{hi} cells, each cell line having been stimulated with EGF for 14 days. Only seven transcripts were conjointly regulated. **B**: Binding of MYC and MIZ1 to the CTH promoter was analyzed by ChIP with chromatin isolated from HeLa cells. As control, chromatin was immunoprecipitated with nonspecific IgG. Bound DNA was analyzed by quantitative real-time PCR. Enrichment compared with input DNA was calculated. As controls, a positive region from the p21 promoter, known to be bound by MYC and MIZ1, and a negative region from the p21 promoter were analyzed. **C, D:** Western blot of Hm^{hi} cells (ctrl), Hm^{hi}-MYC-TA cells and Hm^{hi} pS-*Miz1* cells, showing expression of CTH (**C**) and CBS (**D**). Where indicated, EGF was added. Samples were harvested upon 14 days of treatment. β-actin served as loading control. **E, F:** Real-time PCR analysis of *Mthfr* (**E**) and *Slc7a11* (**F**) in control and EGF-treated Hm^{hi}, Hm^{hi}-MYC-TA and Hm^{hi}-pS-Miz1 cells. EGF treatment was performed for 14 days. Expression levels were normalized to *Hprt*, and values from untreated Hm^{hi} cells were set as 1. *: $p<0.05$.

Figure 5: Inhibition of cystathionase reestablishes ROS-induced senescence of melanocytes.
A: SA-β-Gal staining of Hm^{hi}-MYC-TA cells and Hm^{hi}-pS-*Miz1* cells upon 1 week of EGF stimulation. Where indicated, 10 mM PAG was added. **B:** Effect of CTH overexpression on Hm^{hi}-mediated senescence. Left panel: Western blot showing the overexpression of CTH in Hm^{hi}-CTH cells. β-actin served as loading control. Right panel: SA-β-Gal staining of control Hm^{hi} cells and Hm^{hi}-CTH cells upon 2 weeks of EGF stimulation. Scale bar = 100 µm.

Figure 6: Inhibition of CTH in human melanoma leads to the reappearance of cellular senescence.
A: Western blot showing CTH and MYC expression in the human melanoma cell lines SK-MEL-28, A375, SK-MEL-3, WM-35, Mel Im, Mel Ho, DX-3, LT5.1 and Bro. The immortalized human melanocyte cell line Hermes 3a served as control. β-actin was used as loading control. **B**: DNA damage is induced in response to increasing concentrations of PAG. The Western blot shows expression of the DNA damage indicator γ–H2AX in untreated or

PAG-stressed SK-MEL-28, A375 and LT5.1 cells upon one week of treatment. β-actin served as loading control. **C**: SA β-Gal staining of SK-MEL28, A375 and LT5.1 cells upon one week of continuous treatment with the indicated concentrations of PAG. Untreated SK-MEL-28 and LT5.1 cells were subcultivated during the experiment to prevent overgrowing of the cell cultures. Hence, the cell density in these samples was lower at the timepoint when the picture was taken. Since the proliferation potential of PAG-treated cells was strongly reduced due to senescence induction, subcultivation was not necessary here. Scale bar = 100 µm.

Figure 7: Knockdown of CTH reduces tumorigenic potential of melanoma cells.
A: Western blot showing the siRNA-dependent knockdown of CTH in Mel Ho, SK-MEL-28, A375, and UACC-62 cells. CTH knockdown was accompanied by an increased γ-H2AX signal. β-actin served as loading control. **B**: Proliferation of Mel Ho, SK-MEL-28, A375, and UACC-62 cells transfected with control siRNA or *CTH*-specific siRNA. Data represent mean values of three independent experiments. **C**: Senescence-associated β-galactosidase staining of Mel Ho, SK-MEL-28, A375, and UACC-62 cells transfected with control or *CTH*-specific siRNA. Pictures were taken at day 6 after transfection. Bar size = 100 µm. **D**: *CTH* knockdown sensitizes cells to reactive oxygen stress. SK-MEL-28 and SK-MEL-28 sh*CTH* cells were continuously treated with 25 µM H_2O_2. Representative pictures were taken after one week. **E**: Total intracellular glutathione levels of SK-MEK-28 and SK-MEL-28 sh*CTH* cells after three days of cultivation in starving media alone or with indicated concentrations of H_2O_2. *: $p<0.05$, **: $p<0.01$, ***: $p<0.001$ (Student's t-test, unpaired, two-tailed). Scale bar = 100 µm.

Figure 1

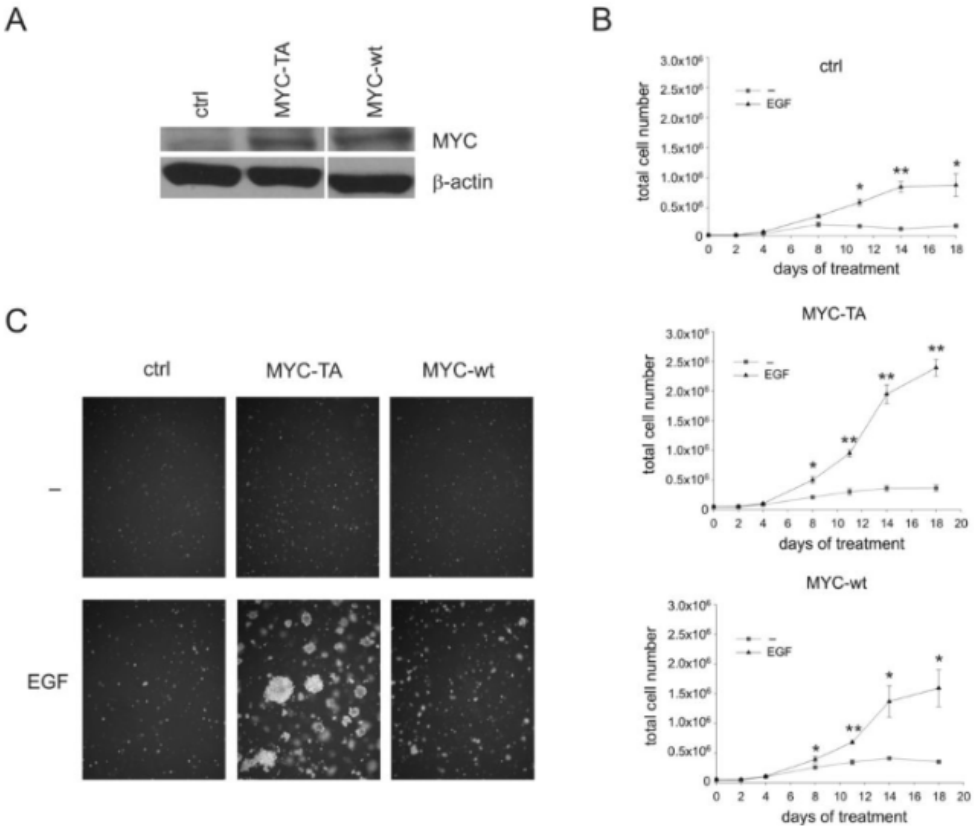
A
ctrl
MYC-TA
MYC-wt
MYC
β-actin
B
ctrl
MYC-TA
MYC-wt
total cell number
days of treatment
–
EGF
C
ctrl
MYC-TA
MYC-wt
–
EGF

Figure 2

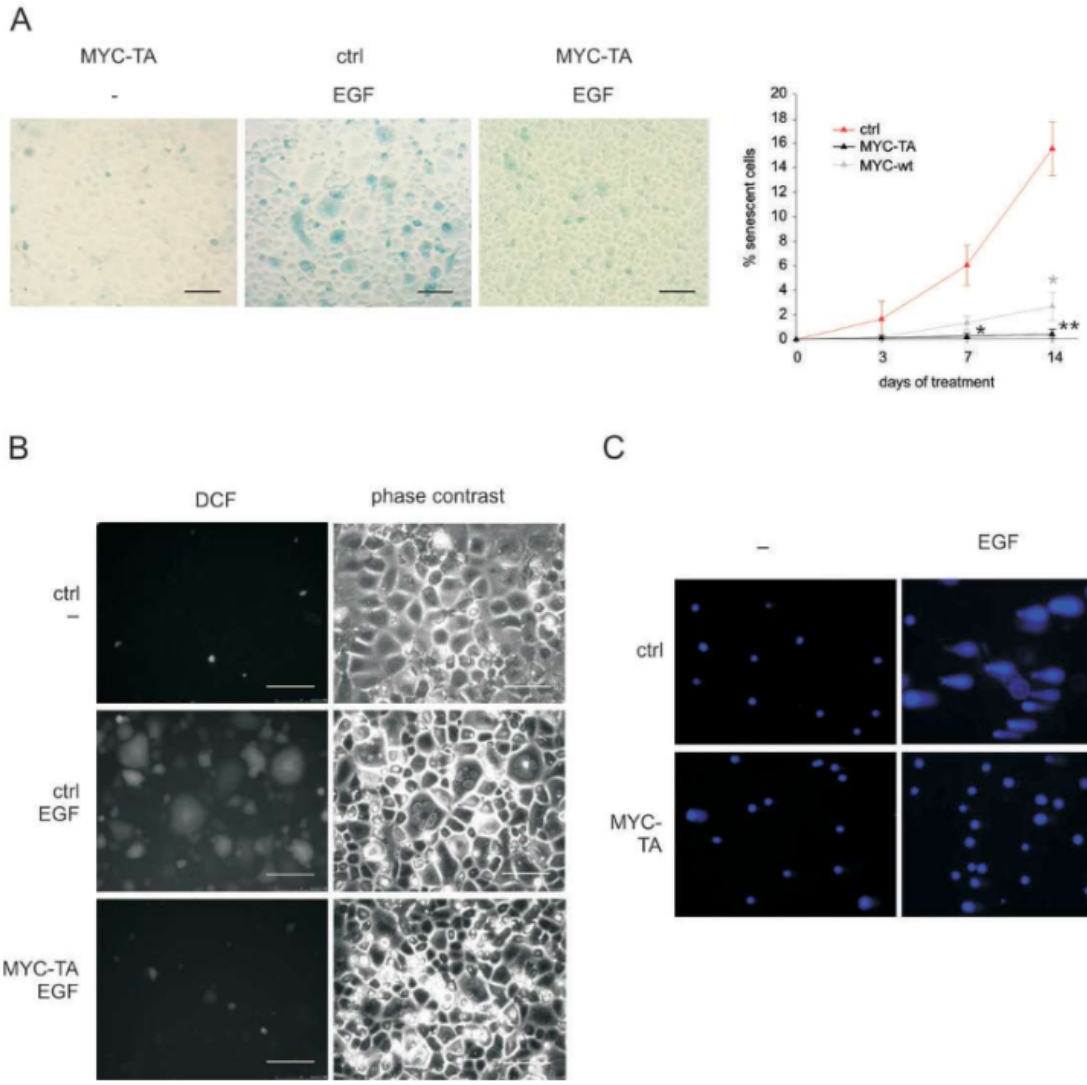
A
MYC-TA
-
ctrl
EGF
MYC-TA
EGF
% senescent cells
days of treatment
ctrl
MYC-TA
MYC-wt
B
DCF
phase contrast
ctrl
–
ctrl
EGF
MYC-TA
EGF
C
–
EGF
ctrl
MYC-
TA

Figure 3

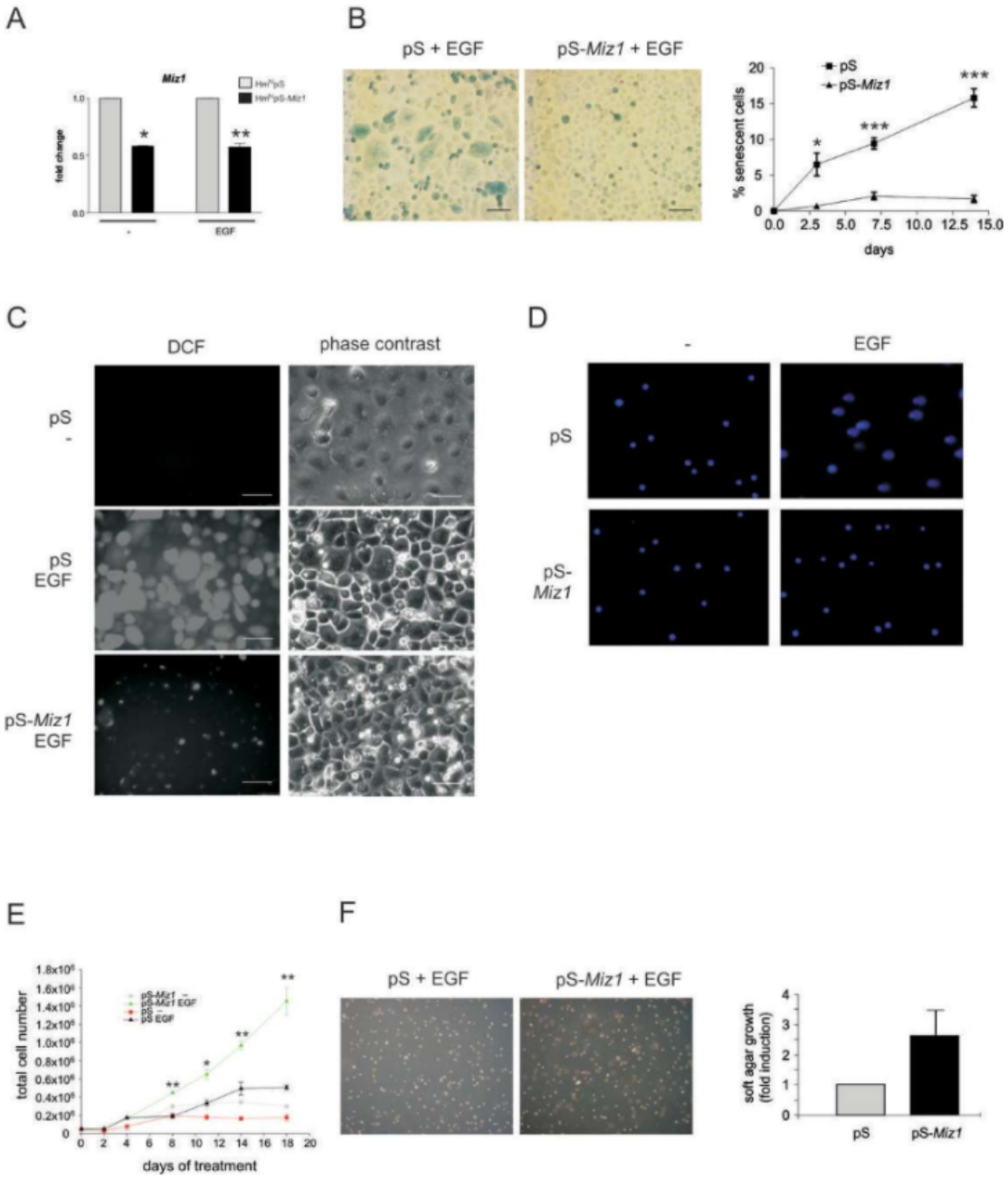
A
Miz1
Hm²pS
Hm²pS-Miz1
fold change
1.0
0.5
0.0
*
**
-
EGF
B
pS + EGF
pS-Miz1 + EGF
pS
pS-Miz1
% senescent cells
20
15
10
5
0
*
***
***
0.0 2.5 5.0 7.5 10.0 12.5 15.0
days
C
DCF
phase contrast
pS
-
pS
EGF
pS-Miz1
EGF
D
-
EGF
pS
pS-
Miz1
E
total cell number
1.8x10⁶
1.6x10⁶
1.4x10⁶
1.2x10⁶
1.0x10⁶
0.8x10⁶
0.6x10⁶
0.4x10⁶
0.2x10⁶
0
pS-Miz1
pS-Miz1 EGF
pS
pS EGF
**
**
*
**
0 2 4 6 8 10 12 14 16 18 20
days of treatment
F
pS + EGF
pS-Miz1 + EGF
soft agar growth
(fold induction)
4
3
2
1
0
pS
pS-Miz1

Figure 4

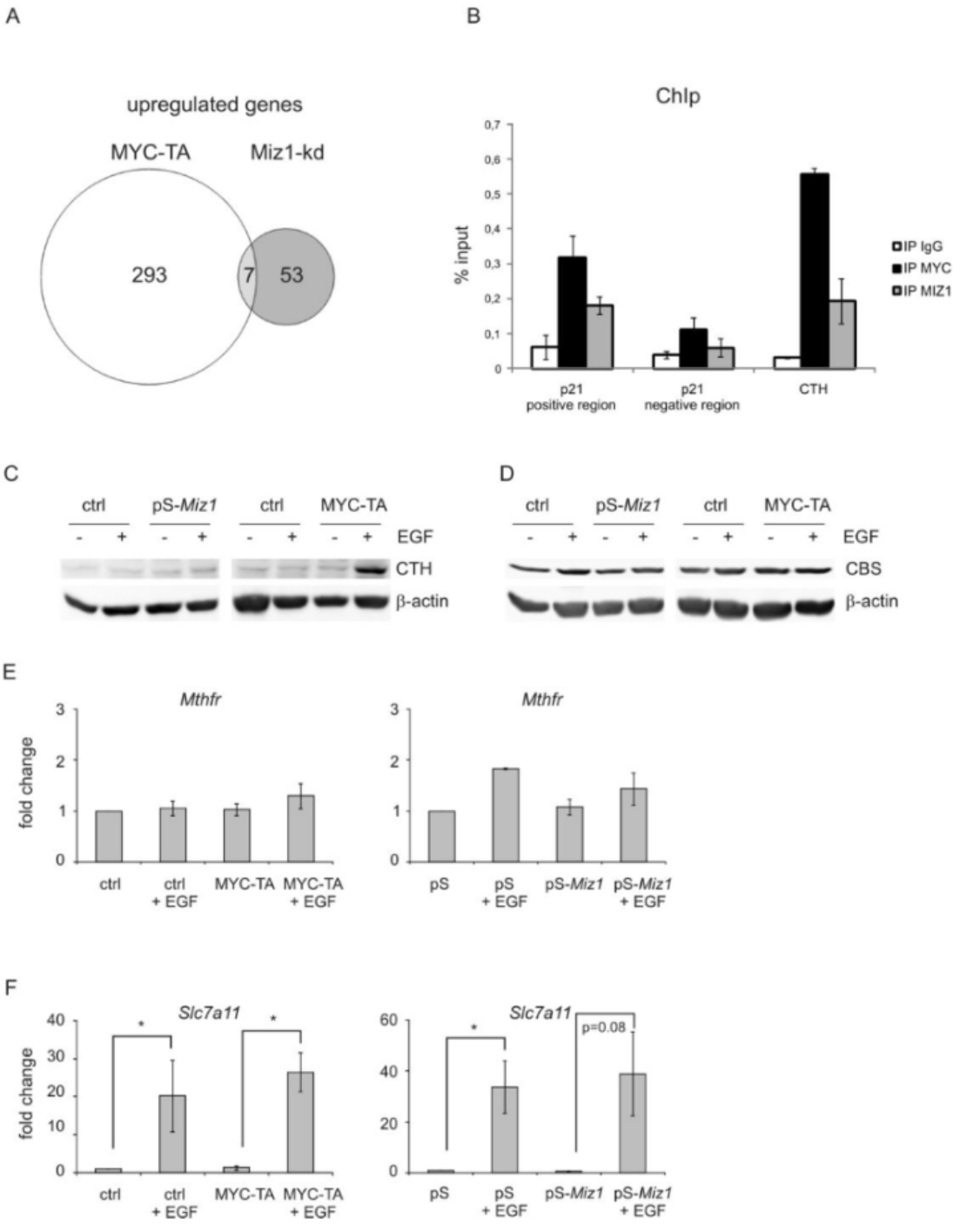
A
upregulated genes
MYC-TA
Miz1-kd
293
7
53
B
ChIp
% input
IP IgG
IP MYC
IP MIZ1
p21 positive region
p21 negative region
CTH
C
ctrl
pS-Miz1
ctrl
MYC-TA
EGF
CTH
β-actin
D
ctrl
pS-Miz1
ctrl
MYC-TA
EGF
CBS
β-actin
E
Mthfr
fold change
ctrl
ctrl + EGF
MYC-TA
MYC-TA + EGF
Mthfr
pS
pS + EGF
pS-Miz1
pS-Miz1 + EGF
F
Slc7a11
fold change
ctrl
ctrl + EGF
MYC-TA
MYC-TA + EGF
Slc7a11
p=0.08
pS
pS + EGF
pS-Miz1
pS-Miz1 + EGF

Figure 5

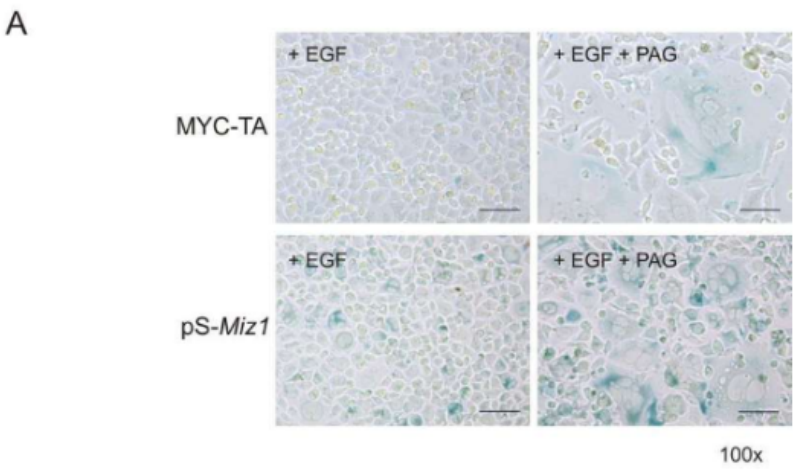
A
+ EGF
+ EGF + PAG
MYC-TA
+ EGF
+ EGF + PAG
pS-Miz1
100x
B
ctrl
CTH
CTH
tubulin
Hm^hi + EGF
Hm^hi-CTH + EGF

Figure 6

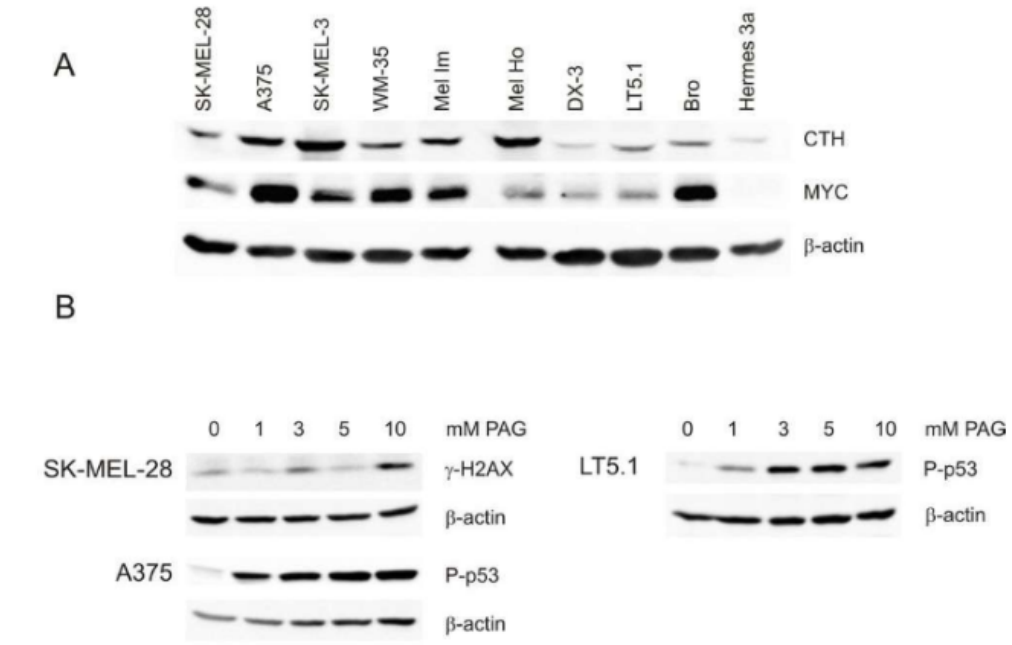
A
SK-MEL-28
A375
SK-MEL-3
WM-35
Mel Im
Mel Ho
DX-3
LT5.1
Bro
Hermes 3a
CTH
MYC
β-actin
B
0 1 3 5 10 mM PAG
SK-MEL-28
γ-H2AX
β-actin
A375
P-p53
β-actin
0 1 3 5 10 mM PAG
LT5.1
P-p53
β-actin
C
-
5 mM PAG
10 mM PAG
SK-MEL-28
A375
LT5.1

Figure 7

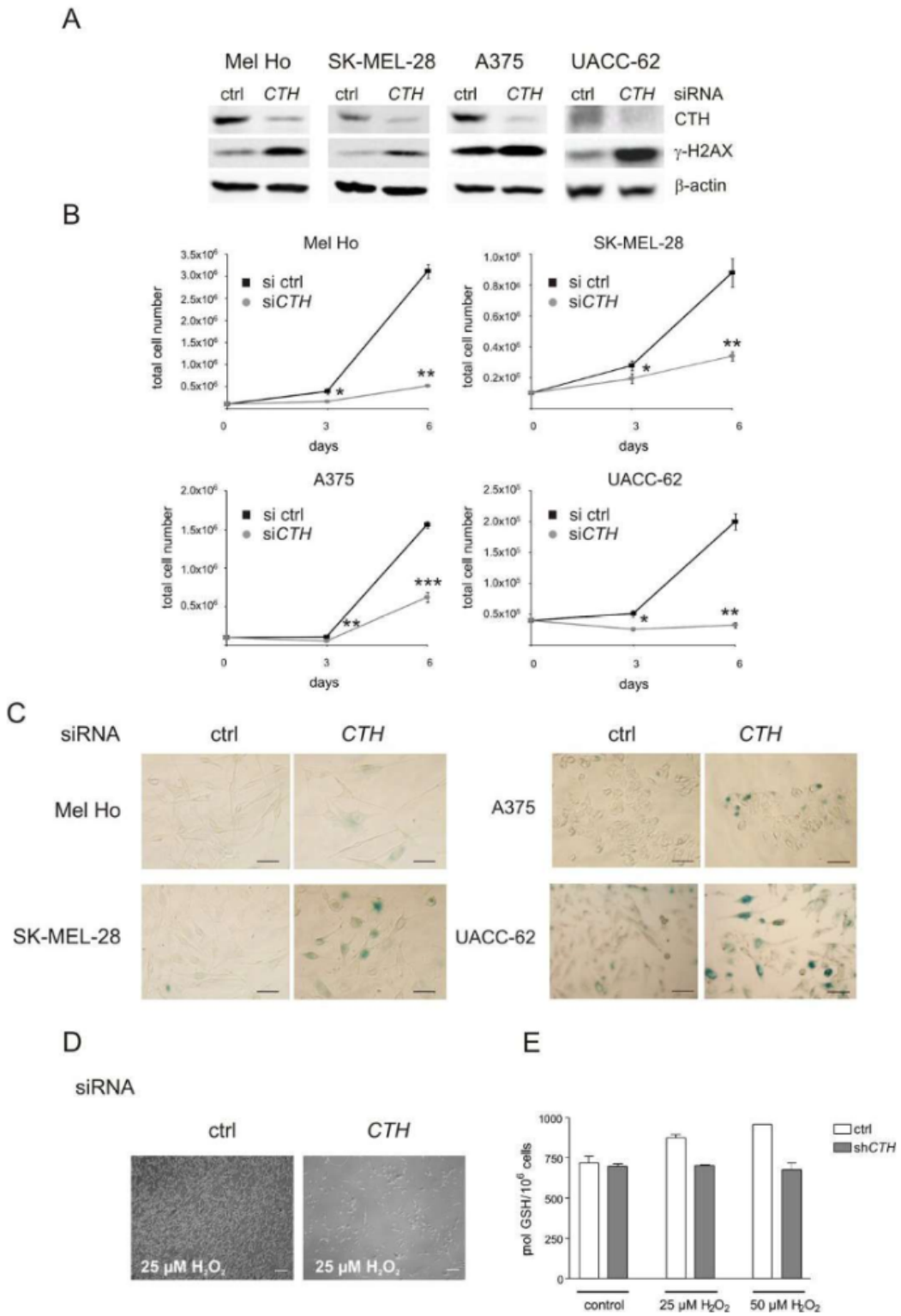
A
Mel Ho
SK-MEL-28
A375
UACC-62
ctrl
CTH
siRNA
γ-H2AX
β-actin
B
si ctrl
siCTH
total cell number
days
C
D
25 μM H2O2
E
pol GSH/10^6 cells
shCTH
control
25 μM H2O2
50 μM H2O2

Supplementary Materials and Methods

Cell culture - Melan-a sut cells were cultivated in RPMI1640 containing 10% FCS, 200 nM 12-O-tetradecanoyl phorbol 13-acetate (TPA), 200 pM cholera toxin, 100 U/ml penicillin, 100 µg/ml streptomycin and, where indicated, 100 µM β-mercaptoethanol, as described previously (Chintala et al 2005). NHEM cells were cultivated in melanocyte growth medium (Promocell).

Microarray – All cells were starved in medium containing 10% dialyzed FCS before EGF stimulation was performed. Hm^{hi} control cells were either stimulated with 100 ng/ml EGF or were left untreated for 14 days. Hm^{hi}-MYC-TA and Hm^{hi} –pS-Miz1 cells were stimulated with 100 ng/ml EGF in starving medium for 14 days. After harvesting, RNA was isolated using the miRNeasy Kit (Qiagen), and analyzed using the Affymetrix Gene Chip Mouse Genome 430 2.0. All data were analyzed using different R packages from the Bioconductor project (www.bioconductor.org). Obtained data are deposited at http://www.ncbi.nlm.nih.gov/geo/query/acc.cgi?token=pjgzficcocyggtu&acc=GSE30473 .

X-celligence analysis – $1.5x10^3$ cells were seeded on wells of a gold-layered 96-well-plate (Roche) and were monitored for the indicated timespan using the X-celligence system (Roche), as instructed by the manufacturer. Every five hours, resistance of the cell population was measured and was recorded as "cell index". The assay was done in triplicate, and two independent biological experiments were performed.

Immunofluorescence - Cells were transfected with control or CTH-specific siRNA before being seeded on glass cover slips the next day. 5 days later, immunofluorescence was performed as previously described (Meierjohann et al 2006). Anti-histone H3K9me3 antibody (1:100; Millipore) and CY3-conjugated goat-anti-rabbit (Jackson ImmunoResearch Laboratories) were used to visualize heterochromatin.

Homocysteine measurement - Homocysteine were measured by ultra performance liquid chromatography coupled to quadrupole/time-of-flight mass spectrometry (Waters) prior derivatisation with AccQ Ultra Kit (Waters). The washed and centrifuged pellets were extracted two times using sonic bath for 15 minutes in methanol containing 1000 mg/l S-methylmethanethiosulphonate and 0.25 mg/l norvalin used as internal standard. The extracts were dried until dryness with SpeedVac, reconstitute in 100 µl MilliQ water and derivatised with 6-aminoquinolyl-N-hydroxysuccinimidyl carbamate according to the kit protocol. 5 µl sample were directly injected on BEH C18 column (2.1*100mm, 1.7µl, Waters) and separated with linear gradient from 0% to 30% acetonitrile in water containing 0.1% formic acid within

12 minutes. The analytes were ionised in positive electrospray ionisation and the intensity of protonated homocysteine derivative (m/z of 352.080) was followed. The retention time of homocysteine was 11.1 min. Internal standard was applied for the quantification (response factor of 0.07) and short validation was performed at each set.

References for Supplementary Material

Chintala S, Li W, Lamoreux ML, Ito S, Wakamatsu K, Sviderskaya EV *et al* (2005). Slc7a11 gene controls production of pheomelanin pigment and proliferation of cultured cells. *Proc Natl Acad Sci U S A* **102:** 10964-10969.

Copie-Bergman C, Plonquet A, Alonso MA, Boulland ML, Marquet J, Divine M *et al* (2002). MAL expression in lymphoid cells: further evidence for MAL as a distinct molecular marker of primary mediastinal large B-cell lymphomas. *Mod Pathol* **15:** 1172-1180.

Meierjohann S, Wende E, Kraiss A, Wellbrock C, Schartl M (2006). The oncogenic epidermal growth factor receptor variant Xiphophorus melanoma receptor kinase induces motility in melanocytes by modulation of focal adhesions. *Cancer Res* **66:** 3145-3152.

Park J, Jung Y, Kim J, Kim KY, Ahn SG, Song K *et al* (2007). TC1 (C8orf4) is upregulated by cellular stress and mediates heat shock response. *Biochem Biophys Res Commun* **360:** 447-452.

Slomnicki LP, Lesniak W (2010). S100A6 (calcyclin) deficiency induces senescence-like changes in cell cycle, morphology and functional characteristics of mouse NIH 3T3 fibroblasts. *J Cell Biochem* **109:** 576-584.

Sunde M, McGrath KC, Young L, Matthews JM, Chua EL, Mackay JP *et al* (2004). TC-1 is a novel tumorigenic and natively disordered protein associated with thyroid cancer. *Cancer Res* **64:** 2766-2773.

Thompson TC (2010). Glioma pathogenesis-related protein 1: tumor-suppressor activities and therapeutic potential. *Yonsei Med J* **51:** 479-483.

Uehara N, Matsuoka Y, Tsubura A (2008). Mesothelin promotes anchorage-independent growth and prevents anoikis via extracellular signal-regulated kinase signaling pathway in human breast cancer cells. *Mol Cancer Res* **6:** 186-193.

van Dieck J, Fernandez-Fernandez MR, Veprintsev DB, Fersht AR (2009). Modulation of the oligomerization state of p53 by differential binding of proteins of the S100 family to p53 monomers and tetramers. *J Biol Chem* **284:** 13804-13811.

Supplementary figure legends

Figure S1: *Myc* is a target gene of HERmrk and is strongly expressed in non-senescent Hm^{me} cells.

A: Short-term induction of *Myc* is similar in Hm^{me} and Hm^{hi} cells. The graph shows the real-time-PCR analysis of *Myc* in response to EGF stimulation at indicated time points. Untreated melan-a cells were used as reference. Expression levels were normalized to *Hprt*. **B**: Western blot showing the expression of endogenous MYC in unstimulated Hm^{me} and Hm^{hi} cells and after 2 h of EGF stimulation. β-actin served as loading control.*: $p<0.05$, **: $p<0.01$, ***: $p<0.001$(Student`s t-test, unpaired, two-tailed).

Figure S2: *p21CIP1/WAF1*is differentially expressed in EGF-treated Hm^{hi} and Hm^{hi}-MYC-TA cells.

Real-time PCR analysis of the indicated cell cycle genes. Untreated control Hm^{hi} cells served as reference. Hm^{hi} and Hm^{hi}-MYC-TA cells were stimulated with EGF for 3, 7 or 14 days before being harvested. Bars represent the fold change of gene expression compared to the untreated Hm^{hi} control. Expression levels were normalized to *Hprt*.*: $p<0.05$(Student`s t-test, unpaired, two-tailed).

Figure S3: MIZ1 is induced in senescent cells.

A: Real-time PCR analysis of *Miz1* gene expression in Hm^{me} and Hm^{hi} cells upon 3, 7 and 14 days of EGF stimulation. Bars represent the fold change of gene expression compared to the respective untreated control. Expression levels were normalized to *Hprt*. **B**: Western blot showing the expression of endogenous MIZ1 in untreated Hm^{me} and Hm^{hi} cells after 14 days of EGF stimulation. β-actin served as loading control. *: $p<0.05$ (Student`s t-test, unpaired, two-tailed).

Figure S4: Senescence prevention also occurs through a second, independent *Miz1*shRNA construct.

A: Knockdown of endogenous *Miz1* upon expression of the pRS-*Miz1* construct in starved and EGF-treated Hm^{hi} cells, as indicated by real-time PCR. The fold change of *Miz1* expression in Hm^{hi}-pRS-*Miz1* cells, compared to the Hm^{hi}-pRS control, is shown. Expression levels were normalized to *Hprt*. **B**: SA β-Gal staining of control Hm^{hi}cells (Hm^{hi}-pRS) and

Hm^{hi}-pRS-*Miz1* cells upon 14 days of EGF treatment. *: p<0.05; **: p<0.01 (Student`s t-test, unpaired, two-tailed). Scale bar = 100 μm.

Figure S5: Senescence prevention does not correlate with reduced levels of $p15^{INK4B}$ and $p21^{CIP/WAF1}$.

Western blot illustrating the expression of $p21^{CIP1/WAF1}$ and $p15^{INK4B}$ in control Hm^{hi}-pS and Hm^{hi}-pS-*Miz1* cells. Cells were left untreated or stimulated with EGF for 3, 7 or 14 days before being harvested. β-actin served as loading control.

Figure S6: Regulation of antioxidant genes by MIZ1 and MYC.

Real-time PCR analysis of *Hmox1*, *Gpx1* and *Prdx1* in transgenic Hm^{hi} melanocytes. **A:** Hm^{hi} control and Hm^{hi}-MYC-TA cells, and **B:** Hm^{hi}-pS and Hm^{hi}-pS-*Miz1* cells were treated with EGF for 14 days before being harvested. **C:** Hm^{hi}cells were left untreated or were treated with EGF, 1 mM glutathione reduced ethyl ester (GRE), or a combination of both for 14 days before being harvested. For **A**-**C**, the bars display the fold change in gene expression compared to the untreated Hm^{hi} control. Expression levels were normalized to *Hprt.**: p<0.05; **: p<0.01.

Figure S7: Regulation of *S100a6*, *Mal*, *Msln*, *Tc1*, *Gliprl* and *Cth* by MIZ1 and MYC.

Real-time PCR analysis of the indicated genes. Control Hm^{hi} cells, Hm^{hi}-MYC-TA cells and Hm^{hi}-pS-*Miz1* cells were treated with EGF for 14 days before being harvested. The bars display the fold change in gene expression compared to the EGF-treated Hm^{hi} control. Expression levels were normalized to *Hprt.* *: p<0.05; **: p<0.01 (Student`s t-test, unpaired, two-tailed).

S100A6 is a Ca^{2+} binding protein that also shows high affinity to proteins of the p53 family and has previously been associated with senescence (Slomnicki and Lesniak 2010, van Dieck et al 2009). For MAL (myelin and lymphocyte protein) and MSLN (mesothelin), aberrant expression has been observed in several cancer types, but their roles are only scarcely investigated (Copie-Bergman et al 2002, Uehara et al 2008). TC1 (thyroid cancer 1) was described to be highly expressed in thyroid cancer (Sunde et al 2004) and can be induced by heat shock and other stresses, including oxidative stress (Park et al 2007). GLIPR1 (glioma pathogenesis-related 1) is described as secreted, matrix-interacting protein whose tumor suppressive role has been discussed for prostate cancer (Thompson 2010).

Figure S8: *Atf4* is induced in senescent Hm^{hi} cells, but unaffected by MYC or MIZ1 expression.

Real-time PCR analysis of *Atf4* in Hm^{hi} controls, Hm^{hi}-MYC-TA, and Hm^{hi}-pS-*Miz1* cells. Cells were treated with EGF for 14 days before being harvested. Bars display the fold change in gene expression compared to the untreated Hm^{hi} control. Expression levels were normalized to *Hprt*. *: $p<0.05$.

Figure S9: MYC regulates CTH expression in human primary melanocytes and four out of six tested tumor cell lines.

A: Western blot showing MYC and CTH expression in NHEM cells transgenic for pBabe-puro-MYC-TA. **B:** γ-H2AX expression in control and CTH-overexpressing NHEM cells after one week of treatment with the indicated H_2O_2 concentration. **C:** NHEM and NHEM-CTH cells were seeded at equal density and subsequently treated with 150 µM H_2O_2. Representative pictures were taken after four days. **D:** Western blot showing MYC and CTH expression in HeLa cells as well as the human melanoma cell lines A375, Mel Im, SK-MEL-3, Mel Ho, and SK-MEL-28, each treated with control siRNA or MYC-specific siRNA. β-actin served as loading control.

Figure S10: Many melanoma cell lines re-establish senescence in response to CTH inhibition by PAG.

A: DNA damage is induced in response to increasing concentrations of PAG. The Western blot shows expression of the DNA damage indicator γ–H2AX in untreated or PAG-stressed MeWo, Mel Ho, DX-3, Bro and WM-35 cells upon one week of treatment. β-actin served as loading control. **B:** SAβ-Gal staining of MeWo, Mel Ho, DX-3, Bro and WM-35 cells upon one week of continuous treatment with 10 mM PAG. Control Mel Ho and DX-3cells were subcultivated during the experiment to prevent overgrowing of the cell cultures, which is the reason for the low cell density shown in these samples. PAG-treated cells grew much slower, and subcultivation was not necessary. Mel Ho, DX-3 and WM-35 became senescent, MeWo and Bro only showed limited proliferation, but no senescence. Scale bar = 100 µm.

Figure S11: Knockdown of *CTH* induces heterochromatin formation in melanoma cells.

Immunofluorescence showing the accumulation of $H3K3^{me3}$ in Mel Ho, SK-MEL-28, A375 and UACC-62 cells transfected with *CTH*-specific siRNA compared to control-siRNA-treated cells. To highlight the differences in fluorescence intensity, images are displayed in false

colours ("rainbow RGB", performed in Image J). The increasing expression is visualized as gradient from blue via green to red. Scale bar = 100 µm.

Figure S12: Cystathionase and SLC7A11 can complement each other.
A: Total number of control-siRNA- and *CTH*-specific siRNA transfected cells after a four-day cultivation in cystine-free medium and medium supplied with 1 mM cystine. Cells were seeded at equal density on day 0. *: $p<0.05$. **B:** X-celligence measurement of melan-a-sut or melan-a-sut-CTH cells in absence or presence of 100 µM β-mercaptoethanol (ME). The experiment was performed in triplicate and was repeated once. The cell index represents the density of the cell population on a well of a 96-well dish. The inlay shows a Western blot demonstrating CTH expression in normal melan-a-sut cells and melan-a-sut cells transfected with pBabe-puro-CTH. **C:** Western blot showing CTH expression in the human melanoma cell lines A375, Mel Ho, and SK-MEL-28, each kept in normal medium (ctrl) or in medium depleted of extracellular cystine (- Cys). Tubulin served as loading control.

Supplementary table legend

Table S1: Homocysteine and total glutathione levels of Hm^{hi} and Hm^{hi}-CTH cells after 14 days of EGF stimulation. Data show pmol/10^5 cells.

Table S2: List of oligonucleotides used throughout this manuscript.

Figure S1

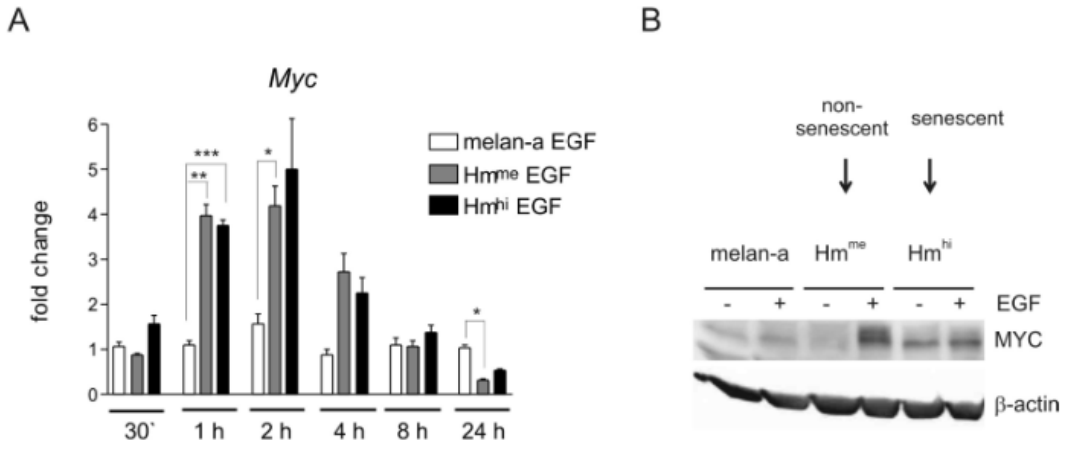
A
Myc
fold change
melan-a EGF
Hm^me EGF
Hm^hi EGF
30`
1 h
2 h
4 h
8 h
24 h
B
non-senescent
senescent
melan-a
Hm^me
Hm^hi
EGF
MYC
β-actin

Figure S2

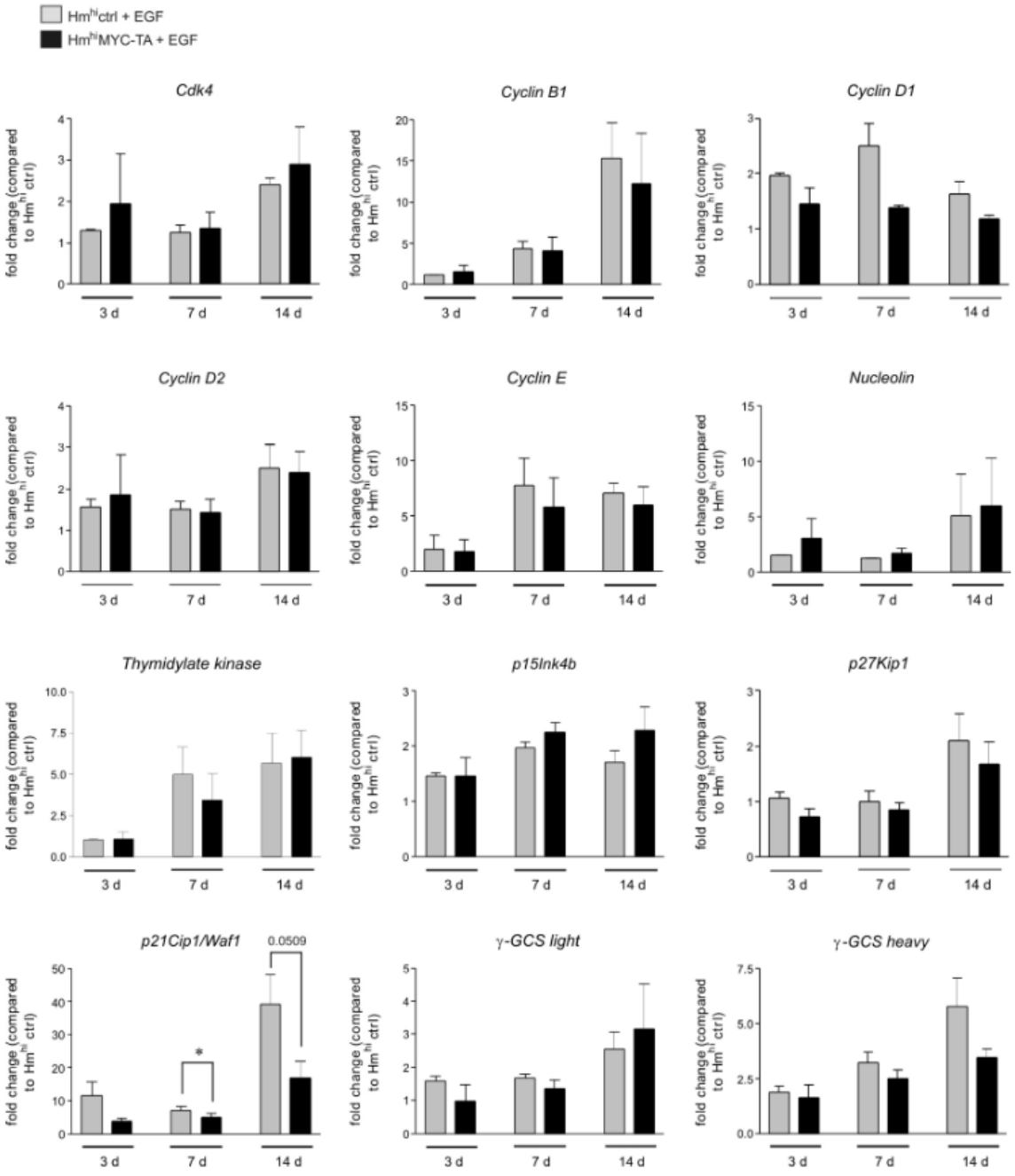
Hm^hi ctrl + EGF
Hm^hi MYC-TA + EGF
Cdk4
Cyclin B1
Cyclin D1
Cyclin D2
Cyclin E
Nucleolin
Thymidylate kinase
p15Ink4b
p27Kip1
p21Cip1/Waf1
0.0509
*
γ-GCS light
γ-GCS heavy
fold change (compared to Hm^hi ctrl)
3 d
7 d
14 d

Figure S3

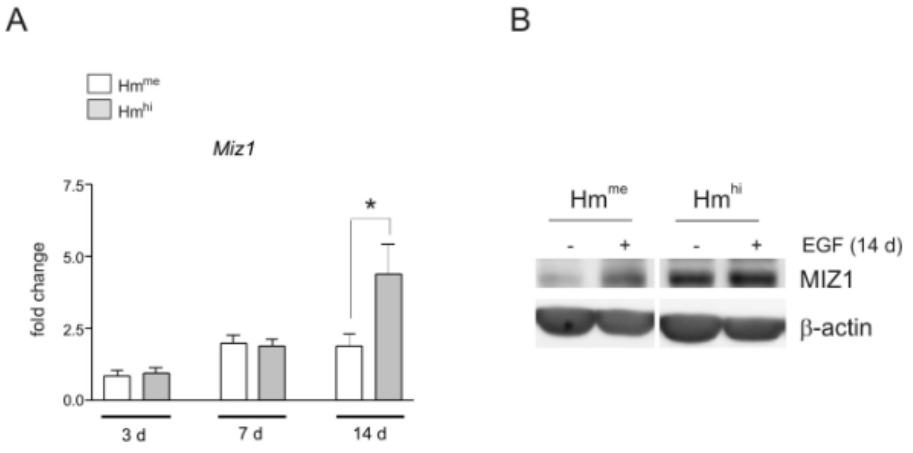
A
Hm^me
Hm^hi
Miz1
fold change
7.5
5.0
2.5
0.0
*
3 d
7 d
14 d
B
Hm^me
Hm^hi
- + - +
EGF (14 d)
MIZ1
β-actin

Figure S4

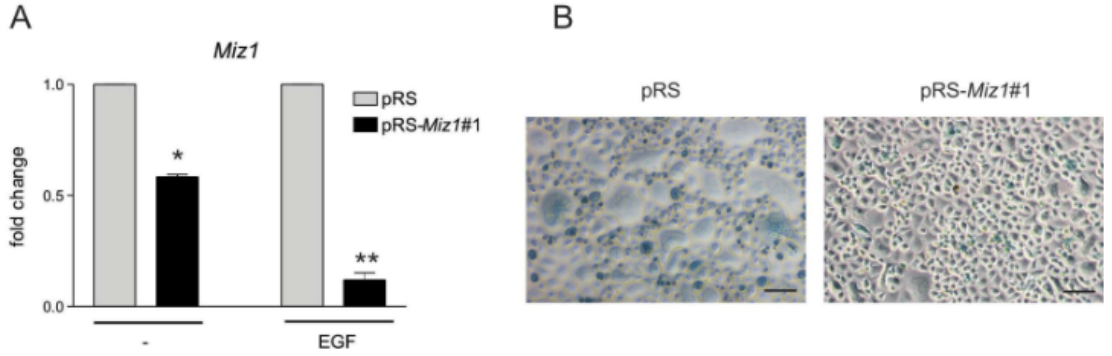

Figure S5

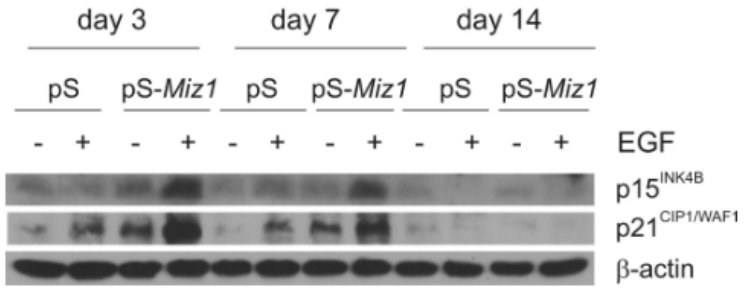
day 3
day 7
day 14
pS
pS-Miz1
pS
pS-Miz1
pS
pS-Miz1
- + - + - + - + - + - +
EGF
p15INK4B
p21CIP1/WAF1
β-actin

Figure S6

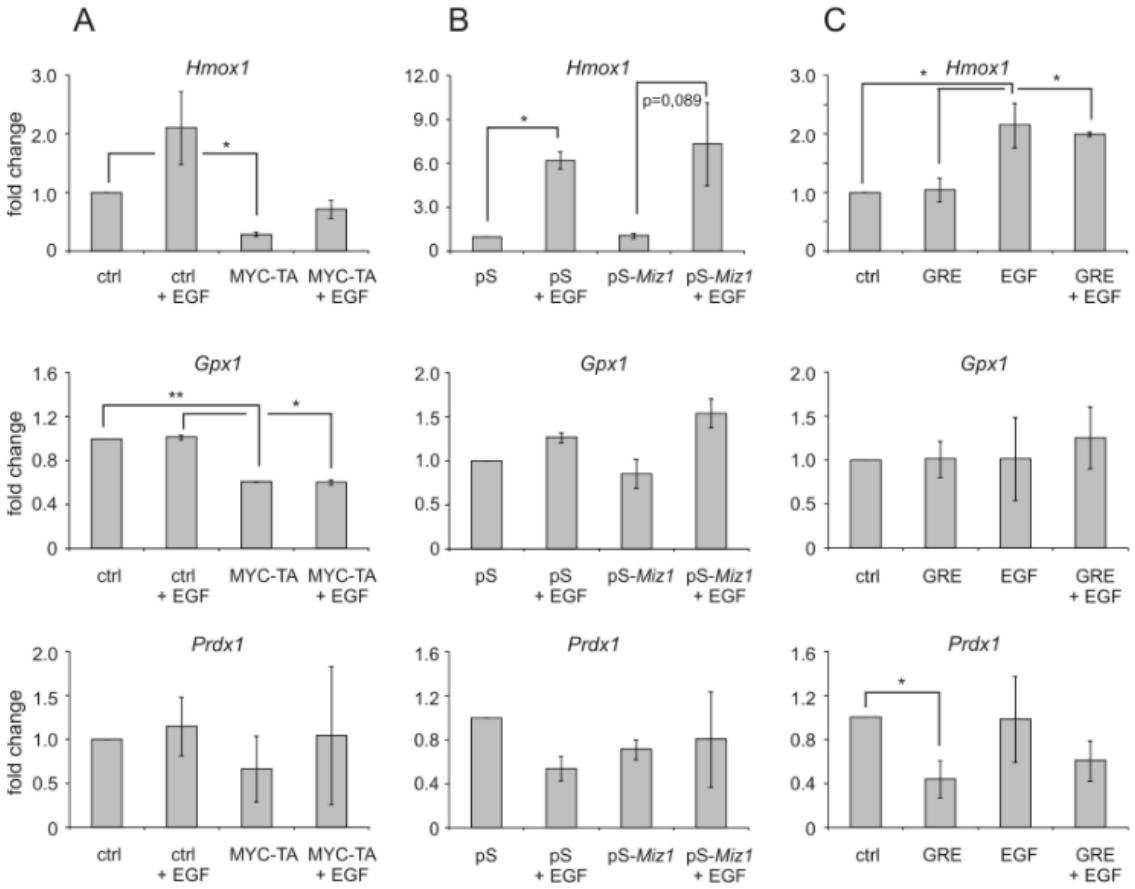
A
B
C
Hmox1
Gpx1
Prdx1
fold change
ctrl
ctrl + EGF
MYC-TA
MYC-TA + EGF
pS
pS + EGF
pS-Miz1
pS-Miz1 + EGF
GRE
GRE + EGF
EGF
p=0,089

Figure S7

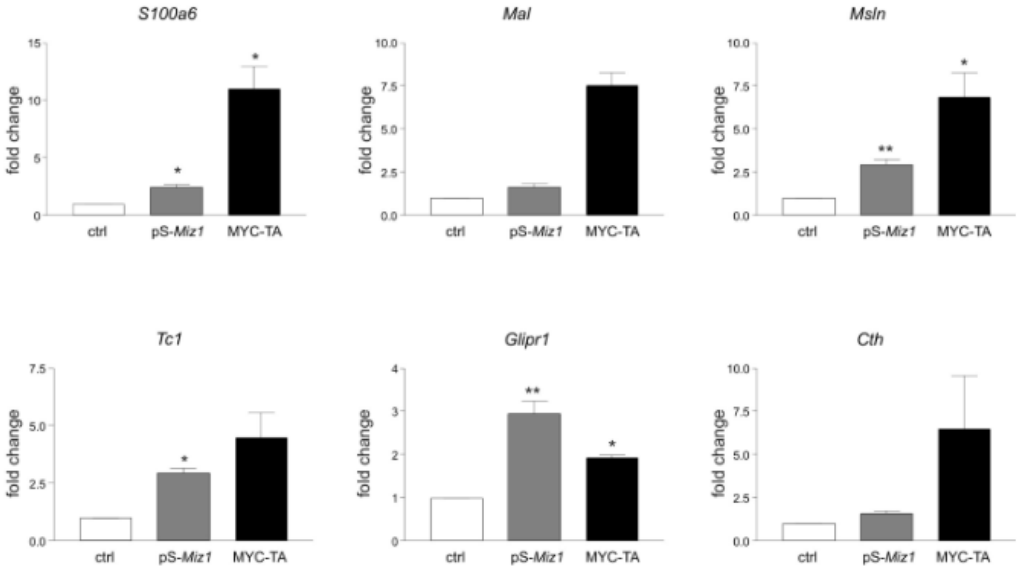
S100a6
Mal
Msln
Tc1
Glipr1
Cth
fold change
ctrl
pS-Miz1
MYC-TA

Figure S8

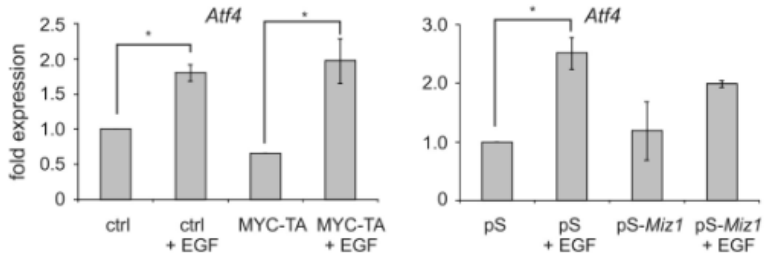
Atf4
fold expression
2.5
2.0
1.5
1.0
0.5
0
*
*
ctrl
ctrl + EGF
MYC-TA
MYC-TA + EGF
Atf4
3.0
2.0
1.0
0
*
pS
pS + EGF
pS-Miz1
pS-Miz1 + EGF

Figure S9

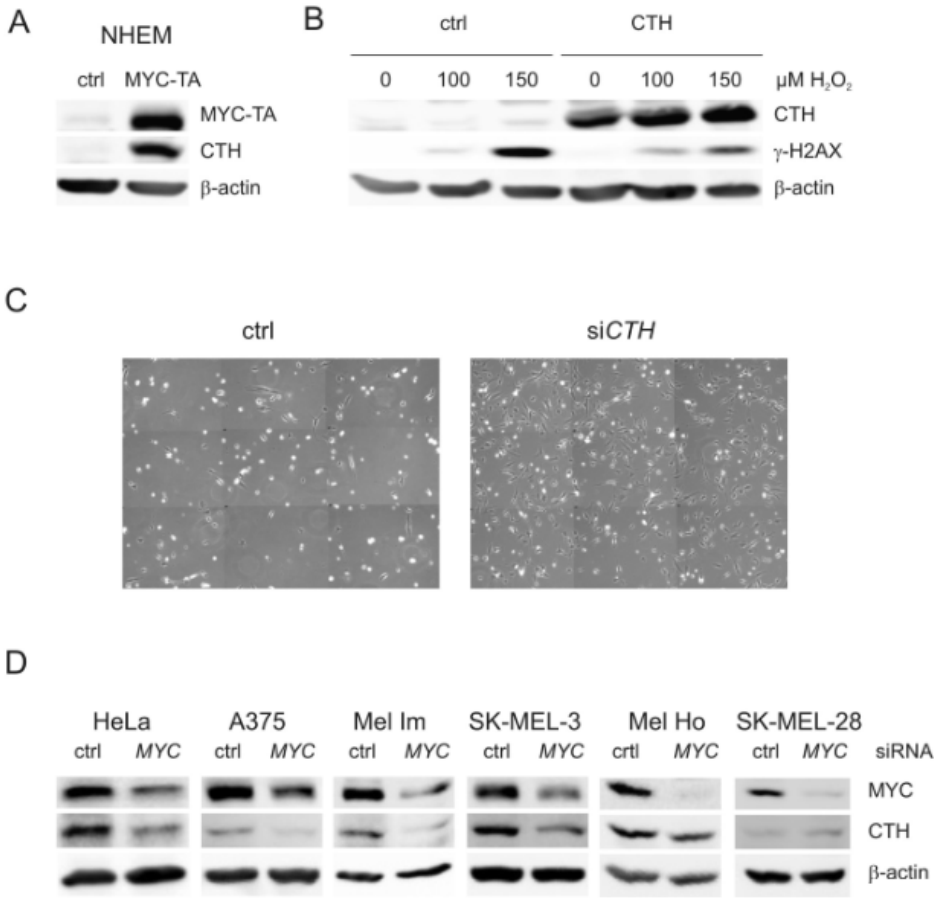
A
NHEM
ctrl
MYC-TA
MYC-TA
CTH
β-actin
B
ctrl
CTH
0
100
150
0
100
150
μM H2O2
CTH
γ-H2AX
β-actin
C
ctrl
siCTH
D
HeLa
A375
Mel Im
SK-MEL-3
Mel Ho
SK-MEL-28
ctrl
MYC
siRNA
MYC
CTH
β-actin

Figure S10

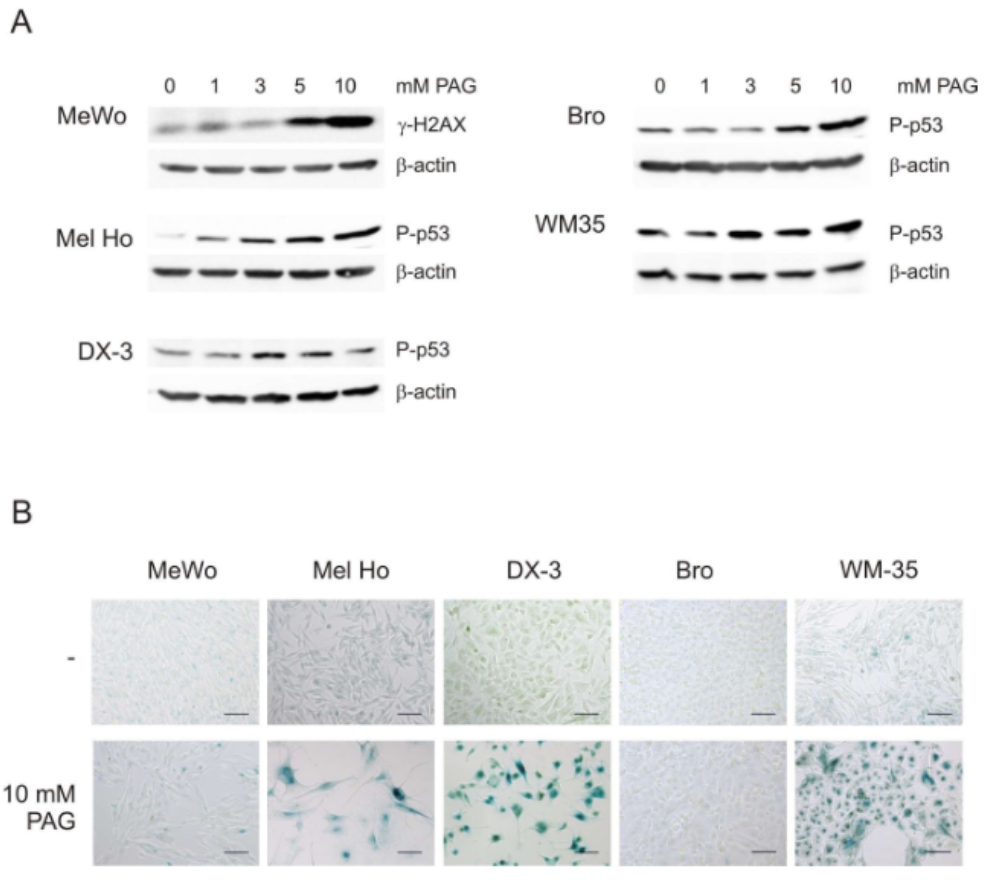
A
0 1 3 5 10 mM PAG
MeWo
γ-H2AX
β-actin
Mel Ho
P-p53
β-actin
DX-3
P-p53
β-actin
0 1 3 5 10 mM PAG
Bro
P-p53
β-actin
WM35
P-p53
β-actin
B
MeWo
Mel Ho
DX-3
Bro
WM-35
-
10 mM PAG

Figure S11

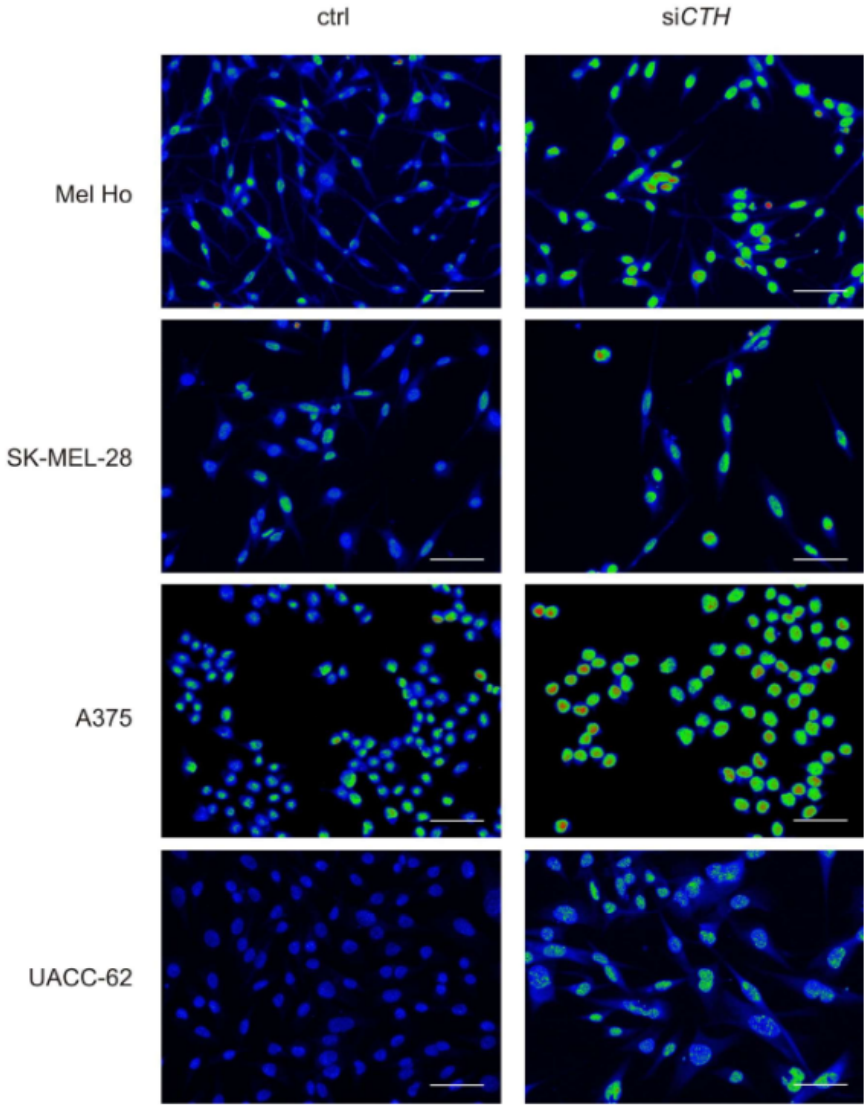

Figure S12

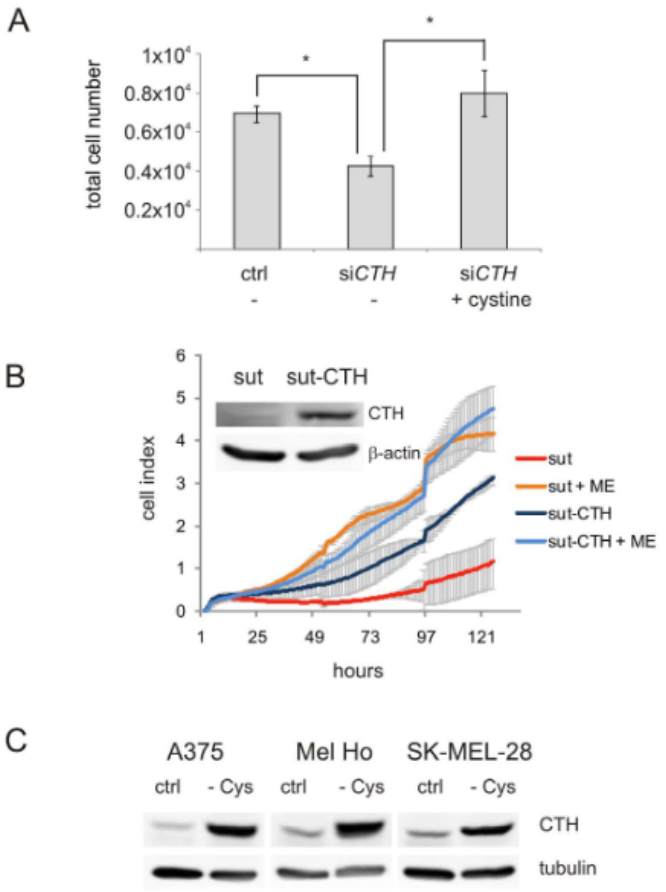
A
total cell number
1x10⁴
0.8x10⁴
0.6x10⁴
0.4x10⁴
0.2x10⁴
*
*
ctrl
-
siCTH
-
siCTH
+ cystine
B
cell index
sut
sut-CTH
CTH
β-actin
sut
sut + ME
sut-CTH
sut-CTH + ME
hours
C
A375
Mel Ho
SK-MEL-28
ctrl
- Cys
ctrl
- Cys
ctrl
- Cys
CTH
tubulin

	Hm-hi	
	ctrl	CTH
homocysteine	60.0 +/- 2.0	70.0 +/- 14.0
glutathione	2380 +/-56.6	2810 +/- 99.0

gene (mouse)	ENSEMBL nr	forward primer (real-time)	reverse primer (real-time)
Atf4	ENSMUSG00000042406	TCGATGCTCTGTTTCGAATG	GGCAACCTGGTCGACTTTTA
Cdk4	ENSMUSG00000006728	GGCCCTCAAGAGTGTGAGAG	CCTTGATGTCCCGATCAGTT
c-Myc	ENSMUSG00000022346	CAACGTCTTGGAACGTCAGA	TCGTCTGCTTGAATGGACAG
Cth	ENSMUSG00000028179	GCACAAATTGTCCACAAAC	CGAAGCCGACTATTGAGGTC
Cyclin B1	ENSMUSG00000041431	TCTTGACAACGGTGAATGGA	TCTTAGCCAGGTGCTGCATA
Cyclin D1	ENSMUSG00000070348	GGCACCTGGATTGTTCTGTT	CAGCTTGCTAGGGAACTTGG
Cyclin D2	ENSMUSG00000000184	TTACCTGGACCGTTTCTTGG	TGCTCAATGAAGTCGTGAGG
Cyclin E1	ENSMUSG00000002068	CACCACTGAGTGCTCCAGAA	CTGTTGGCTGACAGTGGAGA
g-Gcs (heavy)	ENSMUSG00000032350	TGATTGTCGCTGGGGAGT	CCTCTCTCCTCCCGTGTTCT
g-Gcs (light)	ENSMUSG00000028124	GACATTGAAGCCCAGGATTG	GCTCTTCACGATGACCGAGT
Glipr1	ENSMUSG00000056888	TCCTCAGCCATCTCTGCCTGGT	CCACGTTGGGTAATTTCCTGCTGGT
Gpx1	ENSMUSG00000063856	GTCCACCGTGTATGCCTTCT	TCTGCAGATCGTTCATCTCG
Hmox1	ENSMUSG00000005413	CACGCATATACCCGCTACCT	CCAGAGTGTTCATTCGAGCA
Hprt	ENSMUSG00000025630	TGTTGTTGGATATGCCCTTG	ACTGGCAACATCAACAGGACT
Mal	ENSMUSG00000027375	ACTCATGGCGGTGAGACTTCCTGG	TAGGCAAACACCACTGCGGCG
Miz1	ENSMUSG00000006215	GGCAGAAAGTGCATCCAGTG	GGCCCTGCACCCTCTTCCTCTT
Msln	ENSMUSG00000063011	CCCTGCTGGGGTCCTGTGGA	AGGCCTGTGGGGAGACTGGC
Mthfr	ENSMUSG00000029009	ACCATCCTCAGACCCTGTTG	CGTCCACGATGTGGTAGTTG
Nucleolin	ENSMUSG00000026234	AAAGGAGTGAAGCCAGCAAA	TCCTCCTCAGCCACACTCTT
p15Ink4B	ENSMUSG00000073802	TTACCAGACCTGTGCACGAC	GCAGATACCTCGCAATGTCA
p21Cip1/Waf1	ENSMUSG00000023067	ACGGTGGAACTTTGACTTCG	CAGGGCAGAGGAAGTACTGG
p27Kip1	ENSMUSG00000003031	TTGGGTCTCAGGCAAACTCT	TCTGTTCTGTTGGCCCTTTT
Prdx1	ENSMUSG00000028691	TTTTGGGCAGACCAATCTTC	CATGCTGGGGAAACATTCTT
S100a6	ENSMUSG00000001025	GCTGTCGACCGTGCGCTTCT	AGCATCCTGCAGCTTGGAGCC
Tc1	ENSMUSG00000056313	CGAGGATGGAAAGGGACATA	ACGCAGTGTTCTGGTCAGTG
thymidylate kinase	ENSMUSG00000026281	TGTGACCCTTGTTTTGGACA	GCTGCTGGAAACACAACAGA
gene (human)	**ENSEMBL nr**	**forward primer (ChIp)**	**reverse primer (ChIp)**
p21CIP1/WAF1 (pos.)	ENSG00000124762	CCGAAGTCAGTTCCTTGTGG	CGCTCTCTCACCTCCTCTGA
p21CIP1/WAF1 (neg.)	ENSG00000124762	GGAAGGAGGGAATTGGAGAG	TTTCCCTGGAGATCAGGTTG
CTH	ENSG00000116761	CTTCTCGCCTGATCCTTCTG	GAACCGCGAAAGAAGAAGAG

12.3 Oncogenic RAS-induced senescent cells are a source for tumor-initiating cells

Oncogenic RAS-induced senescent cells are a source for tumor-initiating cells.

Leikam, C; Hufnagel, AL; Otto, C; Kneitz, S; Mühling, B; Murphy, DJ; Wagner, TU; Schartl, M; Meierjohann, S.

Paper draft.

Title

Oncogenic RAS-induced senescent cells are a source for tumor-initiating cells

Claudia Leikam[1], Anita L. Hufnagel[1], Christoph Otto[2], Susanne Kneitz[3], Bettina Mühling[2], Daniel J. Murphy[4], Toni U. Wagner[1], Manfred Schartl[1], Svenja Meierjohann[1]

Running head

Senescent cells give rise to tumorigenic offspring

[1]Department of Physiological Chemistry I, University of Wurzburg, Biocenter, Am Hubland, Wurzburg, Germany

[2]Experimental Surgery, Experimental Transplantation Immunology, Clinic of General, Visceral, Vascular and Pediatric Surgery (Surgical Clinic I), University of Wurzburg Hospital, Wurzburg, Germany

[3]Microarray Core Unit, IZKF (Interdisciplinary Center for Clinical Research), University of Wurzburg, Wurzburg, Germany

[4]Department of Physiological Chemistry II, University of Wurzburg, Biocenter, Am Hubland, Wurzburg, Germany

Correspondence and requests for materials should be addressed to S. M. (svenja.meierjohann@biozentrum.uni-wuerzburg.de).

Abstract

Oncogene signaling in non-neoplastic cells usually results in oncogene-induced senescence (OIS), an irreversible G0-like state frequently characterized by a bi- or multinuclear phenotype that represents a major barrier to cancer initiation. Although senescence bypass may be achieved by genetic or epigenetic changes prior to the onset of senescence, the emergence of melanomas from preexisting nevi that comprise a mass of onocogene-induced senescent cells suggests that senescence is not irreversible. How a pre-existing senescent cell can progress to cancer represents a key issue in cancer biology. Here, we show that prolonged expression of the melanoma oncogene N-RAS^{61K} in pigment cells overcomes initial OIS by triggering the emergence of tumor-initiating, mononucleated stem-like cells from multinucleated senescent cells. This progeny is dedifferentiated, highly proliferative, anoikis-resistant and induces fast growing, metastatic tumors upon transplantation into nude mice. Our data demonstrate that induction of OIS is not merely a general cellular failsafe mechanism, but also carries the potential to provide a source for highly aggressive, tumor-initiating cells.

Introduction

Cellular senescence is characterized by cell cycle arrest and alterations of cell shape and metabolism, which can be triggered either by the sequential loss of telomeres {Hayflick, 1965 #1703} or by numerous forms of cellular stress, e.g. UV-irradiation, oxidative stress or aberrant oncogenic signaling (premature senescence) {Mooi, 2006 #1712}. In particular, oncogene-induced senescence (OIS), driven for example by activated RAS or BRAF, is an anti-cancer protection mechanism that prevents tumor generation despite the presence of oncogenic mutations. For example, human nevi display classical characteristics of senescence {Michaloglou, 2005 #1440}, most likely arising from oncogene-activated MAPK signaling caused by mutant B-RAF^{600E} or N-RAS^{61K}, which are present in up to 80% of common benign and congenital nevi, respectively {Dessars, 2009 #1766}{Bauer, 2007 #1803}{Saldanha, 2004 #1806}. However, although oncogenic RAS triggers OIS *in vivo* {Guo, 2009 #1716}{Swarbrick, 2008 #1738}{Braig, 2005 #1745}{Collado, 2005 #1747}, it is clear that senescence bypass is a key feature of cancer and consequently activated RAS is detected in up to 30% of human cancers {DeNicola, 2009 #1750}{Land, 1983 #1762}.

Since senescence is generally considered to be an irreversible event, senescence bypass must be achieved by genetic or epigenetic inactivation of the Rb1 and p53 pathways prior to the induction of pro-senescent oncogenic signals. However, it is evident that a significant minority of melanomas arise from pre-existing nevi, raising the possibility of a mechanism by which tumour progression may arise from post-senescent cells. How a senescent cell might give rise to cancer is a key issue in tumour biology. Here, we reveal that long-term NRAS^{61K} activation in melanocytes triggers the post-senescence generation of tumor-initiating cells with stem-like properties. The results illustrate that senescent multinuclear cells are not inert, but can instead be a source for malignant daughter cells

Results

N-RAS^{61K} triggers senescence and anoikis resistance

N-RAS^{61K} effectively induces senescence in melanocytes, as characterized by induction of reactive oxygen species (ROS), p53 signaling, multinuclear phenotype and senescence-associated β-galactosidase (SA-β-Gal) staining {Leikam, 2008 #1604}{Denoyelle, 2006 #1809}{Haferkamp, 2009 #1834}. To monitor the long-term effects of senescence, we used the melanocyte cell line melan-a expressing human doxycycline-inducible N-RAS^{61K}. After 14 days of continuous doxycycline treatment, the majority of cells had become senescent, demonstrated by their multinucleated phenotype and SA-β-Gal staining (Fig. 1A). However, after 3-4 weeks of N-RAS^{61K} expression, proliferating cells appeared that overgrew the cell culture and formed three-dimensional cellular aggregates a typical feature of transformed cells *in vitro* (Fig. 1A). Concurrently, we noted the appearance of viable, detached cells in the culture supernatant. Replating of these cells was followed by reattachment before they again gave rise to detached cells. We termed these cells "N-RAS^{61K}-AR" (for "anoikis-resistant").

To compare the features of N-RAS^{61K}-AR cells to melan-a control cells (transfected with pTRE2hyg control vector, but simply termed "melan-a hereafter) and N-RAS^{61K} cells, we monitored proliferation under different cell culture conditions. Although tetradecanoyl-12,13-phorbolacetate (TPA) is required for the growth of melanocytes, N-RAS^{61K}-AR cells were entirely independent of TPA, while the growth of melan-a and N-RAS^{61K} cells required TPA (Fig. 1B). Moreover, in doxycycline-containing medium supplemented with 2.5% or 10% growth factor-reduced, dialyzed serum, N-RAS^{61K}-AR cells proliferated strongly, whereas N-RAS^{61K} cells underwent senescence after initial proliferation and melan-a cells showed cellular arrest (Fig. S1A, B). These data provide evidence that N-RAS^{61K}-AR cells can grow independently of TPA and under growth factor-deprived conditions. The unexpected proliferation behavior of N-RAS^{61K}-AR cells was further confirmed by their capacity to efficiently form soft agar colonies (Fig. 1C).

N-RAS^{61K}-AR cells are tumorigenic and de-differentiated

To analyze tumorigenicity *in vivo*, melan-a, N-RAS^{61K}, and N-RAS^{61K}-AR cells were injected into nude mice. Melan-a and N-RAS^{61K} cells only gave rise to subcutaneous, pigmented, nevus-like structures independent of presence or absence of doxycycline (Fig. 2A, C, Fig. S2A, Table S1). N-RAS^{61K}-AR cells, however, formed large tumors at all injection sites after approximately ten days (Fig. 2B, D, E, G, Table S1). Strikingly, tumor formation occurred in the absence of doxycycline, suggesting independence of the initial oncogene. Mitotic figures were abundant in tumor sections (Fig. 2E), and staining of the S phase marker Ki67 as well as the mitosis marker phospho-histone H3 (Ser10) were readily detectable in tumors, but not in nevus-like structures of control mice (Fig. 2H, I), strongly indicating a high *in-vivo* proliferation potential of N-RAS^{61K}-AR cells. The mice were sacrificed after four weeks due to the considerable tumor load. Notably, by this time, the primary tumor had already metastasized to the lung (Figure 2F).

To gain better insight into the process leading to the generation of the highly aggressive N-RAS^{61K}-AR cells from a previously senescent cell culture, expression profiling of N-RAS^{61K} cells after different times of doxycycline stimulation and of N-RAS^{61K}-AR was performed. We found the expression of melanocyte differentiation markers to be highly regulated in response to N-RAS^{61K} expression (Fig. 3A, C). Concurrent with senescence progression, most differentiation markers, such as *Tyrp1*, *Mlana*, *Dct*, *Sox10* and *Mitf,* were strongly induced after 14 days. However, expression of most differentiation markers decreased after 28 days of N-RAS^{61K} induction and in N-RAS^{61K}–AR cells. However, *Mitf* levels were still higher in N-RAS^{61K}-AR when compared to the 6-day sample. It is known that a certain level of MITF is also maintained in human melanoma, consistent with its role for melanocyte and melanoma proliferation as well as survival {Levy, 2006 #1466}. Still, a dampened MITF target gene signature, consisting of *Tyrp1*, *Mlana* and *Dct*, is observed in highly invasive human

melanoma cells, which instead display enhanced levels of Wnt pathway and matrix components {Hoek, 2008 #1893}. These are also markedly upregulated in NRAS^{61K}-AR cells (data not shown).

While the expression of melanocyte differentiation genes decreased over time, numerous neuronally expressed genes were induced (Fig. 3B, C). Many of these genes were still expressed in N-RAS^{61K}-AR cells. During embryonic development, melanocytes arise from the neural crest lineage, which also gives rise to neuronal cells. Thus, the change from melanocytic to neuronal marker gene expression might hint at de- or transdifferentiation of the pigment cells. Interestingly, expression of neuronal markers is also observed in human melanoma cells {Boiko, 2010 #1889}{Florenes, 1994 #1888}. To check whether the N-RAS^{61K}-AR cells indeed underwent dedifferentiation, we looked at the expression of embryonal and stem cell markers. This gene group was very heterogeneously expressed (data not shown). Interestingly, *Pdpn* and *Nanog* belonged to the genes whose expression was strongly increased in N-RAS^{61K}-AR cells (Fig. 4A, B). In particular, NANOG is considered a master transcription factor for the maintenance of the undifferentiated state and cellular self-renewal. Using a NANOG-driven GFP expression vector {Hotta, 2009 #1883}, we found a large fraction of N-RAS^{61K}-AR cells to contain NANOG expression, whereas N-RAS^{61K} cells lacked NANOG expression (Fig. 4C). N-RAS^{61K}-AR cells also displayed a reduction of cytoplasmic volume and consequently a higher nuclear/cytoplasmic ratio compared to N-RAS^{61K} cells (Fig. S3, Movie S1), consistent with the N-RAS^{61K}-AR cells exhibiting stem-like properties. A similar reduction of cytoplasmic volume is often observed during development of dedifferentiated and metastatic cells as well as melanocyte stem cells.

Further analysis of the up-regulated genes distinguishing N-RAS^{61K}-AR cells from all other samples led to two prominent groups: 1. positive regulators of proliferation, and 2. meiosis genes (Fig. S4 and Fig. 4D). The positive regulators of proliferation included numerous genes encoding growth factors (e.g. *Kitl*, *Vegfa*, *Hbegf*, *Btc,* and *Areg*) and growth factor receptors

(*Pdgfra, Flt1*) as well as enzymes involved in generation and transmission of growth-promoting signaling molecules (*Ptgs2, Fabp4*) (Fig. S4A, B). Although the genes represented by the second group are usually up-regulated during meiosis, *Spo11* is also known as cancer/testis gene {Simpson, 2005 #1844}, and *Cyp26b1* is involved in retinoic acid metabolism and plays a role in neural crest-derived tissue development {Maclean, 2009 #1843} (Fig. 4 D, E). Meiosis-related genes are often up-regulated in melanoma cells which are particularly prone to the so-called meiomitosis, describing the partial expression of meiosis machinery in mitotic cells {Grichnik, 2008 #1845}. Taken together, the expression profile provides evidence for melanocyte dedifferentiation upon long-term N-RAS^{61K} activation, which is a typical feature of invasive melanoma cells, and reveals the expression of meiosis-associated genes in N-RAS^{61K}-AR cells.

The development of anoikis resistance is dependent on prior senescence

Senescence induced by oncogenes such as N-RAS^{61K} is not immediately executed after oncogene activation, but only comes into action after a previous proliferation boost caused by strong, growth-promoting signals {Denoyelle, 2006 #1809}{Michaloglou, 2005 #1440}. To determine whether a proliferation stimulus *per se* leads to the observed dedifferentiation and anoikis resistance, we cultivated the parental cell line melan-a for long time periods in presence of the growth stimulus TPA, an efficient activator of PKC and the MAPK pathway. Apart from the addition of TPA, melan-a cells underwent the same treatment as N-RAS^{61K} cells, namely the same initial density and no subcultivation during the experiment. After TPA-treated melan-a cells had reached confluency, pigmentation increased (Fig. 5A). Upon 28 days of treatment, we could neither observe viable, detached melan-a cells in the supernatant, nor the three-dimensional cell colonies we observed in N-RAS^{61K} cells (Fig. 5A, B). Furthermore, melan-a cells upon 28 days of treatment neither showed induction of the pluripotency markers *Pdpn* and *Nanog* nor of the male meiosis marker *Spo11,* whereas the

melanocyte markers *Mlana*, *Tyrp1* and *Dct* remained stable or were even found to be up-regulated (Fig. 5C).

To identify the pathways necessary for mediating the generation of N-RAS^{61K}-AR cells, we blocked either the MAPK or the PI3K pathway, which are both direct effectors downstream of N-RAS^{61K}, using the small molecule inhibitors PD184352 or LY294002, respectively. In both cases, the cells remained viable, but were incapable of producing anoikis-resistant progeny (Fig. 6A). Interestingly, PD184352, but not LY294002 treatment prevented the formation of multinucleated cells (Fig. S5). The receptor tyrosine kinase Xmrk is another efficient inducer of OIS, as described previously {Leikam, 2008 #1604}, and also activates PI3K as well as MAPK signaling. We performed long-term activation of an inducible version of the receptor (termed "HERmrk" or "Hm^{hi}") and again found that senescence of melan-a cells was followed by the generation of three-dimensionally growing cells and anoikis resistance (Fig. S6A). Similar to the observation for N-RAS^{61K}-AR cells, NANOG activity was induced (Fig. S6B). Importantly, oncogene-induced senescence followed by anoikis resistance was not restricted to murine melanocytes, but was also detected in normal human epidermal melanocytes (NHEM) in response to N-RAS^{61K} expression (Fig. S7).

RAS signaling leads to the induction of NADPH oxidase isoforms (Fig. 6B), which is accompanied by the generation of reactive oxygen species {Shinohara, 2010 #1853} (and own unpublished observations). Accordingly, activation of oncogenic N-RAS in melan-a cells causes DNA damage and p53 activation {Leikam, 2008 #1604}. To elucidate the role of DNA damage and senescence induction in N-RAS^{61K}-AR development, we applied the antioxidant glutathione ethyl ester or inhibited NADPH oxidase (diphenyle iodonium, DPI), ATM (caffeine) or p53 (pifithrine). DPI, caffeine and pifithrine, but not the glutathione component, were able to prevent the generation of anoikis-resistant cells, thus demonstrating the involvement of DNA damage and senescence induction in this process (Fig. 6A, C, Fig. S5).

To betterunderstand the generation of anoikis-resistant cells, we conducted time lapse movies of senescent N-RAS^{61K} cells after long-term oncogene stimulation. We recorded several highly multinucleated cells performing asynchronous cytokinesis (Fig. 7, Movie S2). Strikingly, this asynchronous cytokinesis resulted in the budding of small, mononuclear, viable cells that underwent further divisions (Movie S3, Fig. S8). The mother cells remained multinuclear and persisted throughout the experiments.

Discussion

The idea that senescence only operates as tumor-suppressive mechanism was recently challenged by the observation that in their niche, senescent cells secrete factors that provide autocrine inhibitory signals, but also stimulate neighboring premalignant cells or cause low levels of tumor-promoting inflammation {Rodier, 2011 #1894}. Here we reveal a novel mechanism underlying the generation of highly tumorigenic melanoma cells from senescent, multinuclear pigment cells that were induced by oncogenic signaling.

At first sight, it seems paradoxical that the prior induction of senescence is required to enable tumor development. However, the relevance of our findings for animal models and human melanoma is supported by several observations. First, mice with lung-specific expression of oncogenic RAS first develop senescent pre-malignant lung adenomas, which later develop into adenocarcinomas {Collado, 2005 #1747}. As all affected lung cells express oncogenic RAS, and this induces senescence, the tumorigenic process is likely initiated after the induction of senescence. Second, staining of the senescence mediator and DNA damage marker p53 is retained in human melanoma with a history of high cumulative sun exposure, and is even associated with higher Breslow thickness {Purdue, 2005 #1897}, suggesting residual pro-senescent signaling in melanoma and its compatibility with tumor maintenance. Finally, polyploid cells, which we identified as source for the malignant offspring, are not only found in melanoma, but also in melanocytic nevi {Stenzinger, 1984 #1898}{Pilch, 2000 #1899}, and a significant proportion of melanomas arise from pre-existing nevi (e.g. PMID: 6500548 , PMID: 21051009 , PMID: 15253185 , PMID: 18792098 REF).

Senescence is triggered by replication-associated DNA damage that is often accompanied by the development of polyploid cells that appear under physiological and pathological conditions. The superoxide-producing enzyme NADPH oxidase is involved in the generation of polyploid megakaryocytes {McCrann, 2009 #1860}. In the liver, the amount of polyploid

cells increases with age and after situations causing oxidative stress, such as partial hepatectomy {Gorla, 2001 #1856}. In lentigo maligna (LM), also called melanoma *in situ*, multinucleated "star burst cells" are present in up to 85% of patient samples {Cohen, 1996 #1864}. LM mainly occurs in chronically sun-damaged skin and is associated with UV light exposure as well as p53 positivity {Atillasoy, 1998 #1885}{Purdue, 2005 #1897}, suggesting a causal relationship between UV-induced DNA damage and the appearance of starburst cells. Polyploid cells are at increased risk of becoming cancerous through a combination of genomic instability that facilitates the appearance of further mutations {Storchova, 2008 #1859} and aberrant gene expression owing to the presence of multiple copies of many genes. The accumulation of bi- and multinuclear cells is also a common feature of senescent cells *in vitro*, and DNA damage, caused by oncogenic or replicative stress, often mediates senescence {Evan, 2009 #1869}. We observed that the development of N-RAS^{61K}-AR cells was prevented by inhibiting NADPH oxidases, the DNA damage pathway and p53, thus indicating senescence induction as a pre-requisite for anoikis resistance. Furthermore, inhibition of PI3K and MAPK pathways had the same effect. Other oncogenic RAS isoforms such as H-RAS^{G12V} are also capable of inducing genomic instability and lead to micronucleation in a MAPK-dependent manner {Saavedra, 2000 #1882}. In accordance with these observations, MEK inhibition of our N-RAS^{61K} cells prevented the development of multinucleated cells (Fig. S5, 8 days) and consequently AR development. By contrast, PI3K inhibition allowed multinucleation, but prevented anoikis-resistance (Fig. 6, Fig. S5), implicating a role for this pathway at later stages of AR development and highlighting the co-operativity between the MAPK and PI3K pathways in generating tumor-initiating cells from senescent cells..

Our finding of OIS-induced tumorigenesis is reminiscent of a recent observation describing that normal human keratinocytes first become senescent in cell culture, followed by the appearance of so-called "post-senescent emerging cells" {Gosselin, 2009 #1870}. These cells "budded" from senescent cells, and their generation was increased by the addition of H_2O_2.

Similarly, irradiated cells of different origin displayed a comparable behavior, which was termed "neosis" {Sundaram, 2004 #1871}. Here, the post-senescent emerging cells and neotic cells adapted a transformed phenotype. The "budding" or "neotic" behavior strongly resembles the process of "depolyploidisation" by asymmetric division, which was recently described for tetra- or polyploid tumor cells. Here, the cancer cells undergo a ploidy cycle where aneuploid cells give rise to para-diploid cells, thereby re-aligning to normal cell cycle regulation and reducing the risk of lethal accumulation of DNA damage {Salmina, 2010 #1875}{Vitale, 2010 #1872}. A shared phenomenon is the up-regulation of meiotic genes such as *Spo11,* which is associated with depolyploidisation. This up-regulation might reveal a functional parallel between asexual ploidy reduction, e.g. occurring in cancer, and sexual ploidy reduction, occurring during meiosis {Erenpreisa, 2010 #1880}. Importantly, depolyploidisation was also described to go along with increased levels of *OCT4*, *NANOG* and *SOX2* {Sundaram, 2004 #1871}.

Our data for the first time illustrate that this mode of overcoming senescence also takes place in response to naturally occurring oncogenes such as the melanoma oncogene N-RAS^{61K}. This process is not only accompanied by the loss of melanocyte markers but also by the increase of neuronal-like expression patterns. Importantly, the cells display features of highly dedifferentiated cells, such as a high nuclear-cytoplasmic ratio and increased nuclear expression of the transcription factor NANOG, which might explain their aggressive growth and early metastasis *in vivo*. Taken together, polyploidy due to oncogenic senescence stress might constitute a cancer risk comparable to the risk of tumor generation after radiation- or chemotherapy-induced polyploidy.

Materials and Methods

Cell culture: $NRAS^{61K}$ and Hm^{hi}-cells as well as melan-a cells were previously described and cultivated as reported earlier *(1-2)*. For long-term treatment, cells were cultured in starving medium (Dulbecco's Modified Eagle's Medium with 10% dialyzed, foetal calf serum (Gibco/Invitrogen, Karlsruhe, Germany)) for 3 days prior to the assay. Normal human embryonic melanocytes (NHEM) cells were transfected with pCDH-CMV-$NRAS61^{K}$-EF1-copGFP and were cultivated in melanocyte growth medium (Promocell).

RNA isolation and real-time PCR: RNA isolation was performed with TrIR solution (ABGene, Hamburg, Germany) from two independent biological replicates. Whole RNA was reversely transcribed using the RevertAidTM First Strand cDNA Synthesis Kit (Fermentas, Leon-Rot, Germany). Fluorescence-based quantitative real-time PCR was performed using the iCycler (Bio-Rad, Munich, Germany), and for each gene, three independent real-time PCRs were performed with cDNA from each biological replicate. The sequence of oligonucleotides used can be found in the supplementary information (Supplementary Table 2). Gene expression was normalized to hypoxanthine- guanine phosphoribosyltransferase. Relative expression levels were calculated applying REST software.

Soft agar growth: 1 ml of 1.2% agar was mixed with 1 ml 2x DMEM supplemented with 10% FCS (D10) and plated onto 6-well plates. Upon polymerization, the solid agar was overlain with an equal amount of soft agar mix (0.6% agar) containing $4x10^4$ cells per well. The polymerized soft agar was overlain with 100 µl of D10 medium every second day. Phase contrast pictures (25-fold magnification) were taken after 14 days of incubation. Images display equally cropped sections. Scale bars = 100 µm.

In vivo growth: Melan-a control cells (stably transfected with pTRE2hyg as empty vector control) and N-RAS^{61R} cells were cultured in DMEM containing 10% foetal calf serum supplemented with antibiotics, 12 nM cholera toxin to support melanin synthesis and 200 nM **t**etradecanoyl-12,13-phorbolacetate (TPA) to allow proliferation. In contrast, N-RAS^{61R}-AR cells were cultured in the absence of both cholera toxin and TPA. Nude mice (NMRI, Harlan strain) were subcutaneously injected with 2.5x10^{6} melan-a, N-RAS^{61R} or N-RAS^{61R}-AR cells per flank. Where indicated, 2 mg/ml doxycycline (Sigma) dissolved in 10% saccharose solution was supplied *ad libitum* by administration to the drinking water. After four weeks, N-RAS^{61R}-AR mice were sacrificed due to considerable tumor load. In all other mice, growth of injected cells was monitored for 10 weeks after injection before sacrificing the mice. All experiments were in accordance with the institution`s guidelines.

Immunohistochemistry: Ki67 and phospho-Histone H3-S^{10} staining were perfomed using SP6 (Neomarkers) and 06-570 (Upstate/Milipore) as previously described {Murphy, 2008 #1890}. Alexa-Fluor conjugated anti-rabbit secondary antibodies (Invitrogen) were used for detection and tissues were counterstained with Hoechst 33342 (Invitrogen).

Microarray: NRAS^{61K} cells were treated for 6, 14 or 28 days with 1 µg/ml doxycycline (Sigma) and NRAS^{61K}-AR cells underwent the same treatment for 10 days before being harvested. RNA was isolated using the miRNeasy Kit (Qiagen), and analyzed using the Affymetrix Gene Chip Mouse Genome 430 2.0. All data were analyzed using different R packages from the Bioconductor project (www.bioconductor.org). Obtained data are deposited at http://www.ncbi.nlm.nih.gov/geo/query/acc.cgi?acc=GSE27010.

Statistic analysis: Generally, all graphs depict the mean values of at least three independent

experiments, standard deviations are indicated. Student`s t test (two-tailed, paired) revealed statistical significance highlighted by asterisks (*: $p<0.05$; **: $p<0.01$, ***: $p<0.001$).

Acknowledgements

We thank Roland Houben (University of Wurzburg, Germany) for kindly supplying the pCDH-CMV-NRAS61^{K}-EF1-copGFP vector and James Ellis (University of Toronto, Canada) for kindly supplying the PL-SIN-EOS-S(4+)-eGFP vector.

References

Financial disclosure

This work was supported by the Deutsche Forschungsgesellschaft, Transregio 17 ("RAS-dependent pathways in human cancer"). CL was supported by a grant from the German Excellence Initiative, Graduate School of Life Sciences, University of Wurzburg.

Figure legends

Figure 1: Long-term N-RAS^{61K} activation leads to melanocyte senescence followed by anoikis resistance.

(A) Phase contrast (PH) images of N-RAS^{61K} cells after 3, 14, 21 and 28 days of doxycycline treatment (1 µg/ml) and corresponding brightfield images of SA-β-galactosidase-stained N-RAS^{61K}cells after 3 and 14 days. Scale bars, 100µm. **(B)** Proliferation of melan-a, N-RAS^{61K} and N-RAS^{61K}-AR cells in DMEM containing 10% FCS, antibiotics and, where indicated, tetradecanoyl-12,13-phorbolacetate (TPA). **(C)** Soft agar growth assay of N-RAS^{61K} and N-RAS^{61K}-AR cells, cultivated for 14 days in DMEM containing 10% FCS and antibiotics. Scale bars, 100µm.

Figure 2: N-RAS^{61K}-AR cells are tumorigenic *in vivo*.

(A) (B) Macroscopic view of tumor development after subcutaneous injection of melan-a control cells **(A)** or N-RAS^{61K} –AR cells **(B)** into nude mice. **(C-F)**:, Hematoxylin/eosin stained tissue sections. **(C)** shows the subcutaneous accumulation of injected melan-a cells forming a nevus-like structure (scale bar, 50 µm). In **(D)** and **(E)**, N-RAS^{61K} –AR derived tumors are displayed **(D)**: scale bar, 50 µm; **(E)**: scale bar, 20 µm. The arrows in **(E)** indicate mitotic figures. **(F),** Lung metastasis in a N-RAS^{61K}–AR-injected nude mouse. The inlay shows a magnification of the metastasis. Scale bar, 500 µm). **(G)** Time-dependent development of subcutaneous tumours in N-RAS^{61K}–AR injected nude mice. The different colours represent the single tumors from both flanks of each mice. **(H)** Hoechst and Ki67 staining and **(I)** Hoechst and P-H3 staining of a tumor section from N-RAS^{61K}-AR-injected mice visualizing strong mitotic activity throughout the tumor. Scale bars, 100 µm.

Figure 3: Long-term N-RAS^{61K} expression diminishes melanocyte marker expression and increases neuronal gene expression.

(A-C) Heatplot displaying the RNA expression of melanocyte differentiation markers **(A)**, neuronal genes **(B)** and meiosis genes **(C)** in N-RAS^{61K} cells stimulated with doxycycline for 6, 14, and 28 days and in N-RAS^{61K}–AR cells. **(C)**, Confirmation of differential gene expression by real-time PCR using primers directed against *Tyrp1*, *Mlana*, *Dct*, *Sox10*, *Mitf*, *Nefl*, *Smarca*, *Cyp21b1* and *Spo11*.

Figure 4: Pluripotency markers *Nanog* and *Pdpn* are expressed during long-term N-RAS^{61K} induction.

(A) Real-time PCR analysis of *Pdpn* expression and **(B)** RT-PCR analysis of *Nanog* expression (40 cycles, right panel) in N-RAS^{61K} cells stimulated with doxycycline for 6, 14, and 28 days and in N-RAS^{61K}–AR cells. *Hprt* served as control. **(C)** *Nanog*-driven GFP expression in N-RAS^{61K} and N-RAS^{61K}–AR cells, transiently transfected with the PL-SIN-EOS-S(4+)-eGFP vector. Scale bars, 100µm. **(D)** Heatplot displaying the RNA expression of meiosis genes in N-RAS^{61K} cells stimulated with doxycycline for 6, 14, and 28 days and in N-RAS^{61K}–AR cells. **(E)**, Confirmation of differential gene expression by real-time PCR using primers directed against *Cyp21b1* and *Spo11*.

Figure 5: Induction of proliferation is not sufficient to induce anoikis resistance.

(A) Phase contrast images of melan-a cells cultivated for 28 days under starving conditions (10% dialyzed FCS) without any additives (-) or in presence of TPA. Scale bars, 100µm. **(B)** N-RAS^{61K} cells were cultivated for 28 days in presence of doxycycline (Dox), whereas melan-a cells were kept in starving media or TPA-containing media. Upon 28 days of treatment, supernatant was transferred to a new 6-well plate, which was incubated for 24 h to

allow cells to reattach, followed by a 2% crystal violet staining. **(C) left panel:** Real-time PCR analysis of *Tyrp1*, *Dct*, and *Mlana* from melan-a cells starved for 28 days or treated with TPA, respectively. **(C) right panel:** RT-PCR analysis of *Nanog, Spo11* (40 cycles each) and *Pdpn* (33 cycles) expression of melan-a cells starved for 28 days or treated with TPA, respectively. Dox-treated N-RAS^{61K} cells, also harvested after 28 days, served as positive control. *Hprt* was used as reference.

Figure 6: Anoikis resistance is prevented by inhibiting DNA damage pathways and senescence as well as PI3K and MAPK pathways.

(A) N-RAS^{61K} cells were cultivated for 28 days in presence of doxycycline (Dox) and DMSO (ctrl.), the PI3K inhibitor LY294002 (LY, 10 µM), the antioxidant glutathione reduced ethyl ester (GRE, 1 mM), the p53 inhibitor pifithrine (Pifi, 10 µM), the MEK inhibitor PD184352 (PD, 2 µM), or the ATM inhibitor caffeine (Caf, 1 mM). Scale bars, 100µm. **(B)** RT-PCR analysis of NADPH oxidase isoforms *Nox1 and Nox2* in response to N-RAS^{61K} induction by doxycycline (Dox) (40 cycles). *Hprt* served as control. **(C)** As in **A**, but in presence of DMSO (ctrl.) or the NADPH oxidase inhibitor diphenyl iodium salt (DPI, 500 nM). After 28 days, supernatant was transferred to a new 6-well plate and cells were allowed to reattach for 24 h, followed by staining with 2% crystal violet solution.

Figure 7: Multinuclear cells give rise to small cells. N-RAS^{61K} cells were transiently transfected with pBabe-MN [EF1a-red membrane and green nucleus]-2APuro before being plated onto glass cover-slips. Upon 16 days of doxycycline treatment, cells were monitored for 17 hours. Time points are indicated. Scale bars, 50 µm.

Figure 1

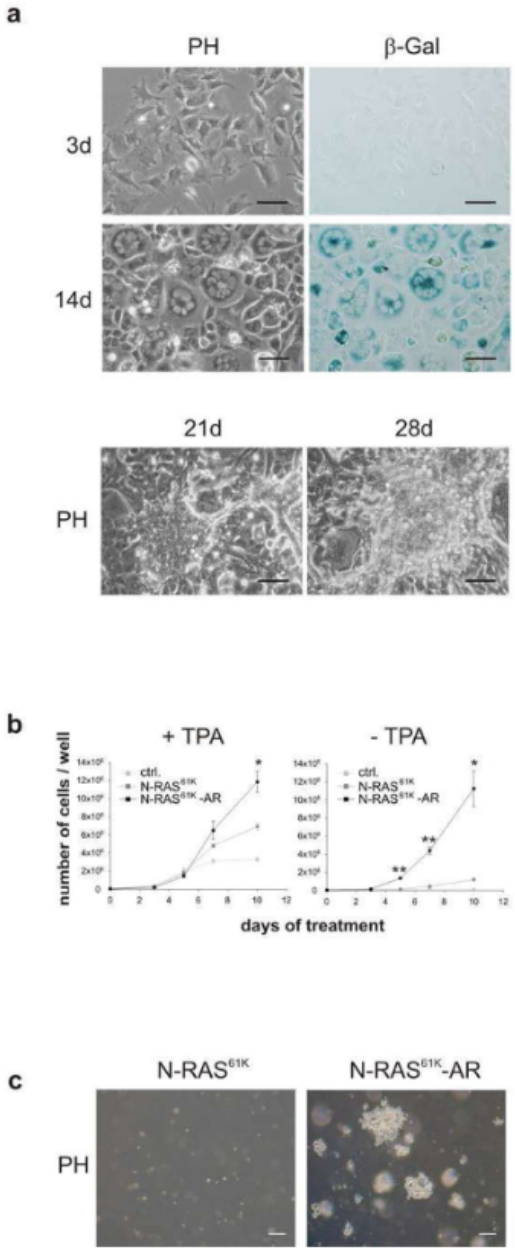
a
PH
β-Gal
3d
14d
21d
28d
PH
b
+ TPA
- TPA
number of cells / well
ctrl.
N-RAS61K
N-RAS61K -AR
days of treatment
c
N-RAS61K
N-RAS61K-AR
PH

Figure 2

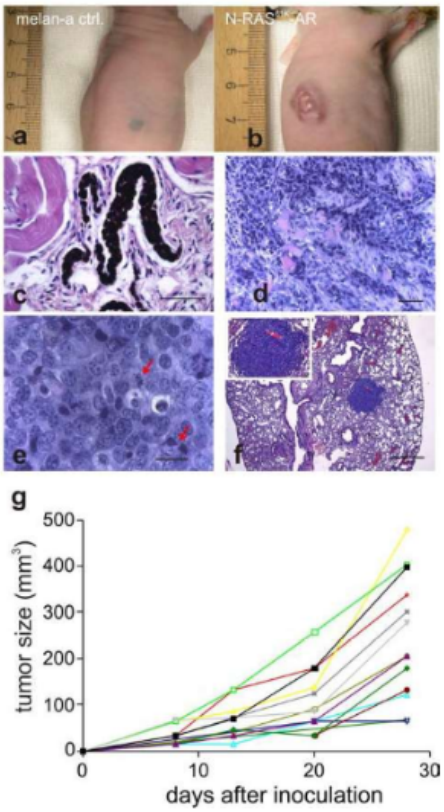
melan-a ctrl.
a
b
c
d
e
f
g
tumor size (mm³)
500
400
300
200
100
0
0
10
20
30
days after inoculation

Figure 3

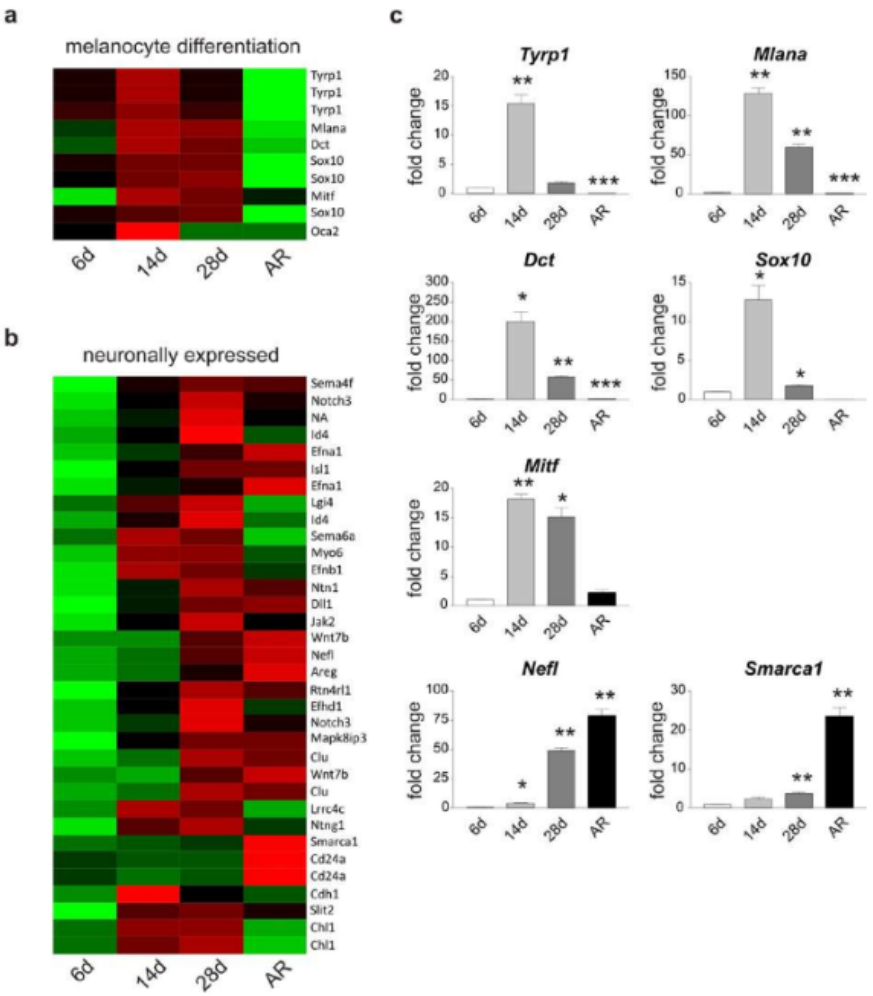
a
melanocyte differentiation
Tyrp1
Tyrp1
Tyrp1
Mlana
Dct
Sox10
Sox10
Mitf
Sox10
Oca2
6d
14d
28d
AR
b
neuronally expressed
Sema4f
Notch3
NA
Id4
Efna1
Isl1
Efna1
Lgi4
Id4
Sema6a
Myo6
Efnb1
Ntn1
Dll1
Jak2
Wnt7b
Nefl
Areg
Rtn4rl1
Efhd1
Notch3
Mapk8ip3
Clu
Wnt7b
Clu
Lrrc4c
Ntng1
Smarca1
Cd24a
Cd24a
Cdh1
Slit2
Chl1
Chl1
6d
14d
28d
AR
c
Tyrp1
Mlana
Dct
Sox10
Mitf
Nefl
Smarca1
fold change
6d
14d
28d
AR

Figure 4

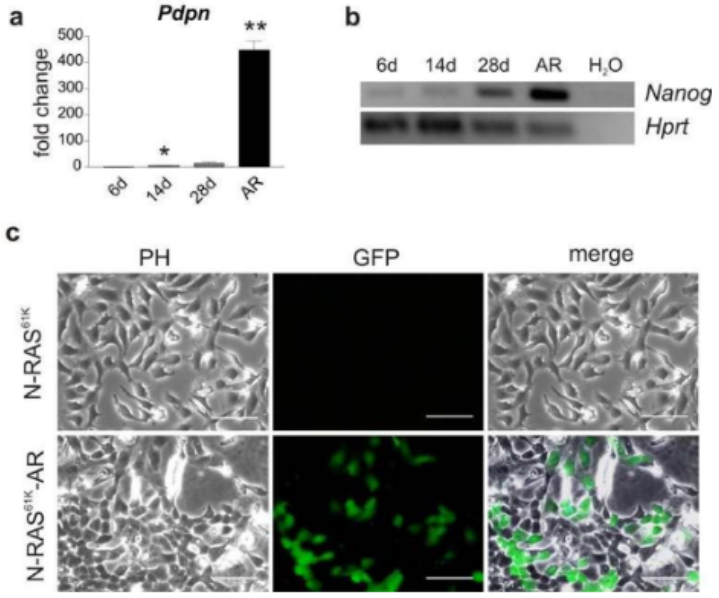
a
Pdpn
fold change
500
400
300
200
100
0
**
*
6d
14d
28d
AR
b
6d
14d
28d
AR
H2O
Nanog
Hprt
c
PH
GFP
merge
N-RAS61K
N-RAS61K-AR

Figure 5

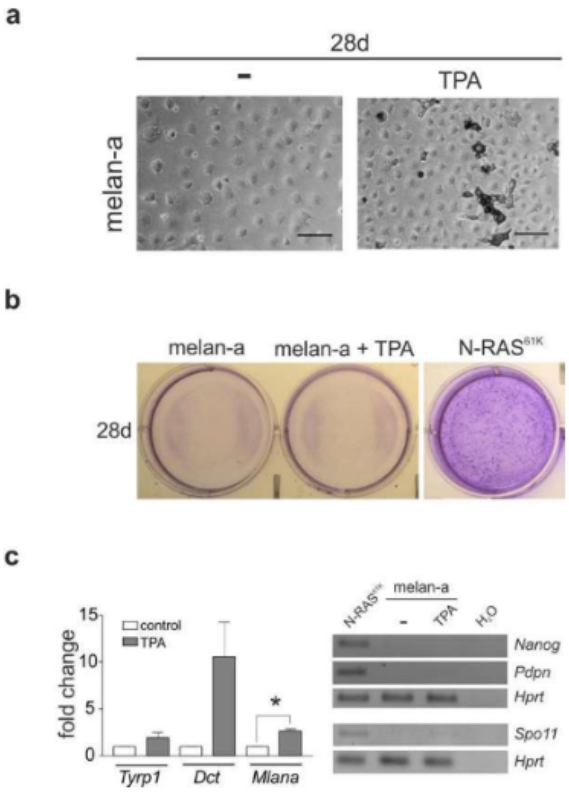
a
28d
-
TPA
melan-a
b
melan-a
melan-a + TPA
N-RAS^{G1K}
28d
c
control
TPA
fold change
15
10
5
0
*
Tyrp1
Dct
Miana
N-RAS^{G1K}
melan-a
-
TPA
H$_2$O
Nanog
Pdpn
Hprt
Spo11
Hprt

Figure 6

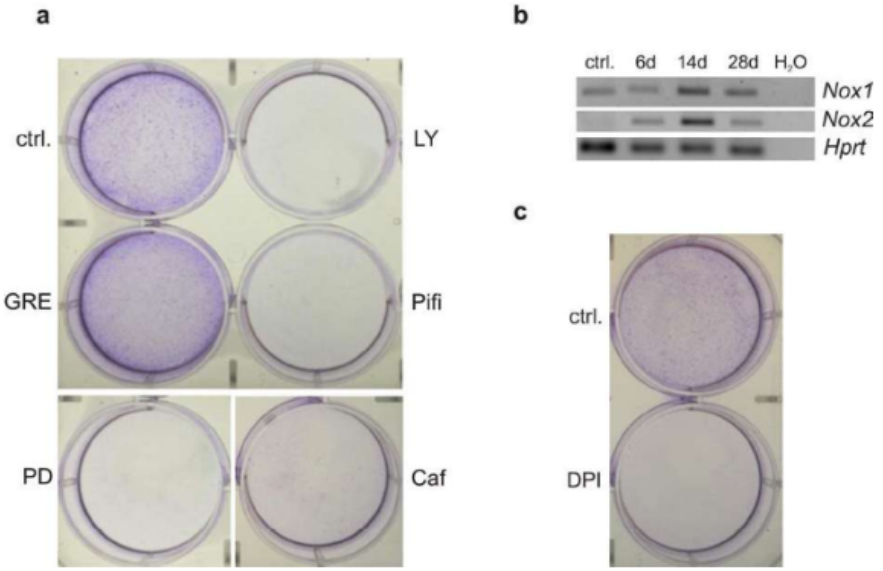
a
ctrl.
LY
GRE
Pifi
PD
Caf
b
ctrl.
6d
14d
28d
H2O
Nox1
Nox2
Hprt
c
ctrl.
DPI

Figure 7